frontiers | Research Topics

Novel anti-cancer agents targeting tumour metastasis and stemness

Edited by
Bo Wang, Zhongrui Li, Jing-Quan Wang and Luping Pang

Published in
Frontiers in Pharmacology

ISSN 1664-8714
ISBN 978-2-8325-5668-9
DOI 10.3389/978-2-8325-5668-9

About Frontiers

Frontiers is more than just an open access publisher of scholarly articles: it is a pioneering approach to the world of academia, radically improving the way scholarly research is managed. The grand vision of Frontiers is a world where all people have an equal opportunity to seek, share and generate knowledge. Frontiers provides immediate and permanent online open access to all its publications, but this alone is not enough to realize our grand goals.

Frontiers journal series

The Frontiers journal series is a multi-tier and interdisciplinary set of open-access, online journals, promising a paradigm shift from the current review, selection and dissemination processes in academic publishing. All Frontiers journals are driven by researchers for researchers; therefore, they constitute a service to the scholarly community. At the same time, the *Frontiers journal series* operates on a revolutionary invention, the tiered publishing system, initially addressing specific communities of scholars, and gradually climbing up to broader public understanding, thus serving the interests of the lay society, too.

Dedication to quality

Each Frontiers article is a landmark of the highest quality, thanks to genuinely collaborative interactions between authors and review editors, who include some of the world's best academicians. Research must be certified by peers before entering a stream of knowledge that may eventually reach the public - and shape society; therefore, Frontiers only applies the most rigorous and unbiased reviews. Frontiers revolutionizes research publishing by freely delivering the most outstanding research, evaluated with no bias from both the academic and social point of view. By applying the most advanced information technologies, Frontiers is catapulting scholarly publishing into a new generation.

What are Frontiers Research Topics?

Frontiers Research Topics are very popular trademarks of the *Frontiers journals series*: they are collections of at least ten articles, all centered on a particular subject. With their unique mix of varied contributions from Original Research to Review Articles, Frontiers Research Topics unify the most influential researchers, the latest key findings and historical advances in a hot research area.

Find out more on how to host your own Frontiers Research Topic or contribute to one as an author by contacting the Frontiers editorial office: frontiersin.org/about/contact

Novel anti-cancer agents targeting tumour metastasis and stemness

Topic editors

Bo Wang — Zhengzhou University, China
Zhongrui Li — Nanjing University of Chinese Medicine, China
Jing-Quan Wang — St. John's University, United States
Luping Pang — Zhengzhou University, China

Citation

Wang, B., Li, Z., Wang, J.-Q., Pang, L., eds. (2024). *Novel anti-cancer agents targeting tumour metastasis and stemness*. Lausanne: Frontiers Media SA.
doi: 10.3389/978-2-8325-5668-9

Table of contents

frontiers | Frontiers in Pharmacology

TYPE Editorial
PUBLISHED 30 October 2024
DOI 10.3389/fphar.2024.1504024

OPEN ACCESS

EDITED AND REVIEWED BY
Olivier Feron,
Université catholique de Louvain, Belgium

*CORRESPONDENCE
Bo Wang,
wangbo0601@zzu.edu.cn

RECEIVED 30 September 2024
ACCEPTED 21 October 2024
PUBLISHED 30 October 2024

CITATION
Pang L and Wang B (2024) Editorial: Novel anti-cancer agents targeting tumour metastasis and stemness.
Front. Pharmacol. 15:1504024.
doi: 10.3389/fphar.2024.1504024

Editorial: Novel anti-cancer agents targeting tumour metastasis and stemness

Luping Pang[1] and Bo Wang[2]*

[1]Department of Medical Genetics and Cell Biology, School of Basic Medical Sciences, Zhengzhou University, Zhengzhou, China, [2]School of Pharmaceutical Sciences, Zhengzhou University, Zhengzhou, China

KEYWORDS

tumor, metastasis, stemness, novel anti-cancer strategy, cancer stem cells

Editorial on the Research Topic
Novel anti-cancer agents targeting tumour metastasis and stemness

Despite extensive efforts in drug development for cancer treatment, only a few successful therapeutic agents and strategies have emerged that specifically target patients with metastatic cancer, particularly those with distant metastasis. Cancer stem cells (CSCs), also known as cancer-initiating cells, represent a small population of cells within cancerous tissue that possess unlimited proliferative potential and the ability to drive tumor formation (Batlle and Clevers, 2017). CSCs are believed to be the primary cause of drug resistance, cancer relapse, and metastasis, largely due to their capacities for self-renewal and differentiation.

Importantly, CSCs can migrate to distant sites by promoting epithelial-to-mesenchymal transition (EMT), evading apoptosis, and escaping immune surveillance, all of which contribute to cancer metastasis and progression. As such, CSCs play a critical role in tumorigenesis, drug resistance, recurrence, and metastasis, highlighting the urgent need to develop targeted therapies to improve patient outcomes in oncology (Chu et al., 2024).

Currently, advanced secondary cancers are typically only detected after multiple metastases have already occurred. The challenges associated with detecting dormant cancer cells or small metastases further complicate cancer treatment. Additionally, drugs targeting cancer metastasis often exhibit high cytotoxicity, inconsistencies in patient outcomes, and contribute to the development of drug resistance. Therefore, there is an urgent need for the development of novel small molecules, biological drugs, and combination therapies that target key processes in cancer metastasis.

Several pathways, such as WNT/β-Catenin, Notch, PI3K/AKT, TGF-β, and PPAR, have been validated as key regulators of cancer metastasis. Effectively targeting these pathways offers promising opportunities for therapeutic interventions that could inhibit tumor growth and reduce cancer stemness (Yang et al., 2020). This research aims to identify innovative small molecules and effective therapeutic strategies to target tumor metastasis and CSC-related processes, with the ultimate goal of improving survival rates for cancer patients.

Metaplastic breast cancer (MpBC) is a Research Topic of morphologically diverse and exceedingly aggressive variant disease, which can be classified as high or low grade based on the pathological features. As one type of high-grade MpBC, squamous cell carcinoma

(SCC) cases usually possess negative expression of estrogen receptor (ER), progesterone receptor (PR), and human epidermal growth factor receptor 2 (HER2), resembling triple-negative breast cancer (TNBC) but with a worse prognosis than conventional TNBC. Wang et al. reported an initial rare case of a patient diagnosed with HER2-positive breast SCC, who achieved favorable outcomes by utilizing HER2-targeted drugs in conjunction with chemotherapeutic drug paclitaxel. These findings suggest that HER2-targeted drugs can also exhibit positive effects on HER2-positive MpBC and SCC patients, thus providing a novel reference point for the subsequent treatment of uncommon pathological subtypes of breast cancer.

Recently, immune checkpoint inhibitors (ICIs) have revolutionized cancer treatment. However, a significant proportion of gastric cancer (GC) patients do not benefit from this therapeutic strategy. To elucidate the mechanisms underlying GC patients resistance to ICIs and identify biomarkers able to predict the response to ICIs at treatment initiation stage, Sun et al. collected GC tissues from 28 patients prior to the administration of anti-programmed death 1 (PD-1) immunotherapy and carried out protein quantification by high-resolution mass spectrometry (MS). Data analysis suggested that the low activity in the complement and coagulation cascades pathway and a high abundance of activated $CD8^+$ T cells are positive signals corresponding to ICIs. They also identified 10 protein biomarkers with potential for predicting the response to PD-1 inhibitor immunotherapy in GC patients, which may provide the impetus for personalized precision immunotherapy.

For anti-cancer drug development, 2D cell culture is the most commonly used method to evaluate tumor metastasis capability, but with limitations in representing cancer hallmarks and phenotypes. Ding et al. reported an innovative approach which combines the advantages of 3D tumor spheroid culture with impedance-based biosensing technologies to establish a high-throughput 3D cell invasion assay for anti-metastasis drug screening through multicellular tumor spheroids. This method could be a promising tool for enhancing the quality of the drug development pipeline by providing a robust platform for predicting the efficacy and safety of anti-metastatic drugs before applying into preclinical or clinical trials.

To improve the therapeutic efficacy and selectivity of chemotherapeutic agents for cancer treatment, the nanodrug delivery and targeting systems are initiated and thrivingly developed in recent years. However, most nanocarriers exhibit drawbacks including an intricate preparation process, limited drug-loading capacity, untargeted drug release, and nanocarrier toxicities. Wang et al. took advantage of natural products with abundant scaffold diversity and structural complexity, and established two carrier-free berberine (BBR)-based nanoparticles (NPs) to increase their synergistic efficacy for tumor treatment. BBR interacts with glycyrrhetinic acid (GA) and artesunate (ART) to self-assemble BBR-GA and BBR-ART NPs, respectively, without any nanocarriers. These BBR-based NPs have been demonstrated to possess significant tumor targeting specificity and enhanced antitumor properties both *in vitro* and *in vivo*. These novel carrier-free self-assemblies based on natural products offer a strategy for synergistic drug delivery and thus shed lights on developing enhanced antitumor drugs.

The stemness of CSCs plays a key role in driving hepatocellular carcinoma (HC) tumorigenesis, apoptotic resistance, and metastasis while functional mitochondria are critical for the stemness maintenance. Cuproptosis is Cu-mediated non-apoptotic pathway by inactivating mitochondrial enzymes pyruvate dehydrogenase (PDH) and succinate dehydrogenase (SDH), leading to mitochondrial dysfunction. Thus, Abu-Serie et al. designed two types of Cu oxide nanoparticles (Cu_4O_3 "C(I + II)" NPs and Cu_2O "C(I)" NPs) combined with an aldehyde dehydrogenase "ALDH" inhibitor diethyldithiocarbamate for anti-HC investigation. Being higher selective accumulation of the former NPs in tumor tissues, it exhibited higher cytotoxicity, mitochondrial membrane potential, and anti-migration impact than the later in the treated human HC cells.

Recently, long noncoding RNAs (lncRNAs) have been reported to be closely related to cancer metastasis. To explore whether lncRNA is also involved in the multi-organ metastasis in gastric cancer (GC), Zhang et al. conducted lncRNA-sequencing analysis of clinical lymph node metastatic GC tissues. They identified lncRNA CADM2-AS1 was aberrantly overexpressed in the metastatic GC tissues. Further mechanistic studies demonstrated overexpressed lncRNA CADM2-AS1 downregulated miR-5047 causing NOTCH4 upregulation to promote metastatic progression in GC. These results suggested that lncRNA CADM2-AS1 could be a potential effective target for metastatic GC prognosis in the clinic.

Non-coding RNAs (ncRNAs) are usually considered to be incapable of coding protein. However, the small peptide encoded by ncRNAs (SPENs) have been recently reported to play important roles in the invasive and migratory abilities of tumor cells, including the regulation of skeleton reorganization, intercellular adhesion, signaling and other processes. Therefore, SPENs have potential applications as therapeutic targets and biomarkers of malignant cancers. Liu et al. summaries the mechanisms of SPENs and their roles in tumor invasion and migration, with the goal of offering new targets for tumor diagnosis and treatment.

As mentioned earlier, CSCs are the leading cause of the anti-tumor treatment failure. These aggressive cancer cells can be preserved and sustained by adjacent cells constructing a specialized microenvironment, in which tumor-associated macrophages (TAMs) are key players. By improving the oxidative metabolism of CSCs and TAMs, cancer cells can extract more energy to survive in nutritionally defective environments. Among these metabolic pathways, mitochondria act as the crucial bioenergetic hub, drawing major hopes for drugs targeting mitochondria. Marrone et al. summarized the literatures on the metabolic adaptations of CSCs and their supporting macrophages, as well as highlighted the resistance and dormancy behaviors that give CSCs a selection advantage and quiescence capacity in particularly aggressive microenvironments and the critical role of TAMs in supporting these attitudes.

Despite extensive research on cervical cancer therapeutics, a bibliometric analysis specifically focused on immunotherapy for advanced, recurrent, or metastatic (A/R/M) cervical malignancies remains unmapped. Duan et al. conducted a systematic search using Web of Science Core Research Topic to identify articles related to A/R/M cervical cancer published between 2000 and 2022, providing

a detailed landscape of immunotherapy research in A/R/M cervical cancer.

In conclusion, through multiple innovative approaches reported, this Research Topic advanced our understanding of the different mechanisms of cancer metastasis and CSCs in different cancer types and their potential drug targets and challenges. Continued research and novel strategies offer hope for investigating more effective therapeutics, eventually improving the life span and quality of cancer patients.

Author contributions

LP: Writing–review and editing. BW: Writing–original draft.

Funding

The author(s) declare that no financial support was received for the research, authorship, and/or publication of this article.

Conflict of interest

The authors declare that the research was conducted in the absence of any commercial or financial relationships that could be construed as a potential conflict of interest.

Generative AI statement

The author(s) declare that no Generative AI was used in the creation of this manuscript.

Publisher's note

References

Batlle, E., and Clevers, H. (2017). Cancer stem cells revisited. *Nat. Med.* 23 1124–1134.

Chu, X., Tian, W., Ning, J., Xiao, G., Zhou, Y., Wang, Z., et al. (2024). Cancer stem cells: advances in knowledge and implications for cancer therapy. *Signal Transduct. Target. Ther.* 9 170.

Yang, L., Shi, P., Zhao, G., Xu, J., Peng, W., Zhang, J., et al. (2020). Targeting cancer stem cell pathways for cancer therapy. *Signal Transduct. Target. Ther.* 5 8.

frontiers | Frontiers in Pharmacology

TYPE Case Report
PUBLISHED 22 February 2024
DOI 10.3389/fphar.2024.1332574

OPEN ACCESS

EDITED BY
Jing-Quan Wang,
St. John's University, United States

REVIEWED BY
Ramcharan Singh Angom,
Mayo Clinic Florida, United States
Bo Wang,
Zhengzhou University, China

*CORRESPONDENCE
Zhen Wang,
tonywang@zju.edu.cn

†These authors have contributed equally to this work and share first authorship

RECEIVED 03 November 2023
ACCEPTED 05 February 2024
PUBLISHED 22 February 2024

CITATION
Wang G, Yang C, Zeng D, Wang J, Mao H, Xu Y, Jiang C and Wang Z (2024), Case report: Successful treatment of a rare HER2-positive advanced breast squamous cell carcinoma. *Front. Pharmacol.* 15:1332574. doi: 10.3389/fphar.2024.1332574

Case report: Successful treatment of a rare HER2-positive advanced breast squamous cell carcinoma

Gui Wang[1,2†], Chenghui Yang[3†], Donglin Zeng[1], Jihao Wang[1], Huaxin Mao[1], Yu Xu[1], Chao Jiang[4] and Zhen Wang[2,5,6*]

[1]Department of General Surgery, Longquan People's Hospital, Lishui, China, [2]Department of Breast Surgery, Second Affiliated Hospital, Zhejiang University School of Medicine, Hangzhou, China, [3]Department of Breast Surgery, First Affiliated Hospital of Wenzhou Medical University, Wenzhou, China, [4]Academy of Chinese Medical Sciences, Zhejiang Chinese Medical University, Hangzhou, China, [5]Key Laboratory of Tumor Microenvironment and Immune Therapy of Zhejiang Province, Second Affiliated Hospital, Zhejiang University School of Medicine, Hangzhou, China, [6]Cancer Center, Zhejiang University, Hangzhou, China

Background: Breast squamous cell carcinoma (SCC) is an uncommon and highly aggressive variant of metaplastic breast cancer. Despite its rarity, there is currently no consensus on treatment guidelines for this specific subtype. Previous studies have demonstrated that chemotherapy alone has limited efficacy in treating breast SCC. However, the potential for targeted therapy in combination with chemotherapy holds promise for future treatment options.

Case presentation: In this case report, we present a patient with advanced HER2-positive breast SCC, exhibiting a prominent breast mass, localized ulcers, and metastases in the lungs and brain. Our treatment approach involved the administration of HER2-targeted drugs in conjunction with paclitaxel, resulting in a sustained control of tumor growth.

Conclusion: This case represents a rare occurrence of HER2-positive breast SCC, with limited available data on the efficacy of previous HER2-targeted drugs in treating such patients. Our study presents the first application of HER2-targeted drugs in this particular case, offering novel therapeutic insights for future considerations. Additionally, it is imperative to conduct further investigations to assess the feasibility of treatment options in a larger cohort of patients.

KEYWORDS

metaplastic breast cancer, breast squamous cell carcinoma, HER2, targeted therapy, antibody drug conjugate

Abbreviations: ADC, Antibody Drug Conjugate; ADCC, Antibody-dependent cell-mediated cytotoxicity; BI-RADS, Breast Imaging Reporting and Data System; ER, Estrogen Receptor; HER2, Human Epidermal Growth Factor Receptor 2; IDC, Invasive ductal carcinoma; MDT, Multi-Disciplinary Team; MpBC, Metaplastic Breast Cancer; MRI, Magnetic Resonance Imaging; pCR, pathological Complete Response; PR, Progesterone Receptor; SCC, Squamous Cell Carcinoma; TKI, Tyrosine Kinase Inhibitor; TNBC, Triple-Negative Breast Cancer; WHO, World Health Organization.

Background

Metaplastic breast cancer (MpBC) is a collection of morphologically diverse and exceedingly aggressive variant diseases with a low prevalence, comprising 0.2%–1.0% of the overall breast cancer cases (Pezzi et al., 2007; DeSantis et al., 2017; Thomas et al., 2023a). In the year 2000, the World Health Organization (WHO) officially classified MpBC as a distinct and heterogeneous form of invasive breast cancer, distinguished by the transformation of neoplastic epithelium into squamous epithelium and/or stromal elements, such as spindle cells, chondrocytes, and osteocytes (Thomas et al., 2023b). MpBC can be categorized into various histological subtypes, consisting of one or multiple components or a combination of carcinoma and metaplasia regions. Based on the pathological features, the histological grade of MpBC can be classified as high or low grade. High-grade MpBC encompasses squamous cell carcinoma (SCC) which accounting for about 0.1%–0.2% of breast cancer (Hennessy et al., 2005), spindle cell carcinoma, metaplastic carcinomas with mesenchymal differentiation (such as cartilage, bone, rhabdomyosarcoma, and nerve differentiation), as well as mixed metaplastic carcinomas. Low-grade MpBC encompasses low-grade adenosquamous carcinoma and fibromatosis-like metaplastic carcinomas. The majority of MpBC cases exhibit negative expression of estrogen receptor (ER), progesterone receptor (PR), and human epidermal growth factor receptor 2 (HER2), resembling triple-negative breast cancer (TNBC) but with a worse prognosis than conventional TNBC (Narayan et al., 2023; Tan et al., 2023; Zheng et al., 2023). In recent

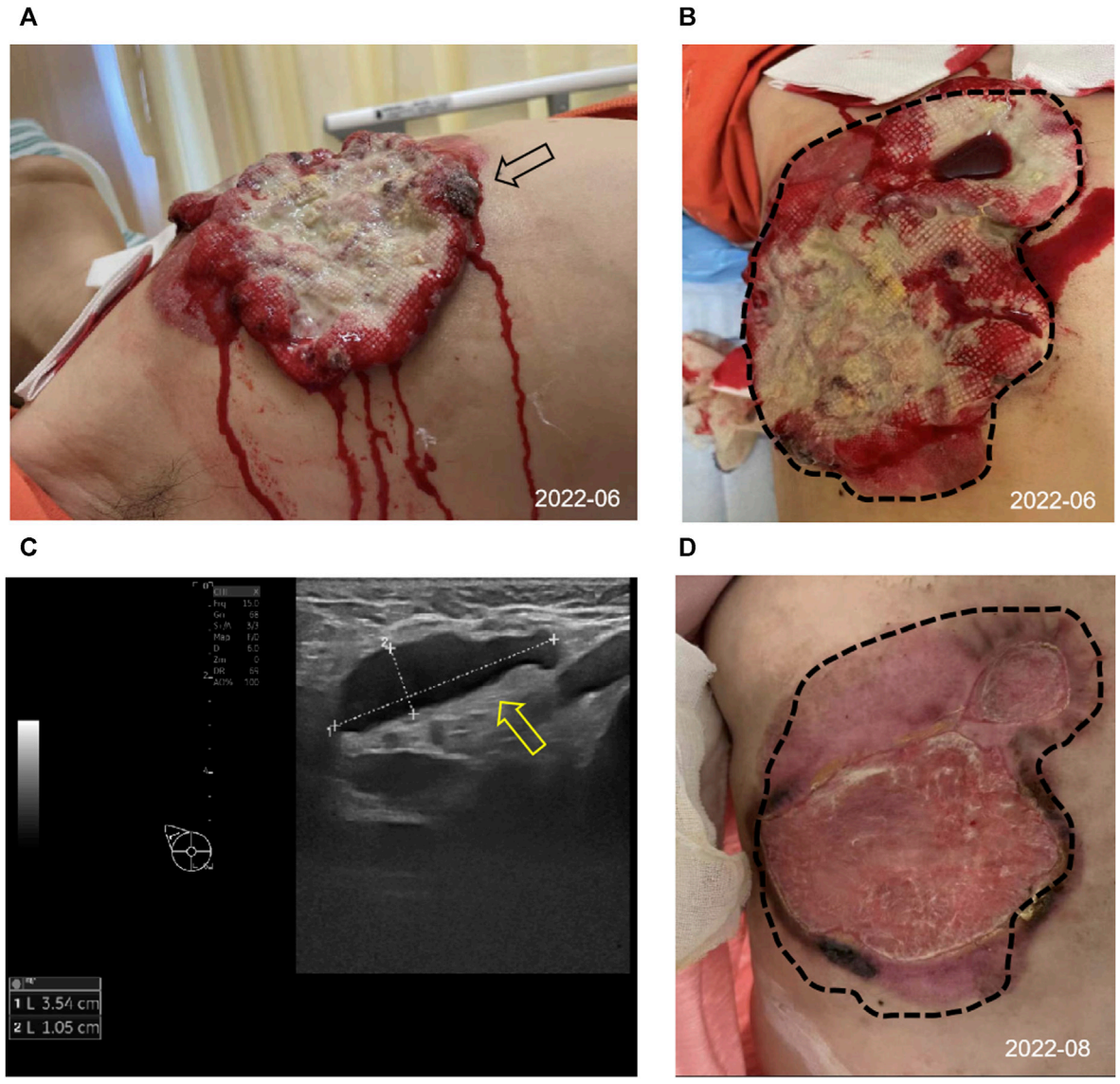

FIGURE 1
Appearance and clinical sign at initial diagnosis and after 2 cycles of treatment. **(A,B)** Image of the right chest mass from side (black arrow) and frontal (tumor lesions outlined with black dashed lines) at the initial diagnosis. **(C)** The ultrasound image showed enlarged right axillary node (3.54*1.05 cm) with disappearance of the normal lymph node structure (shown by the yellow arrow). **(D)** Changes in the right chest mass appearance after 2 cycles of treatment, compared with initial diagnosis (black dashed lines).

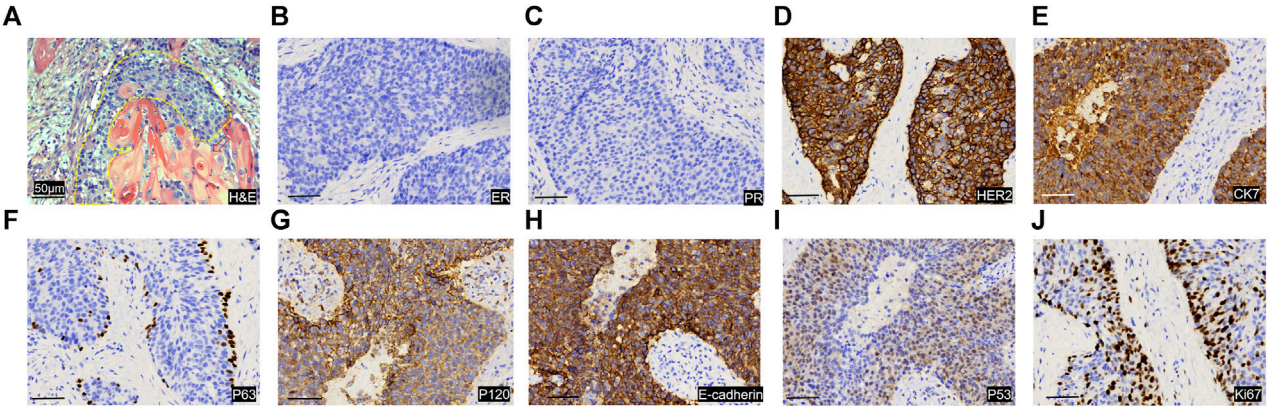

FIGURE 2
Image of pathological sections of tumor puncture. **(A)** H&E image of the pathological section. The yellow dashed line shows the tumor cancer foci, and the tumor cells grow in a nest, with obvious cell specificity, and nuclear division. Significant cell keratosis is seen at the positions indicated by the red arrows. Immunohistochemical staining images of for ER **(B)**, PR **(C)**, HER 2 **(D)**, CK7 **(E)**, P63 **(F)**, P120 **(G)**, E-cadherin **(H)**, P53 **(I)**, Ki-67 **(J)**. Scale Bar = 50 μm.

years, advancements in research technology have led to an enhanced understanding of this uncommon breast tumor, resulting in increased attention and the accumulation of relevant treatment experience for MpBC (Qiu et al., 2022; Corso et al., 2023; Coutant et al., 2023; Kawachi et al., 2023).

Herein, we report the initial case of a patient diagnosed with HER2-positive breast SCC, who achieved sustained tumor control through the utilization of HER2-targeted drugs in conjunction with paclitaxel.;

Case description

In June 2022, a 52-year-old female patient sought medical attention at the clinic, reporting the presence of a right breast mass persisting for a duration of 6 months, accompanied by local skin ulceration lasting over 3 months. The patient described the initial discovery of the breast mass as protruding through the skin, measuring approximately 2*2 cm in size and exhibiting a red coloration. Due to tingling pain, the patient engaged in repeated wiping of the mass, which unfortunately led to its gradual enlargement and subsequent rupture within a span of 2 months, resulting in the exudation of hemorrhagic fluid. Despite these concerning developments, the patient remained unaware of the severity of her condition and refrained from seeking medical attention. Subsequently, there was a significant escalation in the extent of skin ulceration. Upon physical examination, a breast mass exhibiting a concave alteration and surface hemorrhaging was observed, measuring approximately 15*10 cm (Figures 1A, B). Additionally, several enlarged and firm consistency right axillary lymph nodes were detected. The patient denied any familial history of breast cancer.

Consequently, she was admitted to our hospital's breast center for further evaluation. The general condition of the patient was fair including consciousness state, blood pressure, heart rate, respiratory rate, and normal auscultatory findings of heart and lungs. Breast ultrasound examination revealed a hypoechoic mass in the outer quadrant of the right breast, measuring 2.21*1.92 cm, displaying an indistinct border and irregular margins, graded as Breast imaging-reporting and data system (BI-RADS) category 4C. The ultrasound examination of the right axillary lymph nodes revealed the presence of multiple hypoechoic nodules with indistinct boundaries and absence of lymphatic structure (Figure 1C). Subsequently, a biopsy of the breast mass was performed and H&E pathological image showed the tumor cells grow in a nest, with obvious cell specificity, nuclear division and significant cell keratosis, indicated the presence of invasive carcinoma with squamous differentiation (Figures 2A). Immunohistochemistry further revealed negative expression of ER and PR, strongly positive expression of HER2, positive expression of CK7, partial positive expression of P63, membrane positive expression of P120, negative expression of E-cadherin, wild type expression of P53, and approximately 30% positive expression of Ki-67 (Figures 2B–J). Based on the integration of clinical and pathological findings, the diagnosis of MpBC and breast SCC was established. A lung computed tomography (CT) scan revealed the presence of multiple nodules with irregular morphology and burr change in both lungs, suggesting the possibility of metastatic tumor (Figures 3A, B). However, subsequent examinations including abdominal ultrasound, abdominal enhanced CT, brain magnetic resonance imaging (MRI), vertebral CT, and supraclavicular lymph node ultrasound did not reveal any signs of tumor metastasis. A positron emission tomography-computed tomography (PET-CT) examination demonstrated an increased uptake of fluorodeoxyglucose (FDG) in right chest wall soft tissue, right axillary lymph nodes, and multiple parts of both lungs, considering lymph node and multiple lung metastasis (Figures 3C–G). In conjunction with the aforementioned examination findings, the patient received a diagnosis of right breast SCC, cT4N2M1, Stage IV, HER2-positive subtype.

Following a Multi-Disciplinary Team (MDT) consultation, a treatment regimen consisting of weekly chemotherapy with paclitaxel (albumin-bound formulation) and targeted therapy with trastuzumab and pertuzumab every 3 weeks was initiated on 25 June 2022. After 6 weeks of treatment, the patient exhibited significant wound reduction (Figures 1D) and a notable decrease in

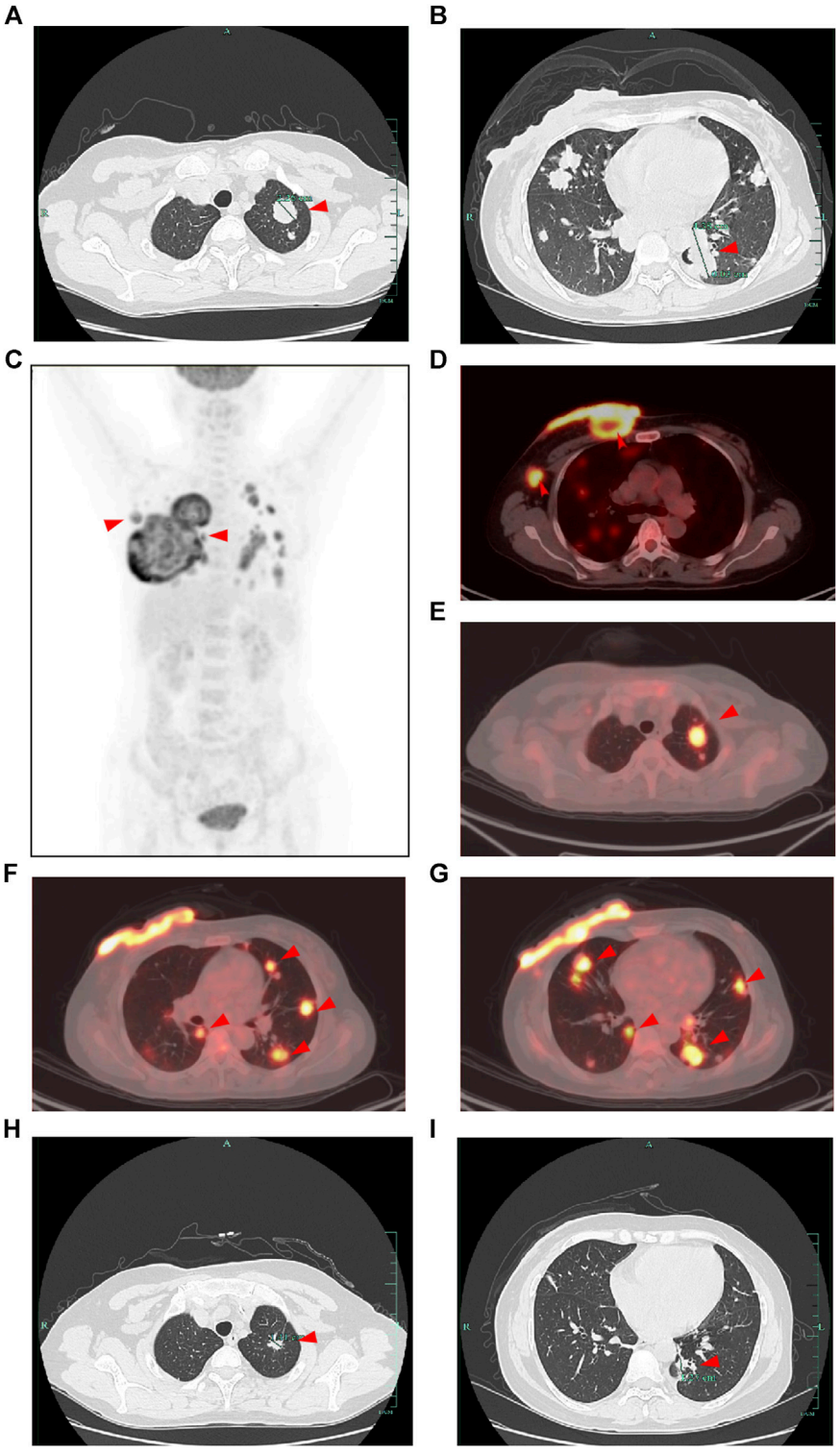

FIGURE 3
CT and PET-CT images of the patient. **(A,B)** CT images of the lung at the initial diagnosis showed multiple lung metastasis (shown by the red arrow). **(C)** Overview of the whole-body PET-CT image. **(D–G)** PET-CT image showed an increased uptake of fluorodeoxyglucose (FDG) in right chest wall soft tissue, right axillary lymph nodes, and multiple parts of both lungs (shown by the red arrow). **(H,I)** CT images of the lung after 2 cycles of treatment showed decreased lung metastasis (shown by the red arrow compared with initial diagnosis).

lung lesions on 18 August 2022 (Figures 3H, I), which was classified as a partial response. At the same time, the evaluation of the patient's physical condition showed that she still had a good mental state and stable vital signs, and no significant side reactions were described. Therefore, the original treatment regimen was maintained until January 2023, at which point the patient experienced bilateral lower

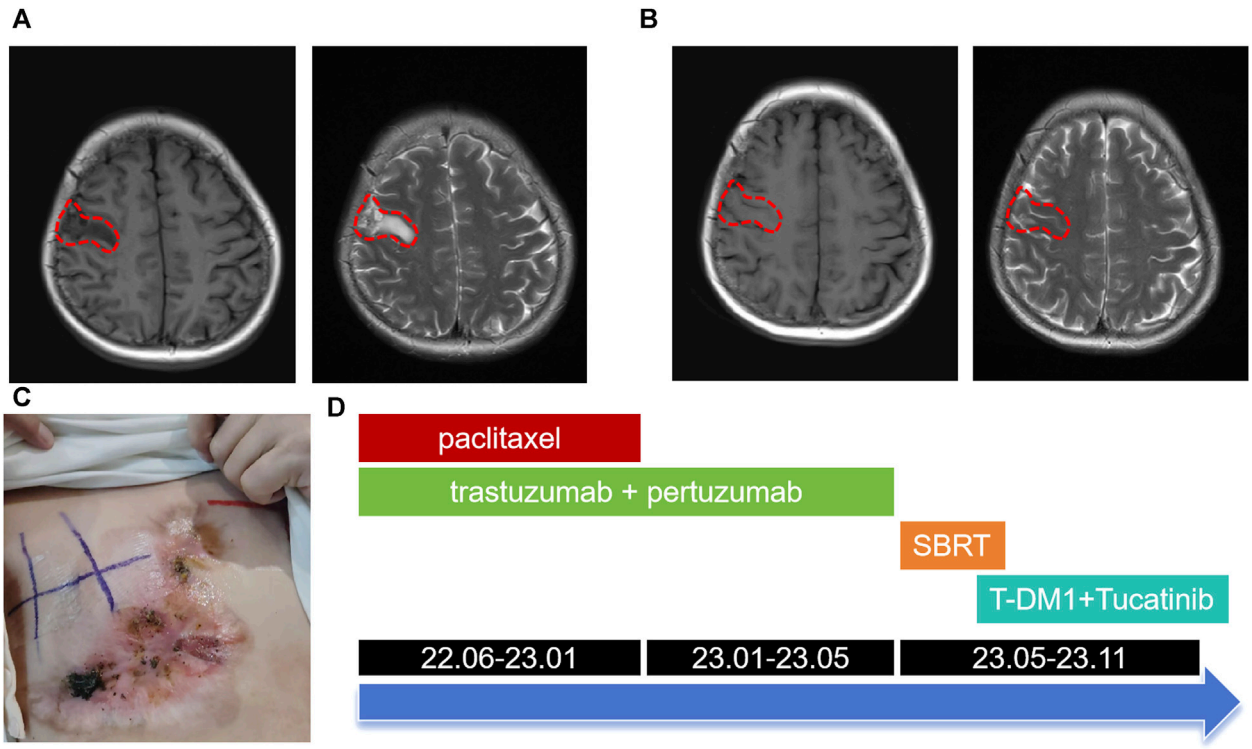

FIGURE 4
Brain MRI images and the overall treatment timeline. **(A)** Brain MRI images at May 2023 showed right frontal lobe nodule accompanied by edema in the adjacent brain tissue (lesions outlined with red dashed lines). **(B)** Brain MRI images after SBRT and combined therapy including T-DM1 combined with Tucatinib. **(C)** Changes in the right chest mass appearance at October 2023. **(D)** Treatment timeline from June 2022 to November 2023.

limb edema with a normal levels of serum protein and creatinine and numbness at the end of the limb (glove anesthesia), which was attributed to paclitaxel. Consequently, paclitaxel was discontinued and the targeted therapy was continued. During the routine systematic evaluation in May 2023, a notable reduction in the right chest ulceration and scab formation on the skin were observed. Additionally, lung CT scan revealed a substantial decrease in lung metastases. However, brain MRI revealed the presence of a right frontal lobe nodule accompanied by edema in the adjacent brain tissue, and metastasis was considered (Figures 4A). Following an MDT discussion, Stereotactic Body Radiotherapy (SBRT) was administered at a dose of 32.5Gy/5F to the planning gross tumor volume (PGTV). Simultaneously, the patient's treatment regimen was modified to include the antibody drug conjugate (ADC) T-DM1 and the tyrosine kinase inhibitor (TKI) Tucatinib, starting from 18 August 2023. Subsequent brain MRI conducted on 26 September 2023, revealed a significant reduction in the size of the brain metastasis compared to previous scans (Figures 4B). During the regimen, the patient had fatigue and platelet reduction (platelet count minimum to lower than 50*10^9/L), which may caused by the simultaneous administration of T-DM1 and radiotherapy as reported before (von Minckwitz et al., 2019). Furthermore, the patient was given daily injection of recombinant human thrombopoietin, until platelet count rose to 80*10^9/L. The patient is presently undergoing ongoing treatment, as depicted in Figures 4C, D.

Discussion

This paper presents a comprehensive analysis of the management of an advanced case of HER2-positive breast SCC, yielding promising outcomes in targeted therapy. The findings of this study offer valuable insights for future clinical interventions in similar cases.

The etiology of MpBC remains uncertain, predominantly affecting women aged over 50 years, with sporadic occurrences and minimal familial clustering (Chaudhary et al., 2023). Limited data exists regarding the demographics, clinical manifestations, tumor attributes, and therapeutic approaches for MpBC, including SCC (Ullah et al., 2023; Wu et al., 2023). The lymph node metastasis rate of MpBC was relatively low, as evidenced by a large-scale study indicating that the incidence of MpBC involving axillary lymph nodes was 21.9%, which is lower than that of invasive ductal carcinoma (IDC) at 34.3% (Pezzi et al., 2007; Lee et al., 2023). Despite this lower lymph node involvement, MpBC is characterized by a higher propensity for local recurrence and distant metastasis, with the lung being the most common site of metastasis (He et al., 2019; Abada et al., 2022).

The majority of MpBC cases present as palpable breast masses, which do not differ from common benign and malignant breast tumors. X-ray and ultrasound are commonly advised for the diagnosis of MpBC. However, the histological complexity of MpBC makes preoperative puncture diagnosis challenging, leading to a higher reliance on postoperative diagnosis. The differential diagnosis of MpBC necessitates the utilization of

multiple immunohistochemical markers. The morphological characteristics of SCC are generally distinctive, making the diagnosis less arduous. Immunohistochemistry for breast SCC typically reveals the presence of Cytokeratin (CK) markers. Additionally, it is crucial to exclude primary SCC originating from other organs, such as the lung or skin.

Due to the limited prevalence of MpBC, there is a scarcity of prospective studies specifically focusing on this subtype. The majority of available data originates from retrospective studies, and currently, there are no established guidelines for the treatment of MpBC. Consequently, its management is predominantly approached similarly to invasive ductal carcinoma (IDC). Surgical intervention is the preferred approach for the management of SCC, and in cases of well-differentiated SCC, complete excision of the tumor may suffice. Endocrine therapy is not recommended for hormone receptor-negative cancer. With the exception of low-grade adenosquamous carcinoma and fibromatosis-like metaplastic carcinomas, MpBC is limited response to conventional chemotherapy. In the event that chemotherapy is deemed necessary, the selection of 5-fluorouracil, doxorubicin, and platinum agents can be considered. Chen et al. (2011) conducted a study involving 12 patients with MpBC, administering either single or combination chemotherapy. Among these patients, only one individual who received chemotherapy containing taxol drugs exhibited a partial response. In another separate study by Takala, 14 patients undergoing palliative chemotherapy were included, with two patients showing a partial response after being treated with amycin or capecitabine (Takala et al., 2019).

The majority of MpBC patients were found to be HER2 negative, with HER2 positivity observed only in a limited number of cases or reported in retrospective studies. Expression rate of HER2 in breast SCC has also been reported to be less than 10% (Pirot et al., 2020). The HER2 protein is classified as a member of the tyrosine protein kinase family. HER2 over-expression plays a significant role in the regulation of cellular processes, specifically cell growth and division. However, when HER2 is over-expressed, it leads to the rapid proliferation of cancer cells and tumor formation. This phenomenon is commonly observed in malignancies, particularly in breast cancer. Consequently, the use of HER2-targeted antibodies, such as trastuzumab and pastuzumab, ADC (T-DM1, T-DXd), and TKI (Pyrrotinib, tukatinib, and neratinib), has become a primary approach to address HER2 over-expression in breast cancer (Swain et al., 2023). The combination of drugs targeting the HER2 protein can effectively induce antibody-dependent cell-mediated cytotoxicity (ADCC) and activate the classical pathway of complement, thereby impeding the proliferation, division, and metastasis of tumor cells. These targeted drugs have been employed in this particular case, yielding favorable therapeutic outcomes within a specific timeframe. Lei et al. (2022) documented notable efficacy in MpBC patients with positive HER2 results following trastuzumab treatment. Further investigation is warranted to ascertain the suitability of HER2-targeted therapy for HER2-positive MpBC patients, given the limited prevalence of HER2 expression in this population. Given the resistance of MpBC to chemotherapy, it is imperative to explore novel treatment options based on the molecular tumor characteristics. Notably, MpBC cases featuring somatic gene mutations in the PI3K/AKT/mTOR signaling pathway demonstrate heightened pathway activity, which is closely linked to primary and secondary resistance to conventional breast cancer therapy (Ng et al., 2017). The high-frequency alterations observed in the PI3K/AKT/mTOR pathway suggest that the use of PI3K inhibitors or mTOR inhibitors may be a viable therapeutic option for the treatment of MpBC. A study conducted by Yang et al. (2019) in 2019 demonstrated that a MpBC patient with a *PIK3CA H1047R* mutation achieved a partial response when treated with weekly paclitaxel therapy and the PI3K inhibitor Bupanisi, resulting in an overall survival of 42 months. Additionally, mTOR inhibitors have shown promise in MpBC patients. A systemic treatment regimen for advanced MpBC patients, consisting of an mTOR inhibitor (sirolimus or everolimus) in combination with liposomal doxorubicin and bevacizumab, has demonstrated efficacy. The objective response rate (ORR) was found to be 21%, with 8% achieving a complete response and 13% achieving a partial response (Dwyer and Clark, 2015). Clinical studies are needed to confirm the potential of PI3K inhibitors and mTOR inhibitors as new treatment options for MpBC patients. Two randomized phase 3 trials, OlympiAD (He et al., 2019) and EMBRACA (Romero, 2018), have demonstrated that PARP inhibitors (PARPi) are more effective than chemotherapy in patients with locally advanced/metastatic breast cancer and BRCA mutations. An additional case of MpBC patients carrying the BRCA2 mutation achieved a pathological complete response (pCR) after 6 months of neoadjuvant treatment with Trapappanib alone, indicating that PARP inhibition may be a potential therapeutic strategy for MpBC (Litton et al., 2020). Additionally, the use of PD-L1/PD-1 immune checkpoint blockade therapy shows promise. Suzanne's study revealed that PD-L1 expression was positive in tumor cells in 18% of the enrolled high-grade MpBC cases and in tumor-infiltrating immune cells in 40% of the cases (Chartier et al., 2023). Sylvia and Anita separately reported a case of pCR achieved through a combination of chemotherapy and Pembrolizumab in MpBC (Adams, 2017; Gul et al., 2023).

Conclusion

This paper presents a unique instance of HER2-positive breast SCC that exhibited favorable outcomes upon the administration of HER2-targeted drugs in combination with chemotherapeutic drugs. These findings suggest that HER2-targeted drugs can also yield positive effects on MpBC and SCC, thereby offering a novel point of reference for the subsequent treatment of uncommon pathological subtypes of breast cancer.

Data availability statement

The raw data supporting the conclusions of this article will be made available by the authors, without undue reservation.

Ethics statement

The studies involving humans were approved by the Ethics Committee of Second Affiliated Hospital of Zhejiang University School of Medicine. The studies were conducted in accordance with the local legislation and institutional requirements. Written informed consent for participation was not required from the participants or the participants' legal guardians/next of kin in accordance with the national legislation and institutional requirements. Written informed consent was obtained from the

individual(s) for the publication of any potentially identifiable images or data included in this article. Written informed consent was obtained from the participant/patient(s) for the publication of this case report.

Author contributions

GW: Writing–original draft, Data curation. CY: Writing–original draft. DZ: Writing–original draft, Investigation. JW: Investigation, Writing–original draft. HM: Writing–review and editing. YX: Writing–review and editing. CJ: Writing–original draft. ZW: Writing–original draft.

Funding

The author(s) declare financial support was received for the research, authorship, and/or publication of this article. This work were supported by grants from the National Natural Science Foundation of China (82273449) and Medical and Health Science and Technology Project of Zhejiang Province (2024KY1039).

Conflict of interest

The authors declare that the research was conducted in the absence of any commercial or financial relationships that could be construed as a potential conflict of interest.

Publisher's note

All claims expressed in this article are solely those of the authors and do not necessarily represent those of their affiliated organizations, or those of the publisher, the editors and the reviewers. Any product that may be evaluated in this article, or claim that may be made by its manufacturer, is not guaranteed or endorsed by the publisher.

References

Abada, E., Daaboul, F., Ebare, K., Jang, H., Fehmi, Z., Kim, S., et al. (2022). Clinicopathologic characteristics and outcome descriptors of metaplastic breast carcinoma. *Archives pathology laboratory Med.* 146 (3), 341–350. doi:10.5858/arpa.2020-0830-OA

Adams, S. (2017). Dramatic response of metaplastic breast cancer to chemo-immunotherapy. *NPJ breast cancer* 3, 8. doi:10.1038/s41523-017-0011-0

Chartier, S., Brochard, C., Martinat, C., Coussy, F., Feron, J. G., Kirova, Y., et al. (2023). TROP2, androgen receptor, and PD-L1 status in histological subtypes of high-grade metaplastic breast carcinomas. *Histopathology* 82 (5), 664–671. doi:10.1111/his.14852

Chaudhary, D., Balhara, K., Mandal, S., Mallya, V., Tomar, R., Khurana, N., et al. (2023). Metaplastic breast carcinoma: analysis of clinical and pathologic features, a five-year study. *J. cancer Res. Ther.* 19 (5), 1226–1230. doi:10.4103/jcrt.jcrt_1229_21

Chen, I. C., Lin, C. H., Huang, C. S., Lien, H. C., Hsu, C., Kuo, W. H., et al. (2011). Lack of efficacy to systemic chemotherapy for treatment of metaplastic carcinoma of the breast in the modern era. *Breast cancer Res. Treat.* 130 (1), 345–351. doi:10.1007/s10549-011-1686-9

Corso, G., Marabelli, M., Calvello, M., Gandini, S., Risti, M., Feroce, I., et al. (2023). Germline pathogenic variants in metaplastic breast cancer patients and the emerging role of the BRCA1 gene. *Eur. J. Hum. Genet. EJHG.* 31 (11), 1275–1282. doi:10.1038/s41431-023-01429-2

Coutant, A., Cockenpot, V., Muller, L., Degletagne, C., Pommier, R., Tonon, L., et al. (2023). Spatial transcriptomics reveal pitfalls and opportunities for the detection of rare high-plasticity breast cancer subtypes. *Laboratory investigation; a J. Tech. methods pathology* 103 (12), 100258. doi:10.1016/j.labinv.2023.100258

DeSantis, C. E., Kramer, J. L., and Jemal, A. (2017). The burden of rare cancers in the United States. *a cancer J. Clin.* 67 (4), 261–272. doi:10.3322/caac.21400

Dwyer, J. B., and Clark, B. Z. (2015). Low-grade fibromatosis-like spindle cell carcinoma of the breast. *Archives pathology laboratory Med.* 139 (4), 552–557. doi:10.5858/arpa.2013-0555-RS

Gul, A., Alberty-Oller, J. J., Sandhu, J., Ayala-Bustamante, E., and Adams, S. (2023). A case of pathologic complete response to neoadjuvant chemotherapy and Pembrolizumab in metaplastic breast cancer. *JCO Precis. Oncol.* 7, e2200506. doi:10.1200/PO.22.00506

He, X., Ji, J., Dong, R., Liu, H., Dai, X., Wang, C., et al. (2019). Prognosis in different subtypes of metaplastic breast cancer: a population-based analysis. *Breast cancer Res. Treat.* 173 (2), 329–341. doi:10.1007/s10549-018-5005-6

Hennessy, B. T., Krishnamurthy, S., Giordano, S., Buchholz, T. A., Kau, S. W., Duan, Z., et al. (2005). Squamous cell carcinoma of the breast. *J. Clin. Oncol. official J. Am. Soc. Clin. Oncol.* 23 (31), 7827–7835. doi:10.1200/JCO.2004.00.9589

Kawachi, K., Tang, X., Kasajima, R., Yamanaka, T., Shimizu, E., Katayama, K., et al. (2023). Genetic analysis of low-grade adenosquamous carcinoma of the breast progressing to high-grade metaplastic carcinoma. *Breast cancer Res. Treat.* 202 (3), 563–573. doi:10.1007/s10549-023-07078-9

Lee, J. H., Ryu, J. M., Lee, S. K., Chae, B. J., Lee, J. E., Kim, S. W., et al. (2023). Clinical characteristics and prognosis of metaplastic breast cancer compared with invasive ductal carcinoma: a propensity-matched analysis. *Cancers* 15 (5), 1556. doi:10.3390/cancers15051556

Lei, T., Pu, T., Wei, B., Fan, Y., Yang, L., Shen, M., et al. (2022). Clinicopathologic characteristics of HER2-positive metaplastic squamous cell carcinoma of the breast. *J. Clin. pathology* 75 (1), 18–23. doi:10.1136/jclinpath-2020-206468

Litton, J. K., Scoggins, M. E., Hess, K. R., Adrada, B. E., Murthy, R. K., Damodaran, S., et al. (2020). Neoadjuvant talazoparib for patients with operable breast cancer with a germline BRCA pathogenic variant. *J. Clin. Oncol. official J. Am. Soc. Clin. Oncol.* 38 (5), 388–394. doi:10.1200/JCO.19.01304

Narayan, P., Kostrzewa, C. E., Zhang, Z., O'Brien, D. A. R., Mueller, B. A., Cuaron, J. J., et al. (2023). Metaplastic carcinoma of the breast: matched cohort analysis of recurrence and survival. *Breast cancer Res. Treat.* 199 (2), 355–361. doi:10.1007/s10549-023-06923-1

Ng, C. K. Y., Piscuoglio, S., Geyer, F. C., Burke, K. A., Pareja, F., Eberle, C. A., et al. (2017). The landscape of somatic genetic alterations in metaplastic breast carcinomas. *Clin. cancer Res. official J. Am. Assoc. Cancer Res.* 23 (14), 3859–3870. doi:10.1158/1078-0432.CCR-16-2857

Pezzi, C. M., Patel-Parekh, L., Cole, K., Franko, J., Klimberg, V. S., and Bland, K. (2007). Characteristics and treatment of metaplastic breast cancer: analysis of 892 cases from the National Cancer Data Base. *Ann. Surg. Oncol.* 14 (1), 166–173. doi:10.1245/s10434-006-9124-7

Pirot, F., Chaltiel, D., Ben Lakhdar, A., Mathieu, M. C., Rimareix, F., and Conversano, A. (2020). Squamous cell carcinoma of the breast, are there two entities with distinct prognosis? A series of 39 patients. *Breast cancer Res. Treat.* 180 (1), 87–95. doi:10.1007/s10549-020-05525-5

Qiu, Y., Chen, Y., Zhu, L., Chen, H., Dai, Y., Bao, B., et al. (2022). Differences of clinicopathological features between metaplastic breast carcinoma and nonspecific invasive breast carcinoma and prognostic profile of metaplastic breast carcinoma. *breast J.* 2022, 2500594. doi:10.1155/2022/2500594

Romero, D. (2018). EMBRACing a new PARP inhibitor? *Nat. Rev. Clin. Oncol.* 15 (11), 655. doi:10.1038/s41571-018-0090-3

Swain, S. M., Shastry, M., and Hamilton, E. (2023). Targeting HER2-positive breast cancer: advances and future directions. *Nat. Rev. Drug Discov.* 22 (2), 101–126. doi:10.1038/s41573-022-00579-0

Takala, S., Heikkilä, P., Nevanlinna, H., Blomqvist, C., and Mattson, J. (2019). Metaplastic carcinoma of the breast: prognosis and response to systemic treatment in metastatic disease. *breast J.* 25 (3), 418–424. doi:10.1111/tbj.13234

Tan, Y., Yang, B., Chen, Y., and Yan, X. (2023). Outcomes of metaplastic breast cancer versus triple-negative breast cancer: a propensity score matching analysis. *World J. Surg.* 47, 3192–3202. doi:10.1007/s00268-023-07106-1

Thomas, A., Douglas, E., Reis-Filho, J. S., Gurcan, M. N., and Wen, H. Y. (2023a). Metaplastic breast cancer: current understanding and future directions. *Clin. breast cancer* 23, 775–783. doi:10.1016/j.clbc.2023.04.004

Thomas, H. R., Hu, B., Boyraz, B., Johnson, A., Bossuyt, V. I., Spring, L., et al. (2023b). Metaplastic breast cancer: a review. *Crit. Rev. oncology/hematology* 182, 103924. doi:10.1016/j.critrevonc.2023.103924

Ullah, A., Khan, J., Yasinzai, A. Q. K., Tracy, K., Nguyen, T., Tareen, B., et al. (2023). Metaplastic breast carcinoma in U.S. Population: racial disparities, survival benefit of adjuvant chemoradiation and future personalized treatment with genomic landscape. *Cancers* 15 (11), 2954. doi:10.3390/cancers15112954

von Minckwitz, G., Huang, C. S., Mano, M. S., Loibl, S., Mamounas, E. P., Untch, M., et al. (2019). Trastuzumab emtansine for residual invasive HER2-positive breast cancer. *N. Engl. J. Med.* 380 (7), 617–628. doi:10.1056/NEJMoa1814017

Wu, P., Chang, H., Wang, Q., Shao, Q., and He, D. (2023). Trends of incidence and mortality in metaplastic breast cancer and the effect of contralateral prophylactic mastectomy: a population-based study. *Asian J. Surg.* 47, 394–401. doi:10.1016/j.asjsur.2023.09.053

Yang, M. H., Chen, I. C., and Lu, Y. S. (2019). PI3K inhibitor provides durable response in metastatic metaplastic carcinoma of the breast: a hidden gem in the BELLE-4 study. *J. Formos. Med. Assoc. = Taiwan yi zhi* 118 (9), 1333–1338. doi:10.1016/j.jfma.2018.12.004

Zheng, C., Fu, C., Wen, Y., Liu, J., Lin, S., Han, H., et al. (2023). Clinical characteristics and overall survival prognostic nomogram for metaplastic breast cancer. *Front. Oncol.* 13, 1030124. doi:10.3389/fonc.2023.1030124

frontiers | Frontiers in Pharmacology

TYPE Original Research
PUBLISHED 12 March 2024
DOI 10.3389/fphar.2024.1333087

OPEN ACCESS

EDITED BY
Ahmed Esmat Abdel Moneim,
Helwan University, Egypt

REVIEWED BY
Wei Song,
Nanjing Drum Tower Hospital, China
Md Nurunnabi,
The University of Texas at El Paso, United States

*CORRESPONDENCE
Renshi Li,
li-renshi@cpu.edu.cn
Chao Han,
hanchao@cpu.edu.cn
Lei Wang,
wanglei@njucm.edu.cn

†These authors have contributed equally to this work

RECEIVED 04 November 2023
ACCEPTED 27 February 2024
PUBLISHED 12 March 2024

CITATION
Wang Y, Li Z, Zhang H, Wu P, Zhao Y, Li R, Han C and Wang L (2024), Berberine-based self-assembly agents with enhanced synergistic antitumor efficacy.
Front. Pharmacol. 15:1333087.
doi: 10.3389/fphar.2024.1333087

Berberine-based self-assembly agents with enhanced synergistic antitumor efficacy

Yun Wang[1†], Zhongrui Li[1,2†], Haili Zhang[1], Peiye Wu[1], Yu Zhao[1], Renshi Li[1*], Chao Han[1*] and Lei Wang[2*]

[1]State Key Laboratory of Natural Medicines, Jiangsu Key Laboratory of Bioactive Natural Product Research, School of Traditional Chinese Pharmacy, China Pharmaceutical University, Nanjing, China, [2]Department of Rehabilitation, College of Acupuncture and Moxibustion and Massage Health Preservation and Rehabilitation, Nanjing University of Chinese Medicine, Nanjing, China

Tumors are still a major threat to people worldwide. Nanodrug delivery and targeting systems can significantly improve the therapeutic efficacy of chemotherapeutic drugs for antitumor purposes. However, many nanocarriers are likely to exhibit drawbacks such as a complex preparation process, limited drug-loading capacity, untargeted drug release, and toxicity associated with nanocarriers. Therefore, new therapeutic alternatives are urgently needed to develop antitumor drugs. Natural products with abundant scaffold diversity and structural complexity, which are derived from medicinal plants, are important sources of new antitumor drugs. Here, two carrier-free berberine (BBR)-based nanoparticles (NPs) were established to increase the synergistic efficacy of tumor treatment. BBR can interact with glycyrrhetinic acid (GA) and artesunate (ART) to self-assemble BBR-GA and BBR-ART NPs without any nanocarriers, respectively, the formation of which is dominated by electrostatic and hydrophobic interactions. Moreover, BBR-GA NPs could lead to mitochondria-mediated cell apoptosis by regulating mitochondrial fission and dysfunction, while BBR-ART NPs induced ferroptosis in tumor cells. BBR-based NPs have been demonstrated to possess significant tumor targeting and enhanced antitumor properties compared with those of simple monomer mixes both *in vitro* and *in vivo*. These carrier-free self-assemblies based on natural products provide a strategy for synergistic drug delivery and thus offer broad prospects for developing enhanced antitumor drugs.

KEYWORDS

carrier-free self-assemblies, natural products, synergistic antitumor, mitochondria-mediated, enhanced efficiency

1 Introduction

The incidence and mortality of cancer are increasing, annually worldwide, which suggests that cancer is a risk factor affecting human health (Hanahan, 2022; Siegel et al., 2023). Cancer treatment includes surgery, chemotherapy, radiation therapy, and immunotherapy, while chemotherapy remains the primary treatment in the early and postoperative stages. However, chemotherapy can cause serious adverse reactions in patients, and long-term use of chemical drugs can also lead to problems such as reduced drug sensitivity and resistance (Bagchi et al., 2021). Therefore, developing new antitumor drugs is still a crucial challenge. Natural medicinal plants have positive effects on postoperative adjunctive therapy for certain cancers and are a source of potential antitumor

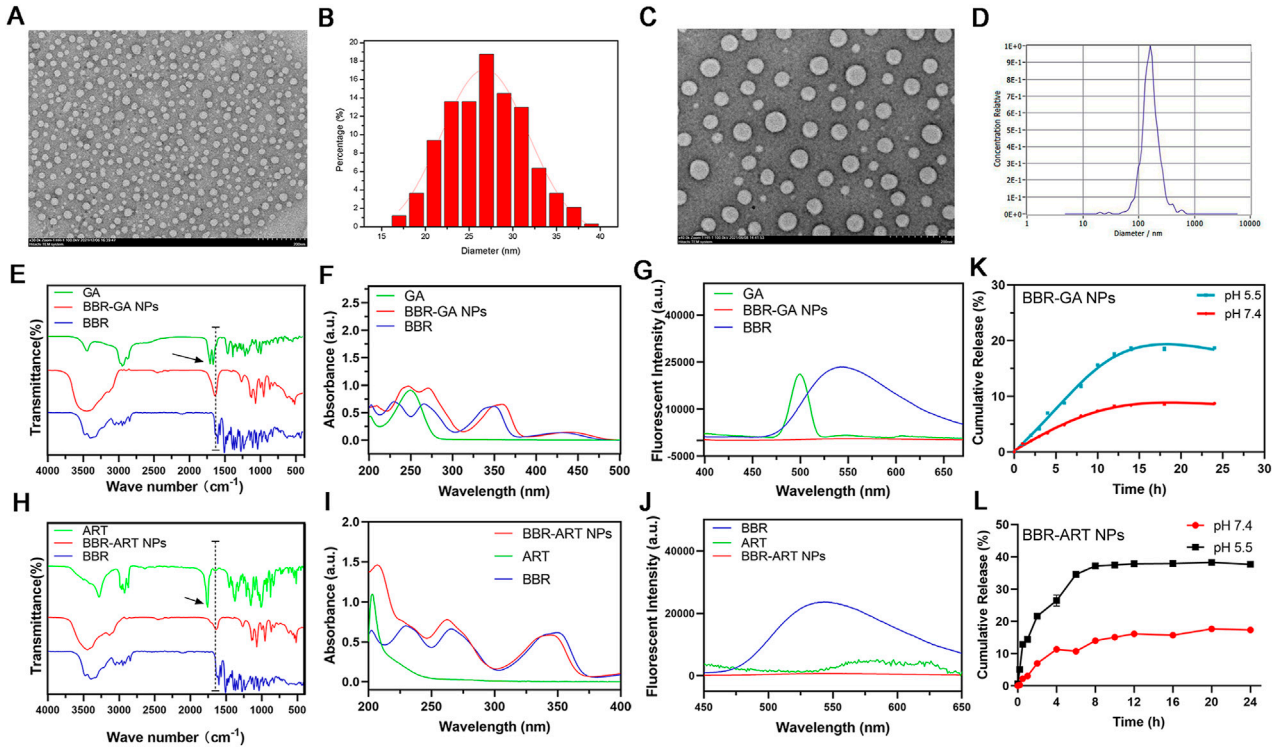

FIGURE 1
Characterization of BBR-based NPs. **(A)** TEM images of BBR-GA NPs. **(B)** The size distribution of BBR-GA NPs as determined by TEM images. **(C)** TEM images of BBR-ART NPs. **(D)** Size distribution of BBR-ART NPs in aqueous solution. **(E)** IR, **(F)** UV–vis, and **(G)** emission spectra of BBR-GA NPs and their monomers. **(H)** IR, **(I)** UV–vis, and **(J)** emission spectra of BBR-ART NPs and their monomers. *In vitro* BBR release from BBR-GA **(K)** and BBR-ART NPs **(L)**. Data are presented as the mean ± SD, $n = 3$.

drugs (Islam et al., 2022; Li et al., 2022). In particular, traditional Chinese medicine has made great contributions to the health of people worldwide for thousands of years. Among the 247 anticancer drugs approved by the U.S. Food and Drug Administration between 1981 and 2019, approximately 45% are natural products or natural product derivatives (Newman and Cragg, 2020; Atanasov et al., 2021). Therefore, the use of natural chemical entities with ample structural complexity and scaffold diversity, which are derived from medicinal plants has been, and will continue to be, a prospective method for antitumor drug research.

Various nanocarriers are widely used to load natural molecules to increase therapeutic efficacy and reduce toxicity for the treatment of cancer (Cabral et al., 2020; Ni et al., 2020). Nanotechnology agents, such as liposomes, micelles, carbon materials, and a metal-organic framework, can improve the solubility and prolong the blood circulation time of natural molecules, after which the molecules are actively or passively released into the tumor. However, most nanodrugs face the problems of a low drug loading rate and unsatisfactory drug percolation (Wolfram and Ferrari, 2019). The assembly process of nanodrugs for achieving targeted delivery and targeted drug release is complex and laborious. Therefore, increasing amounts of attention has been given to carrier-free self-assemblies based on pure drugs in the field of nanomedicine development (Huang et al., 2021; Fu et al., 2022; Li et al., 2023). These self-assemblies without any nanocarrier materials are likely formed through electrostatic interactions, hydrophobicity, hydrogen bonding, or π-π stacking. Moreover, carrier-free nanoscale self-assemblies possess a high drug loading capability (even up to 100%), synergistic therapeutic efficacy, and convenient scalable production. The formation of supramolecular structures is facilitated by natural products with unique stereostructures and multiple chiral centers. By transferring and magnifying molecular chirality through self-assembl, natural molecules have been deemed to one of the ideal building blocks for constructing supramolecular nano self-assemblies.

In this work, we successfully prepared two carrier-free self-assemblies, berberine-glycyrrhizic acid nanoparticles (BBR-GA NPs) and berberine-artesunate nanoparticles (BBR-ART NPs), which were used to increase synergistic effects on tumors. BBR (Song et al., 2020) is a famous alkaloid component of *Coptidis rhizoma* and GA (Kowalska and Kalinowska-Lis, 2019) is a representative triterpenoid from *Glycyrrhiza uralensis*. ART (Zhang et al., 2022) is a derivative of artemisinin that is separated from *Artemisia annua*. GA is a pentacyclic triterpene with a rigid hydrophobic skeleton and multiple chiral centers, while ART is a sesquiterpenoid with a flexible alkyl side chain and a rigid hydrophobic skeleton. These special structural properties make it easy for GA and ART to form orderly arranged aggregates with laminar BBR. The diameters of the BBR-ART NPs were larger than those of the BBR-GA NPs, and were dominated by hydrophobic and electrostatic interactions. BBR and GA are released from NPs into the cytosol via the endocytosis of tumor cells, after which BBR

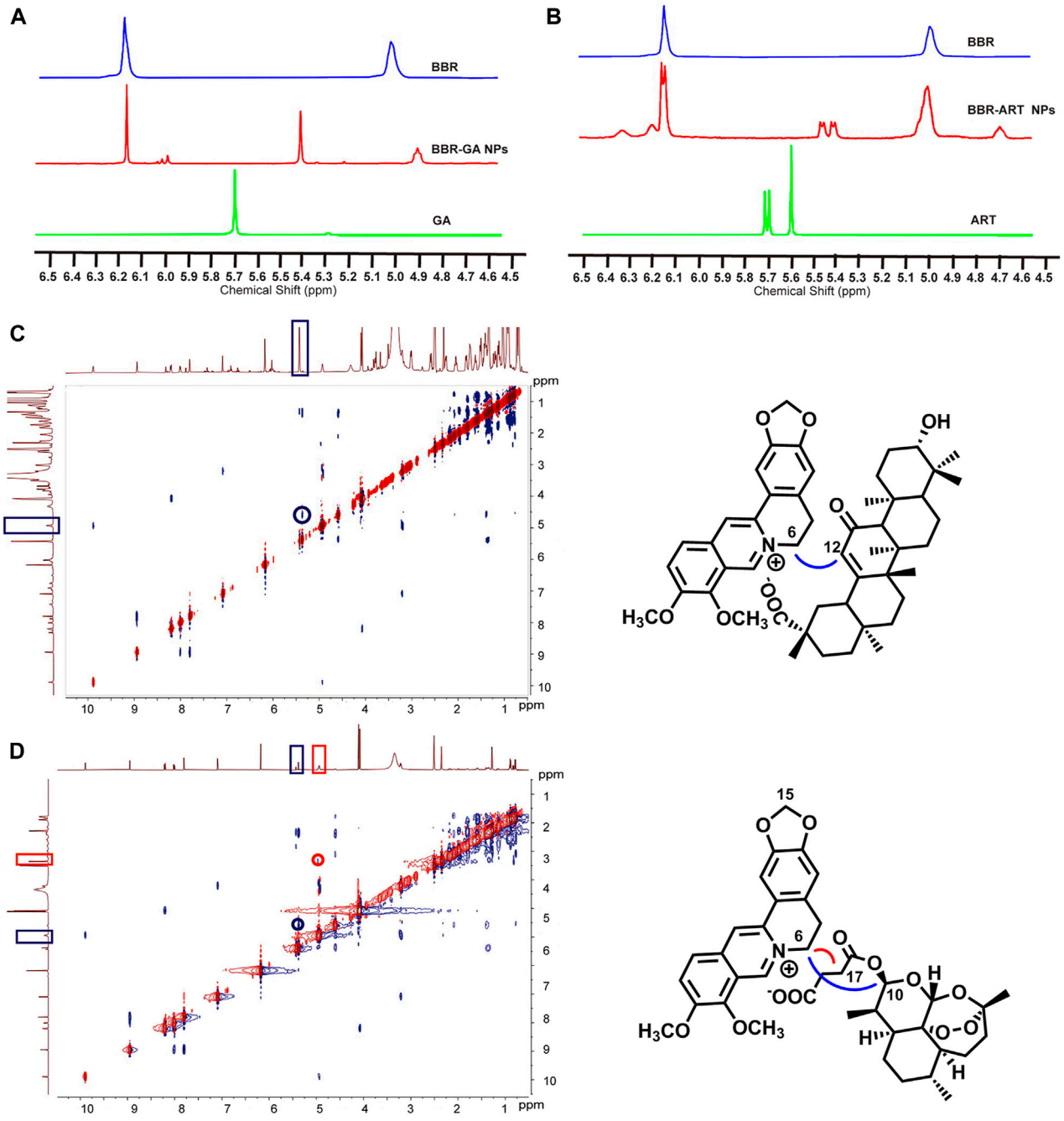

FIGURE 2
Nuclear magnetic resonance spectra of BBR-based NPs. **(A)** ^{1}H NMR spectra of BBR-GA NPs and their monomers (600 MHz, DMSO-d_6). **(B)** ^{1}H NMR spectra of BBR-ART NPs and their monomers (600 MHz, DMSO-d_6). ROESY correlation spectra of BBR-GA **(C)** and BBR-ART NPs **(D)**.

specifically targets mitochondria. After intravenous injection, the assembled BBR-GA NPs may be passively targeted to tumor tissue where they accumulate. BBR-GA NPs could lead to mitochondria-mediated cell apoptosis by regulating mitochondrial fission and dysfunction. In contrast, BBR-ART NPs induced ferroptosis in PANC-1 cells *in vitro* and *in vivo*. BBR-based NPs enabled synergistic antitumor and sensibilized single drug-based antineoplastic effects. This study provides an effective strategy to enhance the antitumor efficacy of carrier-free self-assemblies based on natural products.

2 Materials and methods

2.1 Reagents

BBR, GA, and ART were purchased from Shanghai Aladdin Reagent Co., Ltd., China. An Annexin V-FITC/7ADD apoptosis detection kit, and a bicinchoninic acid protein assay kit were purchased from Jiangsu KeyGen BioTech. Corp., Ltd. (Nanjing, China). DMEM, bovine serum albumin, fetal bovine serum, 2′,7′-dichlorodihydrofluorescein diacetate, BODIPY lipid peroxidation

fluorescent probe, and PBS were purchased from Invitrogen Life Technologies (Carlsbad, USA). Terminal deoxynucleotidyl transferase (TdT)-mediated dUTP nick end labeling apoptosis staining kit and Ki67 cell proliferation detection kit were purchased from Vazyme Biotech, Nanjing, China. Antibodies against FIS1, OPA1, Bcl2, Bax, cleaved caspase 3, xCT, p53, GPX4, HO-1, and GAPDH were purchased from Cell Signaling Technology (Beverly, MA, USA). Other solvents used in this study were of analytical grade, and distilled deionized water was used.

2.2 Preparation and characterization of BBR-based NPs

BBR-based NPs were prepared by simple agitation. Briefly, GA or ART aqueous solutions (0.1 mM) were mixed with hydrochloric acid (BBR) aqueous solution (0.1 mM) in the ratio of 1:1. This mixture was stirred for 12 h at 24°C. The mixture was dialyzed against deionized water for 12 h (M_W = 7,000 Da), after which the unencapsulated GA, ART, and BBR were removed. Then, the obtained BBR-GA NPs or BBR-ART NPs were resuspended in phosphoric acid buffer solution and stored at 4°C.

The morphological characteristics of the BBR-based NPs were determined by HT7700 Transmission Electron Microscopy. A nanoparticle tracking analysis system (Zeta View, Meer Busch, Germany) was used to determine the size of the NPs, and a Zetasizer Nano ZS90 (Malvern, Worcestershire, UK) was used to determine the zeta potential. Ultraviolet–visible (UV–vis, 200–500 nm) and Fourier transform infrared (FT-IR, 4,000 to 400 cm^{-1} with the KBr method) spectra of the samples were obtained by a UV-2450 UV–vis spectrophotometer (Shimadzu, Japan) and a Fourier transform infrared spectrometer (Bruker, Germany), respectively. The fluorescence spectra of the samples were measured on an RF-6000 Spectro fluorophotometer (Shimadzu, Japan) in the range of 400–700 nm. ^{1}H-NMR and ROESY spectra were obtained with a Bruker AVIII-600 NMR spectrometer (^{1}H: 600 MHz) (Bruker, Germany), with tetramethylsilane (TMS) serving as an internal standard. Chemical shift values (δ) are given in parts per million (ppm). The dialysis method was used to investigate the release of BBR from NPs. The NPs (2 mL) were soaked in PBS (35 mL) containing 0.1% tween 80. The NPs in PBS at pH 7.4 or 5.5 were collected at the indicated time points. The release of BBR was analyzed by using a microplate reader (350 nm wavelength), and the release rate was calculated.

2.3 Cellular uptake and subcellular localization of BBR-GA NPs

A549 cells (3×10^3 cells per well) were seeded in glass bottom 96-well plates. When the cells were adherent, they were treated with BBR-GA NPs (at encapsulated BBR concentration of 30 μM) for 0, 1, 2, 4, or 6 h. Cells were cleaned three times. Fluorescence images were captured by using a high-content screening system. To study the subcellular location of BBR-GA NPs, A549 cells (3×10^3 cells per well) were seeded in glass bottom 96-well plates. Cells were treated with NPs (30 μM BBR equiv.) for 2 h or 8 h, after which the cells were washed three times with PBS. Cells were further incubated with 1.0 μM Lyso-Tracker Red or Mito-Tracker for 15 min, and the nuclei were stained with 10 μM DAPI for 15 min. Fluorescence images were taken using an HCS system.

2.4 *In vitro* antitumor efficacy

MTT assays were applied to determine the cytotoxicity of the BBR-based NPs. A549, MCF-7, and PANC-1 cells (3.0×10^3 cells) were seeded in 96-well plates. Cells were incubated with different dosage forms for 24 h. Then, 10 μL of 5 mg mL^{-1} MTT solution in PBS was added to each well. After another 4 h of incubation, 150 μL of DMSO was added to each well to dissolve the generated formazan. After shaking for 15 min, the absorbance of obtained formazan was measured at 570 nm by using a SpectraMax Plus384 microplate reader (Molecular Devices, CA, USA). Clonogenic ability assay was conducted to evaluate the inhibitory effect of BBR-ART NPs on the proliferation of PANC-1 cells. Cells (1.0×10^3 cells per well) were seeded in 6-well plates. Cells were treated with different dosage forms of BBR-ART NPs or 0.1% DMSO for 6 d. The cells in the plates were then stained with crystal violet and imaged. Apoptosis induction by BBR-GA or BBR-ART NPs was measured by using Annexin V-FITC/7ADD double staining assays. A549, MCF-7, or PANC-1 cells (2×10^5 cells per well) were treated with different dosage forms of BBR-based NPs. After another 24 or 48 h of incubation, cells were washed with PBS, digested with trypsin, and stained in binding buffer containing annexin V-FITC and 7ADD for 15 min. Flow cytometry was used to analyze the cells. The mitochondrial membrane potential was measured using a JC-1 assay. After A549 cells were treated with different dosage forms of JC-1, 500 μL JC-1 dye staining solution, was added, and the cells were incubated in the dark at 37°C for 25 min. Cells were washed twice and detected by flow cytometry. Intracellular reactive oxygen species (ROS) production or lipid peroxidation induced by NPs. A549 or PANC-1 cells were cultured with different, treatment regimens and washed with PBS. Then cells were treated with DCFH-DA or BODIP for 30 min at 37°C. Flow cytometry and an HCS system were used to measure the relative ROS or lipid peroxidation levels.

2.5 Western blotting

Western blotting was used to determine the protein expression of FIS1, OPA1, Bcl2, Bax, cleaved caspase 3, xCT, p53, GPX4, and HO-1 in cell lysates. GAPDH was used as the reference protein. Equal amounts of proteins from the total cell lysates were separated via sodium dodecyl sulfate 10% polyacrylamide gel electrophoresis. The proteins were wet-transferred to a polyvinylidene fluoride membrane in the presence of an electric field and blotted with primary antibodies specific for FIS1, OPA1, Bcl2, Bax, cleaved caspase 3, xCT, p53, GPX4, HO-1, and GAPDH, which were used as the internal standards, overnight. Samples were then probed with secondary antibodies for 2 h at 37°C. The prepared

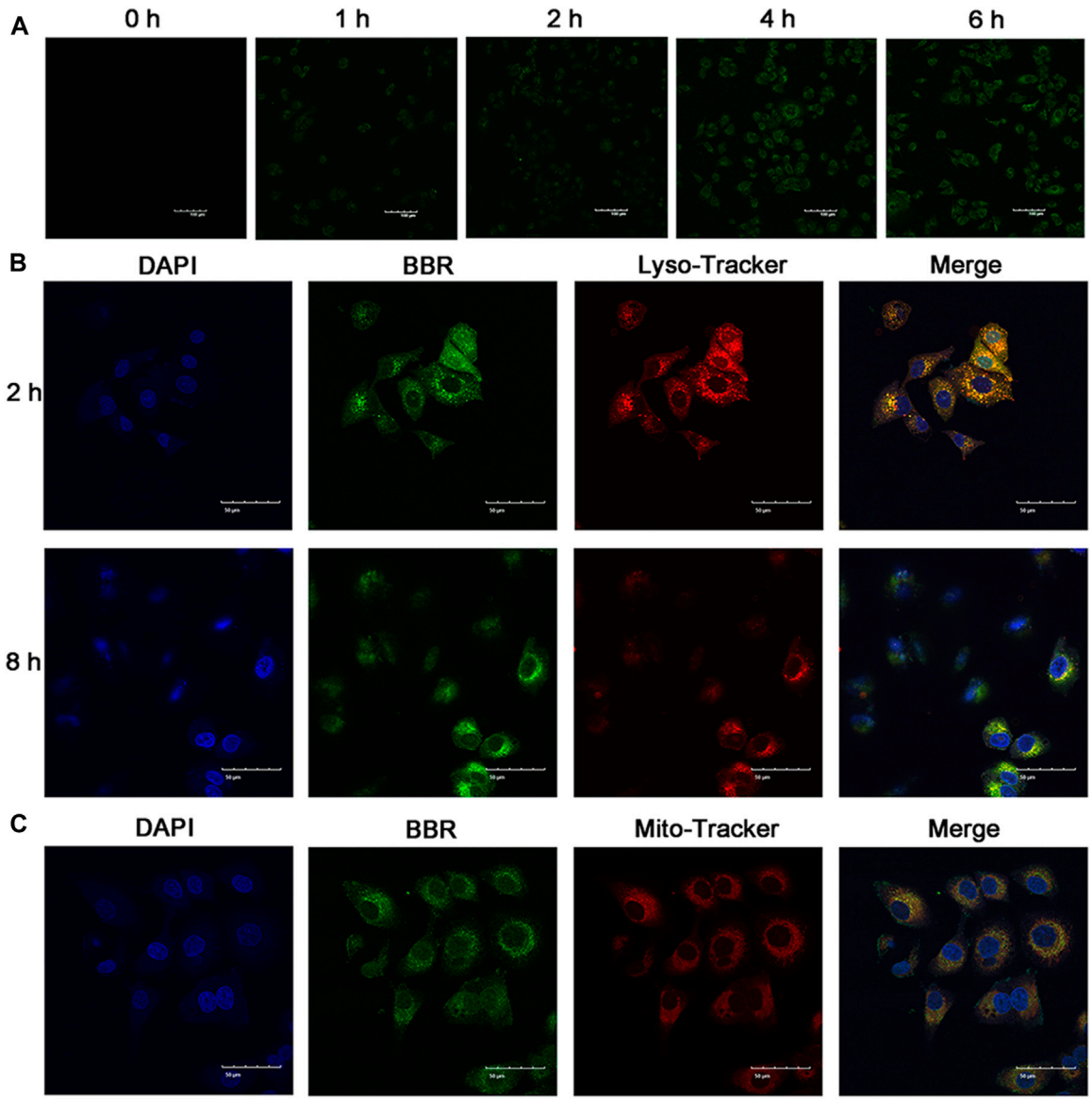

FIGURE 3
Cellular uptake and subcellular distribution *in vitro*. **(A)** Fluorescence images of A549 cells after treatment for 0-6 h with BBR-GA NPs (30 μM BBR equivalent). Scale bar = 100 μm. **(B)** Fluorescence images of BBR-GA NPs with lysosomal localization (30 μM BBR equivalent) in A549 cells after treatment for 2 and 8 h. Scale bar = 50 μm. **(C)** Fluorescence images of BBR-mediated targeting of mitochondria (30 μM BBR equivalent) in A549 cells after treatment for 8 h. Scale bar = 50 μm.

protein samples were tested using the Chemi DOC^{TM} XRS+ system (Bio-Rad Laboratories, Hercules, CA, USA).

2.6 Zebrafish xenograft tumor model

All experiments were approved by the Animal Ethical Committee of China Pharmaceutical University, and the handling procedures were performed on the basis of the National Institutes of Health of Experimental Animals. Wild type zebrafish were purchased from Nanjing Xinjia Medical Technology Co., Ltd. Zebrafish were fed in E3 embryo media at 28°C. A549 cells were incubated with 10 μg mL^{-1} CM-DiI solution (5% DMSO/water) until fluorescence was observed. The labeled cells were microinjected into the yolk space of 48 hpf wild-type zebrafish embryos (400 cells per embryo). Zebrafish xenograft tumor model was established and cultured in a 34°C light incubator (light 14 h, dark 10 h). The tumor-bearing zebrafish were randomly divided into different groups (3 or 6 zebrafish/group). The zebrafish were incubated with BBR + GA or BBR-GA NPs (5 mM BBR equiv.). Fluorescence images were recorded using a fluorescence microscope at 0, 30, and 60 min for detection of tumor targeting. Next, to evaluate anti-tumor efficacy of BBR-GA NPs, tumor-bearing zebrafish were incubated with PBS, BBR + GA, or BBR-GA NPs (5 mM BBR equiv.). Fluorescence images were recorded using a fluorescence

10.3389/fphar.2024.1333087

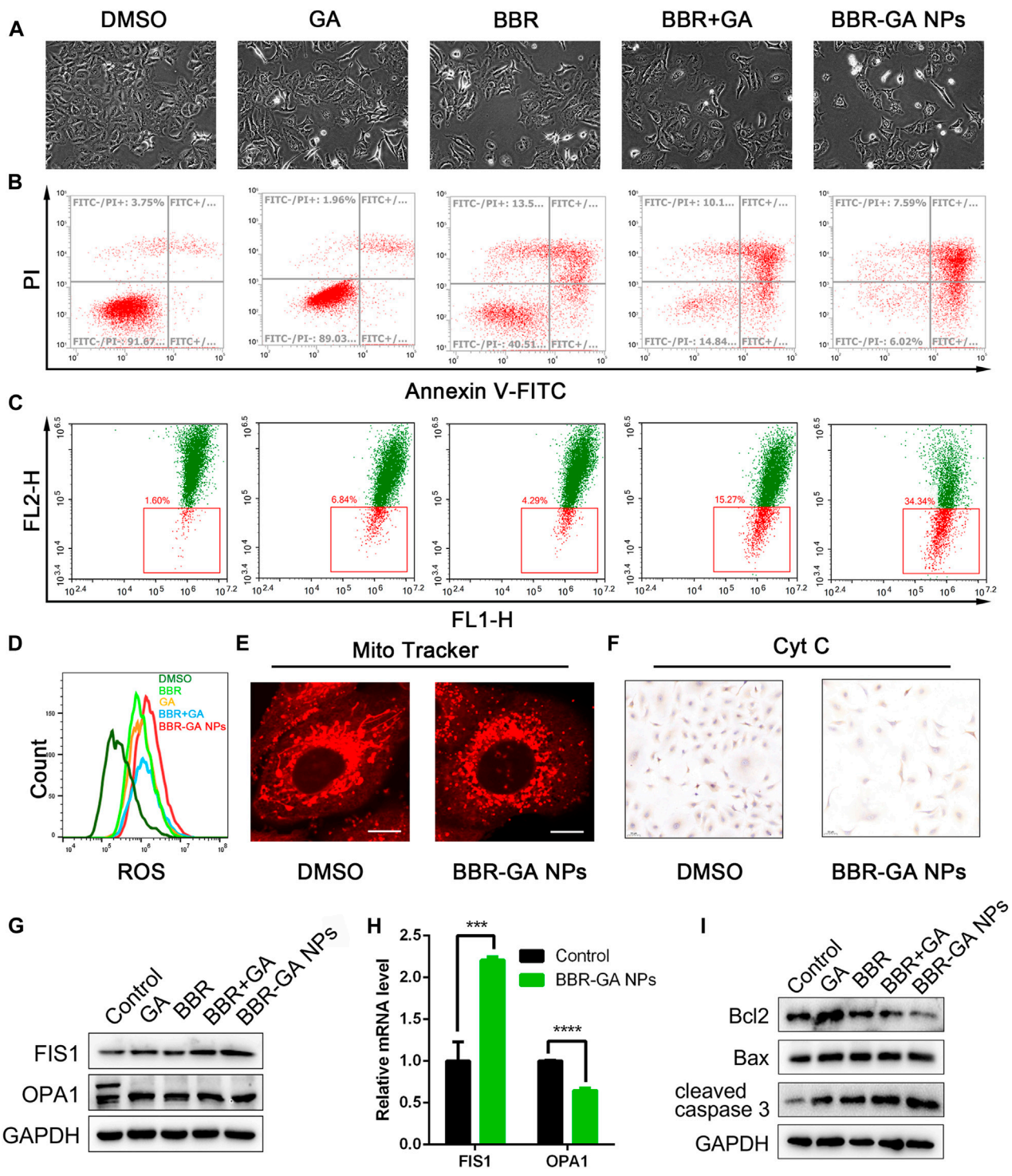

FIGURE 4
In vitro proapoptotic activity of BBR-GA NPs. **(A)** Cellular morphology of A549 cells after treatment with various formulations for 48 h. **(B)** Cell apoptosis after treatment with various formulations determined by annexin V-FITC/7ADD staining. **(C)** ΔΨm of A549 cells after incubation with various formulations determined by JC-1 staining. **(D)** Analysis of ROS production in A549 cells using flow cytometry. **(E)** Confocal microscopy images of BBR-GA NPs-induced mitochondrial fission as determined via MitoTracker staining. Scale bars: 20 μm. **(F)** Immunohistochemical staining images of cytochrome c translocated from mitochondria to cytosol in A549 cells after treatment with BBR-GA NPs. **(G)** The expression of FIS1 and OPA1 in A549 cells after treatment with various formulations was determined by Western blot analysis. **(H)** Relative mRNA levels of FIS1 and OPA1 in A549 cells after treatment with BBR-GA NPs determined by Q-PCR analysis. **(I)** The expression of Bcl2, Bax, and cleaved caspase 3 in A549 cells after treatment with various formulations by Western blot analysis.

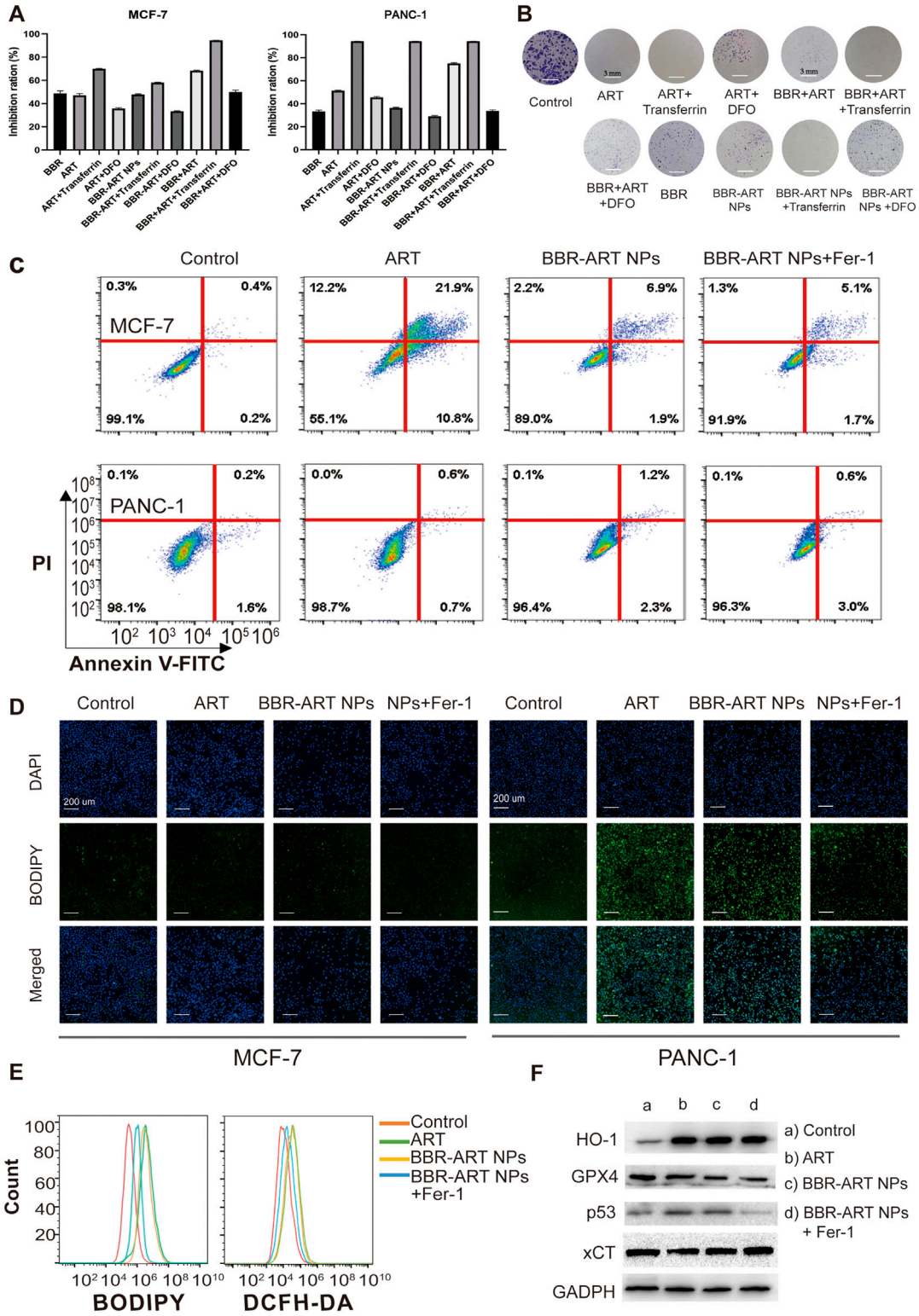

FIGURE 5
In vitro pro-ferroptosis activity of BBR-ART NPs. **(A)** MTT analysis of MCF-7 and PANC-1 cells after exposure to various formulations. The data are presented as the mean ± SD, $n = 3$. **(B)** The clonogenic ability of PANC-1 cells after treatment with various formulations. **(C)** The apoptotic rate of MCF-7 and PANC-1 cells after treatment with various formulations for 24 h determined by annexin V-FITC/7ADD staining. **(D)** Fluorescence microscopic images of lipid ROS in MCF-7 and PANC-1 cells after BODIPY staining. Scale bar = 200 μm. **(E)** Analysis of lipid ROS levels in PANC-1 cells by BODIPY staining and total ROS levels by DCFH-DA staining. **(F)** The expression of HO-1, GPX4, p53, and xCT in PANC-1 cells was determined by Western blot analysis.

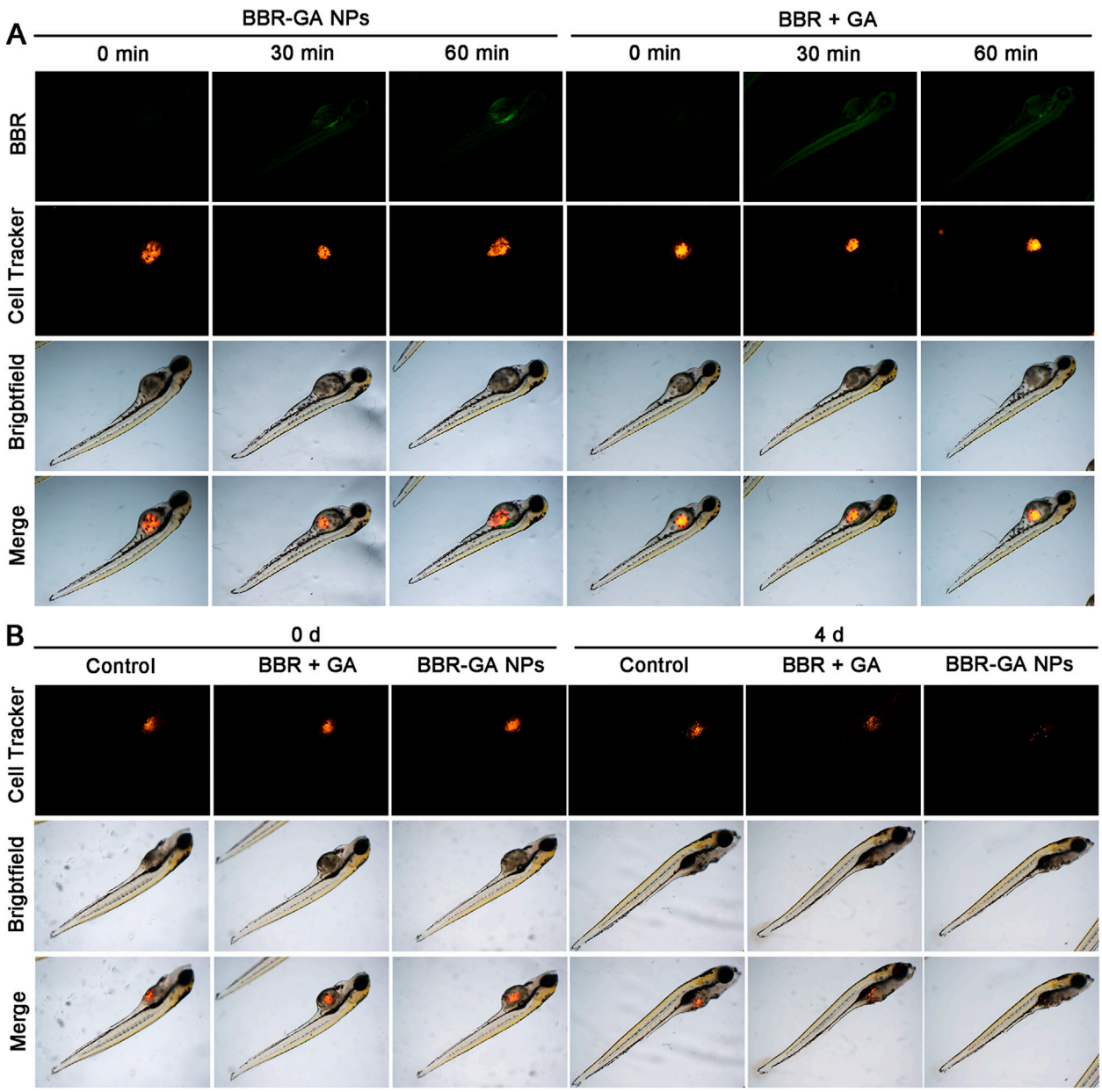

FIGURE 6
In vivo biodistribution and therapeutic efficacy of BBR-GA NPs in A549 tumor-bearing zebrafish. **(A)** Fluorescence images of zebrafish at 0, 30 and 60 min after treatment with BBR-GA NPs or BBR + GA. **(B)** Fluorescence images of zebrafish at 0 and 4 days after treatment with BBR-GA NPs or BBR + GA.

microscope at 0 and 4 days for determination of antitumor effects.

2.7 *In vivo* antitumor efficacy and safety

Five-week-old BALB/c nude mice (GemPharmatech Co., Ltd, Nanjing, China) were selected and injected with A549 or PANC-1 cells (4.0×10^7 cells per mouse) into the right lower limb region. When the tumors reached a size of 100 mm^3, the tumor-bearing mice were randomly divided into different groups (7 mice/group). Then, the mice were intravenously administered different dosage forms every 2 days. Throughout the experiments, the bodies of the mice were observed. Tumor volume (mm^3) was measured using calipers every 2 days and the tumor volume was calculated with the following formula (length × $width^2$ × 0.5). After 14 days of treatment, the mice were euthanized and sacrificed, and the tumor tissues and major organs were harvested for hematoxylin and eosin (H&E) staining, TUNEL assays and immunohistochemical assays. To evaluate the safety of BBR-based NPs *in vivo*, the serum levels of blood urea nitrogen (BUN), creatinine (CRE), aspartate transaminase (AST), alanine

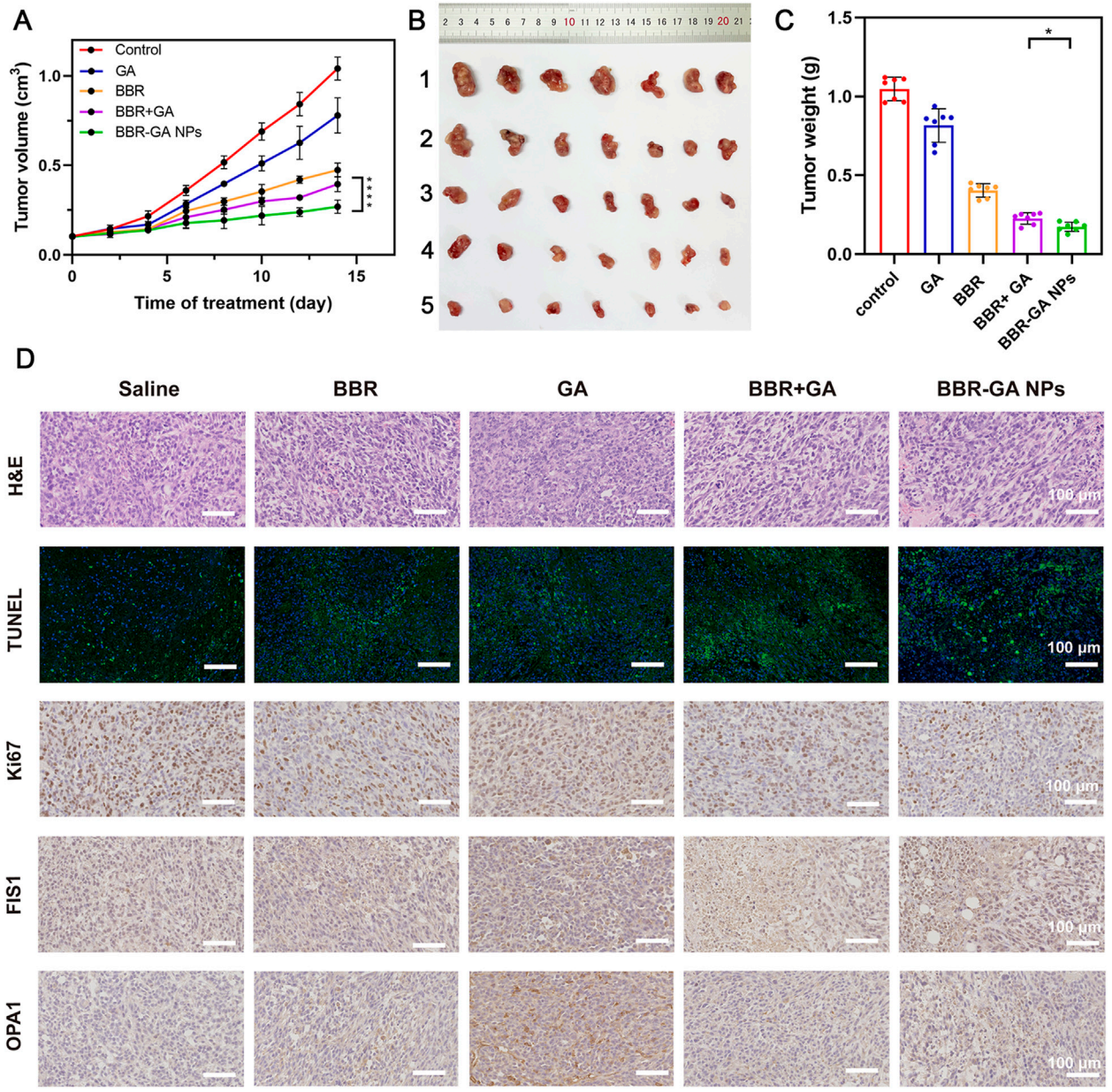

FIGURE 7
Therapeutic efficacy of BBR-GA NPs in tumor-bearing nude mice *in vivo*. **(A)** Tumor growth curves over 14 days (n = 7). ****p < 0.0001. **(B)** Photographs of tumor tissues excised on Day 14. 1: Control; 2: GA; 3: BBR; 4: BBR + GA; 5: BBR-GA NPs. **(C)** Weights of tumor tissues excised on Day 14 (n = 7). *p < 0.05. **(D)** Images of H&E staining, TUNEL staining, Ki67, FIS1, and OPA1 staining in tumor slices after treatment.

transaminase (ALT) were measured by using the corresponding assay kits (KeyGen, China).

2.8 Statistical analysis

All experiments were repeated at least in triplicate and the data are expressed as the mean ± standard deviation (SD). Results were analyzed by one-way analysis of variance (ANOVA) using GraphPad Prism 6.0 (GraphPad Inc., San Diego, CA). A p-value less than 0.05 was considered to indicate a significant difference. *p < 0.05, **p < 0.01, ***p < 0.001, and ****p < 0.0001 were considered to indicate statistical significance.

3 Results and discussion

3.1 Preparation and characterization of BBR-GA and BBR-ART NPs

BBR and GA/ART could self-assemble into NPs in aqueous solution. Several characteristic constants of the self-assemblies were

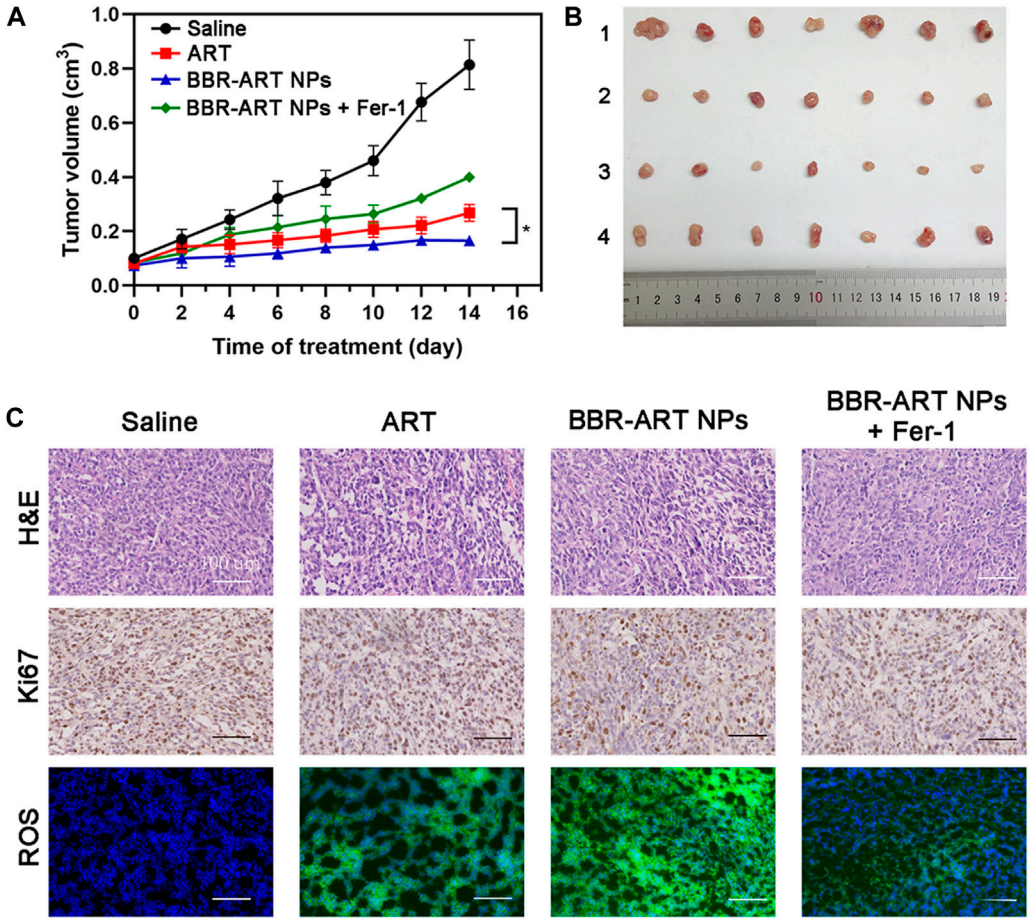

FIGURE 8
Therapeutic efficacy of BBR-ART NPs in PANC-1 tumor-bearing nude mice *in vivo*. **(A)** Tumor growth curves over 14 days (n = 7). *p < 0.05. **(B)** Photographs of tumor tissues excised on Day 14. 1: Control; 2: ART; 3: BBR-ART NPs; 4: BBR-ART NPs + Fer-1; **(C)** Images of H&E staining, TUNEL staining, Ki67, and ROS degree in tumor slices after treatments.

examined. TEM (Figures 1A, B) revealed that the morphology of BBR-GA was uniform, and the particle size was approximately 26.5 nm. The self-assembled form of the BBR-ART system was similar to that of BBR-GA NPs. These NPs were approximately 137.9 nm in diameter, which waw larger than that of the BBR-GA NPs (Figures 1C, D). The zeta potentials of BBR-GA NPs and BBR-ART NPs were −24.5 ± 1.1 and −18.4 ± 1.0 mV (Supplementary Figure S1). Moreover, all of the BBR-GA NPs and BBR-ART NPs exhibited the Tyndall effect in aqueous solution (Supplementary Figure S2). The stability of BBR-GA NPs and BBR-ART NPs in physiological condition (Supplementary Figure S3). Next, IR, UV, and fluorescence emission spectra were used to measure the spectroscopic properties of BBR-based self-assemblies. In IR spectroscopy, GA showed strong absorption peaks at 1706 and 1,664 cm^{-1} (corresponding to the C=O stretching peaks of GA, Figure 1E). However, these peaks became single peak that shifted to a lower wavenumber (1,640 cm^{-1}) in the BBR-GA NPs. BBR-ART NPs exihibited the same IR spectroscopic properties (Figure 1H). This result indicated that electrostatic interactions formed between the carboxyl group of GA/ART and ammonium ion of BBR. The UV–vis spectrum (Figure 1F) of BBR-GA NPs contained three typical absorption bands for GA and BBR (228, 262, and 344 nm). Similar to BBR-GA NPs, BBR-ART also exhibited three typical absorption bands (209, 260, and 347 nm), which are signals of ART and BBR, respectively (Figure 1I). BBR-based NPs exhibited the characteristic UV peaks of their monomers. Furthermore, the fluorescence characteristics of the BBR-based NPs were studied. BBR emitted obvious fluorescence at 550 nm (Figures 1G, J). After being assembled, NPs showed no significant fluorescence absorption. This difference might be due to fluorescence quenching resulting from the energy transfer effect after self-assembly. The *in vitro* profiles of BBR released from NPs in pH 5.5 and pH 7.4 solutions were generated based on incubation times (Figures 1K, L). NPs displayed a higher BBR release rate at pH 5.5 than at pH 7.4, indicating that BBR was released from NPs to a greater extent in an acidic microenvironment than in a neutral environment.

Moreover, ^{1}H-NMR and ROESY spectra were also obtained to confirm the formation of self-assembled BBR-based NPs. For BBR-GA NPs, the chemical shift of H-6 in BBR decreased from 5.02 to 4.93 ppm, while the chemical shift of H-12 of GA decreased from 5.77 to 5.43 ppm (Figure 2A). Correspondingly, the ROESY spectrum of BBR-GA NPs showed strong interactions between

H-6 of BBR and H-12 of GA (Figure 2C), which suggests that the distances between these two hydrogen atoms were closer to each other (less than 5 Å). Combined with the previous IR spectra of BBR-GA NPs, these results further confirmed that the formation of self-assembled NPs was driven by electrostatic interactions between carboxyl group of GA and ammonium ion of BBR. For the BBR-ART NPs, the chemical shift of H-15 of BBR did not change, while the peak shape of these hydrogen atoms changed from singlet to doublet (Figure 2B). The chemical shift of H-17 in ART decreased from 5.61 to 4.75 ppm, while the chemical shift of H-10 in ART decreased from 5.71 to 5.43 ppm. Observably, the peak shape of H-10 for ART changed from a doublet to a double doublet. Next, in the ROESY spectrum of BBR-ART NPs, strong interactions between H-6 of BBR and H-12/-10 of ART were observed (Figure 2D). Overall, electrostatic interactions drove the formation of a one-dimensional BBR-based complex: a parallel conformation between BBR and GA, and a staggered conformation between BBR and ART. Then, hydrophobic interactions drove the formation of three-dimensional BBR-based NPs. The formation processes of these two BBR-based NPs were different. Previous results in which the diameters of BBR-ART NPs were larger than those of the BBR-GA NPs might confirm these findings. In conclusion, BBR-based NPs were validated to be self-assembled nanoplatforms in various assays.

3.2 Cellular uptake and intracellular localization of BBR-GA NPs *in vitro*

Cellular uptake of NPs has a significant influence on their antitumor effect. Thus, to investigate the cellular uptake of BBR-GA NPs, human A549 lung cancer cells were used as a cell model. To study the cellular uptake of BBR-GA NPs, A549 cells were incubated with NPs, and the fluorescence intensity of BBR (green) was used to determine the quantity of BBR-GA NPs taken up. The green fluorescence intensity increased over time within 6 hours (Figure 3A). After endocytosis, the subcellular localization of the BBR-GA NPs was analyzed. To explore the mitochondrial targeting of BBR after the lysosomal capture of BBR-GA NPs in A549 cells, fluorescence imaging assays were performed. The number of lysosomes was determined using LysoTracker. BBR (green fluorescence) was clearly visualized after 2 h (Figure 3B). Orange fluorescence which was green (BBR) combined with red (lysosome) fluorescence, indicated that BBR-GA NPs were trapped by lysosomes. After 8 h of incubation, weak orange fluorescence demonstrated that BBR-GA NPs had escaped from lysosomes. After lysosomal escape, BBR was proven to target mitochondria. DAPI (blue) was used for nuclear staining and Mito-Tracker Red was used for mitochondrial staining. The bright orange fluorescence (Figure 3C) indicated the mitochondrial targeting of BBR. There was a negative large transmembrane potential in the mitochondria, which might drive the positively charged BBR to the mitochondria. Therefore, BBR-GA NPs were endocytosed into tumor cells where they rapidly released BBR and GA after lysosomal escape. Then, BBR targets mitochondria and GA is exposed to the cytoplasm.

3.3 *In vitro* antitumor effects of BBR-based NPs

To explore the cytotoxicity of the BBR-GA self-assemblies, MTT assays were used with A549 cells. The IC_{50} value of BBR-GA NPs was 60.5 ± 0.13 μM (Supplementary Figure S4). BBR-GA NPs at high concentrations (>50 μM) had higher cytotoxic activity than the GA, BBR, or BBR + GA groups. In contrast, the IC_{50} value was lower when human lung bronchial epithelial BEAS-2B cells were treated with BBR-GA NPs (IC_{50} > 100 μM), indicating that self-assemblies produced stronger toxicity particularly in tumor cells. Compared to those in the other groups, BBR-GA NPs caused the cells to become shrunken and sparse (Figure 4A). Similar results were obtained for the apoptosis-inducing effect. The total apoptosis rate induced in the BBR-GA NPs group was 86.4%, which was higher than that in the BBR + GA group (11.3%), BBR group (40.4%), and GA group (77.4%) (Figure 4B; Supplementary Figure S4). Mitochondria-mediated apoptosis is regarded as the major mode of cell death in cancer therapy (Harrington et al., 2023; Peng et al., 2023), and is characterized by a decrease in the mitochondrial membrane potential (ΔΨm), triggering the production of ROS and the release of proapoptotic factors (such as caspase-3). The ability of BBR-GA NPs to reduce the ΔΨm was measured in A549 cells by using the lipophilic dye JC-1. The ΔΨm of cells in all the administration groups was reduced, compared with that of cells in the control group, and BBR-GA NPs were the most effective decreasing the ΔΨm to 65.7% (Figure 4C; Supplementary Figure S4). Next, the cell-permeable fluorophore DCFH-DA was used to assess the production of intracellular ROS. The ROS levels in the BBR-GA group were 1.5, 1.3, and 1.1 times higher than those in GA, BBR, and BBR + GA groups, respectively (Figure 4D; Supplementary Figure S5). Next, MitoTracker Red staining demonstrated that mitochondria of A549 cells showed obvious morphological changes from an oval shape to a truncated and fragmented shape following BBR-GA NPs treatment (Figure 4E). The above results suggested mitochondrial dysfunction could trigger the release of cytochrome c from mitochondria to cytoplasm. BBR-GA NPs significantly reduced the release of cytochrome c by means of streptavidin-peroxidase immunohistochemistry (Figure 4F). Next, Western blotting and Q-PCR were used to evaluate the balance of mitochondrial dynamics. Mitochondria undergo fission when cells are under metabolic or environmental stress (Kraus et al., 2021). Fission 1 (FIS1) is a mitochondrial fission-associated factor, while optic atrophy 1 (OPA1) is related to mitochondrial fusion (Rodrigues and Ferraz, 2020). The expression of FIS1 increased in BBR-GA NPs-treated cells (Figures 4G, H; Supplementary Figure S6). The ratio of L-OPA1 (long isoform of OPA1) to S-OPA1 (short isoform of OPA1) in cells dramatically decreased upon treatment with BBR-GA NPs. Moreover, the ratio of Bax (proapoptotic protein) to Bcl-2 (anti-apoptotic protein), which can initiate the cascade of caspases (Walensky, 2019), was further measured. Similarly, the Bax/Bcl-2 ratios in the BBR-GA NPs group were 1.4-fold, 1.6-fold, and 3.0-fold higher than those in the BBR + GA, BBR, and GA groups, respectively (Figure 4I; Supplementary Figure S7). Consistently, BBR-GA NPs group enhanced cleaved caspase-3 activity by 1.1-fold, 1.4-fold, and 2.0-fold compared to that in the BBR + GA, BBR, and GA groups, respectively. Collectively, BBR-GA NPs reduced imbalance of mitochondrial dynamics to promote

mitochondrial fission, thereby leading to mitochondria-mediated cell apoptosis.

Ferroptosis is a type of cell death characterized by the accumulation of lipid peroxidation products and iron, and is different from apoptosis, autophagy, and cell necrosis (Lei et al., 2022; Liang et al., 2022). Artemisinin derivatives can induce ferroptosis in the treatment of cancer (Zhu et al., 2020; Hu et al., 2022). BBR-ART NPs (50 μM BBR equiv.) induced approximately 36.5% cell death in PANC-1 cells (Figure 5A). Increasing lysosomal free iron by cotreatment with iron-saturated, diferric holo-transferrin significantly increased cell death (94.2%). However, coaddition of the lysosomal iron chelator deferoxamine mesylate (DFO) blocked cell death (29.1%), indicating that BBR-ART NPs-induced ferroptosis in PANC-1 cells. Control MCF-7 cells were insensitive to all conditions. Colony formation assays were subsequently performed to determine the effects of BBR-ART NPs on proliferation. BBR-ART NPs reduced clonogenic growth of PANC-1 cells after 6 days of treatment (Figure 5B; Supplementary Figure S8). Consistent with MTT results, the clonogenic growth of cells was amplified by cotreatment with transferrin and rescued by coaddition of DFO. Annexin V-FITC/PI apoptosis detection showed BBR-ART NPs and BBR-ART NPs + Fer-1 groups (ferrostatin-1, a ferroptosis inhibitor) exhibited very little apoptosis in PANC-1 cells compared with MCF-7 cells (Figure 5C), further highlighting the effect of NPs-mediated ferroptosis in PANC-1 cells. Iron-dependent ROS generation during ferroptosis is the central stressor for cellular death (Wang Y. et al., 2021). A BODIPY probe was used to measure intracellular lipid peroxidation. Green fluorescence (with oxidized BODIPY) was clearly observed in PANC-1 cells compared to MCF-7 cells (Figure 5D). The fluorescence intensities of BBR-ART NPs in PANC-1 cells were approximately 1.2 and 2.0 times higher than those in the ART and BBR-ART NPs + Fer-1 groups, respectively (Supplementary Figure S9). Fer-1 was shown to inhibit lipid peroxidation during ferroptotic cell death. Similarly, flow cytometry yielded similar (Figure 5E; Supplementary Figure S10). Next, Western blot analysis was used to evaluate the expression of ferroptosis-related factors: heme oxygenase-1 (HO-1, which catalyzes the catabolism of heme to ferrous) and glutathione peroxidase 4 (GPX4, a negative regulator). HO-1 expression increased and GPX4 expression decreased in response to BBR-ART NPs treatment (Figure 5F; Supplementary Figure S11), indicating activation of ferroptosis. Moreover, BBR-ART NPs could also decrease the expression of xCT and increase the expression of p53. In general, BBR-ART NPs exhibited antitumor activity in PANC-1 cells by inducing ferroptosis.

3.4 *In vivo* antitumor effects of BBR-based NPs

As expected, BBR-based NPs showed more favorable tumor targeting than the other monomers due to the enhanced permeability and retention (EPR) effect. BBR fluorescence can be used to detect the biodistribution of BBR-GA NPs in A549 tumor-bearing zebrafish. Zebrafish (Astell and Sieger, 2020) are becoming a suitable model for testing tumor targeting of NPs because of the transparency of zebrafish embryos, which enables the visualization of fluorescently labeled cancer cells and NPs through their body wall in real time. In addition, zebrafishes exhibit 87% homology with the human genome (Wang X. et al., 2021; Wu et al., 2021), which can be used to characterize the anticancer effects of NPs. A xenograft model was established by microinjecting Cell-Tracker™ CM-Dil labeled A549 cells into the yolk sacs of zebrafish embryos. BBR signals (green) of BBR + GA group were clearly observed in zebrafish after 30 min of treatment and the green fluorescence intensity was always distributed throughout the body at 60 min (Figure 6A). However, BBR-GA group showed obvious drug accumulation at the tumor site, with green fluorescence approaching the yolk sacs of zebrafish at the treatment time. These data supported the ability of BBR-GA NPs to target tumors *in vivo*. Next, the *in vivo* antitumor activity of BBR-GA NPs was studied in A549 tumor-bearing zebrafish. After 4 days of treatment, BBR-GA NPs and BBR + GA groups all exhibited reduced fluorescence intensity in the zebrafish (Figure 6B). Similarly, compared with those in the control group, the tumor inhibition rates in the BBR-GA NPs and BBR + GA groups were 86.4% and 69.6%, respectively (Supplementary Figure S12). BBR-GA NPs inhibited tumor growth more than the simple monomer mixture in zebrafish model.

After verifying their outstanding tumor targeting efficiency in a zebrafish model, the antitumor efficacy of BBR-based NPs was tested in tumor cell-bearing nude mice. *In vivo* antitumor therapy with BBR-GA NPs was investigated in A549 cell-bearing BALB/c nude mice when the tumor size reached 100 mm^3. The mice were randomly allocated into five groups and intravenously injected with saline, GA, BBR, BBR + GA, or BBR-GA NPs. During treatment, the tumor volume was recorded. The mice treated with BBR-GA NPs exhibited better inhibition of tumor growth than the GA, BBR, and BBR + GA groups throughout the treatment period (Figure 7A). Tissues were harvested after mice were sacrificed. Treatment with BBR-GA NPs resulted in significant inhibition of tumor growth compared to that of the other treatments (Figure 7B). Notably, BBR-GA NPs had a better inhibitory effect than simple monomer mixture. On Day 14 of treatment, the tumor weights of the BBR-GA NPs group were 0.1-, 0.2-, 0.5- and 0.8-fold lower than those of saline, GA, BBR, and BBR + GA groups, respectively (Figure 7C), and the tumor inhibition rates of BBR-GA NPs, BBR + GA, BBR, and GA groups were 72%, 61%, 53%, and 22%, respectively (Supplementary Figure S13). Next, histological assessments of tissues were performed via H&E staining. The different treatment groups exhibited more loosely packed cells and various degrees of necrosis in tumor tissue sections (Figure 7D). For BBR-GA NPs, tumor cells with a high nucleus-to-plasma ratio exhibited diffuse distribution. The nuclei were heteromorphic and cell boundaries were blurry. Tumor cells exhibited necrosis/apoptosis, and the tumor cell death rate was about 60%. In addition, to confirm the inhibition of apoptosis and cell proliferation, TUNEL and Ki-67 immunohistochemistry were used to evaluate the number of apoptotic cells and proliferating cells in tumor tissue sections. The apoptosis rate of the BBR-GA NPs group was 48.0% as compared with the control group. The apoptosis rates of GA, BBR, and BBR + GA groups were 0.30, 0.2, and 0.6 times lower than that of BBR-GA group. Similarly, the number of Ki-67-positive tumor cells in BBR-GA NPs group were 0.4, 0.6, and 0.7 times lower

than that in GA, BBR, and BBR + GA groups, respectively. Next, the expression of two key proteins that regulate mitochondrial homeostasis in tumor tissue were also investigated. Compared to other administration groups, FIS1 and OPA1 in BBR-GA NPs group were obviously highly expressed and expressed at low levels, respectively. In addition to the therapeutic effects, the safety of BBR-GA NPs was also evaluated. The body weights of the mice in all groups increased with no significant differences among groups (Supplementary Figure S14). H&E staining revealed that the cells in main organs exhibited no serious damage among the groups (Supplementary Figure S15). Furthermore, BBR-GA NPs did not induce hepatic or kidney toxicity (Supplementary Figure S16).

Moreover, *in vivo* antitumor effects of BBR-ART NPs were studied in PANC-1 cell-bearing BALB/c nude mice. The mice were randomly allocated to four groups, and the mice were intravenously injected with saline, ART, BBR-ART NPs, or BBR-ART NPs + Fer-1. BBR-ART NPs-treated group exhibited the lowest tumor volume among all the groups during treatment (Figures 8A, B). Similarly, BBR-ART NPs administration group had the lowest tumor weight among all the groups. The average tumor inhibition rates of ART, BBR-ART NPs, and BBR-ART NPs + Fer-1 groups were approximately 69%, 80%, and 51%, respectively, after 14 days treatment (Supplementary Figure S17). As expected, the addition of Fer-1, a ferroptosis inhibitor, hindered the antitumor efficacy of the BBR-ART NPs. H&E staining was further used to analyze the tumor tissues. BBR-ART NPs produced more loosely packed cells and led to the highest amount of tumor cell death (Figure 8C). Ki-67 immunohistochemistry showed cell proliferation in tumor tissues of the BBR-ART NPs, BBR-ART NPs + Fer-1, and ART groups were 0.3, 0.6, and 0.5 times higher than that of in control group. In addition, compared with those in the PBS group, the BBR-ART NPs group exhibited the maximum ROS level (88.50%). The above research results proved the efficient *in vivo* antitumor activity of BBR-ART NPs. The biosafety of BBR-ART NPs was also evaluated. The body weight of each group showed slight increase, and the difference between groups could be ignored (Supplementary Figure S18). According to the H&E staining results, no serious damage was observed in the main organs among the four groups (Supplementary Figure S19). In addition, compared with those in the control group, BBR-ART NPs did not induce obvious hepatic or kidney toxicity, for example, the blood BUN/CRE (a kidney function marker) and GOT/GPT (liver function marker) levels were normal (Supplementary Figure S20). These results suggested that BBR-ART NPs had good biosafety and did not induce severe systemic toxicity. Thus, BBR-based NPs were proven to have a satisfactory safety profile for synergistic drug delivery and enhanced antitumor efficacy *in vivo*.

4 Conclusion

In summary, we developed a carrier-free BBR-based nanoplatform for synergistic tumor treatment. Specifically, BBR can interact with GA or ART to self-assemble BBR-GA or BBR-ART NPs, respectively. The formation of carrier-free self-assemblies were mainly governed by electrostatic and hydrophobic interactions. The diameters of the BBR-ART NPs were larger than those of the BBR-GA NPs indicating different formation processes for these two BBR-based NPs: the parallel conformation between BBR and GA, and the staggered conformation between BBR and ART. After intravenous injection, the assembled BBR-GA NPs accumulated at tumor sites owing to passive targeting effect (EPR). BBR and GA were released into cytosol, after which BBR specially targets the mitochondria in tumor cells. BBR-GA NPs could lead to mitochondria-mediated cell apoptosis by regulating mitochondrial fission and dysfunction. Moreover, *in vivo* and *in vitro* trials showed that BBR-ART NPs could induce ferroptosis in PANC-1 cells. Therefore, BBR-based NPs enabled synergistic antitumor and sensibilized single drug-based antineoplastic effect. These carrier-free self-assemblies based on natural products provide a strategy for synergistic drug delivery and thus offer broad prospects for developing enhanced antitumor drugs. The synergistic strategy we constructed is a promising candidate for clinical application in the treatment of tumors in the future.

Data availability statement

The original contributions presented in the study are included in the article/Supplementary Material, further inquiries can be directed to the corresponding authors.

Ethics statement

The animal studies were approved by Animal Ethics Committee of China Pharmaceutical University. The studies were conducted in accordance with the local legislation and institutional requirements. Written informed consent was obtained from the owners for the participation of their animals in this study.

Author contributions

YW: Formal Analysis, Methodology, Visualization, Writing–original draft. ZL: Formal Analysis, Methodology, Visualization, Writing–original draft. HZ: Formal Analysis, Methodology, Writing–original draft. PW: Formal Analysis, Methodology, Writing–original draft. YZ: Formal Analysis, Methodology, Writing–original draft. RL: Conceptualization, Funding acquisition, Investigation, Supervision, Writing–review and editing. CH: Conceptualization, Funding acquisition, Investigation, Project administration, Supervision, Writing–review and editing. LW: Conceptualization, Funding acquisition, Investigation, Supervision, Writing–review and editing.

Funding

The author(s) declare financial support was received for the research, authorship, and/or publication of this article. This work was co-supported by National Natural Science Foundation of China (82104359), the Fundamental Research Funds for the Central Universities (2632023TD02), the China Postdoctoral Science

Foundation (2021M691647), and the Open Project of State Key Laboratory of Natural Medicines (SKLNMKF202207).

Acknowledgments

We acknowledge the public platform of Animal Experimental Center for the use of SPF laboratory animal, and also thank Shuoshuo Hou for his help with Guidance and training.

Conflict of interest

The authors declare that the research was conducted in the absence of any commercial or financial relationships that could be construed as a potential conflict of interest.

Publisher's note

Supplementary material

The Supplementary Material for this article can be found online at: https://www.frontiersin.org/articles/10.3389/fphar.2024.1333087/full#supplementary-material

References

Astell, K. R., and Sieger, D. (2020). Zebrafish *in vivo* models of cancer and metastasis. *Cold Spring Harb. Perspect. Med.* 10, 0370777–a37117. doi:10.1101/cshperspect.a037077

Atanasov, A. G., Zotchev, S. B., Dirsch, V. M., Orhan, I. E., Banach, M., Rollinger, J. M., et al. (2021). Natural products in drug discovery: advances and opportunities. *Nat. Rev. Drug Discov.* 20, 200–216. doi:10.1038/s41573-020-00114-z

Bagchi, S., Yuan, R., and Engleman, E. G. (2021). Immune checkpoint inhibitors for the treatment of cancer: clinical impact and mechanisms of response and resistance. *Annu. Rev. Pathol. Mech. Dis.* 16, 223–249. doi:10.1146/annurev-pathol-042020-042741

Cabral, H., Kinoh, H., and Kataoka, K. (2020). Tumor-targeted nanomedicine for immunotherapy. *Acc. Chem. Res.* 53, 2765–2776. doi:10.1021/acs.accounts.0c00518

Fu, S., Li, G., Zang, W., Zhou, X., Shi, K., and Zhai, Y. (2022). Pure drug nano-assemblies: a facile carrier-free nanoplatform for efficient cancer therapy. *Acta Pharm. Sin. B* 12, 92–106. doi:10.1016/j.apsb.2021.08.012

Hanahan, D. (2022). Hallmarks of cancer: new dimensions. *Cancer Discov.* 12, 31–46. doi:10.1158/2159-8290.CD-21-1059

Harrington, J. S., Ryter, S. W., Plataki, M., Price, D. R., and Choi, A. M. K. (2023). Mitochondria in health, disease, and aging. *Physiol. Rev.* 103 (4), 2349–2422. doi:10.1152/physrev.00058.2021

Hu, Y., Guo, N., Yang, T., Yan, J., Wang, W., and Li, X. (2022). The potential mechanisms by which artemisinin and its derivatives induce ferroptosis in the treatment of cancer. *Oxid. Med. Cell. Longev.* 2022, 1458143. doi:10.1155/2022/1458143

Huang, L., Zhao, S., Fang, F., Xu, T., Lan, M., and Zhang, J. (2021). Advances and perspectives in carrier-free nanodrugs for cancer chemo-monotherapy and combination therapy. *Biomaterials* 268, 120557. doi:10.1016/j.biomaterials.2020.120557

Islam, M. R., Akash, S., Rahman, M. M., Nowrin, F. T., Akter, T., Shohag, S., et al. (2022). Colon cancer and colorectal cancer: prevention and treatment by potential natural products. *Chem. Biol. Interact.* 368, 110170. doi:10.1016/j.cbi.2022.110170

Kowalska, A., and Kalinowska-Lis, U. (2019). 18β-Glycyrrhetinic acid: its core biological properties and dermatological applications. *Int. J. Cosmet. Sci.* 41, 325–331. doi:10.1111/ics.12548

Kraus, F., Roy, K., Pucadyil, T. J., and Ryan, M. T. (2021). Function and regulation of the divisome for mitochondrial fission. *Nature* 590, 57–66. doi:10.1038/s41586-021-03214-x

Lei, G., Zhuang, L., and Gan, B. (2022). Targeting ferroptosis as a vulnerability in cancer. *Nat. Rev. Cancer* 22, 381–396. doi:10.1038/s41568-022-00459-0

Li, H., Wei, W., and Xu, H. (2022). Drug discovery is an eternal challenge for the biomedical sciences. *Acta Mat. Medica* 1, 1–3. doi:10.15212/amm-2022-1001

Li, Z., Xu, X., Wang, Y., Kong, L., and Han, C. (2023). Carrier-free nanoplatforms from natural plants for enhanced bioactivity. *J. Adv. Res.* 50, 159–176. doi:10.1016/j.jare.2022.09.013

Liang, D., Minikes, A. M., and Jiang, X. (2022). Ferroptosis at the intersection of lipid metabolism and cellular signaling. *Mol. Cell* 82, 2215–2227. doi:10.1016/j.molcel.2022.03.022

Newman, D. J., and Cragg, G. M. (2020). Natural products as sources of new drugs over the nearly four decades from 01/1981 to 09/2019. *J. Nat. Prod.* 83, 770–803. doi:10.1021/acs.jnatprod.9b01285

Ni, K., Luo, T., Nash, G. T., and Lin, W. (2020). Nanoscale metal-organic frameworks for cancer immunotherapy. *Acc. Chem. Res.* 53, 1739–1748. doi:10.1021/acs.accounts.0c00313

Peng, X., Songsong, T., Tang, D., Zhou, D., Li, Y., Chen, Q., et al. (2023). Autonomous metal-organic framework nanorobots for active mitochondria-targeted cancer therapy. *Sci. Adv.* 9, eadh1736–15. doi:10.1126/sciadv.adh1736

Rodrigues, T., and Ferraz, L. S. (2020). Therapeutic potential of targeting mitochondrial dynamics in cancer. *Biochem. Pharmacol.* 182, 114282. doi:10.1016/j.bcp.2020.114282

Siegel, R. L., Miller, K. D., Wagle, N. S., and Jemal, A. (2023). Cancer statistics, 2023. *Ca. Cancer J. Clin.* 73, 17–48. doi:10.3322/caac.21763

Song, D., Hao, J., and Fan, D. (2020). Biological properties and clinical applications of berberine. *Front. Med.* 14, 564–582. doi:10.1007/s11684-019-0724-6

Walensky, L. D. (2019). Targeting BAX to drug death directly. *Nat. Chem. Biol.* 15, 657–665. doi:10.1038/s41589-019-0306-6

Wang, X., Zhang, J. B., He, K. J., Wang, F., and Liu, C. F. (2021a). Advances of zebrafish in neurodegenerative disease: from models to drug discovery. *Front. Pharmacol.* 12, 713963–714019. doi:10.3389/fphar.2021.713963

Wang, Y., Qi, H., Liu, Y., Duan, C., Liu, X., Xia, T., et al. (2021b). The double-edged roles of ROS in cancer prevention and therapy. *Theranostics* 11, 4839–4857. doi:10.7150/thno.56747

Wolfram, J., and Ferrari, M. (2019). Clinical cancer nanomedicine. *Nano Today* 25, 85–98. doi:10.1016/j.nantod.2019.02.005

Wu, J., Sun, T., Yang, C., Lv, T., Bi, Y., Xu, Y., et al. (2021). Tetrazine-mediated bioorthogonal removal of 3-isocyanopropyl groups enables the controlled release of nitric oxide: *in vivo*. *Biomater. Sci.* 9, 1816–1825. doi:10.1039/d0bm01841d

Zhang, J., Li, Y., Wan, J., Zhang, M., Li, C., and Lin, J. (2022). Artesunate: a review of its therapeutic insights in respiratory diseases. *Phytomedicine* 104, 154259. doi:10.1016/j.phymed.2022.154259

Zhu, S., Yu, Q., Huo, C., Li, Y., He, L., Ran, B., et al. (2020). Ferroptosis: a novel mechanism of artemisinin and its derivatives in cancer therapy. *Curr. Med. Chem.* 28, 329–345. doi:10.2174/0929867327666200121124404

frontiers | Frontiers in Pharmacology

TYPE Review
PUBLISHED 10 April 2024
DOI 10.3389/fphar.2024.1375993

OPEN ACCESS

EDITED BY
Bo Wang,
Zhengzhou University, China

REVIEWED BY
Marco A. Velasco-Velazquez,
National Autonomous University of Mexico, Mexico
Ioannis S. Pateras,
National and Kapodistrian University of Athens, Greece

*CORRESPONDENCE
Maria Fiammetta Romano,
mariafiammetta.romano@unina.it
Simona Romano,
simona.romano@unina.it

RECEIVED 24 January 2024
ACCEPTED 25 March 2024
PUBLISHED 10 April 2024

CITATION
Marrone L, Romano S, Malasomma C, Di Giacomo V, Cerullo A, Abate R, Vecchione MA, Fratantonio D and Romano MF (2024), Metabolic vulnerability of cancer stem cells and their niche.
Front. Pharmacol. 15:1375993.
doi: 10.3389/fphar.2024.1375993

Metabolic vulnerability of cancer stem cells and their niche

Laura Marrone[1], Simona Romano[1]*, Chiara Malasomma[1], Valeria Di Giacomo[1], Andrea Cerullo[1], Rosetta Abate[1], Marialuisa Alessandra Vecchione[1], Deborah Fratantonio[2] and Maria Fiammetta Romano[1]*

[1]Department of Molecular Medicine and Medical Biotechnology, University of Naples Federico II, Naples, Italy, [2]Department of Medicine and Surgery, LUM University Giuseppe Degennaro, Bari, Italy

Cancer stem cells (CSC) are the leading cause of the failure of anti-tumor treatments. These aggressive cancer cells are preserved and sustained by adjacent cells forming a specialized microenvironment, termed niche, among which tumor-associated macrophages (TAMs) are critical players. The cycle of tricarboxylic acids, fatty acid oxidation path, and electron transport chain have been proven to play central roles in the development and maintenance of CSCs and TAMs. By improving their oxidative metabolism, cancer cells are able to extract more energy from nutrients, which allows them to survive in nutritionally defective environments. Because mitochondria are crucial bioenergetic hubs and sites of these metabolic pathways, major hopes are posed for drugs targeting mitochondria. A wide range of medications targeting mitochondria, electron transport chain complexes, or oxidative enzymes are currently investigated in phase 1 and phase 2 clinical trials against hard-to-treat tumors. This review article aims to highlight recent literature on the metabolic adaptations of CSCs and their supporting macrophages. A focus is provided on the resistance and dormancy behaviors that give CSCs a selection advantage and quiescence capacity in particularly hostile microenvironments and the role of TAMs in supporting these attitudes. The article also describes medicaments that have demonstrated a robust ability to disrupt core oxidative metabolism in preclinical cancer studies and are currently being tested in clinical trials.

KEYWORDS

cancer stem cells, tumor dormancy, tumor associated macrophages, oxidative metabolism, anti-mitochondrial drugs in clinical trials

Introduction

There is a consensus that conventional cancer treatments fail due to the failure to eliminate tumor stem cells (CSCs), i.e., the stem, regenerative, and undifferentiated component of the tumor. Tumor cells that survive treatment are more difficult to eradicate, are aggressive, are responsible for relapses, and possess stem-like properties overall (Baccelli and Trump, 2012; Fan et al., 2023). The expression of surface stemness markers (e.g., CD44, CD133, CD25, ABC transporters), stemness genes (e.g., OCT4, SOX2, NANOG) and aldehyde dehydrogenase 1-ADH1; the capacity for tumorigenicity when transplanted into mice even at low clonal density and the ability to grow in culture in non-adherent conditions forming spheres are classically used to identify CSCs. Although it is still under debate whether tumor-initiating cell originates from the transformation of normal stem cells or the clonal evolution of genetically unstable cells with a capacity for the

interconversion of different cellular states (Jordan, 2004; Sell, 2010), the concept of plasticity is central in CSC biology (Plaks et al., 2015). The plasticity of CSCs enables them to adapt and survive throughout biological stresses caused by the treatment and the continuous TME changes during tumor evolution, allowing dynamic and reversible transitions between quiescent and proliferative states, epithelial and mesenchymal states, differentiation, and metastasis (Plaks et al., 2015; Agliano et al., 2017; Müller et al., 2020; Romano et al., 2020). Under a persistently hostile environment that can develop at either the primary or metastatic tumor site, CSCs exploit evolutionarily conserved adaptation mechanisms and become dormant (Garimella et al., 2023), leading to a type of clinical remission, in which cancer cells are occult, undetectable, and asymptomatic for a variably protracted period, after which the tumor can recur in primary or distant sites (Enderling et al., 2013). The extreme variability and plasticity of CSCs due to genetic and epigenetic remodeling (Garimella et al., 2023) make their targeting challenging.

The maintenance of CSCs is ensured by adjacent cells in the TME, in particular by tumor-associated macrophages (TAMs) that form a specialized microenvironment that supports their survival against stress and injury and exerts a central role in maintaining their self-renewal and resistance characteristics. Tumor adaptation with the TME and interactions with TAMs throughout cancer progression can also lead differentiated tumor cells to take on CSC characteristics. (Ayob and Ramasamy, 2018).

Over the past decade, thanks to a deeper understanding of the CSC biology of resistant tumors, numerous efforts have focused on designing tailored therapies to target CSCs towards personalized medicine (Khan et al., 2015). However, the results obtained to date are far from conclusive and therapies against cancer stem cells remain an unmet goal (Cole et al., 2020).

In recent years, our understanding of cancer metabolic adaptations in a stressful TME has placed new hopes in modern cancer chemotherapy that can hinder CSCs with their dynamic cellular states by targeting the cornerstone of energy metabolism (Ayob and Ramasamy, 2018). Metabolic adaptations of CSCs and their supporting TAMs actually represent a demanding field of investigation. Our article deals with such an urgent field of investigation that may give new directions to cancer treatment. We review the latest studies that converge on the perception that mitochondrial function and OXPHOS metabolism meet the requirements of CSCs and their supporting TAMs from different tumor types. We offer an overview of therapies that disrupt the core of oxidative metabolism and, having shown a robust ability against CSCs in preclinical cancer studies, are currently studied in phase 1 and phase 2 clinical trials in their aspects of pharmacodynamics, pharmacokinetics, bioavailability, toxicity, together to efficacy on refractory and resistant tumors.

CSCs and the mitochondrial respiratory machinery

The discovery that cancer has metabolic alterations dates back to the early 1920s when the biochemist Otto Warburg first proved that, oppositely to healthy cells, the metabolism of cancer cells mainly relies on glycolysis, uncoupled to OXPHOS, even under normal oxygen concentrations and fully functioning mitochondria. Tumor cells encompass hypoxia and re-oxygenation (Belisario et al., 2020), continuing their growth notwithstanding mutable environmental conditions. High lactate levels in the TME favor tumor acidosis and adaptation of cancer cells to hypoxia (Bononi et al., 2022). Hypoxia exerts a selection pressure that leads to the survival of subpopulations with the genetic machinery for malignant progression induced by HIF-1α and HIF-2α (Allavena et al., 2021). Lactate generated by glycolytic tumor cells is secreted outside the cell through the monocarboxylate transporter (MCT) 4 and can be metabolized by adjacent cells (Martinez-Outschoorn et al., 2017). In oxygenated areas, lactate enters the tumor cell through MCT1 transporters and, upon conversion into pyruvate, produces the so-called “reverse Warburg phenotype” (Marchiq and Pouysségur, 2016). Pyruvate fuels the tricarboxylic acid (TCA) cycle and mitochondrial respiratory chain, increasing the NADH/NAD + ratio and mitochondrial biogenesis. In a physiological system of mouse adipocytes, Yang et al. showed that increased NADH/NAD + ratio induces Sirtuin 1 (SIRT1)-mediated deacetylation of the peroxisome proliferator-activated receptor gamma coactivator-1α (PGC-1α), leading to activation of such a pivotal promoter of mitochondrial biogenesis (Yang et al., 2020).

Several studies highlight expression of MCT trasporters in different cancer settings. Using varied tumor mouse models (colorectal adenocarcinoma, human cervix squamous cell carcinoma, hepatocarcinoma, lung adenocarcinoma), Sonveaux et al. found MCT1 expressed on a subset of resistant cancer stem-like cells and its targeting had clinical antitumor potential (Sonveaux et al., 2008). They demonstrated that MCT1 inhibition induced a switch from lactate-fueled respiration to glycolysis, which overcame cancer resistance and induced sensitivity to ionizing radiation (Sonveaux et al., 2008). Curry et al. interrogated head and neck cancer (HNSCC) tissues to assess metabolic compartmentation in primary tumors typically composed in upper layer of differentiating squamous carcinoma cells and a basal stem cell layer that regenerates the tumor. The basal layer was mitochondrial-rich and specialized for the use of mitochondrial fuels, such as L-lactate and ketone bodies and expressed high levels of MCT1. Conversely, the majority of well-differentiated carcinoma cells and cancer-associated fibroblasts (CAFs) showed strong MCT4 immunoreactivity (Curry et al., 2013).

Pancreatic ductal adenocarcinoma (PDAC) cells do express MCT1 and MCT4 (Kong et al., 2016). Through immunohistochemistry of PDAC tissues, Sandforth et al. demonstrated a co-localization of MCT1 with KLF4 (Sandforth et al., 2020). Moreover, they demonstrated that MCT1 expression on PDAC cell lines conferred greater potential of clonal growth, along with drug resistance and elevated expression of the stemness marker nestin and reprogramming factors (OCT4, KLF4, NANOG). These effects on stemness properties were abrogated by targeting of MCT1 (Sandforth et al., 2020). Pancreatic CSCs, defined using spheres and enriched through CD133 marker, were also shown to express increased levels of PGC-1α, demonstrated to be a relevant determinant of their OXPHOS dependency (Sancho et al., 2015). PGC-1α forced expression in CD133 pancreatic cancer cells accelerated OXPHOS metabolism and enabled their self-renewal and tumorigenic capacity (Valle et al., 2020).

MCT1 and MCT4 are expressed in glioblastoma tumors (Park et al., 2018). Takada et al. measured an upregulation of MCT1 along

with stem cell markers (Nestin, NANOG, CD133, SOX-2, and OCT-4) in sphere-forming glioblastoma cells compared with adherent, non-sphere forming cells. Inhibition of MCT1 decreased the viability of glioblastoma CSCs compared with that of non-CSCs (Takada et al., 2016). Mudassar et al. showed MCT1 transporters were associated with high mitochondrial abundance in high grade glioma cells (Mudassar et al., 2020). PGC-1α suppression hampered spheroid formation of glioblastoma cells *in vitro* and their capability to form *in vivo* tumors (Bruns et al., 2019). Other studies, associate PGC-1α with cancer metastasis and resistance (Vazquez et al., 2013; LeBleu et al., 2014). PGC-1α expression was co-induced with EMT genetic program in breast cancer patients with distant metastasis and poor outcome (LeBleu et al., 2014). Also, PGC-1α supports high bioenergetic and ROS detoxification capacities of resistant melanoma tumors with higher rates of survival under oxidative stress compared to PGC-1α-negative melanomas (Vazquez et al., 2013). Mitochondrial biogenesis is essential for the anchorage-independent survival and propagation of stem-like cancer cells (De Luca et al., 2015). For a review of MCT transporters in cancer and the potential of new selective MCT1 and/or MCT4 inhibitors in cancer therapeutics, we refer to Singh et al. (Singh et al., 2023).

Evidence that oxidative phosphorylation is upregulated in CSCs is increasingly emerging (Abdullah and Chow, 2013; Sancho et al., 2016; Li et al., 2020; Karp and Lyakhovich, 2022). Studying one of the most aggressive and resistant cancers, i.e., pancreatic ductal adenocarcinoma, Viale et al. found that a subpopulation of dormant tumor cells responsible for tumor relapse relied on oxidative phosphorylation for survival and had features of cancer stem cells ($CD133^{+}CD44^{high}$ cells with spherogenic and tumorigenic capabilities) (Viale et al., 2014). Valle et al. by changing the carbon source from glucose to galactose *in vitro*, induced a forced oxidative metabolism in pancreatic cancer cells (Valle et al., 2020). Such a metabolic switch produced enrichment in typical pancreatic CSC biomarkers (Hermann et al., 2007) including pluripotency gene expression, tumorigenic potential, upregulated immune evasion properties and acquisition of plastic features such as a reversible quiescence-like state (Valle et al., 2020). Dependency on mitochondrial metabolism has been demonstrated in CSCs from ovarian cancer, identified through coexpression of CD44 and CD117 and tumor-initiating capacity (Pastò et al., 2014). In ovarian cancer patients, comparative transcriptome analyses from ascites-derived tumor cell spheroids *versus* tumor samples revealed upregulation of genes involved in oxidative phosphorylation process along with those of chemoresistance, cell adhesion and cell-barrier integrity (Ding et al., 2021).

In small cell lung cancer, resistant CSC-like cells, identified based on selective expression of urokinase-type plasminogen activator receptor ($uPAR^{+}$), showed higher dependency on oxidative phosphorylation than non-CSCs ($uPAR^{-}$) (Gao et al., 2016). The glycosylphosphatidylinositol (GPI)-anchored protein uPAR is associated with multidrug resistance and with high clonogenic activity (Gao et al., 2016). Vlashi et al. showed that stem/progenitor cells from neurospheres depended on oxidative phosphorylation and higher ATP content compared with differentiated glioblastoma cells derived from culture in monolayers (Vlashi et al., 2011). They also show that such a OXPHOS dependence is lost during differentiation and accompanied with a switch to aerobic glycolysis (Vlashi et al., 2011). Evidence that mitochondrium is a relevant target to overcome resistance of colorectal CSCs are reviewed by Rainho et al. (Rainho et al., 2023). Following metabolic profiling of primary chronic myeloid leukemia (CML) cells, Kuntz et al. found a three-fold increase in the rate of mitochondrial oxygen consumption along with a pattern of metabolites indicating increased lipolysis and fatty acid oxidation in the stem cell-enriched population ($CD34^{+}CD38^{-}$), compared to differentiated CML cells ($CD34^{-}$) (Kuntz et al., 2017). Inhibition of oxidative phosphorylation by tigecycline, an anti-bacterial FDA-approved antibiotic, produced a selective cytotoxic effect on CSC at clinically administrable doses (Kuntz et al., 2017). This study highlights that although the nature of CSCs differs and different origins of CSCs are postulated between hematological and solid tumors (Bonnet and Dick, 1997; Jordan, 2004), the requirements of CSCs appear to be met by oxidative metabolism across different tumors.

The concept of metabolic symbiosis between hypoxic/glycolytic- and OXPHOS-tumor cells that favors rapid adaptation of cancer to changing environmental oxygen conditions (Nakajima and Van Houten, 2013) can virtually unravel an interplay between non-CSCs and CSCs in which differentiated tumor cells provide glycolysis products that fuel oxidative metabolism of the stem, regenerative and resistant cellular component of the tumor. (Figure 1).

OXPHOS and multidrug resistance

Increased activity of ATP binding cassette (ABC) transporter family members involved in multidrug resistance is a common feature of CSCs (Begicevic and Falasca, 2017). There are several efforts focused on creating druggable molecules to inhibit these transporters. Five-cyano-6-phenylpyrimidin derivatives containing an acylurea moiety demonstrated efficacy in inhibiting P-glycoprotein ABCB1, a leading member of ABC transport proteins found to be widely overexpressed in human solid tumors and hematologic malignancies (Wang et al., 2018a; Wang et al., 2018b). ABC transporters are highly dependent on ATP since they use the energy from ATP hydrolysis to pump substrates out of cells (Linton and Higgings, 2007). ATP generated by the respiration of mitochondria in the proximity of the plasma membrane and transported from the mitochondrial matrix to the cytosol nearby plasma membrane produces a local rise of ATP level for the active transporter's need (Linton and Higgings, 2007), thus explaining why mitochondrial and not glycolytic ATP preferentially fuels ABC transporter activity in chemoresistant cancer cells (Linton and Higgings, 2007). In a model of chemoresistant cancer cells, Giddings et al. found that methylation-controlled J protein (MCJ) affected ABC transporter function through regulation of mitochondrial respiration (Giddings et al., 2021). MCJ localizes on the inner membrane of mitochondria and negatively regulates Complex I thus acting as an endogenous brake on mitochondrial respiration (Hatle et al., 2013) As MCJ is often downregulated in the tumors, the authors generated MCJ mimetics and investigated their capability to inhibit ABC transporter function and therapeutic efficacy in combination with doxorubicin, using ovarian and mammary cancer cells and an *in vivo* mouse model of mammary

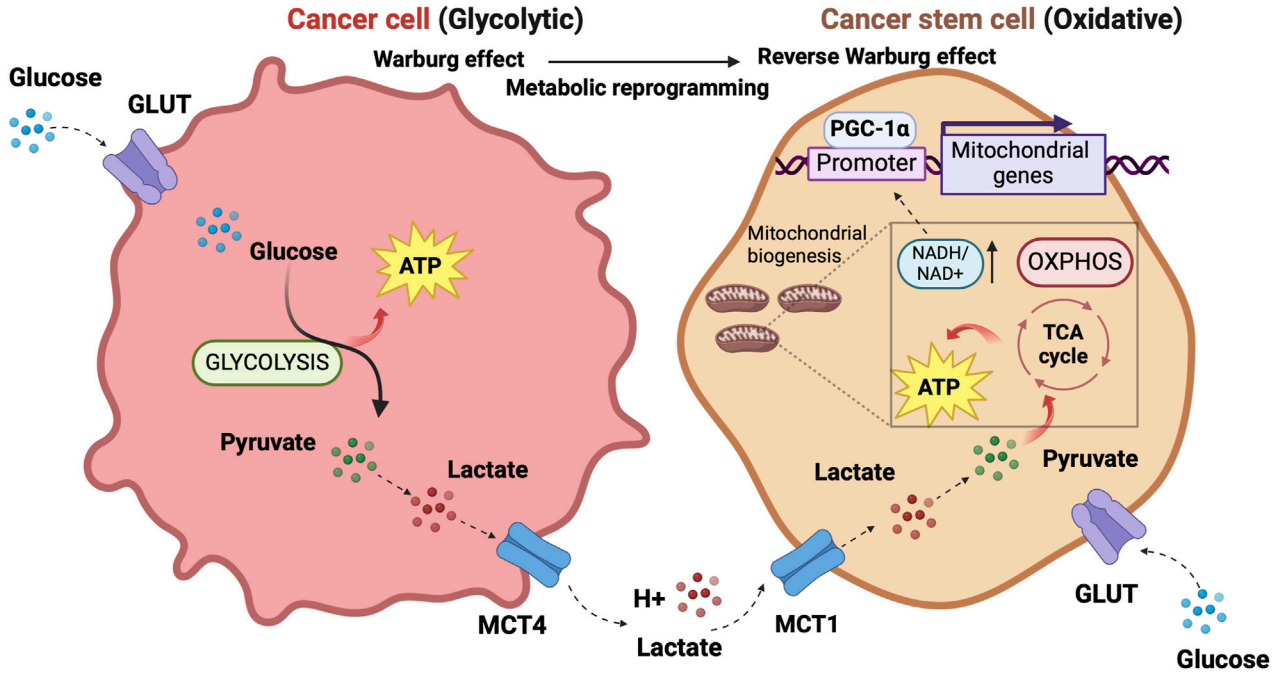

FIGURE 1
The prevalent metabolism adaptations in differentiated tumor cells compared to stem cell-like tumor cells support a metabolic symbiosis between the different cellular states. The illustration was started from scratch, created with BioRender.com original design.

tumor (Giddings et al., 2021). MCJ mimetics attenuated mitochondrial respiration in chemoresistant cells and reversed cancer chemoresistance *in vivo* tumor model MCJ-KO. The tumors of mice treated with a combination of MCJ mimetics and doxorubicin showed a prominent size reduction compared to those treated with doxorubicin alone. There was no evidence of liver and heart toxicity by MCJ mimetics nor effect on mouse body weight (Giddings et al., 2021). Although not selectively involving CSCs, the study by Giddings et al. sheds light on the aspect of chemoresistance closely linked to the stem-cell-like concept.

OXPHOS and tumor dormancy

Dormancy is a strategy adopted by a tumor cell placed in a persistently hostile environment that exploits evolutionarily conserved adaptation mechanisms to succeed in tumor progression (Merlo et al., 2006). Proliferation arrest, metabolic quiescence, and immune occultation are the main features of tumor dormancy (Enderling et al., 2013). Dormant cancer cells can reawaken in response to signals which are not yet fully understood, resulting in recurrence and metastasis (Gao et al., 2016; Park and Nam, 2020). Adapting newly arrived cancer cells to the microenvironment of distal organs is a stringent rate-limiting step in metastasis, and the probability of completing this step varies widely depending on the tumor type and the target organ. A study of the metabolic signature associated with disseminated cancer cells suggested an activation of mitochondrial bioenergetic pathways (TCA cycle and OXPHOS) and the pentose-phosphate pathway (Dudgeon et al., 2020) upon seeding. Newly seeded cancer cells slow down bioenergetics and become dormant to survive in secondary sites (Ganguly and Kimmelman, 2023). Although how and when dormant tumor cells become reactivated after inactivity remains not well understood, a role for lipid metabolism in reawakening is emerging (Luo et al., 2017; Watt et al., 2019). Pascual et al. (Pascual et al., 2017) found a subpopulation of CD44bright slow-cycling cells in human oral carcinomas with a unique ability to initiate metastasis that expressed high levels of the fatty acid receptor CD36 and lipid metabolism genes (Pascual et al., 2017). Using neutralizing antibodies for CD36 blockade, they were able to inhibit metastasis formation in orthotopic mouse models of human oral cancer. Conversely, palmitic acid or a high-fat diet increased the metastatic potential of $CD36^{+}$ cancer cells (Pascual et al., 2017). Ladanyi et al. demonstrated a role for adipocytes in the stimulation of CD36 and Fatty acid transport protein 1 (FATP1) in ovarian cancer cells (Ladanyi et al., 2018) suggesting a significant role for cancer-associated adipocytes in tumor growth and metastasis through favoring lipid utilization and uptake and metabolic reprogramming (Yao and He, 2021). Intriguingly, the oxidation of Cys272 and Cys333 promoted the activation of CD36, suggesting a regulatory effect of the redox signaling in the reactivation of dormant cancer cells (Wang et al., 2019). Also, oxidative stress enabled P450 epoxygenases to synthesize epoxyeicosatrienoic acids, metabolites of arachidonic acid, with a vasodilation effect facilitating exit from the dormant state (Borin et al., 2017).

The CSC niche and tumor associated macrophages

Adjacent cells to CSC form a specialized microenvironment, termed niche, essential for preserving and sustaining CSC against stress and injuries with growth factors, cytokines, and extracellular

matrix compounds (Allavena et al., 2021). In analogy to the physiological stem cell niche, this specialized tissue structure allows CSCs to survive and remain quiescent and also provides cues for reactivation of proliferation, differentiation, and migration. (Allavena et al., 2021).

CSCs niche dynamics vary between leukemia and solid tumors. Tracing the cellular origins of human cancers has long been a complex and contentious area in cancer research. Pioneering work by John Dick and colleagues in the 1990s introduced the hierarchical model in acute myeloid leukemia (AML), proposing that a primitive stem or early progenitor cell serves as the cell of origin for malignant transformation in AML (Lapidot et al., 1994; Bonnet and Dick, 1997). This model delineates a rare population of leukemic stem cells (LSCs) with high self-renewal potential and immunophenotypic resemblance to healthy hematopoietic stem cells (HSCs), which are exclusively capable of reinitiating leukemia in immunodeficient mice (Lapidot et al., 1994; Bonnet and Dick, 1997). In leukemia, the bone marrow serves as primary niche, populated by healthy stem cells with which CSCs compete (Marchand and Pinho, 2021). The leukemic niche is populated by different cell types, such as mesenchymal stem cells (MSCs), endothelial cells, megakaryocytes, macrophages, osteoblasts, and nerve cells (Schepers et al., 2015). Bidirectional interactions between leukemic cells and the bone marrow microenvironment promote leukemic progression at the expense of healthy hematopoiesis, implicating bone marrow mesenchymal stem cells in the predisposition, manifestation, and evolution of hematological malignancies (Korn and Méndez-Ferrer, 2017).

In contrast, solid tumors exhibit phenotypic plasticity, where tumor cells can can interconvert between differentiated and stem-like states across a continuum of cell fate specification (Quail et al., 2012). Moreover, despite the presence of founder mutations within the parental clones, a large number of additional mutations between primitive and metastatic tumor implicate the concept of clonal evolution in CSC development (Campbell et al., 2010; Kreso and Dick, 2014). The fact that melanoma, breast, prostate, ovarian, and lung cancer cells are all able to alter their gene expression to resemble cell types that are not part of their original lineage (Quail et al., 2012) exemplifies cancer cell plasticity that enables cancer cells to gain/lose stem cell properties (Passalidou et al., 2002; Shirakawa et al., 2002; Lim et al., 2009). Solid tumors contain non-tumor stromal cells supporting CSCs including CAFs, MSCs, TAMs and other immune cells, and extracellular matrix proteins (Mancini et al., 2021). The niche is characterized by conditions of hypoxia, acidity, and low glucose levels (Olivares-Urbano et al., 2020). The niche concept extends to specialized pre-metastatic microenvironments that play a crucial role in the colonization of disseminated tumor cells at secondary sites, with organ-specific exosomes derived from primary tumors facilitating colonization (Fong et al., 2015; Hoshino al.al 2015). Once the pre-metastatic niche has finished priming, the metastatic niche generates a microenvironment that sustains metastatic cancer stem cells, providing physical anchorage, survival, immune surveillance protection, and metabolic requirements for CSCs in distant metastatic sites (Joseph et al., 2023).

TAMs are the leading players in the CSC niche, they physically interact with CSCs and secrete a variety of soluble factors to protect them from environmental damage (Jinushi et al., 2011; Fan et al., 2014; Zhou et al., 2015; Oshimori, 2020). Notably, similarities exist between TAMs from leukemias and solid tumors within their respective niches. Such similarities consist in abundant localization of TAMs in both leukemic and solid tumor niches that positively correlate with CSC distribution (Wang and Zheng, 2019; Basak et al., 2023) and accumulation within hypoxic tumor regions, where CSCs are also prevalent (Wang and Zheng, 2019; Basak et al., 2023). CSCs exert significant influence over TME by recruiting and polarizing macrophages toward a pro-tumor M2 phenotype. In turn, M2-TAMs actively support CSC maintenance, thus promoting a symbiotic relationship between these cellular populations (Wang and Zheng, 2019; Basak et al., 2023).

TAMs are able to activate signaling pathways essential to CSCs, including those driven by Sonic Hedgehog (SHH), Neurogenic locus notch homolog protein (NOTCH), STAT3, PI3k/Akt, Wingless integrated (WNT)/b-catenin and NANOG, through soluble factors or direct physical interaction with CSC (Allavena et al., 2021). Tumor cells produce chemotactic factors (Allavena et al., 2021), exosomes (Su et al., 2021) and metabolites (Diskin et al., 2021) to recruit circulating monocytes and tissue-resident macrophages and induce their polarization towards anti-inflammatory, angiogenic and protumor (M2) phenotype typical of TAMs. TAMs initiate reciprocal crosstalk with CSC to exert their trophic action in the niche (Allavena et al., 2021). Transcription factors involved in maintaining the pluripotency and self-renewal characteristics of CSCs are highly expressed by TAMs (Shang et al., 2023). The CSC's role in modulating the TME and driving the recruitment and alternative polarization of macrophages and crosstalk between CSCs and TAMs have been extensively reviewed in several articles (Sainz et al., 2016; Muller et al., 2020; Allavena et al., 2021; Chae et al., 2023).

The primary tumor secretome influences the immune milieu at distant organs, thus preparing the permissive soil for colonization of disseminated cancer cells by re-educating the metabolic and epigenetic state of resident cells in the host organs (Ganguly and Kimmelman, 2023). Macrophages play a special role in priming and disseminating tumor cells for dormancy and stemness (Borriello et al., 2022). Using a technique termed Window for High-Resolution Imaging of the Lung (WHRIL) (Entenberg et al., 2018), Borriello et al. quantitatively measured, in real-time, spontaneously disseminating tumor cells during the process of metastasis to the lung, in a breast cancer mouse model (Borriello et al., 2022). They found a subset of macrophages within the primary tumor that caused activation of genetic programs related to dissemination, dormancy, and stemness in tumor cells approaching the intravasation site. Upon tumor cell contact with macrophages, tumor cell expresses high levels of the actin-regulatory protein MenaINV (Roussos et al., 2011). This actin isoform plays an active role in tumor cell migration during intravasation within the primary tumor (Pignatelli et al., 2016). Moreover, contact with macrophages activated in tumor cells expression of stem-like SOX-9 phenotype and Nuclear Receptor Subfamily 2 Group F Member 1 (NR2F1), the orphan nuclear receptor and one of the best molecular markers of dormancy that regulates expression of pluripotency genes (Sosa et al., 2015). The depletion of macrophages significantly reduced NR2F1 levels in the tumor cells and prevented dormancy (Borriello et al., 2022). Before disseminating, tumor cells establish microenvironmental niches incorporating macrophages in the primary tumor that enable them to acquire a pro-dissemination,

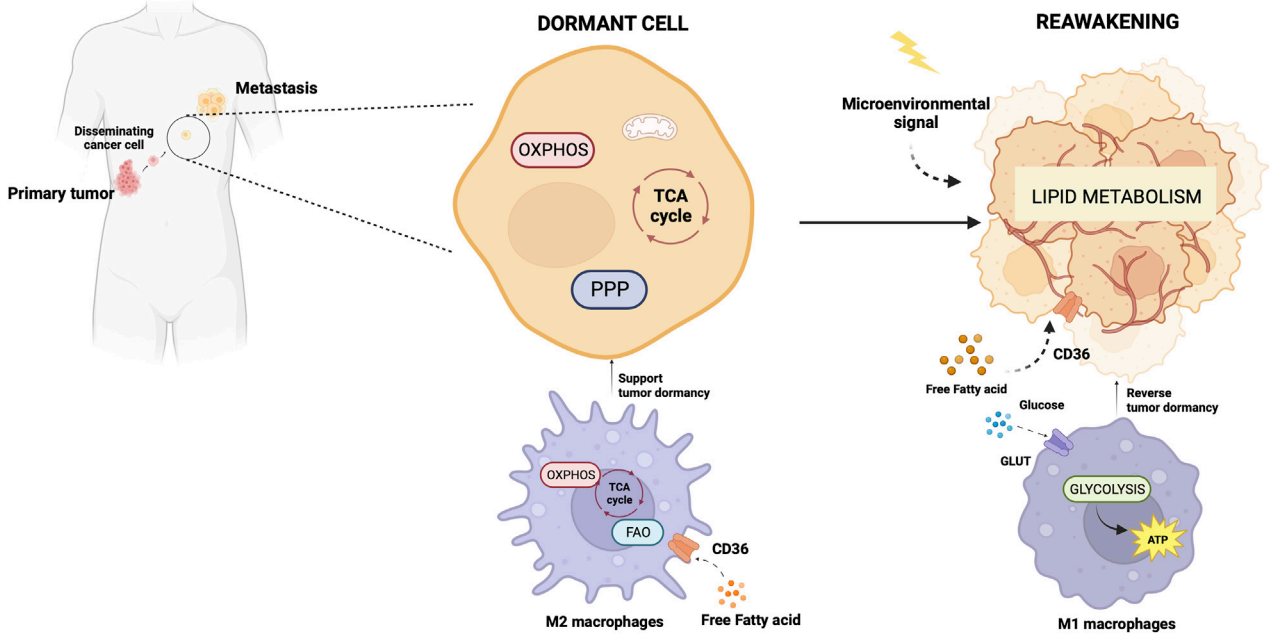

FIGURE 2
Metabolic aspects of TAMs in tumor dormancy and reawakening. The illustration was started from scratch, created with BioRender.com original design.

stem-like dormancy phenotype that is carried to the secondary site and is lost during metastatic growth (Borriello et al., 2022). Dormancy represents a typical risk for long-term breast cancer survivors. Dormant breast cancer cells preferentially reside in the bone marrow. A study by Walker et al. in a breast cancer mouse model showed that bone marrow M2 macrophages supported tumor dormancy. Upon the M2 to M1 switch through activation of TLR4 with LPS, M1 macrophages reversed dormancy and induced sensitivity to carboplatin of breast cancer cells (Walker et al., 2019). The authors demonstrated that M1-derived exosomes produced clinical evidence of metastasis due to the activation of NF-κB in quiescent breast cancer cells to reverse non-cycling to cycling cells (Walker et al., 2019). Crosstalk between macrophages and dormant cancer cells has been extensively reviewed by Batoon and McCauley (Batoon et al., 2021). Figure 2 illustrates the interplay between dormant cell and macrophages.

The mitochondrial respiratory machinery is a significant driving force in TAM polarization

Phenotype, function, and metabolic state are closely interconnected aspects in macrophages and coordinated with each other (Minhas et al., 2019; Emtenani et al., 2022; Gonzalez et al., 2023). Through single-cell transcriptomic profiling of macrophages phagocytosing neoplastic cells, Gonzales et al. demonstrated a strict linkage between phagocytosis, immune-suppressive phenotype, and gene expression changes toward OXPHOS, ribosomal, and other metabolic genes (Gonzalez et al., 2023). The correlation of the metabolic gene signature with worse clinical outcomes was validated in human lung cancer (Gonzalez et al., 2023). Consistent with the findings by Gonzales et al., Minhas et al. showed that genetic or pharmacological blockade of *de novo* NAD + synthesis, suppressed mitochondrial NAD + -dependent signaling and respiration, and impaired phagocytosis and resolution of inflammation due to changes in macrophage polarization state. (Minhas et al., 2019). Emtenani et al. (Emtenani et al., 2022), investigating gene expression in macrophages during the first migratory stages of the tissue invasion, found a metabolic reprogramming towards OXPHOS and ribosome biogenesis of migrating macrophages. In this cell model, the authors identified Atossa, a transcriptional regulator inducing expression of an RNA helicase termed Porthos. This factor increased the translation efficiency of short 5′UTR mRNAs that included a subset of mitochondrial OXPHOS genes of the respiratory complexes (Emtenani et al., 2022).

Like CSCs, M2 macrophages can resist and remain functional in adverse environmental conditions such as low nutrients, low pH, hypoxia, and oncometabolite abundance (Liu et al., 2021). Like CSCs, M2 macrophage metabolism exploits the mitochondrial respiratory machinery that is a significant driving force in alternative macrophage polarization (O'Neill et al., 2016; Liu et al., 2021). While aerobic glycolysis produces most of the ATP and intermediates for biosynthetic pathways required for effector (microbicidal and antitumor) functions of M1 macrophages (Warburg and Minami, 1923; Altenberg and Greulich, 2004; Tannahill et al., 2013), to sustain their activities, M2 macrophages use the TCA cycle to obtain reducing equivalents, assuring constant energy production in concert with mitochondrial OXPHOS (Figure 3). Acetyl-CoA oxidized in the TCA cycle mainly derives from fatty acid oxidation (Odegaard and Chawla, 2011; O'Neill et al., 2016). M2 macrophages actively extract fatty acids from circulating lipoproteins internalized through CD36 (Evans et al., 1993) and endocytosis (Huang et al., 2014). The pivotal role of fatty acids oxidation in alternative macrophage polarization is underscored by the observation that blocking palmitate entry into the

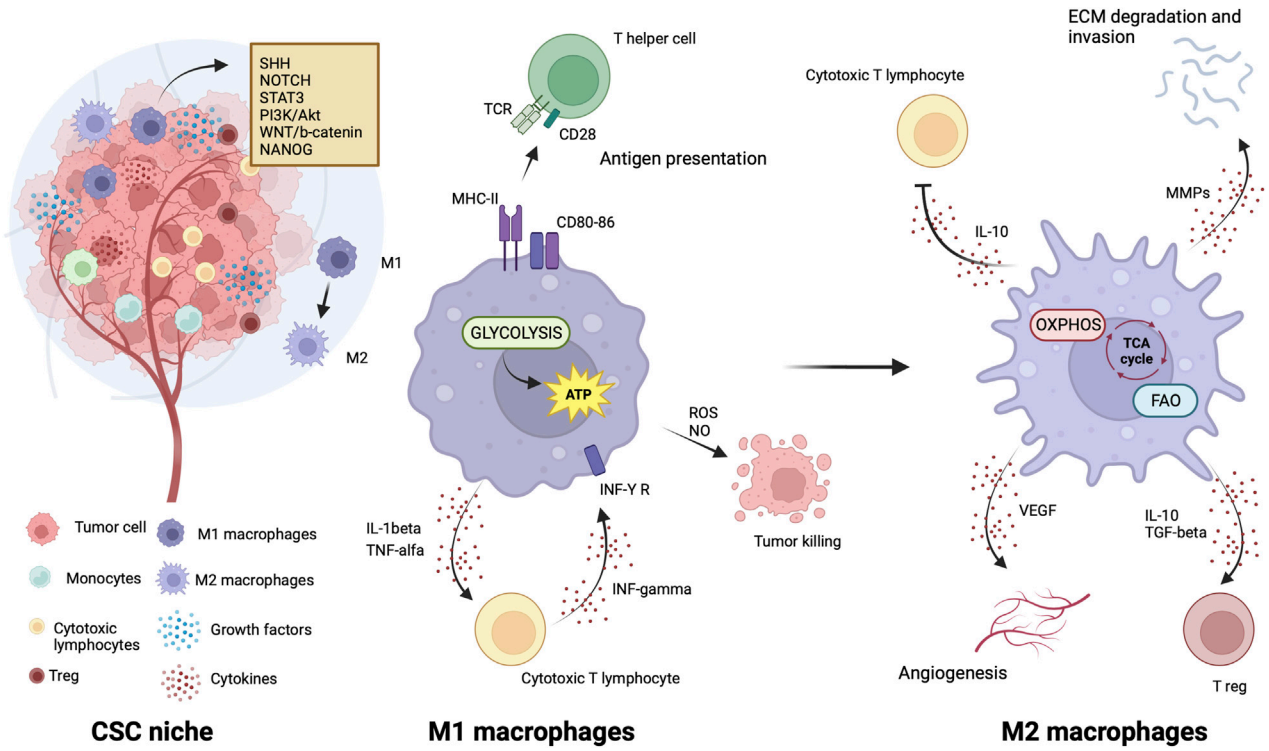

FIGURE 3
Metabolic features of TAMs in CSC niche. The illustration was started from scratch, created with BioRender.com original design.

mitochondrial matrix hampers IL-4-induced M2 polarization (Malandrino et al., 2015). Enhanced fatty acid oxidation in palmitate-incubated macrophages reduced the inflammatory profile (Malandrino et al., 2015). Proliferator-activated receptors of peroxisomes, organules involved in the oxidation of long-chain fatty acids and eicosanoid-CoA esters (Reddy and Hashimoto, 2001) were shown to regulate the transcription of M2 genes, (Odegaard et al., 2008; Chawla, 2010; Nelson et al., 2018).

OXPHOS-targeted drugs in clinical trials

Efforts in recent years led to design of numerous clinical trials for the assessment of the anticancer effectiveness of drugs targeting mitochondrial metabolism with the aim of hindering CSCs and microenvironmental signaling together.

The electron transport chain has indepth been explored for development of inhibitors for each complex (Sainero-Alcolado et al., 2022). However, these compounds can exhibit remarkable toxicity that prevents their use in clinical practice (Sainero-Alcolado et al., 2022). The antidiabetic agent metformin (Watanabe, 1918) counts more than 400 registered clinical trials in the last 5 years as a cancer chemopreventive or therapeutic agent, alone or in combination with neoadjuvant chemo-radiation therapy (https://www.clinicaltrials.gov). The master pathway of metformin anticancer activity is the activation of the adenosine monophosphate-activated protein kinase (AMPK) that inhibits mammalian target of rapamycin (mTOR) (Zhou et al., 2001) pathway triggered by inhibition of complex I through drug binding in the quinone channel (Owen et al., 2000). Recently, metformin was found to cause a mitochondrial effect independent of inhibition of complex1 by direct molecular targeting PEN2, a subunit of γ-secretase (Ma et al., 2022). PEN2 binds to ATPase H^+transporting accessory protein 1, inhibits the activity of ATPase without increasing AMP or ADP, and then activates the lysosomal AMP-independent AMPK pathway (Ma et al., 2022). Still, other mechanisms concur to its anticancer activity that are still not well understood. Metformin reduces cancer risk, decreases cancer-related mortality in patients with diabetes (Decensi et al., 2010), and has excellent performance in preclinical studies. Particularly, a preclinical study shows that metformin selectively targets cancer stem cells and acts together with chemotherapy to block tumor growth and prolong remission (Hirsch et al., 2009). A prospective phase I clinical trial (NCT01442870) assessing the safety of metformin in combination with chemotherapy in patients with solid tumors suggests that metformin can be given safely with chemotherapy (Saif et al., 2019). Brown et al. evaluated the impact of metformin on CSC number and clinical outcomes in nondiabetic patients with advanced-stage epithelial ovarian cancer. Metformin decreased by 2.4-folds the number of ALDH+CD133+ CSCs and increased sensitivity to cisplatin *ex vivo*. Translational studies confirm an impact of metformin on ovarian cancer CSCs and suggest epigenetic change in the tumor stroma, specifically MSCs, may drive the platinum sensitivity *ex vivo*. Metformin treatment was associated with increased overall survival, supporting the use of metformin in phase III studies (Brown et al., 2020). However, benefits in cancer treatment are often quite vague in clinical trials; thus, there are challenges in the clinical translation of metformin. In a very recent review, Hua et al. (Hua et al., 2023) point out that the mechanisms of action of metformin must be seen in the context of

cancer hallmarks, the well-standardized set of crucial functional capabilities for malignant transformation (Hanahan, 2022). In their article, after summarizing the current knowledge on the antitumor action of metformin, the authors elaborate the underlying mechanisms in terms of cancer hallmarks and propose new perspectives of metformin use potentially applicable to cancer treatment (Hanahan, 2022).

IACS-010759, an inhibitor of complex I, was found to reduce mitochondrial function of enriched tumor cell spheroids from the ascites of high-grade serous ovarian cancer patients. Also, IACS-010759 treatment reduced the fraction of $CD34^+$ progenitor AML cells in a dose-dependent manner (Molina et al., 2018). Current clinical trials with IACS-010759 involve advanced tumors (phase 1, NCT03291938) and AML (phase 1, NCT02882321). Tamoxifen was found to interact with the flavin mononucleotide site of complex I leading to mitochondrial failure (Moreira et al., 2006). It is investigated in cancers other than breast, and genito-urinary tract, as intraocular melanoma, in combination with cisplatin (phase 2, NCT00489944); high risk stage III melanoma in combination with sorafenib (phase 2, NCT00492505); oesophageal cancer (phase 1, NCT02513849); osteosarcoma (phase 1, NCT00001436). Pyrvinium pamoate is a lipophilic cation belonging to the cyanine dye family, inhibiting complex I. (Schultz and Nevler, 2022). It has been used in the clinic as a safe and effective anthelminthic for over 70 years (Schultz and Nevler, 2022) and currently is investigated in pancreatic cancer to determine its safety and tolerability (phase 1, NCT05055323). Atovaquone, with a structure similar to protozoan ubiquinone, is an inhibitor of complex III (Mather et al., 2005) approved by the US Food and Drug Administration against plasmodium falciparum. Atovaquone reduced the tumorsphere formation and invasion ability of $EpCAM^+CD44^+$ CSCs isolated from HCT-116 colon carcinoma cell lines (Fu et al., 2020). It was found to inhibit proliferation and induce apoptosis of CSCs ($CD44^+CD24Low^-$ and $ALDH^+$) derived from the mammary breast cancer cell line MCF7 (Fiorillo et al., 2016b) and of $ALDH^+CD133^+$ cancer stem-like cells from two high-grade serous ovarian cancer patients (Kapur et al., 2022). Atovaquone anti-cancer efficacy has been assessed in varied mouse cancer models (Rodriguez-Berriguette et al., 2024) and is currently investigated in NSCLC (phase 1, NCT04648033), ovarian cancer (phase 2, NCT05998135), AML (phase 1, NCT03568994). Niclosamide is an uncoupler of electron transport chain (Chen et al., 2018). Jin et al., showed that niclosamide is a potent inhibitor of the NF-κB pathway and exerts a synergism with Ara-C or VP-16 against primary AML cells. They also suggested that this drug has the potential to eradicate AML blasts since they demonstrated that niclosamide kills AML $CD34^+CD38^-$stem-cells, while sparing normal bone marrow progenitors (Jin et al., 2010). Niclosamide efficiently decreased therapy resistance in colorectal cancers by reducing CSC populations and their self-renewal activity, thereby attenuating the survival potential of CSCs following chemoradiation (Park et al., 2019). Clinical trials with niclosamide involved treatment of refractory AML (phase 1, NCT05188170), colorectal cancer (phase 1, NCT02687009; phase 2, NCT02519582), and castration resistant prostate cancer (phase 1, NCT03123978; phase1, NCT02532114; phase 2, NCT02807805). Table 1 lists active or recently completed clinical trials investigating outcomes with respiratory-complex inhibitors in refractory tumors, ONC201 and ONC206 are imidazo-pyrido-pyrimidine derivatives that bind to the mitochondrial serine protease termed caseinolytic protease proteolytic subunit (ClpP) with the ability to reduce mitochondrial oxidative phosphorylation, oxygen consumption rate, ATP production and increase mitochondrial generation of reactive oxygen species (Przystal et al., 2022). They were found for the first time to affect mitochondrial activity in diffuse midline glioma cells in children and young adults and considered two promising agents against Histone three lysine27-to-methionine (H3.3K27M)-mutated gliomas. Treatment with ONC201 reduced self-renewal, clonogenicity and cell viability of GBM cells (He et al., 2021). Similar results of inhibition of tumorsphere formation, CSC genes NANOG and SOX2, and CSC frequency were obtained by Jeon et al., due to selective antagonism of dopamine receptor (Jeon et al., 2023). Moreover, ONC201 targets chemotherapy-resistant colorectal cancer stem-like cells (Prabhu et al., 2015) and significantly decreased CSC frequency and tumor initiation capability in a breast cancer mouse model (Greer et al., 2022). In chemo-refractory AML patient samples, ONC201 induced apoptosis in leukemia stem/progenitor cells ($CD34^+/CD38^-$) to an extent that was equivalently observed in non-CSCs (Ishizawa et al., 2016) Especially ONC201 is an investigational agent that has shown a favorable safety profile in phase 1 and phase 2 clinical trials in advanced cancers. Several clinical trials have been designed to assess efficacy of ONC201 and ONC206, alone or in combination with chemo or immunotherapy, against several cancer types, including colorectal cancer, pediatric H3. K27M-mutant gliomas, adults with recurrent H3.K27M-mutant gliomas, recurrent gliomas, rare primary central nervous system neoplasms, neuroendocrine tumors, multiple myeloma, endometrial cancer, advanced solid tumors, metastatic breast cancer, relapsed/refractory non-Hodgkin's lymphoma, relapsed or refractory acute leukemias, oral cancer (Table 2). Two completed clinical trials (NCT02250781, NCT02324621) evaluated the safety, pharmacokinetics, and pharmacodynamics of ONC201 in patients with advanced solid tumor that is refractory to standard treatment, or for which no standard therapy is available. Results from these studies indicated that oral ONC201 is well-tolerated and had immunostimulatory activity. Patients treated with ONC201, who experienced at least stable disease by RECIST for 12 or more weeks, broad induction of immune cytokines and effector molecules was observed (Stein et al., 2019). Also, increased intratumoral infiltration of cytotoxic NK cells and granzyme B was observed in a metastatic prostate cancer patient in response to ONC201.

In a recent review article, Karp and Lyakhovich outlined antibiotics that, by inducing mitochondrial dysfunction, hinder OXPHOS and the rate of oxygen consumption, reduce ATP and $\Delta\Psi m$ levels, and increase ROS (Karp and Lyakhovich, 2022). Antibiotics act on the prokaryotic ribosomal complex by binding to the bacterial 30S ribosomal subunit, thus preventing association with aminoacyl transfer RNAs (tRNAs) and counteract translation with a consequent bacteriostatic effect (Luger et al., 2018). Translation of mitochondria-encoded proteins occurs within the mitoribosome organelle and produces 13 proteins that are components of respiratory complexes (Luger et al., 2018). The evolutionary conserved link between mitochondria and bacteria supports the use of these drugs to target CSC metabolism (Luger et al., 2018; Karp and Lyakhovich, 2022). Bedaquiline is an anti-

TABLE 1 Clinical trials investigating the outcomes of the treatments of refractory tumors with inhibitors of mitochondrial respiratory complexes.

Title	ClinicalTrials.gov ID	Phase	Primary outcome measure	Study completion, actual/estimated	Enrollment, actual/estimated
Oxidative Phosphorylation Inhibitor IACS-010759 in Treating Patients With Relapsed or Refractory Acute Myeloid Leukemia	NCT02882321	1	Maximum tolerated dose	2022–04	17
			Clinical response (duration, progression free survival, overall survival)	The study terminated for apparent lack of effectiveness	
A Study to Determine if the Drug, Pyrvinium Pamoate, is Safe and Tolerable in Patients With Pancreatic Cancer	NCT05055323	1	Safety and tolerability	2024–04	18
			Pharmacokinetic, pharmacodynamic profile and bioavailability in humans		
Atovaquone With Radical ChemorADIotherapy in Locally Advanced NSCLC (ARCADIAN)	NCT04648033	1	Dose limiting toxicity; maximum tolerated dose; recommended phase II dose	2023–10	21
Repurposing Atovaquone for the Treatment of Platinum-Resistant Ovarian Cancer	NCT05998135	2	Progression free survival	2025–06	28
Atovaquone (Mepron®) Combined With Conventional Chemotherapy for *de Novo* Acute Myeloid Leukemia (AML) (ATACC AML)	NCT03568994	1	Atovaquone plasma levels at time points including bone marrow assessment. Toxicity and steady state concentrations when given in combination with standard chemotherapy	2025–10	26
Niclosamide in Pediatric Patients With Relapsed and Refractory AML	NCT05188170	1	Dose-limiting toxicity; clinical response	2026–12	16
Enzalutamide and Niclosamide in Treating Patients With Recurrent or Metastatic Castration-Resistant Prostate Cancer	NCT03123978	1	Safety and recommended dose	2022–04	6
Abiraterone Acetate, Niclosamide, and Prednisone in Treating Patients With Hormone-Resistant Prostate Cancer	NCT02807805	2	PSA response rate; dose limiting toxicity; clinical response	2024–06	37

microbial agent that is approved by the FDA for the treatment of resistant tuberculosis. It significantly blocks the expansion CSCs generated by breast cancer MCF7 cell line, as determined by reduced expression of CD44 and ALDH1, under anchorage-independent growth conditions and the mammosphere assay (Fiorillo et al., 2016a). Several preclinical studies support efficacy of doxycycline against CSCs (Lamb et al., 2015; Yang et al., 2015; Liu et al., 2022). Lamb et al. found that doxycycline was effective against tumor-sphere formation across different cancer types including breast, ovarian, prostate, lung, pancreatic cancers, melanoma, and glioblastoma (Lamb et al., 2015). In early breast cancer patients, Scatena et al. conducted a clinical pilot study with doxycycline finding a significant decrease in cancer tissues of two CSC markers, namely, CD44 and ALDH1 (Scatena et al., 2018). Yang et al. show that doxycycline severely affected colony formation and viability of human cervical carcinoma stem cells (He-La CSCs), decreased expression of SOX-2 and surface markers CD133 and CD49f. Moreover, upon injection into NOD-SCID mice the doxycycline pretreated HeLa-CSCs had drastically reduced capacity of tumor growth (Yang et al., 2015). Liu et al. showed that the drug significantly inhibited the CSC-like properties of pancreatic cancer cells, namely, mammosphere formation and CD133 expression (Liu et al., 2022). Treatment of Panc-1 with doxycycline significantly enhanced the effect of chemotherapy drugs (i.e., cisplatin, oxaliplatin, 5-FU, sorafenib, and gemcitabine) in comparison with the results obtained when only chemotherapy drugs were used. Among the antibiotics with preclinical evidence of efficacy to suppress CSCs, for which we refer *ad hoc* review articles (Karp and Lyakhovich, 2022; Garimella et al., 2023), doxycycline, a tetracycline derivative is the most investigated in clinical trials. Clinical trials investigating the drug alone or in combination with standard therapy involve varied tumors, among which: pancreatic cancer (phase 2, NCT02775695); pleural neoplasm (observational, NCT03465774; interventional, NCT02583282; phase 2, NCT01411202); cutaneous T-cell lymphoma (phase 2, NCT02341209); advanced melanoma, in association with temozolomide and ipilimumab (phase 1, NCT01590082); relapsed NHL (phase 2, NCT02086591); bone metastatic breast cancer, in association with bisphosphonates (NCT01847976); in localized breast cancer and uterine cancer (phase2, NCT02874430) or head and neck cancer (phase 2, NCT03076281), in association with metformin. Tigecycline, a glycylcycline designed to overcome tetracycline resistance was shown to interfere with the generation of CSCs ($LGR5^+CD44^+$) in a colon adenocarcinoma murine model (Ruiz-Malagón et al., 2023). Moreover, tigecycline impacted tumorsphere formation in a number of cancer cell lines, including ER (−) breast, ovarian, lung, prostate, and pancreatic cancers and melanoma (Lamb et al., 2015). Currently, tigecycline is investigated in acute and chronic myeloid leukemia (phase 1, NCT01332786; observational, NCT02883036). The macrolide azithromycin exerted a very

TABLE 2 Clinical trials investigating the outcomes of tumor treatments with ONC2091 and ONC206 (Imipridones).

Title	ClinicalTrials.gov ID	Phase	Primary outcome measure	Study completion, actual/estimated	Enrollment, actual/estimated
Testing ONC201 to Prevent Colorectal Cancer	NCT05630794	1	To determine the optimal cancer preventive dose of ONC201	2028-01-01	24
ONC201 in Pediatric H3 K27M Gliomas	NCT03416530	1	Determination of recommended Phase 2 dose, as a single agent or in combination with radiation	2023-09-30 active	130
ONC201 and Atezolizumab in Obesity-Driven Endometrial Cancer	NCT05542407	1	Determination of recommended phase 2 dose in combination with Atezolizumab; tumor response according to RECIST Criteria	2025-01-15	58
ONC201 in Adults with Recurrent H3 K27M-mutant Glioma	NCT03295396	2	Overall response rate	2023-09-30 active	95
Oral ONC201 in Recurrent GBM, H3 K27M Glioma, and Midline Glioma	NCT02525692	2	Progression-free survival as assessed by using RANO-HGG criteria	2023–12 active	89
ONC201 in Recurrent or Metastatic Type II Endometrial Cancer Endometrial Cancer	NCT03485729	2	Progression-free survival	2022-12-31 active	30
ONC201 for the Treatment of Newly Diagnosed H3 K27M-mutant Diffuse Glioma Following Completion of Radiotherapy: A Randomized, Double-Blind, Placebo-Controlled, Multicenter Study	NCT05580562	3	Overall survival; progression free survival as assessed by using RANO-HGG criteria	2026–08	450
Phase II Study of ONC201 Plus Weekly Paclitaxel in Patients with Platinum-Resistant Refractory or Recurrent Epithelial Ovarian, Fallopian Tube, or Primary Peritoneal Cancer	NCT04055649	2	Incidence of treatment related adverse events; incidence of dose limiting toxicities	2026-04-28	62
			objective response rate		
			progression free survival		
Phase I/II Study of Oral ONC201 in Patients with Relapsed or Refractory Acute Leukemias and High-Risk Myelodysplastic Syndromes	NCT02392572	1 and 2	Maximum tolerated dose (Phase I); objective response (Phase II)	2024-11-30	120
Phase I Study of Oral ONC206 in Recurrent and Rare Primary Central Nervous System Neoplasms	NCT04541082	1	Maximum tolerated dose of single-agent, oral; number of participants who experienced dose-limiting toxicities	2025–02	102
ONC206 for Treatment of Newly Diagnosed, Recurrent Diffuse Midline Gliomas, and Other Recurrent Malignant CNS Tumors (PNOC023)	NCT04732065	1	Proportion of participants with dose-limiting toxicities; maximum tolerated dose	2027-12-31	256

significant inhibitory effect on mammosphere formation when combined with doxycycline (Fiorillo et al., 2019). It is investigated in Familial Adenomatous Polyposis (FAP) carrying premature nonsense mutations (phase 4, NCT04454151). Table 3 resumes active or recently completed clinical trials investigating outcomes of antibiotics in refractory tumors.

CPI-613 (devimistat) is a nonredox active lipoate analog developed by Cornerstone Pharmaceuticals. CPI-613 mimics the cofactor of the E2 catalytic subunit of pyruvate dehydrogenase and ketoglutarate dehydrogenase (Stuart et al., 2014), inhibiting the enzymatic activity of these complexes operating on the TCA cycle (Stuart et al., 2014) and impairs ATP synthesis (Anderson et al., 2022). Also, TCA cycle inhibition leads to increased mitochondrial turnover due to mitophagy (Anderson et al., 2022).

In ovarian cancer, CPI-613 treatment was found to negatively impact CSC-rich spheres and resulted in a decrease in tumorigenicity *in vivo*. Moreover, CPI-613 treatment induced a decrease in $CD133^+$ and $CD117^+$ cell frequency *in vitro* and *in vivo* (Bellio et al., 2019). In early clinical trials in pancreatic cancer patients, devimistat produced impressive response rates (Alistar et al., 2017) leading to a phase 3 clinical trial (Philip et al., 2019). Moreover, in preclinical models, devimistat sensitized AML cells to chemotherapy and decreased mitochondrial respiration, leading to a phase I study in relapsed and refractory AML patients (Pardee et al., 2018). However, devimistat did not improve overall survival in the multi-center phase 3 randomized clinical trial (NCT03504423) where 528 patients with metastatic pancreatic adenocarcinoma were randomized to receive either devimistat in combination

TABLE 3 Clinical trials investigating the outcomes of tumor treatments with antibiotics.

Title	ClinicalTrials.gov ID	Phase	Primary outcome measure	Study completion, actual/estimated	Enrollment, actual/estimated
Efficacy of Doxycycline on Metakaryote Cell Death in Patients with Resectable Pancreatic Cancer	NCT02775695	2	The number of dead/dying metakaryotes per 1 g of tissue. and the plasma drug concentrations	2022–05	12
Indwelling Pleural Catheters with or without Doxycycline in Treating Patients With Malignant Pleural Effusions	NCT03465774	Observational	Time to pleural catheter removal; recurrence of effusion; quality-adjusted survival; dyspnea	2025–04	208
Metformin Hydrochloride and Doxycycline in Treating Patients with Localized Breast or Uterine Cancer	NCT02874430	2	To percentage of cells that express caveolin-1, MCT1, MCT4 and TOMM20 at baseline and after treatment; safety and tolerability	2023–06	27
Azithromycin Treatment for Readthrough of APC Gene Stop Codon Mutations in Familial Adenomatous Polyposis (FAP)	NCT04454151	4	Evaluation of changes in number and size of adenomas measured by upper endoscopy	2022–04	10

with modified Folfirinox or Folfirinox (Rafael Pharmaceuticals, Inc., 2021). Similarly, the phase 3 study ARMADA 2000 (NCT03504410) was not completed due to a lack of efficacy in patients with relapsed or refractory AML (Anderson et al., 2022). Despite preliminary unsuccessful results, investigations in the clinics continue with the aim of assessing with more precision devimistat capabilities against difficult-to-treat tumors and defining the best condition for devimistat use. Table 4 lists active clinical trials evaluating this drug in the treatment of advanced/refractory tumors. Figure 4 illustrates the mechanism of action of anti-mitochondrial drugs used in clinical trials.

OXPHOS-targeted drugs affect TAMs

Several studies suggest that the effects of pharmacological agents inhibiting mitochondrial metabolism, well reported for bulk tumor cells and cancer stem cells, extend beyond tumor cells and apply also to TAMs, which can contribute to their efficacy. Metformin has the potential to shift the balance of TAMs from an immunosuppressive M2 phenotype to an antitumor M1 phenotype (Wu et al., 2022; Abdelmoneim et al., 2023). A plethora of studies on different cancer models report its efficacy against TAMs (Liu et al., 2018; Wang et al., 2020; Munoz et al., 2021; Wei et al., 2021; Kang et al., 2022; Taylor et al., 2022; Cao et al., 2023). In mice-bearing prostate tumors, metformin remarkably suppressed the infiltration of TAMs mechanistically by inhibiting the cyclooxygenase-COX-2/prostaglandin-PGE2 axis in tumors. The reduction of TAMs following administration of metformin was responsible for the suppression of tumor growth and metastasis (Liu et al., 2018). Evaluating matched pre- and post-treatment tumor specimens from esophageal cancer patients in a phase II clinical trial of low-dose metformin treatment found significant changes in the TME. Precisely, metformin produced a decrease in tumor-promoting $CD163^+$ macrophages and an increase in tumor-suppressive $CD11c^+$ macrophages, in $CD8^+$ cytotoxic T lymphocytes and $CD20^+$ B lymphocytes. Also, metformin augmented macrophage-mediated phagocytosis of esophageal cancer cells *in vitro*. Similar results of TME reprogramming were obtained with short-term metformin treatment of an esophagus cancer mouse model together with inhibition of tumor growth. (Wang et al., 2020). Employing microparticles loading metformin, Wei et al. showed their efficacy in repolarizing M2-like TAMs to into M1-like phenotype and remodeling TME by increasing the recruitment of $CD8^+$ T cells into tumor tissues and decreasing immunosuppressive infiltration of myeloid-derived suppressor cells and regulatory T cells (Wei et al., 2021). Metformin combined with a tumor vaccine significantly increased the expression of M1 markers CD86 and MHC-II in TME, reduced tumor growth and inhibited lung metastasis in select tumor models (Munoz et al., 2021). A study on epithelial ovarian cancer patients showed that metformin combined with platinum, in comparison with platinum alone, significantly reduced $CD68^+$ macrophages and cancer-associated MSCs in TME of 38 cancer samples (Taylor et al., 2022). Two studies of colorectal cancer TME showed that metformin decreases $CD206^+$ and $CD163^+$ M2 macrophages in an AMPK-dependent manner (Kang et al., 2022) and promotes the polarization of TAMs to M1 through inhibition of HIF-1α and mTOR signal (Cao et al., 2023). A role for tamoxifen in TAM reprogramming to the M1 phenotype has been demonstrated in pituitary adenoma, resulting in inhibition of the migration of cancer cells. Mechanistically, such reprogramming was mediated by STAT6 inactivation and inhibition of the macrophage-specific protein tyrosine phosphatase SHP (Lv et al., 2022). Tamoxifen in combination with clodronate caused TAM depletion in castration-resistant ER-positive subtype of prostate cancer tumors (Semenas et al., 2021). It should be however noted that an expansion of an M2 population in the TME connoted tamoxifen resistance in the postmenopausal breast cancer (Xuan et al., 2014). Atovaquone, used within a stabilizer drug delivery platform composed by protoporphyrin IX nanoparticles, induced M2-type TAMs polarization toward M1-type TAMs, transforming "cold tumor" into "hot tumor" and synergized with anti-PD-L1 immunotherapy in a murine model of colon carcinoma (Feng et al., 2023). ONC201 affects macrophage immunometabolism and leads to a pro-inflammatory TME in glioblastoma (Geiß et al., 2021).

TABLE 4 Clinical trials investigating the outcomes of the treatments of refractory tumors with CPI-613 (Devimistat).

Title	ClinicalTrials.gov ID	Phase	Primary outcome measure	Study completion, actual/estimated	Enrollment, actual/estimated
A Study of CPI-613 for Patients with Relapsed or Refractory Burkitt Lymphoma/Leukemia or High-Grade B-Cell Lymphoma with High-Risk Translocations	NCT03793140	2	Overall response rate will be defined as rate of complete response + partial response + minor response + stable disease as determined as per the criteria for response assessment in lymphoma (RECIL)	2024–12	24
Open Label Phase I/II Clinical Trial to Evaluate CPI-613 in Patients with Advanced Malignancies	NCT00741403	1	To evaluate the safety, tolerability, maximum tolerated dose, and efficacy pharmacokinetics of CPI-613 given twice weekly for three consecutive weeks in cancer patients	2016–12 actual	39
Phase 2 Safety, Tolerability and Efficacy Study of CPI-613 in Cancer Patients	NCT01832857	2	Overall survival	2016–12 actual	7
CPI-613 (Devimistat) in Combination with Chemoradiation in Patients with Pancreatic Adenocarcinoma	NCT05325281	1	Maximum tolerated dose will be determined by testing increasing doses of CPI-613, starting from 500 mg/m2 and up to 1,500 mg/m2, on dose escalation cohorts of three patients in combination with Gem-RT therapy	2027–08	24
A Study of CPI-613 for Patients with Relapsed or Refractory Burkitt Lymphoma/Leukemia or High-Grade B-Cell Lymphoma with High-Risk Translocations	NCT03793140	2	Overall response rate will be defined as rate of complete response + partial response + minor response + stable disease as determined as per the criteria for response assessment in lymphoma (RECIL)	2024–12	24
CPI-613 in Combination with Modified FOLFIRINOX in Locally Advanced Pancreatic Cancer	NCT03699319	1 and 2	Overall survival Maximum tolerated dose of CPI-613 in combination with mFOLFIRINOX in the added small cohort of participants with higher doses of CPI-613 developed to redefine maximum tolerated dose	2024–10	49
CPI-613 Given with Metformin in Patients with Relapsed or Refractory Acute Myeloid Leukemia (AML)	NCT05854966	2	Number of participants to receive at least one cycle of maintenance therapy -feasibility	2025–09	17
CPI-613 in Combination with Bendamustine in Patients with Relapsed/Refractory T-Cell Non-Hodgkin Lymphoma	NCT04217317	2	Number of participants to successfully complete therapy regimen	2025–06	12
Gemcitabine and Cisplatin with or Without CPI-613 as First Line Therapy for Patients with Advanced Unresectable Biliary Tract Cancer (BilT-04)	NCT04203160	1 and 2	Maximum tolerated dose Overall response rate according to the RECIST criteria	2025–06	78
CPI-613 (Devimistat) in Combination with Hydroxychloroquine and 5-fluorouracil or Gemcitabine in Treating Patients with Advanced Chemorefractory Solid Tumors	NCT05733000	2	Overall response rate according to the RECIST criteria	2030-03-04	94

Doxycycline inhibits M2-type polarization of human and bone marrow-derived mouse macrophages in a dose-dependent manner and *in vivo* M2-mediated neovascularization in a laser injury model of choroidal neovascularization (He and Marneros, 2014). In pulmonary metastases of osteosarcoma, doxycycline affects macrophage polarization by skewing the tumor induced M2-like TAMs to anti-tumor M1-like subsets, through this mechanism it prevents the progress of pulmonary micro-metastases to macro-metastases at early-stage disease. (Hadjimichael et al., 2022). Table 5 illustrates studies investigating the effects of OXPHOS-targeted drugs on TAMs.

Non-pharmacological disruption of energy metabolism

Studies conducted on triple-negative breast cancer (TNBC) suggest that starvation could have a therapeutic value in cancer.

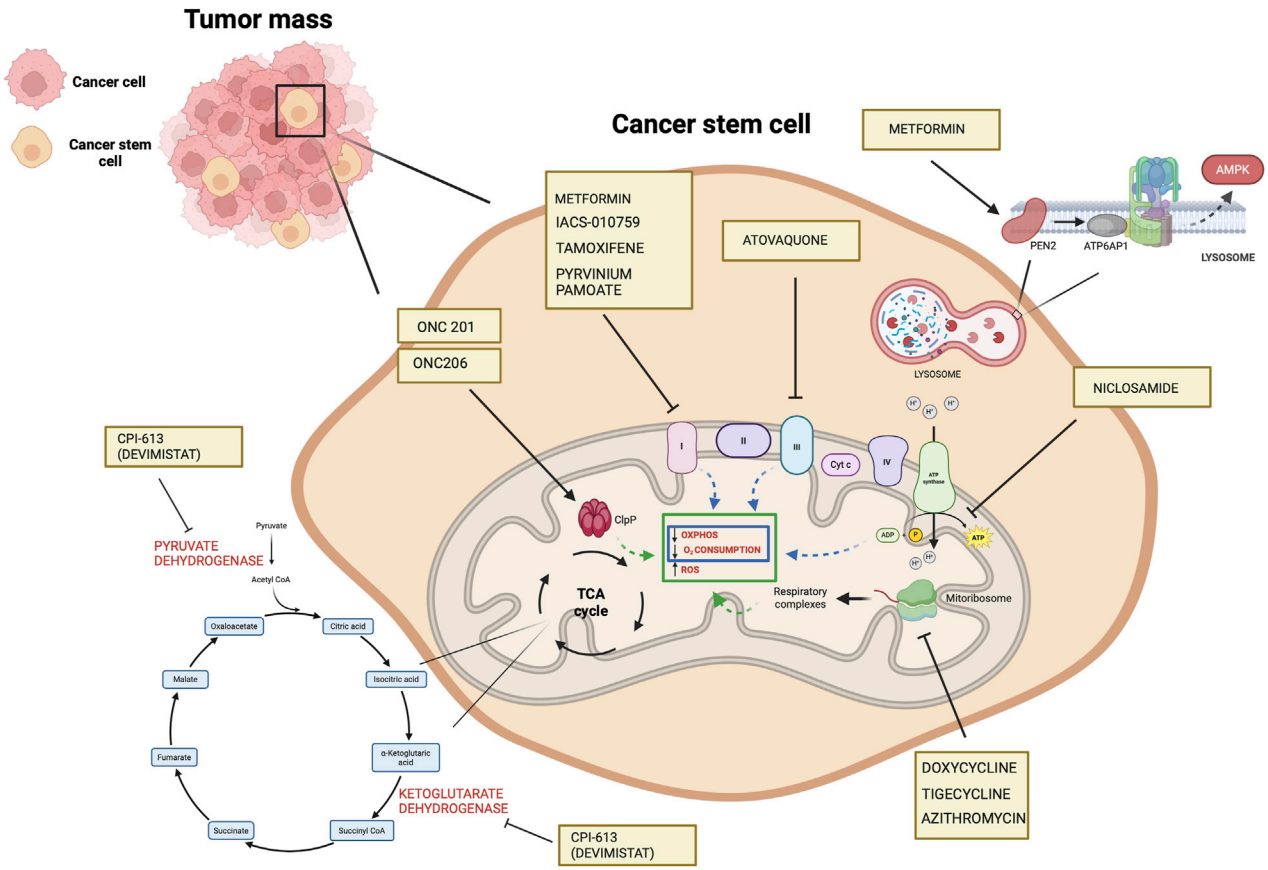

FIGURE 4
Mechanisms of the mitochondrial drugs used in clinical trials that have been shown to target CSCs in preclinical setting (https://www.clinicaltrials.gov). The illustration was started from scratch, created with BioRender.com original design.

Specifically, Salvadori et al., showed that fasting mimicking (FMD) starvation produced a significant impairment of CSCs ($CD44^{+}CD24^{-}$) compared with non-CSC in TNBC murine model and decreased mammosphere generation and volume. FMD delayed tumor progression in a syngeneic TNBC mouse model. Moreover, combining FMD cycles with PI3K/AKT/mTOR inhibitors resulted in long-term animal survival and reduced the treatment-induced side effects (Salvadori et al., 2021). The authors suggest that FMD-induced depletion of TNBC CSCs when tumors are in a less advanced stage could enormously enhance the efficacy of subsequent treatments targeting both CSCs (such as the FMD) and more differentiated cancer cells (such as PI3K/AKT/mTORC1 inhibitors) in late-stage cancers (Salvadori et al., 2021).

Similarly, Pateras et al. showed that short-term starvation increased sensitivity to DNA-damaging chemotherapeutic agents (doxorubicin or cisplatin) and inhibited oxidative stress-induced DNA damage repair in TBNC cells. Mechanistically, the combination of STS and chemotherapy-induced an increase of ROS production in such cancer cells through a collapse of mitochondrial respiration and an altered ATP production. In contrast, in normal, non-transformed cells, this combination has a protective effect (Pateras et al., 2023). The reasons for the differential response of normal *versus* cancer cells to dietary restriction remain unknown. More insights into starvation-induced mechanisms may lead to safe and effective anti-cancer treatments and help to overcome the chemotherapy resistance of cancer. Future *ad hoc* designed clinical trials are needed to assess dietary recommendations as an adjunct to chemotherapy for TNBC treatment and to confirm the efficacy of the combined approach.

Concluding remarks

In various tumors, CSCs and their supporting macrophages have been shown to be highly dependent on mitochondrial function and OXPHOS metabolism. Such a metabolic dependency of CSCs has stimulated modern chemotherapy targeting mitochondria/OXPHOS for cancer cure. To date, numerous clinical trials are underway across a wide range of advanced, resistant, and refractory tumors with a wide range of anti-mitochondrial and anti-metabolic agents. Numerous further agents are the subject of preclinical investigations linking laboratory drug discovery to the initiation of human clinical trials. However, the clinical use of pharmacological agents targeting such metabolic vulnerabilities of CSCs presents numerous challenges. There are issues related to the toxicity of antimitochondrial drugs; also, results so far obtained with clinical trials are sometimes vague or unflattering. More studies are needed to codify and quantify drug effects on healthy cells and find a therapeutic window and valuable tools that assist

TABLE 5 Effects of OXPHOS-targeted drugs on TAMs.

Treatment	Effect on TAMs	Mechanism	Cancer Type/Model	Reference
Metformin	Shifts TAMs from M2 to M1 phenotype	COX-2/PGE2 axis inhibition	Prostate tumors	Liu et al. (2018)
		Reprogrammed TAMs ↓CD163+, ↑CD11c+	Esophageal	Wang et al. (2020)
		Increased recruitment of $CD8^+$ T cells	Hepatocellular carcinoma	Wei et al. (2021)
		Reprogrammed TAMs ↑CD86+	Breast cancer	Munoz et al. (2021)
			Lung carcinoma	
			Oral Squamous Cell Carcinoma	
		Reprogrammed TAMs ↓CD68+	Epithelial ovarian cancer	Taylor et al. (2022)
		AMPK-dependent ↓CD206+	Colorectal cancer	Kang et al. (2022)
		HIF-1α and mTOR inhibition	Colorectal cancer	Cao et al. (2023)
Tamoxifen	Shifts TAMs from M2 to M1 phenotype	STAT6 inactivation, SHP inhibition	Pituitary Adenoma	Lv et al. (2022)
	TAMs depletion	PIP5K1α/AKT and MMP9/VEGF axis inhibition	Prostate (ER-positive subtype)	Semenas et al. (2021)
	Expansion of M2 population	↑CD163+ macrophages infiltration	Postmenopausal Breast	Xuan et al. (2014)
Atovaquone	Shifts TAMs from M2 to M1 phenotype	Reprogrammed TAMs ↓CD206+, ↑CD11c+	Colon carcinoma	Feng et al. (2023)
ONC201	Inhibition of OXPHOS	Activation of ClpP	Glioblastoma	Geiß et al. (2021)
Doxycycline	Inhibits M2-type polarization of macrophages	IL-4-induced luciferase activity and MRC1 inhibition	Choroidal neovascularization	He L et al. (2014)
	Shifts TAMs from M2 to M1 phenotype	↓MMPs, ↓VEGF	Pulmonary metastases of osteosarcoma	Hadjimichael et al. (2022)

personalized therapies for precise administration indication. Despite these issues, awareness of the metabolic plasticity of CSCs supports perseverance in the anti-mitochondrial therapeutic approach. An increasing number of investigations of anti-mitochondrial medications in clinical trials are underway to hinder hard-to-treat tumors. The precise definitions of the therapeutic window and dose of the drug, mode of administration, optimization strategies for selective delivery to tumor cells, and combination with distinct targeted agents are currently being investigated in an attempt to guarantee a safety profile and at the same time undermine CSCs and their selection advantage that causes relapse. Moreover, the implementation of *ad hoc* phase 1 and 2 studies could accelerate the combined use of drugs potentially active against CSCs with those of standard cancer protocols, thus improving helpful information to adopt the use of such combination as the first line of intervention against tumors with a high frequency of recurrence.

Limitation

We have not described the influence of all the components of the niches that vary between solid tumor, and leukemia, as well as primary and metastatic tumor. Still, we focused on TAMs because the study of the niche components would have opened up very broad scenarios that deserve to be treated and explored in depth in a separate article. Furthermore, the studies we have presented often extend to the concept of stem cell-like cells and refer to specific tumors and experimental contexts that are not generalizable to different CSCs from all kinds of tumors.

Author contributions

LM: Conceptualization, Writing–original draft, Writing–review and editing, Data curation, Resources, Software. SR: Conceptualization, Data curation, Resources, Writing–original draft, Visualization, Writing–review and editing. CM: Data curation, Visualization, Writing–original draft, Resources. VD: Data curation, Resources, Visualization, Software, Writing–original draft. AC: Data curation, Resources, Visualization, Writing–original draft. RA: Data curation, Resources, Visualization, Writing–original draft. MV: Data curation, Resources, Visualization, Writing–original draft. DF: Data curation, Visualization, Writing–original draft. MR: Visualization, Conceptualization, Funding acquisition, Supervision, Validation, Writing–original draft, Writing–review and editing.

Funding

The author(s) declare financial support was received for the research, authorship, and/or publication of this article. This work was funded by National Center for Gene Therapy and Drugs based on RNA Technology MUR-CN3 CUP E63C22000940007.

Conflict of interest

The authors declare that the research was conducted in the absence of any commercial or financial relationships that could be construed as a potential conflict of interest.

Publisher's note

References

Abdelmoneim, M., Aboalela, M. A., Naoe, Y., Matsumura, S., Eissa, R. I., Bustos-Villalobos, I., et al. (2023). The impact of metformin on tumor-infiltrated immune cells: preclinical and clinical studies. *Int. J. Mol. Sci.* 24 (17), 13353. doi:10.3390/ijms241713353

Abdullah, L. N., and Chow, E. K. (2013). Mechanisms of chemoresistance in cancer stem cells. *Clin. Transl. Med.* 2 (1), 3. doi:10.1186/2001-1326-2-3

Agliano, A., Calvo, A., and Box, C. (2017). The challenge of targeting cancer stem cells to halt metastasis. *Semin. Cancer Biol.* 44, 25–42. doi:10.1016/j.semcancer.2017.03.003

Alistar, A., Morris, B. B., Desnoyer, R., Klepin, H. D., Hosseinzadeh, K., Clark, C., et al. (2017). Safety and tolerability of the first-in-class agent CPI-613 in combination with modified FOLFIRINOX in patients with metastatic pancreatic cancer: a single-centre, open-label, dose-escalation, phase 1 trial. *Lancet Oncol.* 18 (6), 770–778. doi:10.1016/S1470-2045(17)30314-5

Allavena, P., Digifico, E., and Belgiovine, C. (2021). Macrophages and cancer stem cells: a malevolent alliance. *Mol. Med.* 27 (1), 121. doi:10.1186/s10020-021-00383-3

Altenberg, B., and Greulich, K. O. (2004). Genes of glycolysis are ubiquitously overexpressed in 24 cancer classes. *Genomics* 84 (6), 1014–1020. doi:10.1016/j.ygeno.2004.08.010

Anderson, R., Miller, L. D., Isom, S., Chou, J. W., Pladna, K. M., Schramm, N. J., et al. (2022). Phase II trial of cytarabine and mitoxantrone with devimistat in acute myeloid leukemia. *Nat. Commun.* 13 (1), 1673. doi:10.1038/s41467-022-29039-4

Ayob, A. Z., and Ramasamy, T. S. (2018). Cancer stem cells as key drivers of tumour progression. *J. Biomed. Sci.* 25 (1), 20. doi:10.1186/s12929-018-0426-4

Baccelli, I, and Trumpp, A., (2012). The evolving concept of cancer and metastasis stem cells. *J. Cell Biol.* 198 (3), 281–293. doi:10.1083/jcb.201202014

Basak, U., Sarkar, T., Mukherjee, S., Chakraborty, S., Dutta, A., Dutta, S., et al. (2023). Tumor-associated macrophages: an effective player of the tumor microenvironment. *Front. Immunol.* 14, 1295257. doi:10.3389/fimmu.2023.1295257

Batoon, L., and McCauley, L. K. (2021). Cross talk between macrophages and cancer cells in the bone metastatic environment. *Front. Endocrinol. (Lausanne)* 12, 763846. doi:10.3389/fendo.2021.763846

Begicevic, R. R., and Falasca, M. (2017). ABC transporters in cancer stem cells: beyond chemoresistance. *Int. J. Mol. Sci.* 18 (11), 2362. doi:10.3390/ijms18112362

Belisario, D. C., Kopecka, J., Pasino, M., Akman, M., De Smaele, E., Donadelli, M., et al. (2020). Hypoxia dictates metabolic rewiring of tumors: implications for chemoresistance. *Cells* 9 (12), 2598. doi:10.3390/cells9122598

Bellio, C., DiGloria, C., Spriggs, D. R., Foster, R., Growdon, W. B., and Rueda, B. R. (2019). The metabolic inhibitor CPI-613 negates treatment enrichment of ovarian cancer stem cells. *Cancers (Basel)* 11 (11), 1678. doi:10.3390/cancers11111678

Bonnet, D., and Dick, J. E. (1997). Human acute myeloid leukemia is organized as a hierarchy that originates from a primitive hematopoietic cell. *Nat. Med.* 3 (7), 730–737. doi:10.1038/nm0797-730

Bononi, G., Masoni, S., Di Bussolo, V., Tuccinardi, T., Granchi, C., and Minutolo, F. (2022). Historical perspective of tumor glycolysis: a century with Otto Warburg. *Semin. Cancer Biol.* 86 (Pt 2), 325–333. doi:10.1016/j.semcancer.2022.07.003

Borin, T. F., Angara, K., Rashid, M. H., Achyut, B. R., and Arbab, A. S. (2017). Arachidonic acid metabolite as a novel therapeutic target in breast cancer metastasis. *Int. J. Mol. Sci.* 18 (12), 2661. doi:10.3390/ijms18122661

Borriello, L., Coste, A., Traub, B., Sharma, V. P., Karagiannis, G. S., Lin, Y., et al. (2022). Primary tumor associated macrophages activate programs of invasion and dormancy in disseminating tumor cells. *Nat. Commun.* 13 (1), 626. doi:10.1038/s41467-022-28076-3

Brown, J. R., Chan, D. K., Shank, J. J., Griffith, K. A., Fan, H., Szulawski, R., et al. (2020). Phase II clinical trial of metformin as a cancer stem cell-targeting agent in ovarian cancer. *JCI Insight* 5 (11), e133247. doi:10.1172/jci.insight.133247

Bruns, I., Sauer, B., Burger, M. C., Eriksson, J., Hofmann, U., Braun, Y., et al. (2019). Disruption of peroxisome proliferator-activated receptor γ coactivator (PGC)-1α reverts key features of the neoplastic phenotype of glioma cells. *J. Biol. Chem.* 294 (9), 3037–3050. doi:10.1074/jbc.RA118.006993

Campbell, P. J., Yachida, S., Mudie, L. J., Stephens, P. J., Pleasance, E. D., Stebbings, L. A., et al. (2010). The patterns and dynamics of genomic instability in metastatic pancreatic cancer. *Nature* 467 (7319), 1109–1113. doi:10.1038/nature09460

Cao, Y., Wo, M., Xu, C., Fei, X., Jin, J., and Shan, Z. (2023). An AMPK agonist suppresses the progress of colorectal cancer by regulating the polarization of TAM to M1 through inhibition of HIF-1α and mTOR signal pathway. *J. Cancer Res. Ther.* 19 (6), 1560–1567. doi:10.4103/jcrt.jcrt_2670_22

Chae, C. W., Choi, G., Kim, Y. J., Cho, M., Kwon, Y. W., and Kim, H. S. (2023). The maintenance mechanism of hematopoietic stem cell dormancy: role for a subset of macrophages. *BMB Rep.* 56 (9), 482–487. doi:10.5483/BMBRep.2023-0092

Chawla, A. (2010). Control of macrophage activation and function by PPARs. *Circ. Res.* 106 (10), 1559–1569. doi:10.1161/CIRCRESAHA.110.216523

Chen, W., Mook, R. A., Jr., Premont, R. T., and Wang, J. (2018). Niclosamide: beyond an antihelminthic drug. *Cell Signal* 41, 89–96. doi:10.1016/j.cellsig.2017.04.001

Cole, A. J., Fayomi, A. P., Anyaeche, V. I., Bai, S., and Buckanovich, R. J. (2020). An evolving paradigm of cancer stem cell hierarchies: therapeutic implications. *Theranostics* 10 (7), 3083–3098. doi:10.7150/thno.41647

Curry, J. M., Tuluc, M., Whitaker-Menezes, D., Ames, J. A., Anantharaman, A., Butera, A., et al. (2013). Cancer metabolism, stemness and tumor recurrence: MCT1 and MCT4 are functional biomarkers of metabolic symbiosis in head and neck cancer. *Cell Cycle* 12 (9), 1371–1384. doi:10.4161/cc.24092

Decensi, A., Puntoni, M., Goodwin, P., Cazzaniga, M., Gennari, A., Bonanni, B., et al. (2010). Metformin and cancer risk in diabetic patients: a systematic review and meta-analysis. *Cancer Prev. Res. (Phila)* 3 (11), 1451–1461. doi:10.1158/1940-6207.CAPR-10-0157

De Luca, A., Fiorillo, M., Peiris-Pagès, M., Ozsvari, B., Smith, D. L., Sanchez-Alvarez, R., et al. (2015). Mitochondrial biogenesis is required for the anchorage-independent survival and propagation of stem-like cancer cells. *Oncotarget* 6 (17), 14777–14795. doi:10.18632/oncotarget.4401

Ding, Y., Labitzky, V., Legler, K., Qi, M., Schumacher, U., Schmalfeldt, B., et al. (2021). Molecular characteristics and tumorigenicity of ascites-derived tumor cells: mitochondrial oxidative phosphorylation as a novel therapy target in ovarian cancer. *Mol. Oncol.* 15 (12), 3578–3595. doi:10.1002/1878-0261.13028

Diskin, C., Ryan, T. A. J., and O'Neill, L. A. J. (2021). Modification of proteins by metabolites in immunity. *Immunity* 54 (1), 19–31. doi:10.1016/j.immuni.2020.09.014

Dudgeon, C., Harris, C. R., Chen, Y., Ghaddar, B., Sharma, A., and Shah, M. M., (2020), A novel model of pancreatic cancer dormancy reveals mechanistic insights and a dormancy gene signature with human relevance, *bioRxiv* 2020.04.13.037374. doi:10.1101/2020.04.13.037374

Emtenani, S., Martin, E. T., Gyoergy, A., Bicher, J., Genger, J. W., Köcher, T., et al. (2022). Macrophage mitochondrial bioenergetics and tissue invasion are boosted by an Atossa-Porthos axis in Drosophila. *EMBO J.* 41 (12), e109049. doi:10.15252/embj.2021109049

Enderling, H., Almog, N., and Hlatky, L. (2013). *Systems biology of tumor dormancy*. New York, NY, USA: Springer. doi:10.1007/978-1-4614-1445-2

Entenberg, D., Voiculescu, S., Guo, P., Borriello, L., Wang, Y., Karagiannis, G. S., et al. (2018). A permanent window for the murine lung enables high-resolution imaging of cancer metastasis. *Nat. Methods* 15 (1), 73–80. doi:10.1038/nmeth.4511

Evans, A. J., Sawyez, C. G., Wolfe, B. M., Connelly, P. W., Maguire, G. F., and Huff, M. W. (1993). Evidence that cholesteryl ester and triglyceride accumulation in J774 macrophages induced by very low-density lipoprotein subfractions occurs by different mechanisms. *J. Lipid Res.* 34 (5), 703–717. doi:10.1016/s0022-2275(20)39692-9

Fan, M., Shi, Y., Zhao, J., and Li, L. (2023). Cancer stem cell fate determination: mito-nuclear communication. *Cell Commun. Signal* 21 (1), 159. doi:10.1186/s12964-023-01160-x

Fan, Q. M., Jing, Y. Y., Yu, G. F., Kou, X. R., Ye, F., Gao, L., et al. (2014). Tumor-associated macrophages promote cancer stem cell-like properties via transforming growth factor-beta1-induced epithelial–mesenchymal transition in hepatocellular carcinoma. *Cancer Lett.* 352 (2), 160–168. doi:10.1016/j.canlet.2014.05.008

Feng, X., Chen, Z., Liu, Z., Fu, X., Song, H., and Zhang, Q. (2023). Self-delivery photodynamic-hypoxia alleviating nanomedicine synergizes with anti-PD-L1 for cancer immunotherapy. *Int. J. Pharm.* 639, 122970. doi:10.1016/j.ijpharm.2023.122970

Fiorillo, M., Lamb, R., Tanowitz, H. B., Cappello, A. R., Martinez-Outschoorn, U. E., Sotgia, F., et al. (2016a). Bedaquiline, an FDA-approved antibiotic, inhibits mitochondrial function and potently blocks the proliferative expansion of stem-like cancer cells (CSCs). *Aging* 8, 1593–1607. doi:10.18632/aging.100983

Fiorillo, M., Lamb, R., Tanowitz, H. B., Mutti, L., Krstic-Demonacos, M., Cappello, A. R., et al. (2016b). Repurposing atovaquone: targeting mitochondrial complex III and OXPHOS to eradicate cancer stem cells. *Oncotarget* 7 (23), 34084–34099. doi:10.18632/oncotarget.9122

Fiorillo, M., Tóth, F., Sotgia, F., and Lisanti, M. P. (2019). Doxycycline, Azithromycin and Vitamin C (DAV): a potent combination therapy for targeting mitochondria and eradicating cancer stem cells (CSCs). *Aging (Albany NY)* 11 (8), 2202–2216. doi:10.18632/aging.101905

Fong, M. Y., Zhou, W., Liu, L., Alontaga, A. Y., Chandra, M., Ashby, J., et al. (2015). Breast-cancer-secreted miR-122 reprograms glucose metabolism in premetastatic niche to promote metastasis. *Nat. Cell Biol.* 17 (2), 183–194. doi:10.1038/ncb3094

Fu, C., Xiao, X., Xu, H., Lu, W., and Wang, Y. (2020). Efficacy of atovaquone on $EpCAM^{+}CD44^{+}$ HCT-116 human colon cancer stem cells under hypoxia. *Exp. Ther. Med.* 20 (6), 286. doi:10.3892/etm.2020.9416

Ganguly, K., and Kimmelman, A. C. (2023). Reprogramming of tissue metabolism during cancer metastasis. *Trends Cancer* 9 (6), 461–471. doi:10.1016/j.trecan.2023.02.005

Gao, C., Shen, Y., Jin, F., Miao, Y., and Qiu, X. (2016). Cancer stem cells in small cell lung cancer cell line H446: higher dependency on oxidative phosphorylation and mitochondrial substrate-level phosphorylation than non-stem cancer cells. *PLoS One* 11 (5), e0154576. doi:10.1371/journal.pone.0154576

Gao, H., Chakraborty, G., Zhang, Z., Akalay, I., Gadiya, M., Gao, Y., et al. (2016). Multi-organ site metastatic reactivation mediated by non-canonical discoidin domain receptor 1 signaling. *Cell* 166 (1), 47–62. doi:10.1016/j.cell.2016.06.009

Garimella, S. V., Gampa, S. C., and Chaturvedi, P. (2023). Mitochondria in cancer stem cells: from an innocent bystander to a central player in therapy resistance. *Stem Cells Cloning* 16, 19–41. doi:10.2147/SCCAA.S417842

Geiß, C., Witzler, C., Poschet, G., Ruf, W., and Régnier-Vigouroux, A. (2022). Metabolic and inflammatory reprogramming of macrophages by ONC201 translates in a pro-inflammatory environment even in presence of glioblastoma cells. *Eur. J. Immunol.* 2021 (5), 1246–1261. doi:10.1002/eji.202048957

Giddings, E. L., Champagne, D. P., Wu, M. H., Laffin, J. M., Thornton, T. M., Valenca-Pereira, F., et al. (2021). Mitochondrial ATP fuels ABC transporter-mediated drug efflux in cancer chemoresistance. *Nat. Commun.* 12 (1), 2804. doi:10.1038/s41467-021-23071-6

Gonzalez, M. A., Lu, D. R., Yousefi, M., Kroll, A., Lo, C. H., Briseño, C. G., et al. (2023). Phagocytosis increases an oxidative metabolic and immune suppressive signature in tumor macrophages. *J. Exp. Med.* 220 (6), e20221472. doi:10.1084/jem.20221472

Greer, Y. E., Hernandez, L., Fennell, E. M. J., Kundu, M., Voeller, D., Chari, R., et al. (2022). Mitochondrial matrix protease ClpP agonists inhibit cancer stem cell function in breast cancer cells by disrupting mitochondrial homeostasis. *Cancer Res. Commun.* 2 (10), 1144–1161. doi:10.1158/2767-9764.CRC-22-0142

Hadjimichael, A. C., Foukas, A. F., Papadimitriou, E., Kaspiris, A., Peristiani, C., Chaniotakis, I., et al. (2022). Doxycycline inhibits the progression of metastases in early-stage osteosarcoma by downregulating the expression of MMPs, VEGF and ezrin at primary sites. *Cancer Treat. Res. Commun.* 32, 100617. doi:10.1016/j.ctarc.2022.100617

Hanahan, D. (2022). Hallmarks of cancer: new dimensions. *Cancer Discov.* 12 (1), 31–46. doi:10.1158/2159-8290.CD-21-1059

Hatle, K. M., Gummadidala, P., Navasa, N., Bernardo, E., Dodge, J., Silverstrim, B., et al. (2013). MCJ/DnaJC15, an endogenous mitochondrial repressor of the respiratory chain that controls metabolic alterations. *Mol. Cell Biol.* 33 (11), 2302–2314. doi:10.1128/MCB.00189-13

He, L., Bhat, K., Ioannidis, A., Zhang, L., Nguyen, N. T., Allen, J. E., et al. (2021). Effects of the DRD2/3 antagonist ONC201 and radiation in glioblastoma. *Radiother. Oncol.* 161, 140–147. doi:10.1016/j.radonc.2021.05.027

He, L., and Marneros, A. G. (2014). Doxycycline inhibits polarization of macrophages to the proangiogenic M2-type and subsequent neovascularization. *J. Biol. Chem.* 289 (12), 8019–8028. doi:10.1074/jbc.M113.535765

Hermann, P. C., Huber, S. L., Herrler, T., Aicher, A., Ellwart, J. W., Guba, M., et al. (2007). Distinct populations of cancer stem cells determine tumor growth and metastatic activity in human pancreatic cancer. *Cell Stem.* 1 (3), 313–323. doi:10.1016/j.stem.2007.06.002

Hirsch, H. A., Iliopoulos, D., Tsichlis, P. N., and Struhl, K. (2009). Metformin selectively targets cancer stem cells, and acts together with chemotherapy to block tumor growth and prolong remission. *Cancer Res.* 69 (19), 7507–7511. doi:10.1158/0008-5472.CAN-09-2994

Hoshino, A., Costa-Silva, B., Shen, T. L., Rodrigues, G., Hashimoto, A., Tesic Mark, M., et al. (2015). Tumour exosome integrins determine organotropic metastasis. *Nature* 527 (7578), 329–335. doi:10.1038/nature15756

Hua, Y., Zheng, Y., Yao, Y., Jia, R., Ge, S., and Zhuang, A. (2023). Metformin and cancer hallmarks: shedding new lights on therapeutic repurposing. *J. Transl. Med.* 21 (1), 403. doi:10.1186/s12967-023-04263-8

Huang, S. C., Everts, B., Ivanova, Y., O'Sullivan, D., Nascimento, M., Smith, A. M., et al. (2014). Cell-intrinsic lysosomal lipolysis is essential for alternative activation of macrophages. *Nat. Immunol.* 15 (9), 846–855. doi:10.1038/ni.2956

Ishizawa, J., Kojima, K., Chachad, D., Ruvolo, P., Ruvolo, V., Jacamo, R. O., et al. (2016). ATF4 induction through an atypical integrated stress response to ONC201 triggers p53-independent apoptosis in hematological malignancies. *Sci. Signal* 9 (415), ra17. doi:10.1126/scisignal.aac4380

Jeon, H. M., Oh, Y. T., Shin, Y. J., Chang, N., Kim, D., Woo, D., et al. (2023). Dopamine receptor D2 regulates glioblastoma survival and death through MET and death receptor 4/5. *Neoplasia* 39, 100894. doi:10.1016/j.neo.2023.100894

Jin, Y., Lu, Z., Ding, K., Li, J., Du, X., Chen, C., et al. (2010). Antineoplastic mechanisms of niclosamide in acute myelogenous leukemia stem cells: inactivation of the NF-kappaB pathway and generation of reactive oxygen species. *Cancer Res.* 70 (6), 2516–2527. doi:10.1158/0008-5472.CAN-09-3950

Jinushi, M., Chiba, S., Yoshiyama, H., Masutomi, K., Kinoshita, I., Dosaka-Akita, H., et al. (2011). Tumor-associated macrophages regulate tumorigenicity and anticancer drug responses of cancer stem/initiating cells. *Proc. Natl. Acad. Sci. U. S. A.* 108 (30), 12425–12430. doi:10.1073/pnas.1106645108

Jones, C. L., Inguva, A., and Jordan, C. T. (2021). Targeting energy metabolism in cancer stem cells: progress and challenges in leukemia and solid tumors. *Cell Stem Cell* 28 (3), 378–393. doi:10.1016/j.stem.2021.02.013

Jordan, C. T. (2004). Cancer stem cell biology: from leukemia to solid tumors. *Curr. Opin. Cell Biol.* 16 (6), 708–712. doi:10.1016/j.ceb.2004.09.002

Joseph, S. S., Tran, D. H. V., Islam, F., and Gopalan, V. (2023). "Cancer stem cells and metastasis," in *Cancer stem cells: basic concept and therapeutic implications*. Editors F. Islam, and A. K. Lam (Singapore: Springer). doi:10.1007/978-981-99-3185-9_8

Kang, J., Lee, D., Lee, K. J., Yoon, J. E., Kwon, J. H., Seo, Y., et al. (2022). Tumor-suppressive effect of metformin via the regulation of M2 macrophages and myeloid-derived suppressor cells in the tumor microenvironment of colorectal cancer. *Cancers (Basel)* 14 (12), 2881. doi:10.3390/cancers14122881

Kapur, A., Mehta, P., Simmons, A. D., Ericksen, S. S., Mehta, G., Palecek, S. P., et al. (2022). Atovaquone: an inhibitor of oxidative phosphorylation as studied in gynecologic cancers. *Cancers (Basel)* 14 (9), 2297. doi:10.3390/cancers14092297

Karp, I., and Lyakhovich, A. (2022). Targeting cancer stem cells with antibiotics inducing mitochondrial dysfunction as an alternative anticancer therapy. *Biochem. Pharmacol.* 198, 114966. doi:10.1016/j.bcp.2022.114966

Khan, I. N., Al-Karim, S., Bora, R. S., Chaudhary, A. G., and Saini, K. S. (2015). Cancer stem cells: a challenging paradigm for designing targeted drug therapies. *Drug Discov. Today* 20 (10), 1205–1216. doi:10.1016/j.drudis.2015.06.013

Kong, S. C., Nøhr-Nielsen, A., Zeeberg, K., Reshkin, S. J., Hoffmann, E. K., Novak, I., et al. (2016). Monocarboxylate transporters MCT1 and MCT4 regulate migration and invasion of pancreatic ductal adenocarcinoma cells. *Pancreas* 45 (7), 1036–1047. doi:10.1097/MPA.0000000000000571

Korn, C., and Méndez-Ferrer, S. (2017). Myeloid malignancies and the microenvironment. *Blood* 129 (7), 811–822. doi:10.1182/blood-2016-09-670224

Kreso, A., and Dick, J. E. (2014). Evolution of the cancer stem cell model. *Cell Stem Cell* 14 (3), 275–291. doi:10.1016/j.stem.2014.02.006

Kuntz, E. M., Baquero, P., Michie, A. M., Dunn, K., Tardito, S., Holyoake, T. L., et al. (2017). Targeting mitochondrial oxidative phosphorylation eradicates therapy-resistant chronic myeloid leukemia stem cells. *Nat. Med.* 23 (10), 1234–1240. doi:10.1038/nm.4399

Ladanyi, A., Mukherjee, A., Kenny, H. A., Johnson, A., Mitra, A. K., Sundaresan, S., et al. (2018). Adipocyte-induced CD36 expression drives ovarian cancer progression and metastasis. *Oncogene* 37 (17), 2285–2301. doi:10.1038/s41388-017-0093-z

Lamb, R., Ozsvari, B., Lisanti, C. L., Tanowitz, H. B., Howell, A., Martinez-Outschoorn, U. E., et al. (2015). Antibiotics that target mitochondria effectively eradicate cancer stem cells, across multiple tumor types: treating cancer like an infectious disease. *Oncotarget* 6 (7), 4569–4584. doi:10.18632/oncotarget.3174

Lapidot, T., Sirard, C., Vormoor, J., Murdoch, B., Hoang, T., Caceres-Cortes, J., et al. (1994). A cell initiating human acute myeloid leukaemia after transplantation into SCID mice. *Nature* 367 (6464), 645–648. doi:10.1038/367645a0

LeBleu, V. S., O'Connell, J. T., Gonzalez Herrera, K. N., Wikman, H., Pantel, K., Haigis, M. C., et al. (2014). PGC-1α mediates mitochondrial biogenesis and oxidative phosphorylation in cancer cells to promote metastasis. *Nat. Cell Biol.* 16 (10), 992–1003. doi:10.1038/ncb3039

Li, H., Feng, Z., and He, M. L. (2020). Lipid metabolism alteration contributes to and maintains the properties of cancer stem cells. *Theranostics* 10 (16), 7053–7069. doi:10.7150/thno.41388

Lim, E., Vaillant, F., Wu, D., Forrest, N. C., Pal, B., Hart, A. H., et al. (2009). Aberrant luminal progenitors as the candidate target population for basal tumor development in BRCA1 mutation carriers. *Nat. Med.* 15 (8), 907–913. doi:10.1038/nm.2000

Linton, K. J., and Higgins, C. F. (2007). Structure and function of ABC transporters: the ATP switch provides flexible control. *Pflugers Arch.* 453 (5), 555–567. doi:10.1007/s00424-006-0126-x

Liu, H., Tao, H., Wang, H., Yang, Y., Yang, R., Dai, X., et al. (2022). Corrigendum: doxycycline inhibits cancer stem cell-like properties *via* PAR1/FAK/PI3K/AKT pathway in pancreatic cancer. *Front. Oncol.* 12, 830506. doi:10.3389/fonc.2022.830506

Liu, Q., Tong, D., Liu, G., Gao, J., Wang, L. A., Xu, J., et al. (2018). Metformin inhibits prostate cancer progression by targeting tumor-associated inflammatory infiltration. *Clin. Cancer Res.* 24 (22), 5622–5634. doi:10.1158/1078-0432.CCR-18-0420

Liu, Y., Xu, R., Gu, H., Zhang, E., Qu, J., Cao, W., et al. (2021). Metabolic reprogramming in macrophage responses. *Biomark. Res.* 9 (1), 1. doi:10.1186/s40364-020-00251-y

Luger, A. L., Sauer, B., Lorenz, N. I., Engel, A. L., Braun, Y., Voss, M., et al. (2018). Doxycycline impairs mitochondrial function and protects human glioma cells from hypoxia-induced cell death: implications of using tet-inducible systems. *Int. J. Mol. Sci.* 19 (5), 1504. doi:10.3390/ijms19051504

Luo, X., Cheng, C., Tan, Z., Li, N., Tang, M., Yang, L., et al. (2017). Emerging roles of lipid metabolism in cancer metastasis. *Mol. Cancer* 16 (1), 76. doi:10.1186/s12943-017-0646-3

Lv, T., Zhang, Z., Yu, H., Ren, S., Wang, J., Li, S., et al. (2022). Tamoxifen exerts anticancer effects on pituitary adenoma progression via inducing cell apoptosis and inhibiting cell migration. *Int. J. Mol. Sci.* 23 (5), 2664. doi:10.3390/ijms23052664

Ma, T., Tian, X., Zhang, B., Li, M., Wang, Y., Yang, C., et al. (2022). Low-dose metformin targets the lysosomal AMPK pathway through PEN2. *Nature* 603 (7899), 159–165. doi:10.1038/s41586-022-04431-8

Malandrino, M. I., Fucho, R., Weber, M., Calderon-Dominguez, M., Mir, J. F., Valcarcel, L., et al. (2015). Enhanced fatty acid oxidation in adipocytes and macrophages reduces lipid-induced triglyceride accumulation and inflammation. *Am. J. Physiol. Endocrinol. Metab.* 308 (9), E756–E769. doi:10.1152/ajpendo.00362.2014

Mancini, S. J. C., Balabanian, K., Corre, I., Gavard, J., Lazennec, G., Le Bousse-Kerdilès, M. C., et al. (2021). Deciphering tumor niches: lessons from solid and hematological malignancies. *Front. Immunol.* 12, 766275. doi:10.3389/fimmu.2021.766275

Marchand, T., and Pinho, S. (2021). Leukemic stem cells: from leukemic niche biology to treatment opportunities. *Front. Immunol.* 12, 775128. doi:10.3389/fimmu.2021.775128

Marchiq, I., and Pouysségur, J. (2016). Hypoxia, cancer metabolism and the therapeutic benefit of targeting lactate/H+ symporters. *J. Mol. Med.* 94, 155–171. doi:10.1007/s00109-015-1307-x

Martinez-Outschoorn, U. E., Peiris-Pagés, M., Pestell, R. G., Sotgia, F., and Lisanti, M. P. (2017). Cancer metabolism: a therapeutic perspective. *Nat. Rev. Clin. Oncol.* 14 (1), 11–31. doi:10.1038/nrclinonc.2016.60

Mather, M. W., Darrouzet, E., Valkova-Valchanova, M., Cooley, J. W., McIntosh, M. T., Daldal, F., et al. (2005). Uncovering the molecular mode of action of the antimalarial drug atovaquone using a bacterial system. *J. Biol. Chem.* 280 (29), 27458–27465. doi:10.1074/jbc.M502319200

Merlo, L. M., Pepper, J. W., Reid, B. J., and Maley, C. C. (2006). Cancer as an evolutionary and ecological process. *Nat. Rev. Cancer* 6 (12), 924–935. doi:10.1038/nrc2013

Minhas, P. S., Liu, L., Moon, P. K., Joshi, A. U., Dove, C., Mhatre, S., et al. (2019). Macrophage *de novo* NAD^+ synthesis specifies immune function in aging and inflammation. *Nat. Immunol.* 20 (1), 50–63. doi:10.1038/s41590-018-0255-3

Molina, J. R., Sun, Y., Protopopova, M., Gera, S., Bandi, M., Bristow, C., et al. (2018). An inhibitor of oxidative phosphorylation exploits cancer vulnerability. *Nat. Med.* 24 (7), 1036–1046. doi:10.1038/s41591-018-0052-4

Moreira, P. I., Custódio, J., Moreno, A., Oliveira, C. R., and Santos, M. S. (2006). Tamoxifen and estradiol interact with the flavin mononucleotide site of complex I leading to mitochondrial failure. *J. Biol. Chem.* 281 (15), 10143–10152. doi:10.1074/jbc.M510249200

Mudassar, F., Shen, H., O'Neill, G., and Hau, E. (2020). Targeting tumor hypoxia and mitochondrial metabolism with anti-parasitic drugs to improve radiation response in high-grade gliomas. *J. Exp. Clin. Cancer Res.* 39 (1), 208. doi:10.1186/s13046-020-01724-6

Müller, L., Tunger, A., Plesca, I., Wehner, R., Temme, A., Westphal, D., et al. (2020). Bidirectional crosstalk between cancer stem cells and immune cell subsets. *Front. Immunol.* 11, 140. doi:10.3389/fimmu.2020.00140

Munoz, L. E., Huang, L., Bommireddy, R., Sharma, R., Monterroza, L., Guin, R. N., et al. (2021). Metformin reduces PD-L1 on tumor cells and enhances the anti-tumor immune response generated by vaccine immunotherapy. *J. Immunother. Cancer* 9 (11), e002614. doi:10.1136/jitc-2021-002614

Nakajima, E. C., and Van Houten, B. (2013). Metabolic symbiosis in cancer: refocusing the Warburg lens. *Mol. Carcinog.* 52 (5), 329–337. doi:10.1002/mc.21863

Nelson, V. L., Nguyen, H. C. B., Garcìa-Cañaveras, J. C., Briggs, E. R., Ho, W. Y., DiSpirito, J. R., et al. (2018). PPARγ is a nexus controlling alternative activation of macrophages via glutamine metabolism. *Genes Dev.* 32 (15-16), 1035–1044. doi:10.1101/gad.312355.118

Odegaard, J. I., and Chawla, A. (2011). Alternative macrophage activation and metabolism. *Annu. Rev. Pathol.* 6, 275–297. doi:10.1146/annurev-pathol-011110-130138

Odegaard, J. I., Ricardo-Gonzalez, R. R., Red Eagle, A., Vats, D., Morel, C. R., Goforth, M. H., et al. (2008). Alternative M2 activation of Kupffer cells by PPARdelta ameliorates obesity-induced insulin resistance. *Cell Metab.* 7 (6), 496–507. doi:10.1016/j.cmet.2008.04.003

Olivares-Urbano, M. A., Griñán-Lisón, C., Marchal, J. A., and Núñez, M. I. (2020). CSC radioresistance: a therapeutic challenge to improve radiotherapy effectiveness in cancer. *Cells* 9 (7), 1651. doi:10.3390/cells9071651

O'Neill, L. A., Kishton, R. J., and Rathmell, J. (2016). A guide to immunometabolism for immunologists. *Nat. Rev. Immunol.* 16 (9), 553–565. doi:10.1038/nri.2016.70

Oshimori, N. (2020). Cancer stem cells and their niche in the progression of squamous cell carcinoma. *Cancer Sci.* 111 (11), 3985–3992. doi:10.1111/cas.14639

Owen, M. R., Doran, E., and Halestrap, A. P. (2000). Evidence that metformin exerts its anti-diabetic effects through inhibition of complex 1 of the mitochondrial respiratory chain. *Biochem. J.* 348 (Pt 3), 607–614. doi:10.1042/bj3480607

Pardee, T. S., Anderson, R. G., Pladna, K. M., Isom, S., Ghiraldeli, L. P., Miller, L. D., et al. (2018). A phase I study of CPI-613 in combination with high-dose cytarabine and mitoxantrone for relapsed or refractory acute myeloid leukemia. *Clin. Cancer Res.* 24 (9), 2060–2073. doi:10.1158/1078-0432.CCR-17-2282

Park, S. J., Smith, C. P., Wilbur, R. R., Cain, C. P., Kallu, S. R., Valasapalli, S., et al. (2018). An overview of MCT1 and MCT4 in GBM: small molecule transporters with large implications. *Am. J. Cancer Res.* 8 (10), 1967–1976.

Park, S. Y., Kim, J. Y., Choi, J. H., Kim, J. H., Lee, C. J., Singh, P., et al. (2019). Inhibition of LEF1-mediated DCLK1 by niclosamide attenuates colorectal cancer stemness. *Clin. Cancer Res.* 25 (4), 1415–1429. doi:10.1158/1078-0432.CCR-18-1232

Park, S. Y., and Nam, J. S. (2020). The force awakens: metastatic dormant cancer cells. *Exp. Mol. Med.* 52 (4), 569–581. doi:10.1038/s12276-020-0423-z

Pascual, G., Avgustinova, A., Mejetta, S., Martín, M., Castellanos, A., Attolini, C. S., et al. (2017). Targeting metastasis-initiating cells through the fatty acid receptor CD36. *Nature* 541 (7635), 41–45. doi:10.1038/nature20791

Passalidou, E., Trivella, M., Singh, N., Ferguson, M., Hu, J., Cesario, A., et al. (2002). Vascular phenotype in angiogenic and non-angiogenic lung non-small cell carcinomas. *Br. J. Cancer* 86 (2), 244–249. doi:10.1038/sj.bjc.6600015

Pastò, A., Bellio, C., Pilotto, G., Ciminale, V., Silic-Benussi, M., Guzzo, G., et al. (2014). Cancer stem cells from epithelial ovarian cancer patients privilege oxidative phosphorylation, and resist glucose deprivation. *Oncotarget* 5 (12), 4305–4319. doi:10.18632/oncotarget.2010

Pateras, I. S., Williams, C., Gianniou, D. D., Margetis, A. T., Avgeris, M., Rousakis, P., et al. (2023). Short term starvation potentiates the efficacy of chemotherapy in triple negative breast cancer via metabolic reprogramming. *J. Transl. Med.* 21 (1), 169. doi:10.1186/s12967-023-03935-9

Philip, P. A., Buyse, M. E., Alistar, A. T., Rocha Lima, C. M., Luther, S., Pardee, T. S., et al. (2019). A Phase III open-label trial to evaluate efficacy and safety of CPI-613 plus modified FOLFIRINOX (mFFX) versus FOLFIRINOX (FFX) in patients with metastatic adenocarcinoma of the pancreas. *Future Oncol.* 15 (28), 3189–3196. doi:10.2217/fon-2019-0209

Pierce, S. R., Fang, Z., Yin, Y., West, L., Asher, M., Hao, T., et al. (2021). Targeting dopamine receptor D2 as a novel therapeutic strategy in endometrial cancer. *J. Exp. Clin. Cancer Res.* 40 (1), 61. doi:10.1186/s13046-021-01842-9

Pignatelli, J., Bravo-Cordero, J. J., Roh-Johnson, M., Gandhi, S. J., Wang, Y., Chen, X., et al. (2016). Macrophage-dependent tumor cell transendothelial migration is mediated by Notch1/MenaINV-initiated invadopodium formation. *Sci. Rep.* 6 37874. doi:10.1038/srep37874

Plaks, V., Kong, N., and Werb, Z. (2015). The cancer stem cell niche: how essential is the niche in regulating stemness of tumor cells? *Cell Stem Cell* 16 (3), 225–238. doi:10.1016/j.stem.2015.02.015

Prabhu, V. V., Allen, J. E., Dicker, D. T., and El-Deiry, W. S. (2015). Small-Molecule ONC201/TIC10 targets chemotherapy-resistant colorectal cancer stem-like cells in an akt/foxo3a/TRAIL-dependent manner. *Cancer Res.* 75 (7), 1423–1432. doi:10.1158/0008-5472.CAN-13-3451

Przystal, J. M., Cianciolo Cosentino, C., Yadavilli, S., Zhang, J., Laternser, S., Bonner, E. R., et al. (2022). Imipridones affect tumor bioenergetics and promote cell lineage differentiation in diffuse midline gliomas. *Neuro Oncol.* 24 (9), 1438–1451. doi:10.1093/neuonc/noac041

Quail, D. F., Taylor, M. J., and Postovit, L. M. (2012). Microenvironmental regulation of cancer stem cell phenotypes. *Curr. Stem Cell Res. Ther.* 7 (3), 197–216. doi:10.2174/157488812799859838

Rainho, M. A., Siqueira, P. B., de Amorim, Í. S. S., Mencalha, A. L., and Thole, A. A. (2023). Mitochondria in colorectal cancer stem cells - a target in drug resistance. *Cancer Drug Resist* 6 (2), 273–283. doi:10.20517/cdr.2022.116

Reddy, J. K., and Hashimoto, T. (2001). Peroxisomal beta-oxidation and peroxisome proliferator-activated receptor alpha: an adaptive metabolic system. *Annu. Rev. Nutr.* 21, 193–230. doi:10.1146/annurev.nutr.21.1.193

Rodriguez-Berriguete, G., Puliyadi, R., Machado, N., Barberis, A., Prevo, R., McLaughlin, M., et al. (2024). Antitumour effect of the mitochondrial complex III inhibitor Atovaquone in combination with anti-PD-L1 therapy in mouse cancer models. *Cell Death Dis.* 15 (1), 32. doi:10.1038/s41419-023-06405-8

Romano, S., Tufano, M., D'Arrigo, P., Vigorito, V., Russo, S., and Romano, M. F. (2020). Cell stemness, epithelial-to-mesenchymal transition, and immunoevasion: intertwined aspects in cancer metastasis. *Semin. Cancer Biol.* 60, 181–190. doi:10.1016/j.semcancer.2019.08.015

Roussos, E. T., Balsamo, M., Alford, S. K., Wyckoff, J. B., Gligorijevic, B., Wang, Y., et al. (2011). Mena invasive (MenaINV) promotes multicellular streaming motility and

transendothelial migration in a mouse model of breast cancer. *J. Cell Sci.* 124 (Pt 13), 2120–2131. doi:10.1242/jcs.086231

Ruiz-Malagón, A. J., Hidalgo-García, L., Rodríguez-Sojo, M. J., Molina-Tijeras, J. A., García, F., Diez-Echave, P., et al. (2023). Tigecycline reduces tumorigenesis in colorectal cancer via inhibition of cell proliferation and modulation of immune response. *Biomed. Pharmacother.* 163, 114760. doi:10.1016/j.biopha.2023.114760

Saif, M. W., Rajagopal, S., Caplain, J., Grimm, E., Serebrennikova, O., Das, M., et al. (2019). A phase I delayed-start, randomized and pharmacodynamic study of metformin and chemotherapy in patients with solid tumors. *Cancer Chemother. Pharmacol.* 84 (6), 1323–1331. doi:10.1007/s00280-019-03967-3

Sainero-Alcolado, L., Liaño-Pons, J., Ruiz-Pérez, M. V., and Arsenian-Henriksson, M. (2022). Targeting mitochondrial metabolism for precision medicine in cancer. *Cell Death Differ.* 29 (7), 1304–1317. doi:10.1038/s41418-022-01022-y

Sainz, B., Jr., Carron, E., Vallespinós, M., and Machado, H. L. (2016). Cancer stem cells and macrophages: implications in tumor biology and therapeutic strategies. *Mediat. Inflamm.* 2016, 9012369. doi:10.1155/2016/9012369

Salvadori, G., Zanardi, F., Iannelli, F., Lobefaro, R., Vernieri, C., and Longo, V. D. (2021). Fasting-mimicking diet blocks triple-negative breast cancer and cancer stem cell escape. *Cell Metab.* 33 (11), 2247–2259.e6. doi:10.1016/j.cmet.2021.10.008

Sancho, P., Barneda, D., and Heeschen, C. (2016). Hallmarks of cancer stem cell metabolism. *Br. J. Cancer* 114 (12), 1305–1312. doi:10.1038/bjc.2016.152

Sancho, P., Burgos-Ramos, E., Tavera, A., Bou Kheir, T., Jagust, P., Schoenhals, M., et al. (2015). MYC/PGC-1α balance determines the metabolic phenotype and plasticity of pancreatic cancer stem cells. *Cell Metabol.* 22, 590–605. doi:10.1016/j.cmet.2015.08.015

Sandforth, L., Ammar, N., Dinges, L. A., Röcken, C., Arlt, A., Sebens, S., et al. (2020). Impact of the monocarboxylate transporter-1 (MCT1)-Mediated cellular import of lactate on stemness properties of human pancreatic adenocarcinoma cells. *Cancers (Basel)* 12 (3), 581. doi:10.3390/cancers12030581

Scatena, C., Roncella, M., Di Paolo, A., Aretini, P., Menicagli, M., Fanelli, G., et al. (2018). Doxycycline, an inhibitor of mitochondrial biogenesis, effectively reduces cancer stem cells (CSCs) in early breast cancer patients: a clinical pilot study. *Front. Oncol.* 8, 452. doi:10.3389/fonc.2018.00452

Schepers, K., Campbell, T. B., and Passegué, E. (2015). Normal and leukemic stem cell niches: insights and therapeutic opportunities. *Cell Stem Cell* 16 (3), 254–267. doi:10.1016/j.stem.2015.02.014

Schultz, C. W., and Nevler, A. (2022). Pyrvinium pamoate: past, present, and future as an anti-cancer drug. *Biomedicines* 10 (12), 3249. doi:10.3390/biomedicines10123249

Sell, S. (2010). On the stem cell origin of cancer. *Am. J. Pathol.* 176 (6), 2584–3494. doi:10.2353/ajpath.2010.091064

Semenas, J., Wang, T., Sajid Syed Khaja, A., Firoj Mahmud, A., Simoulis, A., Grundström, T., et al. (2020). Targeted inhibition of ERα signaling and PIP5K1α/Akt pathways in castration-resistant prostate cancer. *Mol. Oncol.* 15 (4), 968–986. doi:10.1002/1878-0261.12873

Shang, S., Yang, C., Chen, F., Xiang, R. S., Zhang, H., Dai, S. Y., et al. (2023). ID1 expressing macrophages support cancer cell stemness and limit $CD8^+$ T cell infiltration in colorectal cancer. *Nat. Commun.* 14 (1), 7661. doi:10.1038/s41467-023-43548-w

Shirakawa, K., Kobayashi, H., Heike, Y., Kawamoto, S., Brechbiel, M. W., Kasumi, F., et al. (2002). Hemodynamics in vasculogenic mimicry and angiogenesis of inflammatory breast cancer xenograft. *Cancer Res.* 62 (2), 560–566.

Singh, M., Afonso, J., Sharma, D., Gupta, R., Kumar, V., Rani, R., et al. (2023). Targeting monocarboxylate transporters (MCTs) in cancer: how close are we to the clinics? *Semin. Cancer Biol.* 90, 1–14. doi:10.1016/j.semcancer.2023.01.007

Sonveaux, P., Végran, F., Schroeder, T., Wergin, M. C., Verrax, J., Rabbani, Z. N., et al. (2008). Targeting lactate-fueled respiration selectively kills hypoxic tumor cells in mice. *J. Clin. Invest.* 118 (12), 3930–3942. doi:10.1172/JCI36843

Sosa, M. S., Parikh, F., Maia, A. G., Estrada, Y., Bosch, A., Bragado, P., et al. (2015). NR2F1 controls tumour cell dormancy via SOX9-and RARβ-driven quiescence programmes. *Nat. Commun.* 6, 6170. doi:10.1038/ncomms7170

Stein, M. N., Malhotra, J., Tarapore, R. S., Malhotra, U., Silk, A. W., Chan, N., et al. (2019). Safety and enhanced immunostimulatory activity of the DRD2 antagonist ONC201 in advanced solid tumor patients with weekly oral administration. *J. Immunother. Cancer* 7 (1), 136. doi:10.1186/s40425-019-0599-8

Stuart, S. D., Schauble, A., Gupta, S., Kennedy, A. D., Keppler, B. R., Bingham, P. M., et al. (2014). A strategically designed small molecule attacks alpha-ketoglutarate dehydrogenase in tumor cells through a redox process. *Cancer Metab.* 2 (1), 4. doi:10.1186/2049-3002-2-4

Su, C., Zhang, J., Yarden, Y., and Fu, L. (2021). The key roles of cancer stem cell-derived extracellular vesicles. *Signal Transduct. Target Ther.* 6 (1), 109. doi:10.1038/s41392-021-00499-2

Takada, T., Takata, K., and Ashihara, E. (2016). Inhibition of monocarboxylate transporter 1 suppresses the proliferation of glioblastoma stem cells. *J. Physiol. Sci.* 66, 387–396. doi:10.1007/s12576-016-0435-6

Tannahill, G. M., Curtis, A. M., Adamik, J., Palsson-McDermott, E. M., McGettrick, A. F., Goel, G., et al. (2013). Succinate is an inflammatory signal that induces IL-1β through HIF-1α. *Nature* 496 (7444), 238–242. doi:10.1038/nature11986

Taylor, S. E., Chan, D. K., Yang, D., Bruno, T., Lieberman, R., Siddiqui, J., et al. (2022). Shifting the soil: metformin treatment decreases the protumorigenic tumor microenvironment in epithelial ovarian cancer. *Cancers (Basel)* 14 (9), 2298. doi:10.3390/cancers14092298

Valle, S., Alcalá, S., Martin-Hijano, L., Cabezas-Sáinz, P., Navarro, D., Muñoz, E. R., et al. (2020). Exploiting oxidative phosphorylation to promote the stem and immunoevasive properties of pancreatic cancer stem cells. *Nat. Commun.* 11 (1), 5265. doi:10.1038/s41467-020-18954-z

Vazquez, F., Lim, J. H., Chim, H., Bhalla, K., Girnun, G., Pierce, K., et al. (2013). PGC1α expression defines a subset of human melanoma tumors with increased mitochondrial capacity and resistance to oxidative stress. *Cancer Cell* 23 (3), 287–301. doi:10.1016/j.ccr.2012.11.020

Viale, A., Pettazzoni, P., Lyssiotis, C. A., Ying, H., Sánchez, N., Marchesini, M., et al. (2014). Oncogene ablation-resistant pancreatic cancer cells depend on mitochondrial function. *Nature* 514 (7524), 628–632. doi:10.1038/nature13611

Vlashi, E., Lagadec, C., Vergnes, L., Matsutani, T., Masui, K., Poulou, M., et al. (2011). Metabolic state of glioma stem cells and nontumorigenic cells. *Proc. Natl. Acad. Sci. U. S. A.* 108 (38), 16062–16067. doi:10.1073/pnas.1106704108

Walker, N. D., Elias, M., Guiro, K., Bhatia, R., Greco, S. J., Bryan, M., et al. (2019). Exosomes from differentially activated macrophages influence dormancy or resurgence of breast cancer cells within bone marrow stroma. *Cell Death Dis.* 10 (2), 59. doi:10.1038/s41419-019-1304-z

Wang, B., Ma, L. Y., Wang, J. Q., Lei, Z. N., Gupta, P., Zhao, Y. D., et al. (2018a). Discovery of 5-Cyano-6-phenylpyrimidin derivatives containing an acylurea moiety as orally bioavailable reversal agents against P-Glycoprotein-Mediated mutidrug resistance. *J. Med. Chem.* 61 (14), 5988–6001. doi:10.1021/acs.jmedchem.8b00335

Wang, B., Zhao, B., Chen, Z. S., Pang, L. P., Zhao, Y. D., Guo, Q., et al. (2018b). Exploration of 1,2,3-triazole-pyrimidine hybrids as potent reversal agents against ABCB1-mediated multidrug resistance. *Eur. J. Med. Chem.* 143, 1535–1542. doi:10.1016/j.ejmech.2017.10.041

Wang, L., and Zheng, G. (2019). Macrophages in leukemia microenvironment. *Blood Sci.* 1 (1), 29–33. doi:10.1097/BS9.0000000000000014

Wang, R., Tao, B., Fan, Q., Wang, S., Chen, L., Zhang, J., et al. (2019). Fatty-acid receptor CD36 functions as a hydrogen sulfide-targeted receptor with its Cys333-Cys272 disulfide bond serving as a specific molecular switch to accelerate gastric cancer metastasis. *EBioMedicine* 45, 108–123. doi:10.1016/j.ebiom.2019.06.037

Wang, S., Lin, Y., Xiong, X., Wang, L., Guo, Y., Chen, Y., et al. (2020). Low-dose metformin reprograms the tumor immune microenvironment in human esophageal cancer: results of a phase II clinical trial. *Clin. Cancer Res.* 26 (18), 4921–4932. doi:10.1158/1078-0432.CCR-20-0113

Warburg, O., and Minami, S. (1923). Versuche an überlebendem carcinom-gewebe. *Klin. Wochenschr* 2, 776–777. doi:10.1007/BF01712130

Watanabe, C. K. (1918). Studies in the metabolism changes induced by administration of guanidine bases: i. Influence of injected guanidine hydrochloride upon blood sugar content. *J. Biol. Chem.* 33 (2), 253–265. doi:10.1016/S0021-9258(18)86579-6

Watt, M. J., Clark, A. K., Selth, L. A., Haynes, V. R., Lister, N., Rebello, R., et al. (2019). Suppressing fatty acid uptake has therapeutic effects in preclinical models of prostate cancer. *Sci. Transl. Med.* 11 (478), eaau5758. doi:10.1126/scitranslmed.aau5758

Wei, Z., Zhang, X., Yong, T., Bie, N., Zhan, G., Li, X., et al. (2021). Boosting anti-PD-1 therapy with metformin-loaded macrophage-derived microparticles. *Nat. Commun.* 12 (1), 440. doi:10.1038/s41467-020-20723-x

Wu, Z., Zhang, C., and Najafi, M. (2022). Targeting of the tumor immune microenvironment by metformin. *J. Cell Commun. Signal* 16 (3), 333–348. doi:10.1007/s12079-021-00648-w

Xuan, Q. J., Wang, J. X., Nanding, A., Wang, Z. P., Liu, H., Lian, X., et al. (2014). Tumor-associated macrophages are correlated with tamoxifen resistance in the postmenopausal breast cancer patients. *Pathol. Oncol. Res.* 20 (3), 619–624. doi:10.1007/s12253-013-9740-z

Yang, B., Lu, Y., Zhang, A., Zhou, A., Zhang, L., Zhang, L., et al. (2015). Doxycycline induces apoptosis and inhibits proliferation and invasion of human cervical carcinoma stem cells. *PLoS One* 10 (6), e0129138. doi:10.1371/journal.pone.0129138

Yang, X., Liu, Q., Li, Y., Tang, Q., Wu, T., Chen, L., et al. (2020). The diabetes medication canagliflozin promotes mitochondrial remodelling of adipocyte via the AMPK-Sirt1-Pgc-1α signalling pathway. *Adipocyte* 9 (1), 484–494. doi:10.1080/21623945.2020.1807850

Yao, H., and He, S. (2021). Multi-faceted role of cancer-associated adipocytes in the tumor microenvironment (Review). *Mol. Med. Rep.* 24 (6), 866. doi:10.3892/mmr.2021.12506

Zhou, G., Myers, R., Li, Y., Chen, Y., Shen, X., Fenyk-Melody, J., et al. (2001). Role of AMP-activated protein kinase in mechanism of metformin action. *J. Clin. Invest.* 108 (8), 1167–1174. doi:10.1172/JCI13505

Zhou, W., Ke, S. Q., Huang, Z., Flavahan, W., Fang, X., Paul, J., et al. (2015). Periostin secreted by glioblastoma stem cells recruits M2 tumour-associated macrophages and promotes malignant growth. *Nat. Cell Biol.* 17 (2), 170–182. doi:10.1038/ncb3090

frontiers | Frontiers in Pharmacology

TYPE Systematic Review
PUBLISHED 10 May 2024
DOI 10.3389/fphar.2024.1351363

OPEN ACCESS

EDITED BY
Bo Wang,
Zhengzhou University, China

REVIEWED BY
Praveen Sonkusre,
Center for Cancer Research, National Cancer Institute (NIH), United States
Ming Yi,
Zhejiang University, China

*CORRESPONDENCE
Rutie Yin,
yinrutie@scu.edu.cn

†These authors have contributed equally to this work

RECEIVED 06 December 2023
ACCEPTED 24 April 2024
PUBLISHED 10 May 2024

CITATION
Duan Y, Yang L, Wang W, Zhang P, Fu K, Li W and Yin R (2024), A comprehensive bibliometric analysis (2000–2022) on the mapping of knowledge regarding immunotherapeutic treatments for advanced, recurrent, or metastatic cervical cancer.
Front. Pharmacol. 15:1351363.
doi: 10.3389/fphar.2024.1351363

A comprehensive bibliometric analysis (2000–2022) on the mapping of knowledge regarding immunotherapeutic treatments for advanced, recurrent, or metastatic cervical cancer

Yuanqiong Duan[1,2†], Lin Yang[1,2†], Wenxiang Wang[1,2†], Peixuan Zhang[1,2], Kaiyu Fu[1,2], Wen Li[1,2] and Rutie Yin[1,2*]

[1]Department of Obstetrics and Gynecology, West China Second University Hospital of Sichuan University, Chengdu, Sichuan, China, [2]Key Laboratory of Birth Defects and Related Diseases of Women and Children, Ministry of Education, Sichuan University, Chengdu, China

Background: Despite extensive literature on therapeutic strategies for cervical cancer, a bibliometric analysis specifically focused on immunotherapy for advanced, recurrent, or metastatic (A/R/M) cervical malignancies remains unexplored. This study aims to address this gap by presenting a comprehensive overview that includes general characteristics, research focal points, the trajectory of evolution, and current emerging trends in this under-researched area.

Methods: A systematic search was conducted using the Web of Science Core Collection (WOSCC) to identify articles related to A/R/M cervical cancer published between 2000 and 2022. Citespace and VOS viewer were the primary tools used to identify research focal points, intriguing future patterns, and to evaluate contributions and co-occurrences among authors, institutions, countries, and journals.

Results: A total of 1,001 original articles were identified, involving 6,387 authors from 66 countries and 1,474 institutions, and published across 366 academic journals. The United States contributed most significantly. The most productive researcher was Van der Burg SH from Leiden University Medical Center. The International Journal of Cancer and Cancer Research were identified as the most productive and influential journals, respectively. Analysis of co-citation clusters highlighted 25 clusters, primarily focusing on potential predictive biomarkers, dendritic cell-based tumor vaccines, therapeutic HPV vaccinations, peptide-based cancer vaccines, tumor immune microenvironments, and adoptive cell transfer (ACT). The latest significant trends in A/R/M cervical cancer immunotherapy research included ACT, CAR-T, and immune checkpoint inhibitors (ICIs), as revealed by keyword and reference burst detection.

Conclusion: This pioneering study provides a detailed landscape of immunotherapy research in A/R/M cervical cancer. It underscores the importance of global collaboration, enriches our understanding of the immunology of A/R/M cervical cancer, expands on potential beneficiaries of immunotherapy, and explores clinical applications of various therapies, including

therapeutic vaccines, adoptive cell transfer, and ICIs, particularly in combination with established treatments such as chemotherapy, radiotherapy, and targeted therapy.

KEYWORDS

cervical cancer, immunotherapy, bispecific antibodies, citespace, bibliometrics analysis

1 Introduction

Cervical cancer (CC) remains a significant global health challenge, ranking as the fourth most prevalent cancer among women worldwide. Despite the preventive potential of the human papillomavirus (HPV) vaccine and regular screening, GLOBOCAN 2020 reports about 604,000 new cases and approximately 341,000 deaths in 2020, emphasizing the urgent need for more effective treatment strategies (Ferrall et al., 2021; Sung et al., 2021). The prognosis for cervical cancer varies considerably with the stage at diagnosis: early-stage cancers, when detected and managed with surgery and chemoradiation, exhibit a 5-year survival rate exceeding 90%. In contrast, this rate drops to below 20% for patients with advanced or metastatic disease (Monk et al., 2022). Unfortunately, therapeutic advancements have not significantly improved survival rates since the 1970s (Feng et al., 2020; Siegel et al., 2022; Suran, 2022), underscoring the critical need for innovative therapeutic approaches, particularly for advanced, recurrent, or metastatic (A/R/M) cervical malignancies.

Immunotherapy is a rapidly evolving field that holds promise for treating a variety of malignancies, including cervical cancer. The unique interplay between persistent HPV infections and the immune system offers a valuable opportunity for targeted immunotherapy (Vinokurova et al., 2008; Pal and Kundu, 2019; Attademo et al., 2020). Additionally, factors such as high tumor mutation burden (TMB) and microsatellite instability (MSI) provide further rationale for employing immunotherapy in cervical cancer cases (Zhao et al., 2019; Tan et al., 2020). Early phase clinical trials have demonstrated the efficacy of this approach, showing sustained responses and a manageable safety profile (Duska et al., 2020; Frumovitz et al., 2020; Huang et al., 2022; Vicier et al., 2022; Xu et al., 2022). Moreover, numerous phase II and III studies are currently investigating the use of immunotherapy, both as a standalone treatment and in conjunction with chemotherapy and radiotherapy, for locally advanced and metastatic cervical cancer (Sugiyama et al., 2014; Harper et al., 2019; Mayadev et al., 2020; Takeuchi et al., 2020; O'Malley et al., 2021). Immunotherapy represents a significant anti-cancer strategy that harnesses and directs the host's immune system to target cancer cells with increased specificity and efficacy, showing great potential to improve therapies and survival rates in advanced, recurrent, or metastatic cervical cancer.

The breadth of research on immunotherapy for A/R/M cervical cancer is extensive and continues to expand rapidly, posing challenges in distilling and synthesizing the vast amount of available information. In this context, bibliometric analysis proves to be an indispensable tool, offering a comprehensive perspective on the evolution of the field and facilitating the identification of pivotal trends and focal points within the research landscape (Chen, 2004). This methodology, which goes beyond traditional review mechanisms by utilizing mathematical and statistical techniques, provides a structured framework of knowledge, enabling more efficient assimilation of the literature (Ellegaard and Wallin, 2015; Chen and Song, 2019).

Despite the wealth of data, there is a noticeable dearth of bibliometric studies specifically targeting the immunology of A/R/M cervical cancer. To address this deficiency, our study undertakes a thorough bibliometric analysis of the literature from 2000 to 2022. We aim to deliver a detailed overview of the existing knowledge base and the emergent trends in the immunotherapy of A/R/M cervical carcinoma. This analysis will yield both quantitative and qualitative insights, laying the foundation for future research in this vital field.

2 Materials and methods

2.1 Origins of bibliometric data

Given the broad scope of the Science Citation Index Expanded (SCI-E) and its relevance to our study, we selected it as the primary database for our bibliometric analysis (Lawson McLean, 2019; Yao et al., 2020). We conducted a systematic literature review of publications from 2000 to 2022. To ensure the precision and relevance of our dataset, we utilized two principal search terms: 'A/R/M cervical cancer' (Strategy A) and 'immunotherapy' (Strategy B). A Boolean search algorithm using "A AND B" (Strategy C) refined our search, ensuring that all articles retrieved were directly relevant to immunotherapy for cervical cancer.

The literature retrieval process was rigorously conducted by two researchers independently. In cases of disagreement, issues were resolved through discussions with the corresponding author, ensuring a balanced and comprehensive selection of articles. Additionally, we restricted our search to articles published in English to maintain clarity and uniformity in our analysis, thereby enhancing the academic rigor of our study. This decision was also supported by the tendency of journal articles to introduce new and innovative findings. Furthermore, our study was meticulously structured according to PRISMA guidelines to ensure a robust and transparent research methodology. The procedural flow of our study, from the initial data collection to the final article selection, is illustrated in the flowchart presented in Figure 1.

2.2 Methods of analysis and visualization

Bibliometric analysis, an emerging field, employs visualization and statistical methods to examine structures and trends within specific subjects or domains (Jiang et al., 2018). Its primary objective is to identify significant nodes and extract valuable insights from extensive data repositories. For data processing and visualization, we

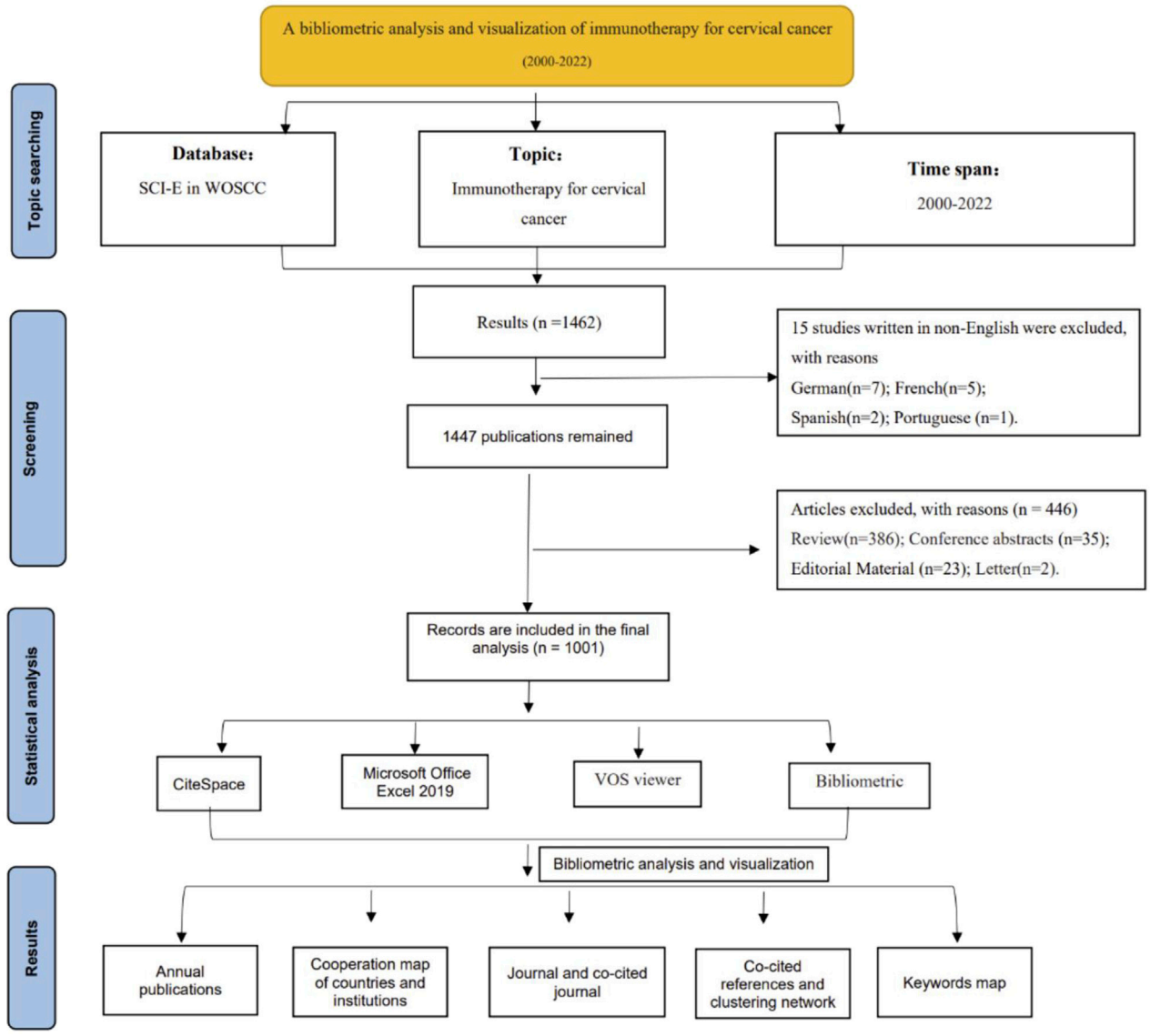

FIGURE 1
Flowchart of the exclusion and incorporation of literature.

primarily utilized CiteSpace and VOS Viewer for their distinctive features and advantages, alongside other industry-standard tools such as NetDraw, HistCite, and SCI2 (Qin et al., 2020).

CiteSpace, a publicly accessible Java application, is specifically designed to uncover patterns and trends in scientific literature. Developed by Professor Chaomei Chen, it aids in identifying critical junctures and turning points in the evolution of disciplines, enabling the visualization of knowledge domains (Synnestvedt et al., 2005). CiteSpace excels at illustrating collaboration networks, identifying key elements, mapping internal structures, forecasting trends, and tracking changes within specific fields (Chen, 2004). We used CiteSpace to analyze and depict the co-presence of nations, regions, and organizations, as well as trends in frequently occurring keywords, co-cited references, and bursts in reference citations.

The VOS Viewer, developed by the Center for Science and Technology Studies at Leiden University, facilitates the creation, display, and exploration of maps based on network data (van Eck and Waltman, 2010). This software streamlines the visualization of scientific networks. Employing VOS Viewer (version 1.6.18.0), we effectively identified productive academic journals, their co-citations, and associated knowledge maps through bibliographic data analysis. Additionally, Microsoft Office Excel 2019 was employed for annual publication analysis and database management. The impact factor (IF), H-index, and Journal Citation Reports (JCR) rankings of journals for 2022 were obtained from the Incites Journal Citation Reports of the Web of Science and the bibliometric online analysis platform (https://bibliometric.com/app).

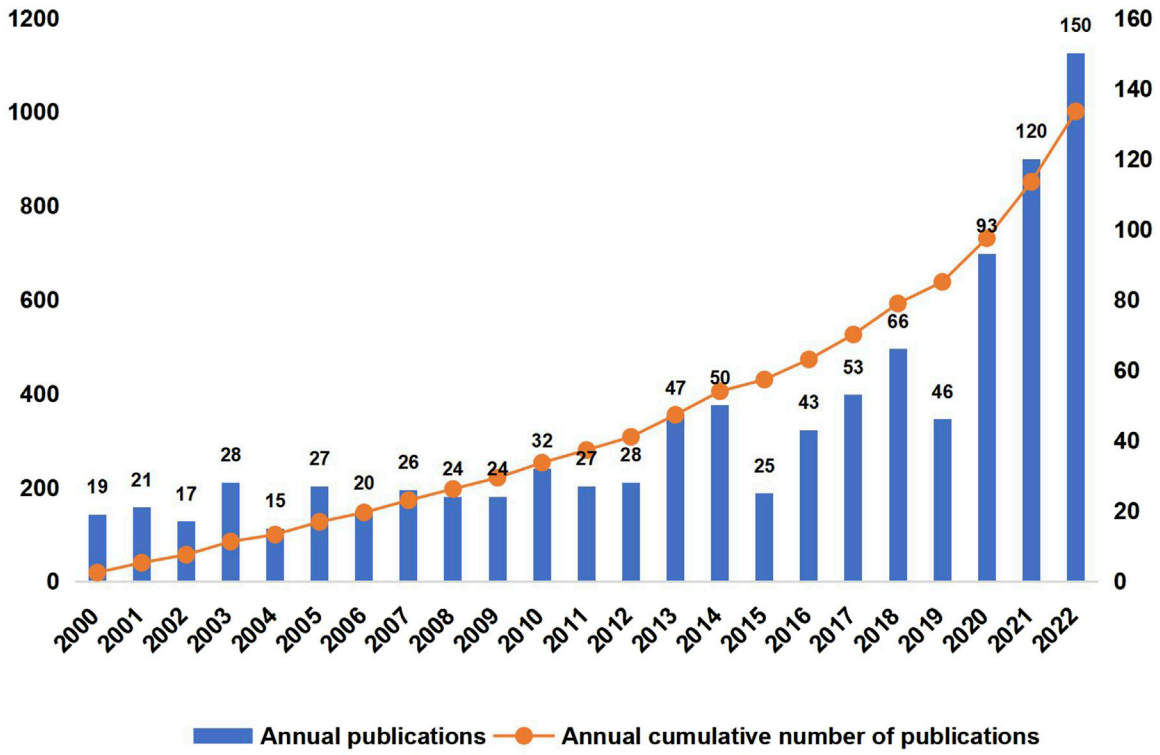

FIGURE 2
Trends in annual publications concerning immunotherapeutic interventions for advanced, recurrent, or metastatic (A/R/M) cervical cancer.

3 Results

3.1 Annual publication trends

From 2000 to 2022, we identified 1,001 distinct articles through our data collection strategy, representing a substantial corpus of research in the field of A/R/M cervical cancer immunotherapy. Figure 2 illustrates the annual distribution of these articles. The initial phase, spanning 2000 to 2019, demonstrates a steady increase in publication volume. The subsequent phase, from 2020 to 2022, is characterized by a significant surge in research activity, reflecting a heightened focus on this area.

3.2 Map of international and institutional cooperation

3.2.1 Contributions of countries

The global endeavor in cervical cancer immunotherapy involves contributions from sixty-six countries. Utilizing CiteSpace, we visualized the collaboration network, displayed in Figure 3A, which highlights the extensive contributions from various nations. In this network, the size of each node corresponds to the total number of publications from specific countries, institutions, or authors (Chen et al., 2012), with connecting lines indicating citation relationships. Notably, the United States, China, Germany, the Netherlands, France, Italy, and Spain are marked in purple, signifying their central role and potential to drive research breakthroughs. Figure 3B shows that the United States leads with 279 publications, accounting for 27.9% of the total, followed by China with 235 publications (23.5%). Other prominent contributors include Japan, Germany, the Netherlands, and Italy. Figure 3C depicts the patterns of international collaboration, with the United States and China, as well as the United States and Italy, being the most frequent collaborators.

3.2.2 Contributions of institutions

The field of immunotherapy for advanced, recurrent, or metastatic (A/R/M) cervical cancer has attracted contributions from 1,474 academic institutions globally. Figure 4A, generated using CiteSpace, displays a network map of these institutions, illustrating their distribution and interconnections. Leiden University is highlighted as the foremost contributor with 42 publications, as depicted in Figure 4B. Other prominent institutions include the National Cancer Institute (NCI), the University of Texas MD Anderson Cancer Center, Johns Hopkins University, and Shanghai Jiao Tong University, with the majority of the top ten institutions located in the US and China. This distribution underscores the pivotal role these countries play in advancing research in immunotherapy for A/R/M cervical cancer. Figure 4C lists the eight most cited institutions, ranked by the duration of their citation bursts, further highlighting the significant impact of these organizations.

3.3 Journals and co-cited journals

Utilizing VOS Viewer for the analysis of co-citations and identification of key journals in A/R/M cervical cancer

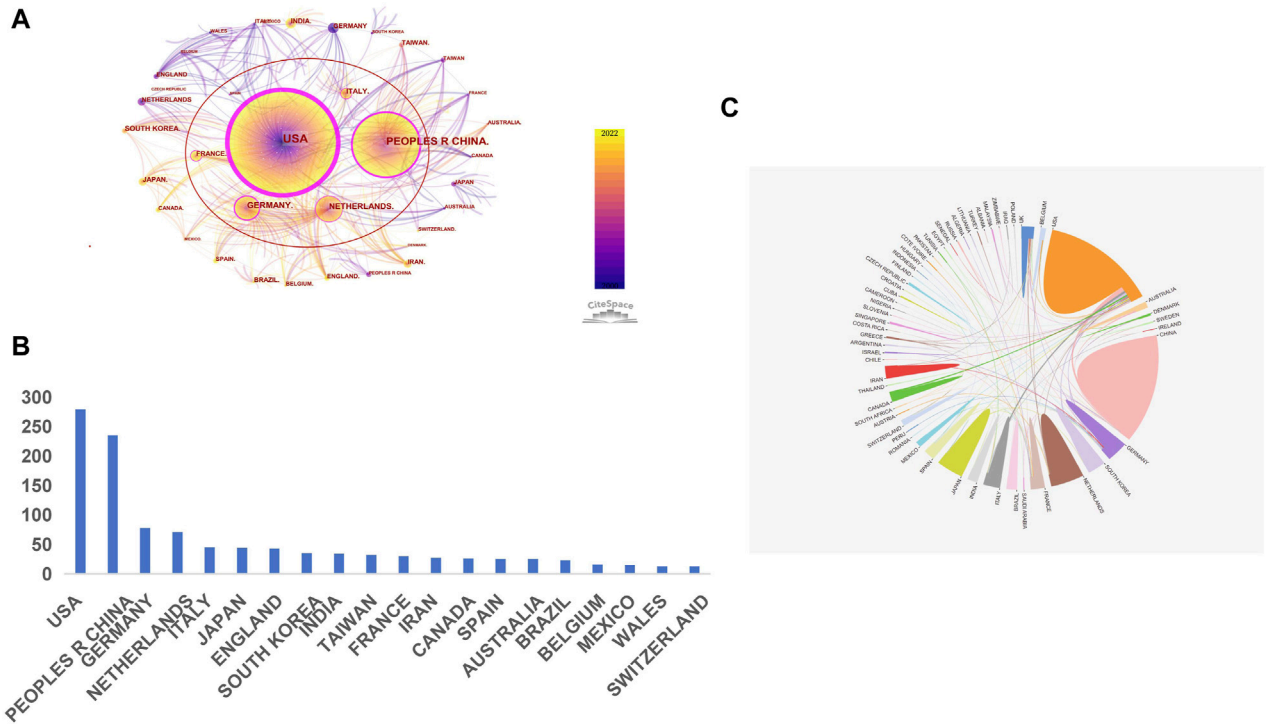

FIGURE 3
A map of international interactions based on a geographic analysis of collaboration **(A)**. Visualization of the network of country co-occurrences (There are 66 nodes and 726 connecting connections in the network. The magnitude of the nodes and the length of the lines represent, respectively, the quantity of a country's publications and the extent of its cooperation within a given geography. Variable-colored lines represent various years, and the presence of a red ellipse indicates an increase in citations or frequency for a particular country.) **(B)**. Count of publications for the top 20 countries **(C)**. Interactions and collaborations among countries.

immunotherapy, we observed significant publication and citation trends. As indicated in Supplementary Table S1, the International Journal of Cancer leads with 3.1% of the total publications (31 publications), followed by Cancer Immunology Immunotherapy, Vaccine, Gynecologic Oncology, and Oncoimmunology, each making substantial contributions to the field. Notably, four of the top ten journals boast impact factors above five and H-indexes exceeding one hundred, highlighting their significant influence within the scientific community. These journals include Clinical Cancer Research (IF: 11.5; H-Index: 292), Cancer Research (IF: 13.2; H-Index: 411), International Journal of Cancer (IF: 6.4; H-Index: 212), and Cancer Immunology Immunotherapy (IF: 5.8; H-Index: 104). Furthermore, Cancer Research leads in citation volume with 630 citations, as detailed in Supplementary Table S2, followed by Clinical Cancer Research and the International Journal of Cancer.

3.4 Authors and co-cited authors

A total of 6,387 authors have contributed to the field of immunotherapy for A/R/M cervical cancer. The ten most productive researchers are listed in Supplementary Table S3, with Van der Burg SH from Leiden University Medical Center leading with 25 publications. This author also ranks highest in total citations, amassing 1,878 citations, followed closely by Kenter GG and Melief CJM. Notably, Melief CJM has the highest H-index, underscoring the impact and relevance of his contributions. This comprehensive analysis underscores the critical roles played by authors such as Van der Burg SH and Melief CJM in advancing this field. Figure 5 depicts the emergence of dominant academic clusters and the patterns of collaboration within and between these groups. For example, Van der Burg SH (yellow cluster) is shown to collaborate closely with Welters MJP, and cross-cluster collaborations are evident between Van der Burg SH and other key researchers such as Kenter GG (red cluster) and Hung CF (green cluster). These collaborative networks illustrate the interconnected nature of research in this field and emphasize the importance of academic teamwork in advancing knowledge.

3.5 Co-cited references and networking cluster analysis

Co-cited references, which are scholarly works frequently cited together, establish a knowledge base that reflects the research community's focal points and trends (Synnestvedt et al., 2005; Lu et al., 2020). To examine this aspect within the realm of A/R/M cervical cancer immunotherapy, we performed a co-citation analysis on 1,001 articles using CiteSpace. Supplementary Table S4 displays the ten most-cited references in this domain. Notably, "Global cancer statistics 2018: GLOBOCAN estimates of incidence and

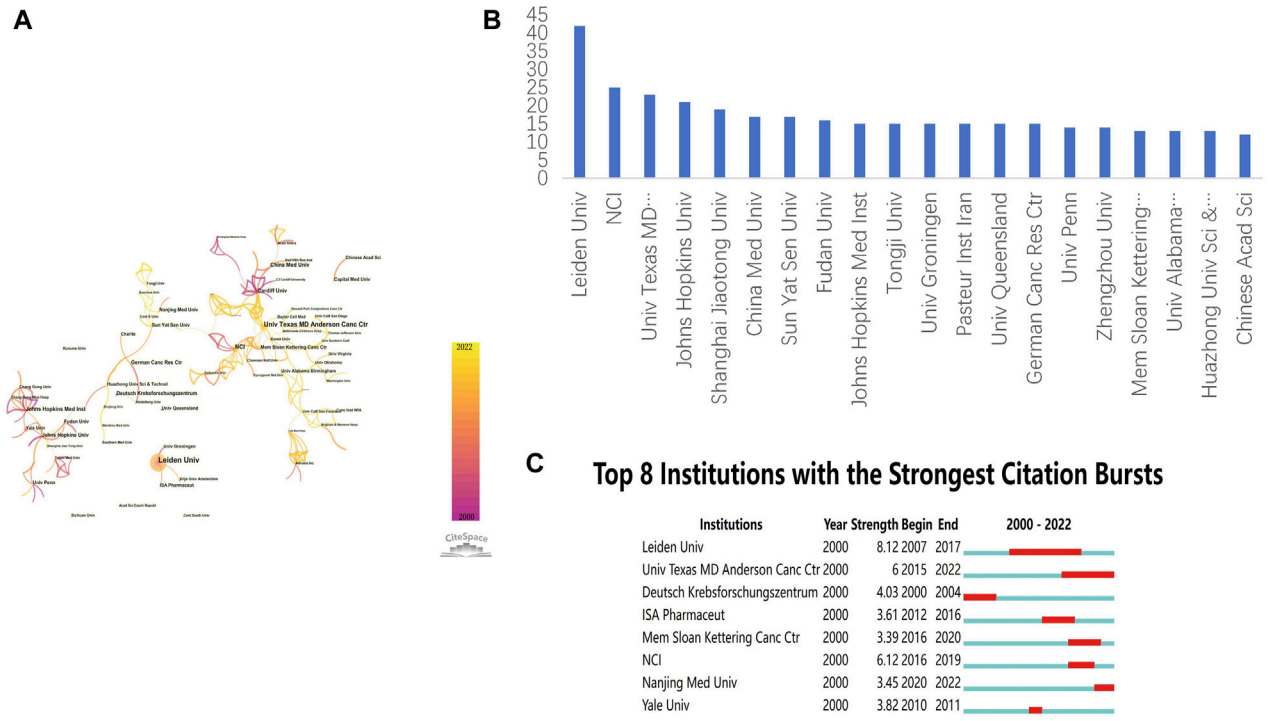

FIGURE 4
Collaborative Infrastructure Map of Institutions **(A)**. Co-occurrence network among institutions (the network consists of 1,474 nodes and 2,940 connecting lines. The sizes of the nodes and lines correspond to the quantity of an institute's publications and the scale of cooperative interactions within the institute, respectively. Lines of assorted colors correlate to different years.) **(B)**. Publication quantity for the top 20 institutions **(C)**. Top 8 institutions experiencing the most pronounced citation surges (Red bars denote periods when a certain institution garners frequent citations, sorted by the duration of the burst.).

mortality worldwide for 36 cancers in 185 countries" stands out as the most cited, offering essential insights into the global impact of cervical cancer. Other significant co-cited references include studies on the "safety and efficacy of PD-1 inhibitors," "integrated genomic and molecular characterization of cervical cancer," and "therapeutic vaccines," each playing a crucial role in advancing immunotherapy for this condition.

We employed CiteSpace to generate a co-citation map, illustrating the interconnections among co-cited references and clustering them to delineate research boundaries in A/R/M cervical cancer immunotherapy. This analysis produced 25 distinct clusters, visualized in Figure 6A. The clustering structure, characterized by a mean silhouette value of 0.9178 and a modularity Q score of 0.8162, demonstrates robust and meaningful groupings. Each cluster represents a specific research area within the field. The largest identified clusters were "cervical cancer" (cluster #0), "potential prognostic biomarker" (cluster #1), "dendritic cell-based tumor vaccine" (cluster #2), and "therapeutic human papillomavirus vaccination" (cluster #3). Other noteworthy clusters include "peptide-based cancer vaccine," "T-lymphocyte," "MHC class-I downregulation," "synthetic long peptide vaccine," and "HPV 16 E7," which suggest significant advancements or breakthroughs in this domain. Furthermore, we analyzed the citation dynamics of these references, highlighting the top 50 with notable citation surges as depicted in Figure 6B. These surges underscore references that are gaining traction over time within the research community. Notably, the reference by Bray F. (2018) exhibited the highest citation strength at 21.63, followed by Chung et al. (2019) at 19.55 and Kenter et al. (2009) at 14.48, underscoring their substantial impact in the field.

3.6 Key topics of research hotspots

In bibliometrics, keywords serve as indicators of trends and focal points within a research domain (Li et al., 2016). They capture the essence of an academic article and, when analyzed collectively, reveal the central themes and directions of a field. Networks of co-keyword and keyword co-occurrence commonly feature overlapping keywords across articles on related topics, allowing for an in-depth analysis of the field's topological properties and their evolution.

3.6.1 Analysis of clusters and co-occurrence of keywords

To visualize keyword co-occurrence maps in the field of A/R/M cervical cancer immunotherapy, we utilized VOS Viewer (van Eck and Waltman, 2010). This tool enabled the creation of a keyword density map and a network illustrating keyword co-occurrences (Figure 7A, B). Additionally, we employed an online bibliometric analysis platform to identify and categorize annual high-frequency keywords (Figure 7C). The cluster analysis of these keywords provides insights into the knowledge structure of this field.

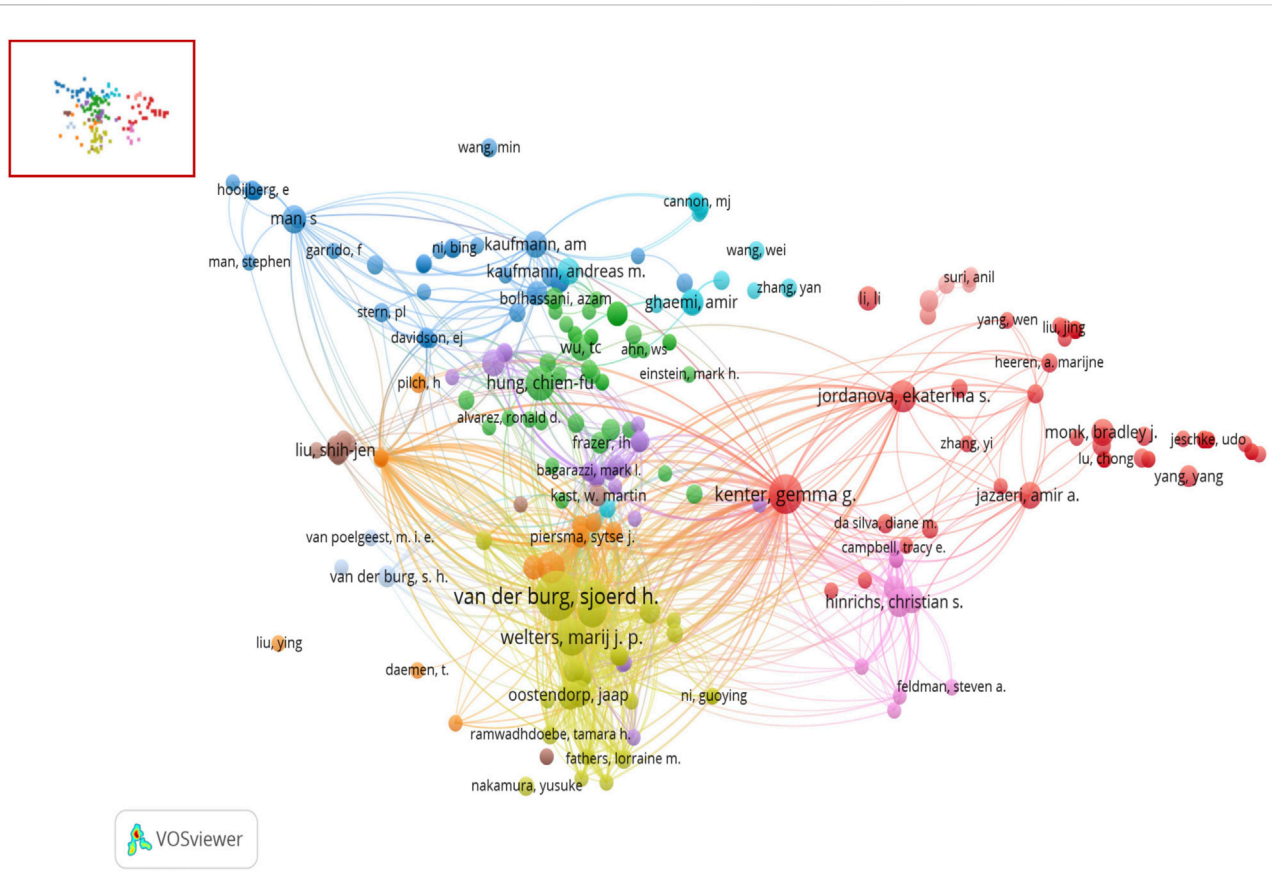

FIGURE 5
Collaborative network map among authors.

As depicted in Figure 7A, the network was divided into seven clusters based on the strength of the connections between co-occurring terms. Cluster 1 (green) contains 86 keywords focused on immune checkpoint inhibitors and related mechanisms. These keywords include activation, apoptosis, checkpoint blockade, B7-H1 (PD-L1), CTLA-4, FoxP3, tumor immune microenvironment, neoantigens, and IDO. Cluster 2 (red), with 82 keywords, primarily discusses immunotherapy strategies such as adoptive cell transfer (ACT), antitumor activity, immune checkpoint inhibitors, cytolytic T-lymphocytes, tumor-infiltrating lymphocytes, and CAR-T immunotherapy. Cluster 3 (blue) consists of 74 terms related to HPV vaccines and includes adenovirus, E6, E7, antigen presentation, antitumor immunity, cancer vaccine, DNA vaccine, and therapeutic vaccine. Cluster 4 (yellow) features 51 terms mostly associated with vaccination strategies, including adoptive transfer, antigens, cytokines, $CD4^+$, cytotoxic T-lymphocytes, IL-12, peptides, and helper immunity. Cluster 5 (purple) focuses on 47 terms concerning adoptive immunotherapy, such as biomarkers, monoclonal antibodies, natural killer cells, toll-like receptors, peptide vaccines, MHC class-I downregulation, and $CD8^+$ T cells. Cluster 6 (light blue) centers on HPV infection, comprising 23 terms like CD4, CD8, cell responses, CIN, regression, and natural history. Finally, Cluster 7 (orange) contains 19 terms related to immunoregulation, including regulatory T-cells, TGF-beta, hypoxia, and more.

3.6.2 Burst detection and overlay visualization of keywords

CiteSpace's keyword burst detection function is instrumental in identifying frequently appearing keywords within specific time frames, highlighting emerging topics in the field. As illustrated in Figure 8A, significant research hotspots over the past decade include vaccination (strength, 3.85; 2012–2016), PD-L1 expression (strength, 3.94; 2017–2020), nivolumab (strength, 5.95; 2017–2020), blockade (strength, 7.03; 2019–2022), pembrolizumab (strength, 6.43; 2019–2022), and apoptosis (strength, 3.36; 2019–2022). These terms indicate ongoing areas of research emphasis. Furthermore, an overlay visualization of the co-citation network's keyword timeline (2000–2022) was generated using CiteSpace, providing an in-depth view of the evolution of these keywords over time, as depicted in Figure 8B.

4 Discussion

4.1 General information

This bibliometric analysis offers a pioneering exploration of the intellectual foundation and research fronts of immunotherapy for A/R/M cervical cancer. Employing bibliometric and visual analysis techniques, this study examines global research trends from 2000 to 2022, encompassing publication patterns, contributing countries,

FIGURE 6
Visual representation of co-cited references in the domain of A/R/M cervical cancer immunotherapy **(A)**. Visualization of clusters formed by co-cited references **(B)**. The top 50 most frequently cited references (Red bars are sorted based on the starting year of the citation surge, indicating strong citation surges.).

institutions, journals, and key terms. The search captured 1,001 Web of Science publications involving 6,387 authors from 66 countries and 1,474 institutions, published across 366 scholarly journals. The increasing recognition of this field is largely attributed to significant innovations, such as the "KEYNOTE-158″Phase II study, which assessed the safety and efficacy of Pembrolizumab in previously treated advanced cervical carcinoma (Chung et al., 2019). A notable surge in publications over the past 3 years underscores the field's growing relevance and its potential for future advancements.

Only two of the 66 countries involved have published over 100 papers, with the United States and China clearly leading in A/R/M cervical cancer immunotherapy research. The United States, with a centrality score of 1.15, has played a pivotal role in fostering international collaboration. China stands out as the only developing country among the top five most productive nations. Among research institutions, Leiden University in the US is notable for having the highest number of publications and attracting significant attention. Economic disparities and varying national policies likely contribute to regional differences in the production of knowledge on cervical cancer immunotherapy. As illustrated in Figure 3A and 4A, while extensive collaboration is evident among many nations and organizations, others remain less connected. Therefore, it is recommended that countries and institutions involved in similar research increase their collaborative efforts to further develop and enhance this field.

4.2 Knowledge base

The utilization of co-citation analysis has been instrumental in delineating a shared body of knowledge among highly cited sources, underscoring the interconnectedness of seminal works within the field (Chen, 2004; Chen and Wu, 2017). In this bibliometric study, the co-citation cluster network and the ten most-cited references are displayed in Figure 6A and Supplementary Table S1, respectively. Notably, there is a significant overlap between our top 10 co-cited sources and the top 50 sources recognized for frequent citation bursts. Moving forward, we plan to conduct a comprehensive review of the key literature on cervical cancer immunology, focusing on the top ten sources that are frequently cited together. This analysis will aim to provide a holistic view of the subject, encompassing both fundamental scientific research and clinical studies.

Currently, preventive vaccines provide almost complete protection against persistent HPV infections and the development of severe genital lesions (Lowy and Schiller, 2006; Wheeler, 2007). However, women already infected with HPV strains covered by the vaccine do not benefit from it (Hildesheim et al., 2016). Consequently, there is a need for a therapeutic vaccine that can protect infected individuals. T-cell-based immunotherapeutic strategies effectively target the HPV16 E6 and E7 oncoproteins, which are present in all cervical cancer cells caused by HPV16(Hung et al., 2007; Vici et al., 2016; Saxena et al., 2021). *Clinical Cancer*

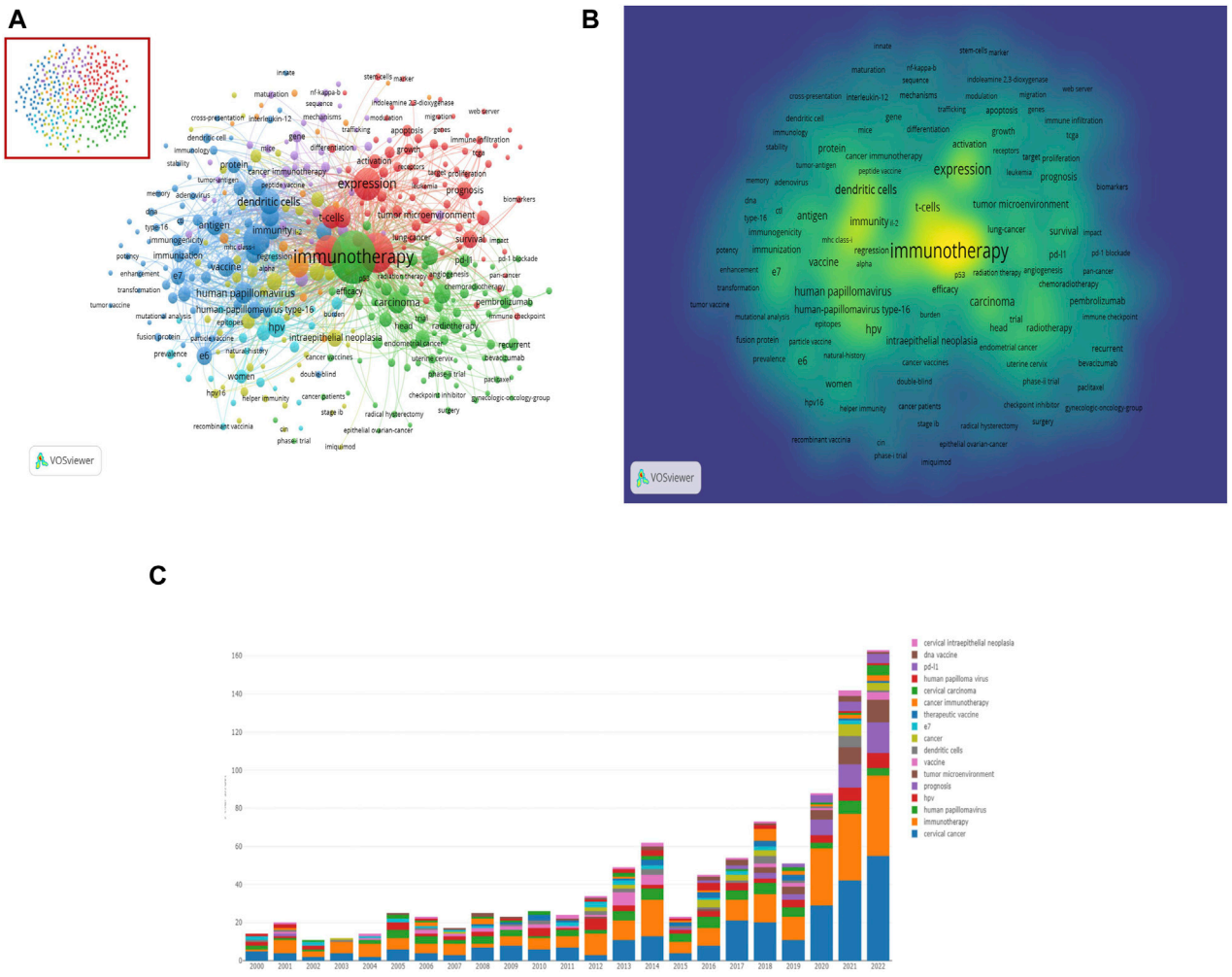

FIGURE 7
Keyword map in the domain of A/R/M cervical cancer immunotherapy **(A)**. Co-occurrence network and clusters of keywords (There are 641 keywords with a relevance score of at least 0.081. These keywords form a co-occurrence network and are organized into 7 clusters, resulting in a total of 42107 links. The connections and sizes of the nodes and words reflect the co-occurrence frequencies, indicating the co-occurrence relationship. Nodes of the same color serve as cluster representations) **(B)**. The keyword density map (Correlations exist between the co-cited frequency and the dimensions of the word, the roundness of the size, and the opacity of the yellow. It is capable of locating high-frequency co-occurrence terms, which indicate research centers.) **(C)**. Annual high-frequency keywords.

Research published the ninth most-cited study in 2008 (Welters et al., 2008), which discussed a synthetic long-peptide vaccine targeting HPV16 E6 and E7. This vaccine significantly increases $CD4^+$ and $CD8^+$ T-cell responses specific to HPV16, targeting various epitopes. Following this, *the New England Journal of Medicine* published the eighth co-cited study (Kenter et al., 2009), which demonstrated that women with grade 3 vulvar intraepithelial neoplasia caused by HPV-16 could achieve clinical responses after being vaccinated with a similar synthetic long-peptide vaccine. This innovation has been pivotal in advancing the development of therapeutic vaccines based on oncoproteins for cervical cancer. Over recent decades, there has been a resurgence in the development of therapeutic cancer vaccines. Enhanced understanding of tumor-associated antigens, advances in innovative antigen delivery methods, and insights into the natural immune response have collectively improved vaccine design (Sahin and Türeci, 2018; Saxena et al., 2021). Nevertheless, tumor-induced immunosuppression and the emergence of resistance to immune responses pose significant challenges in achieving effective treatments. Current efforts to target HPV E6 and E7 with therapeutic vaccines have yet to yield significant success in treating A/R/M cervical cancer (van Elsas et al., 2020; Saxena et al., 2021). To achieve a substantial clinical impact, it will be necessary to design a multi-therapeutic approach tailored to the specific challenges of A/R/M cervical cancer. Integrating vaccines with other treatments, such as chemotherapy, radiation therapy, or additional immunotherapies, may enhance treatment outcomes.

Adoptive T cell therapies (ACT), also known as T-cell-based vaccines, entail the extraction of T cells from the host, followed by their enhancement and reinfusion. This process allows T cells to selectively proliferate and attack tumor antigens *ex vivo*, ultimately inducing tumor regression (Rohaan et al., 2019; Sukari et al., 2019). ACT primarily utilizes T cells modified with chimeric antigen

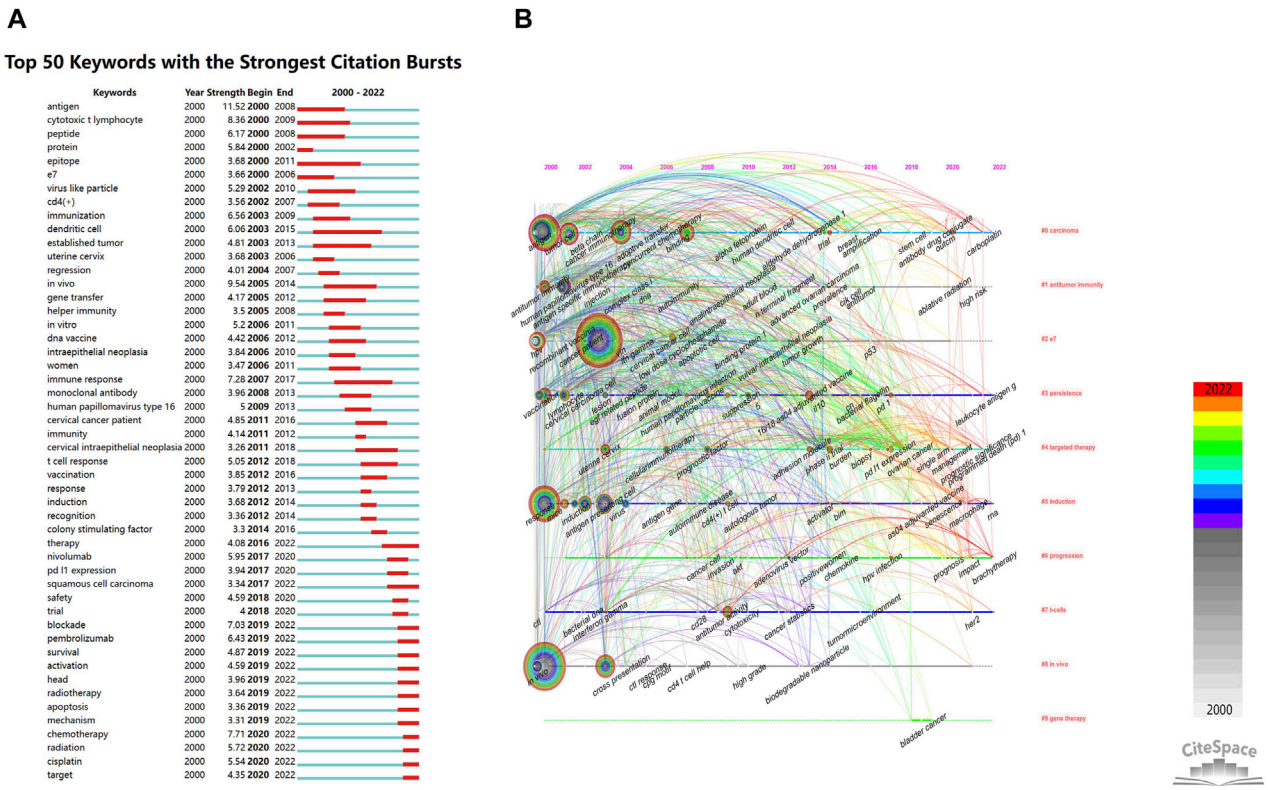

FIGURE 8
Scholastic cartography of keyword bursts and overlay visualization in the domain of immunotherapy for A/R/M cervical cancer **(A)**. Top 50 keywords with the strongest citation bursts (Red bars arranged according to the initial year of explosion indicate which keywords are frequently cited during a specific time period.) **(B)**. The temporal perspective of co-citation clusters (A time map represents the co-citation network for the given keyword from 2000–2022. A horizontal line represents the year of publication of each node in each cluster of this time map. Identifying the most recent and actively cited clusters is feasible within the time frame of 2019–2022).

receptors (CARs), engineered T-cell receptors (TCRs), and tumor-infiltrating lymphocytes (TILs) (Draper et al., 2015). A study published in *the Journal of Clinical Oncology* highlighted ACT as a novel treatment for metastatic cervical cancer (Stevanović et al., 2015). In a pivotal study, three of nine patients receiving a single infusion of selected TILs exhibited objective tumor responses—two complete and one partial. The complete responses were sustained for 22 and 15 months, respectively. Importantly, TILs targeting the HPV oncogenes E6 and E7 have proven effective in reducing tumor sizes in advanced cervical cancer cases. Alternatively, ACT can use genetically engineered TCRs designed to target specific tumor antigens (Draper et al., 2015). A completed Phase I/II trial suggested that E6 TCR therapy could induce remission in HPV-associated epithelial malignancies. Consequently, further research into this treatment is imperative (Klebanoff et al., 2016; Doran et al., 2019). Several ongoing clinical trials are evaluating the efficacy of HPV oncoprotein-specific TCR T cells in treating cervical cancer, with results expected soon (NCT03578406, NCT04476251, and NCT02858310). ACT represents a highly personalized, innovative therapy that may overcome the limitations of traditional chemotherapy in treating A/R/M cervical cancer.

Immunotherapeutic strategies targeting immunological checkpoint molecules, such as CTLA-4 and PD-1 on activated T cells, have induced complete and durable responses in various cancers, including melanoma and bladder malignancies (Wheeler, 2007; Powles et al., 2014). A study in *Modern Pathology* found that squamous cell carcinoma and adenocarcinoma differentially express PD-L1, with squamous cell carcinomas showing significantly higher PD-L1 expression and tumor-associated macrophage levels than adenocarcinomas. These findings underscore PD-L1's critical role in cervical cancer's immune evasion and support therapeutic targeting of the PD-1/PD-L1 pathway (Heeren et al., 2016). Between 2017 and 2019, the *Journal of Clinical Oncology* published several trials confirming these observations (Frenel et al., 2017; Chung et al., 2019; Naumann et al., 2019). Notably, pembrolizumab monotherapy has demonstrated sustained anticancer efficacy and tolerability in patients with advanced cervical cancer (Chung et al., 2019). Consequently, the FDA expedited approval of pembrolizumab for patients with advanced, PD-L1-positive cervical cancer showing progression during or after treatment. In 2017, *Nature* reported a record number of genomic studies on cervical cancer, revealing critical mutations in genes such as CASP8, SHKBP1, ERBB3, HLA-A, and TGFBR2. The studies also highlighted APOBEC mutation patterns, the impact of BCAR4 lncRNA on lapatinib response, and new amplifications in immune targets CD274/PD-L1 and PDCD1LG2/PD-L2. These insights, derived from a comprehensive molecular analysis of 228 primary cervical cancers, suggest potential new therapeutic targets and advocate for personalized treatment strategies for advanced/recurrent/metastatic cervical cancers. In conclusion, the advancement of

immunotherapeutic approaches targeting the PD-1/PD-L1 pathway represents a significant breakthrough in improving cervical cancer treatments. The integration of these innovations with personalized therapy and continued research efforts is redefining the possibilities of cancer treatment, offering a promising future for individuals facing this challenging disease.

4.3 Progression of hotspots and emerging subjects

The recent advances in therapeutic development, particularly in harnessing the host immune system to manage and potentially eliminate cancer, are reflected in the prevalent keywords in current research. Several studies (Cohen et al., 2019; van Elsas et al., 2020; Wang et al., 2020; Ferrall et al., 2021; Norberg and Hinrichs, 2023) demonstrate a growing interest within the scientific community in integrating immunotherapy with traditional cancer treatments such as radiotherapy and chemotherapy. The goal of combining these modalities is to improve therapeutic outcomes and develop more effective cancer control strategies. To highlight these advancements, we present key summaries and discussions from the 2023 ASCO conference, focusing on significant breakthroughs in the field of immunotherapy for A/R/M cervical cancer.

The KEYNOTE-826 study (NCT03635567), highlighted by Bradley J. Monk at the 2023 ASCO conference, reported compelling survival results (Monk et al., 2023). Pembrolizumab achieved a final overall survival of 28.6 months in patients with PD-L1 CPS≥1, 26.4 months across all participants, and a peak of 29.6 months for those with PD-L1 CPS≥10. Progression-free survival was noteworthy, reaching 10.5 and 10.4 months for PD-L1 CPS≥1 and all patients, respectively. These outcomes were statistically significant, regardless of bevacizumab co-administration. In patients with PD-L1 CPS≥1, pembrolizumab significantly increased the objective response rate (68.5% *versus* 50.9% for placebo) and complete response rate (25.6% *versus* 14.5% for placebo). These results affirm the combined use of pembrolizumab and chemotherapy, with or without bevacizumab, as a first-line treatment for advanced/recurrent/metastatic cervical cancer, echoing previous interim findings (Colombo et al., 2021). Furthermore, the phase II CAESURA trial (NCT03912402) assessed the efficacy and safety of prolgolimab combined with platinum-based chemotherapy and bevacizumab in advanced cervical cancer (Fogt et al., 2023). The objective response rate was 63.8% per RECIST 1.1 criteria, with two complete and 35 partial responses. Under iRECIST criteria, the response rate improved to 70.7%, including the same two complete and an increased 39 partial responses. At 12 months, progression-free survival was recorded at 8.5 months per RECIST 1.1 and 13.1 months per iRECIST. The median overall survival had not yet been reached. Notably, 98% of participants experienced adverse events, with 69% considered treatment-related. There were 12 severe events (grade 3 or higher), and immune-related adverse events were noted in approximately 38% of patients. Despite these challenges, the trial demonstrated that the combination of prolgolimab, chemotherapy, and bevacizumab offers promising efficacy and an acceptable safety profile for treating advanced cervical cancer. A phase III placebo-controlled trial (NCT03912402) exploring this treatment regimen as a potential first-line therapy is currently underway, with results highly anticipated by the oncological community.

While the KEYNOTE and CAESURA studies underscore the effectiveness of PD-1 inhibitors in managing A/R/M cervical cancer, locally advanced cervical cancer (LACC) remains a significant clinical challenge. Despite innovative treatments, the relapse rate for LACC exceeds 40% following standard chemoradiation. This underscores the urgent need for improved therapeutic strategies in this setting. Notably, an elevated CD8+/FOXP3+ ratio in tumor cells post-neoadjuvant chemotherapy has been associated with better clinical outcomes (Liang et al., 2018), indicating potential biomarkers for therapeutic efficacy. The use of immune checkpoint inhibitors (ICIs) has shown survival benefits in recurrent cases (Colombo et al., 2021; Tewari et al., 2022). However, the CALLA trial did not demonstrate a significant prolongation in progression-free survival for high-risk LACC patients treated with adjuvant defactinib compared to radiotherapy and chemotherapy alone. This highlights the variability in response to new treatments and the need for further investigation. The COLIBRI trial (NCT04256213), as reported by France's Isabelle Ray-Coquard (Ray-Coquard et al., 2023), focuses on the pre-radio-chemotherapy effects of dual immune therapy with nivolumab and ipilimumab in patients with cervical squamous cell carcinoma stages FIGO IB3-IVA. This trial confirmed the safety and potential efficacy of using nivolumab and ipilimumab as preemptive neoadjuvant treatments, followed by sustained nivolumab monotherapy after radio-chemotherapy. Significant increases in $CD8^+$ cell proliferation, the CD8+/FOXP3+ ratio, and Histo-Cytometry Optimization Threshold (HOT) scores were observed after this dual immune therapy, analyzed using multi-lF or HTG technologies. These findings advocate for the continued exploration of ICIs as a neoadjuvant and sequential treatment strategy in LACC management. The initial results from the COLIBRI trial provide a promising basis for future integrated ICI strategies, suggesting a potential paradigm shift that could enhance survival rates and improve treatment outcomes for LACC patients. This ongoing research highlights the dynamic nature of cancer treatment innovations and the need for tailored strategies to address different stages and types of cervical cancer.

The inclusion of an anti-CTLA-4 antibody alongside PD-1 inhibition has notably extended the duration of response (DoR) and survival, resulting in an increased overall response rate (ORR) (Larkin et al., 2019; Xu et al., 2022). However, this combination therapy significantly raises the frequency of immune-related adverse events (irAEs) compared to anti-PD-1 monotherapy (Hellmann et al., 2019). Recently, alternative strategies have been explored, including a bispecific antibody capable of binding two different antigens or the same antigen at different epitopes, showing substantial promise in clinical trials (Wu et al., 2021; Wang et al., 2022; Wu et al., 2022). Another innovative approach involves QL1706 (PSB205), a bifunctional PD-1/CTLA-4 dual blocker. This engineered monoclonal antibody combines anti-CTLA-4 IgG1 with a novel bifunctional MabPair platform. QL1706 is characterized by a shortened elimination half-life (t1/2) for the CTLA-4 component, which may enhance tolerability by maintaining prolonged anti-PD-1 activity while reducing exposure to CTLA-4, potentially allowing patients to continue

treatment longer without severe CTLA-4-related adverse effects. In a phase I trial on advanced solid tumors, including pretreated advanced cervical cancer, QL1706 demonstrated an ORR of 27.3% (15/55) with a median duration of response (mDoR) not reached; these results are comparable to the ORR of 25.6% reported for the dual PD-1 and CTLA-4 checkpoint blockade with balstilimab and zalifrelimab (O'Malley et al., 2022). As the first of its kind, this bifunctional MabPair product has shown promising antitumor activity and a favorable safety profile, indicating the potential for further development as a foundational agent in dual immunotherapy. This opens the door to the integration of multiple immunotherapeutic strategies, which could significantly enhance effectiveness. Such an approach may involve amplifying antigen-specific T cells, mitigating immunosuppression in the tumor microenvironment, or enhancing effector immune functions, potentially in combination with traditional treatments like chemotherapy or radiotherapy. This holistic immunotherapy approach could prove more effective than focusing on a single strategy, offering a robust framework for combating cancer.

Immunotherapy, particularly targeting the PD-1/PD-L1 pathway, has markedly transformed the treatment landscape for solid tumors, including A/R/M cervical cancers (Motzer et al., 2019; Herbst et al., 2020; An et al., 2022). Frequently, targeting a single signaling pathway does not sufficiently restore robust antitumor immunity, leading to resistance and recurrence (Yi et al., 2018). This is partly due to various factors within the tumor microenvironment (TME) that suppress immune responses, among which transforming growth factor-beta (TGF-β) plays a critical role (Batlle et al., 2019). TGF-β functions as a tumor suppressor in early-stage breast cancers by inducing cell cycle arrest and apoptosis (Moses et al., 2011). However, in advanced cancers, it paradoxically promotes tumor growth by facilitating metastasis, resistance to radiotherapy and chemotherapy, and remodeling the TME (Colak et al., 2017; Yi et al., 2022). TGF-β also extensively suppresses immune activities in the TME, affecting tumor-infiltrating lymphocytes (TILs), macrophage polarization, regulatory T cell (Treg) differentiation, and dendritic cell (DC) activity (Bagati et al., 2021). Additionally, it enhances the production of peritumoral collagen by cancer-associated fibroblasts (CAFs), which hinders the movement of TILs (Trimble et al., 2015). To overcome immunotherapy resistance, strategies that inhibit both PD-1 and TGF-β pathways, such as the use of bifunctional antibodies like M7824 and SHR1701, are gaining attention (Khalili-Tanha et al., 2023; Tan et al., 2022). These second-generation bifunctional agents, targeting both the TGF-β and PD-1 pathways, have been developed as fusion proteins targeting PD-L1/TGF-β. Preclinical studies suggest that M7824, for instance, not only suppresses tumor growth but also significantly enhances both innate and adaptive immunity more effectively than PD-1 inhibitors alone (Lan et al., 2018). Initial clinical trials highlighted M7824s potent anticancer capabilities (Yi et al., 2022). However, subsequent phase 2/3 trials in specific cancers such as bile duct and non-small-cell lung cancers have shown less efficacy than anticipated (Lind et al., 2020). The reasons for these discrepancies are not fully understood, but enhancing the identification of responsive patients through predictive markers could significantly improve the effectiveness of these bifunctional antibodies. This approach promises to refine and optimize the therapeutic strategies in immunotherapy, potentially leading to more personalized and effective cancer treatments.

The immune normalization approach focuses on restoring impaired anti-tumor immune responses by targeting key pathways such as PD-1/PD-L1 to modify the TME (Sanmamed et al., 2018; Bai, et al., 2019). However, for most patients, the immune imbalance in the TME is complex, and addressing additional abnormalities is often crucial to overcome resistance to PD-1/PD-L1 inhibitors. In this context, the development of bispecific antibodies, such as YM101, which targets both PD-L1 and murine TGF-β with a ScFv-IgG-like structure, represents a significant advancement (Yi et al., 2021). YM101 is designed to mitigate the dominant inhibitory effects of TGF-β, shifting the "cancer-immunity set point" from immune tolerance to active T cell immunity, enhancing the therapeutic landscape. Functional assays have demonstrated that YM101 effectively counters the suppressive actions of both the PD-1 and TGF-β pathways. *In vivo* studies reveal that YM101 significantly reduces tumor growth in mouse models, affirming its potential as a dual-targeting therapeutic agent. Moreover, YM101 has been shown to be both effective and safe in preclinical evaluations (Yi et al., 2021). Another analogous bispecific molecule, BiTP, tailored for further clinical investigations, exhibits high affinity for its targets and effectively inhibits subsequent signaling pathways (Yi et al., 2022). Preclinical tests indicate that BiTP can slow tumor growth and extend survival in animal models, showing particular promise against triple-negative breast cancer (Yi et al., 2022). In the TME, BiTP is noted for reducing stromal collagen buildup, enhancing T cell penetration, and diminishing immune-suppressive elements, suggesting a robust candidate for advancing to clinical trials. Additionally, TQB2858, another bispecific antibody targeting PD-L1 and TGF-β, is currently under clinical evaluation and demonstrates potential as a therapeutic option (Xing et al., 2023). The evolution of anti-PD-L1/TGF-β bispecific antibodies signifies a major shift from traditional PD-1/PD-L1 monoclonal antibodies, offering a synergistic approach that may transform immune-excluded tumors into immune-inflamed ones, thereby amplifying the efficacy of existing therapies and broadening the horizons of immunotherapy. While initial results are promising, extensive studies are required to fully ascertain the therapeutic potential of TGF-β targeting in cervical cancer treatment. Furthermore, the integration of TGF-β inhibitors with other immunotherapeutic strategies, such as vaccines or cell-based treatments, could potentially enhance overall therapeutic outcomes, providing a comprehensive approach to combating this malignancy.

4.4 Limitations

This study represents the first bibliometric analysis of original articles focused on immunotherapy for A/R/M cervical cancer. By conducting a quantitative review of the literature, this research summarizes the development of immunotherapy in this field and aims to guide future scholarly inquiries. However, there are several limitations to consider. Firstly, the exclusive use of the Web of Science database for data collection may introduce a publication bias. Moreover, the restriction to English-language publications could have introduced a language-specific publication bias,

potentially overlooking relevant studies published in other languages. Additionally, using bibliometric tools that are based on artificial intelligence and computational linguistics, as suggested by earlier research (Yan et al., 2021), could make it harder to get all the information that is needed. Even with these problems, our results are mostly the same as those of recent traditional reviews (Roden and Stern, 2018; Ferrall et al., 2021). These results give researchers more unbiased information that helps them understand and from see things a different point of view in the field of immunotherapy for A/R/M cervical cancer. These limitations underscore the need for broader and more inclusive research methodologies that expand beyond single-database searches and English-language constraints to ensure a more comprehensive global perspective in future bibliometric analyses.

5 Conclusion

In general, this work employs a methodical bibliometric approach to analyze the articles on immunotherapy for advanced, recurrent, and metastatic cervical cancer. It offers useful insights through quantitative evaluations and knowledge mapping. In order to advance research, it will be crucial to strengthen international and institutional relationships in the future. Currently, there is a strong focus on enhancing our knowledge of the immune features of A/R/M cervical cancer, identifying patient populations that are most likely to respond well to immunotherapy, and exploring the practical uses of therapeutic vaccines, adoptive T cell therapies (ACT), immune checkpoint inhibitors (ICIs), and innovative dual-specificity treatments that target both TGF-beta and PD-L1. These therapeutic techniques are progressively being integrated with conventional treatments such as chemotherapy, radiation, and targeted therapies. The future of cervical cancer immunotherapy will likely include enhancing treatment effectiveness, minimizing adverse effects, and developing more powerful, individualized treatment strategies that cater to different disease phases.

Data availability statement

The raw data supporting the conclusion of this article will be made available by the authors, without undue reservation.

Author contributions

YD: Conceptualization, Data curation, Formal Analysis, Investigation, Methodology, Project administration, Resources, Software, Supervision, Validation, Visualization, Writing–original draft. LY: Conceptualization, Data curation, Formal Analysis, Methodology, Project administration, Resources, Supervision, Validation, Visualization, Writing–original draft. WW: Conceptualization, Data curation, Formal Analysis, Funding acquisition, Investigation, Methodology, Resources, Software, Validation, Visualization, Writing–original draft. PZ: Conceptualization, Data curation, Formal Analysis, Methodology, Project administration, Resources, Visualization, Writing–original draft. KF: Conceptualization, Data curation, Formal Analysis, Methodology, Validation, Visualization, Writing–original draft. WL: Conceptualization, Formal Analysis, Investigation, Methodology, Resources, Visualization, Writing–original draft. RY: Conceptualization, Data curation, Formal Analysis, Funding acquisition, Investigation, Methodology, Project administration, Resources, Software, Supervision, Validation, Visualization, Writing–review and editing.

Funding

The author(s) declare financial support was received for the research, authorship, and/or publication of this article. This research was funded by the Scientific Research Project of Cadre Healthcare in Sichuan Province (2023-1702): "study on the diversity of TCR in peripheral blood of women with different cervical cancer" and the "Key Project" of the Sichuan Provincial Department of Science and Technology (2019YFS0532): "Study on the Key Factors Affecting the Diagnosis and Treatment of Major Disease in Obstetrics and Gynecology" (Approved Medical Ethics Committee of West China Second University Hospital, Sichuan University). Ethical Lot Number: 20220129. Efficacy and safety of Sintilimab combined with chemoradiotherapy in patients with advanced and recurrent/metastatic uterine malignancies. WU JIEPIING Medical Foundation: 320.6750.2021-02-129.

Conflict of interest

The authors declare that the research was conducted in the absence of any commercial or financial relationships that could be construed as a potential conflict of interest.

Publisher's note

Supplementary material

The Supplementary Material for this article can be found online at: https://www.frontiersin.org/articles/10.3389/fphar.2024.1351363/full#supplementary-material

References

Attademo, L., Tuninetti, V., Pisano, C., Cecere, S. C., Di Napoli, M., Tambaro, R., et al. (2020). Immunotherapy in cervix cancer. *Cancer Treat. Rev.* 90, 102088. doi:10.1016/j.ctrv.2020.102088

Chen, C. (2004). Searching for intellectual turning points: progressive knowledge domain visualization. *Proc. Natl. Acad. Sci. U.S.A.* 101 (Suppl. 1), 5303–5310. doi:10.1073/pnas.0307513100

Chen, C., Hu, Z., Liu, S., and Tseng, H. (2012). Emerging trends in regenerative medicine: a scientometric analysis in CiteSpace. *Expert Opin. Biol. Ther.* 12, 593–608. doi:10.1517/14712598.2012.674507

Chen, C., and Song, M. (2019). Visualizing a field of research: a methodology of systematic scientometric reviews. *PLoS ONE* 14, e0223994. doi:10.1371/journal.pone.0223994

Chen, Y., and Wu, C. (2017). The hot spot transformation in the research evolution of maker. *Scientometrics* 113, 1307–1324. doi:10.1007/s11192-017-2542-4

Chung, H. C., Ros, W., Delord, J. P., Perets, R., Italiano, A., Shapira-Frommer, R., et al. (2019). Efficacy and safety of pembrolizumab in previously treated advanced cervical cancer: results from the phase II KEYNOTE-158 study. *J. Clin. Oncol.* 37, 1470–1478. doi:10.1200/JCO.18.01265

Cohen, P. A., Jhingran, A., Oaknin, A., and Denny, L. (2019). Cervical cancer. *Lancet* 393, 169–182. doi:10.1016/S0140-6736(18)32470-X

Colombo, N., Dubot, C., Lorusso, D., Caceres, M. V., Hasegawa, K., Shapira-Frommer, R., et al. (2021). Pembrolizumab for persistent, recurrent, or metastatic cervical cancer. *N. Engl. J. Med.* 385, 1856–1867. doi:10.1056/NEJMoa2112435

Da Silva, D. M., Skeate, J. G., Chavez-Juan, E., Lühen, K. P., Wu, J. M., Wu, C. M., et al. (2019). Therapeutic efficacy of a human papillomavirus type 16 E7 bacterial exotoxin fusion protein adjuvanted with CpG or GPI-0100 in a preclinical mouse model for HPV-associated disease. *Vaccine* 37, 2915–2924. doi:10.1016/j.vaccine.2019.04.043

Doran, S. L., Stevanović, S., Adhikary, S., Gartner, J. J., Jia, L., Kwong, M., et al. (2019). T-cell receptor gene therapy for human papillomavirus-associated epithelial cancers: a first-in-human, phase I/II study. *J. Clin. Oncol.* 37, 2759–2768. doi:10.1200/JCO.18.02424

Draper, L. M., Kwong, M. L., Gros, A., Stevanović, S., Tran, E., Kerkar, S., et al. (2015). Targeting of HPV-16+ epithelial cancer cells by TCR gene engineered T cells directed against E6. *Clin. Cancer Res.* 21, 4431–4439. doi:10.1158/1078-0432.CCR-14-3341

Duska, L. R., Scalici, J. M., Temkin, S. M., Schwarz, J. K., Crane, E. K., Moxley, K. M., et al. (2020). Results of an early safety analysis of a study of the combination of pembrolizumab and pelvic chemoradiation in locally advanced cervical cancer. *Cancer* 126, 4948–4956. doi:10.1002/cncr.33136

Ellegaard, O., and Wallin, J. A. (2015). The bibliometric analysis of scholarly production: how great is the impact. *Scientometrics* 105, 1809–1831. doi:10.1007/s11192-015-1645-z

Feng, C. H., Mell, L. K., Sharabi, A. B., McHale, M., and Mayadev, J. S. (2020). Immunotherapy with radiotherapy and chemoradiotherapy for cervical cancer. *Semin. Radiat. Oncol.* 30, 273–280. doi:10.1016/j.semradonc.2020.05.003

Ferrall, L., Lin, K. Y., Roden, R., Hung, C. F., and Wu, T. C. (2021). Cervical cancer immunotherapy: facts and hopes. *Clin. Cancer Res.* 27, 4953–4973. doi:10.1158/1078-0432.CCR-20-2833

Fogt, S., Andabekov, T., Shamsutdinova, Y., Dvorkin, M., Artamonova, E., Chistyakov, V., et al. (2023). Final results of a phase II trial of prolgolimab with platinum-based therapy and bevacizumab in patients with advanced cervical cancer. *J. Clin. Oncol. Clin. Oncol.* 41, 5536. doi:10.1200/JCO.2023.41.16_suppl.5536

Frenel, J. S., Le Tourneau, C., O'Neil, B., Ott, P. A., Piha-Paul, S. A., Gomez-Roca, C., et al. (2017). Safety and efficacy of pembrolizumab in advanced, programmed death ligand 1-positive cervical cancer: results from the phase ib KEYNOTE-028 trial. *J. Clin. Oncol.* 35, 4035–4041. doi:10.1200/JCO.2017.74.5471

Frumovitz, M., Westin, S. N., Salvo, G., Zarifa, A., Xu, M., Yap, T. A., et al. (2020). Phase II study of pembrolizumab efficacy and safety in women with recurrent small cell neuroendocrine carcinoma of the lower genital tract. *Gynecol. Oncol.* 158, 570–575. doi:10.1016/j.ygyno.2020.05.682

Gao, N., Li, M., Wang, W., Liu, Z., and Guo, Y. (2023). A bibliometrics analysis and visualization study of TRPV1 channel. *Front. Pharmacol.* 14, 1076921. doi:10.3389/fphar.2023.1076921

Han, Q., Li, Z., Fu, Y., Liu, H., Guo, H., Guan, X., et al. (2023). Analyzing the research landscape: mapping frontiers and hot spots in anti-cancer research using bibliometric analysis and research network pharmacology. *Front. Pharmacol.* 14, 1256188. doi:10.3389/fphar.2023.1256188

Harper, D. M., Nieminen, P., Donders, G., Einstein, M. H., Garcia, F., Huh, W. K., et al. (2019). The efficacy and safety of Tipapkinogen Sovacivec therapeutic HPV vaccine in cervical intraepithelial neoplasia grades 2 and 3: randomized controlled phase II trial with 2.5 years of follow-up. *Gynecol. Oncol.* 153, 521–529. doi:10.1016/j.ygyno.2019.03.250

Heeren, A. M., Punt, S., Bleeker, M. C., Gaarenstroom, K. N., van der Velden, J., Kenter, G. G., et al. (2016). Prognostic effect of different PD-L1 expression patterns in squamous cell carcinoma and adenocarcinoma of the cervix. *Mod. Pathol.* 29, 753–763. doi:10.1038/modpathol.2016.64

Hellmann, M. D., Paz-Ares, L., Bernabe Caro, R., Zurawski, B., Kim, S. W., Carcereny Costa, E., et al. (2019). Nivolumab plus ipilimumab in advanced non-small-cell lung cancer. *N. Engl. J. Med.* 381, 2020–2031. doi:10.1056/NEJMoa1910231

Hildesheim, A., Gonzalez, P., Kreimer, A. R., Wacholder, S., Schussler, J., Rodriguez, A. C., et al. (2016). Impact of human papillomavirus (HPV) 16 and 18 vaccination on prevalent infections and rates of cervical lesions after excisional treatment. *Am. J. Obstet. Gynecol.* 215, 212.e1–212.e15. doi:10.1016/j.ajog.2016.02.021

Huang, H., Nie, C. P., Liu, X. F., Song, B., Yue, J. H., Xu, J. X., et al. (2022). Phase I study of adjuvant immunotherapy with autologous tumor-infiltrating lymphocytes in locally advanced cervical cancer. *J. Clin. Invest.* 132, e157726. doi:10.1172/JCI157726

Huh, W. K., Brady, W. E., Fracasso, P. M., Dizon, D. S., Powell, M. A., Monk, B. J., et al. (2020). Phase II study of axalimogene filolisbac (ADXS-HPV) for platinum-refractory cervical carcinoma: an NRG oncology/gynecologic oncology group study. *Gynecol. Oncol.* 158, 562–569. doi:10.1016/j.ygyno.2020.06.493

Hung, C. F., Monie, A., Alvarez, R. D., and Wu, T. C. (2007). DNA vaccines for cervical cancer: from bench to bedside. *Exp. Mol. Med.* 39, 679–689. doi:10.1038/emm.2007.74

Jiang, M., Qi, Y., Liu, H., and Chen, Y. (2018). The role of nanomaterials and nanotechnologies in wastewater treatment: a bibliometric analysis. *Nanoscale Res. Lett.* 13, 233. doi:10.1186/s11671-018-2649-4

Kenter, G. G., Welters, M. J., Valentijn, A. R., Lowik, M. J., Berends-van der Meer, D. M., Vloon, A. P., et al. (2009). Vaccination against HPV-16 oncoproteins for vulvar intraepithelial neoplasia. *N. Engl. J. Med.* 361, 1838–1847. doi:10.1056/NEJMoa0810097

Klebanoff, C. A., Rosenberg, S. A., and Restifo, N. P. (2016). Prospects for gene-engineered T cell immunotherapy for solid cancers. *Nat. Med.* 22, 26–36. doi:10.1038/nm.4015

Larkin, J., Chiarion-Sileni, V., Gonzalez, R., Grob, J. J., Rutkowski, P., Lao, C. D., et al. (2019). Five-year survival with combined nivolumab and ipilimumab in advanced melanoma. *N. Engl. J. Med.* 381, 1535–1546. doi:10.1056/NEJMoa1910836

Lawson McLean, A. (2019). Publication trends in transcranial magnetic stimulation: a 30-year panorama. *Brain Stimul.* 12, 619–627. doi:10.1016/j.brs.2019.01.002

Li, H., An, H., Wang, Y., Huang, J., and Gao, X. (2016). Evolutionary features of academic articles co-keyword network and keywords co-occurrence network: based on two-mode affiliation network. *Phys. A Stat. Mech. its Appl.* 450, 657–669. doi:10.1016/j.physa.2016.01.017

Liang, Y., Lü, W., Zhang, X., and Lü, B. (2018). Tumor-infiltrating CD8+ and FOXP3+ lymphocytes before and after neoadjuvant chemotherapy in cervical cancer. *Diagn Pathol.* 13, 93. doi:10.1186/s13000-018-0770-4

Lowy, D. R., and Schiller, J. T. (2006). Prophylactic human papillomavirus vaccines. *J. Clin. Invest.* 116, 1167–1173. doi:10.1172/JCI28607

Lu, C., Liu, M., Shang, W., Yuan, Y., Li, M., Deng, X., et al. (2020). Knowledge mapping of angelica sinensis (oliv.) diels (danggui) research: a scientometric study. *Front. Pharmacol.* 11, 294. doi:10.3389/fphar.2020.00294

Mayadev, J. S., Enserro, D., Lin, Y. G., Da Silva, D. M., Lankes, H. A., Aghajanian, C., et al. (2020). Sequential ipilimumab after chemoradiotherapy in curative-intent treatment of patients with node-positive cervical cancer. *JAMA Oncol.* 6, 92–99. doi:10.1001/jamaoncol.2019.3857

Monk, B. J., Enomoto, T., Kast, W. M., McCormack, M., Tan, D., Wu, X., et al. (2022). Integration of immunotherapy into treatment of cervical cancer: recent data and ongoing trials. *Cancer Treat. Rev.* 106, 102385. doi:10.1016/j.ctrv.2022.102385

Monk, B. J., Tewari, K. S., Dubot, C., Caceres, M. V., Hasegawa, K., Shapira-Frommer, R., et al. (2023). Health-related quality of life with pembrolizumab or placebo plus chemotherapy with or without bevacizumab for persistent, recurrent, or metastatic cervical cancer (KEYNOTE-826): a randomised, double-blind, placebo-controlled, phase 3 trial. *Lancet Oncol.* 24, 392–402. doi:10.1016/S1470-2045(23)00052-9

Morris, M., Eifel, P. J., Lu, J., Grigsby, P. W., Levenback, C., Stevens, R. E., et al. (1999). Pelvic radiation with concurrent chemotherapy compared with pelvic and para-aortic radiation for high-risk cervical cancer. *N. Engl. J. Med.* 340, 1137–1143. doi:10.1056/NEJM199904153401501

Naumann, R. W., Hollebecque, A., Meyer, T., Devlin, M. J., Oaknin, A., Kerger, J., et al. (2019). Safety and efficacy of nivolumab monotherapy in recurrent or metastatic cervical, vaginal, or vulvar carcinoma: results from the phase I/II CheckMate 358 trial. *J. Clin. Oncol.* 37, 2825–2834. doi:10.1200/JCO.19.00739

Norberg, S. M., and Hinrichs, C. S. (2023). Engineered T cell therapy for viral and non-viral epithelial cancers. *Cancer Cell* 41, 58–69. doi:10.1016/j.ccell.2022.10.016

O'Malley, D. M., Neffa, M., Monk, B. J., Melkadze, T., Huang, M., Kryzhanivska, A., et al. (2022). Dual PD-1 and CTLA-4 checkpoint blockade using balstilimab and zalifrelimab combination as second-line treatment for advanced cervical cancer: an open-label phase II study. *J. Clin. Oncol.* 40, 762–771. doi:10.1200/JCO.21.02067

O'Malley, D. M., Oaknin, A., Monk, B. J., Selle, F., Rojas, C., Gladieff, L., et al. (2021). Phase II study of the safety and efficacy of the anti-PD-1 antibody balstilimab in patients

with recurrent and/or metastatic cervical cancer. *Gynecol. Oncol.* 163, 274–280. doi:10.1016/j.ygyno.2021.08.018

Pal, A., and Kundu, R. (2019). Human papillomavirus E6 and E7: the cervical cancer hallmarks and targets for therapy. *Front. Microbiol.* 10, 3116. doi:10.3389/fmicb.2019.03116

Powles, T., Eder, J. P., Fine, G. D., Braiteh, F. S., Loriot, Y., Cruz, C., et al. (2014). MPDL3280A (anti-PD-L1) treatment leads to clinical activity in metastatic bladder cancer. *Nature* 515, 558–562. doi:10.1038/nature13904

Qin, Y., Zhang, Q., and Liu, Y. (2020). Analysis of knowledge bases and research focuses of cerebral ischemia-reperfusion from the perspective of mapping knowledge domain. *Brain Res. Bull.* 156, 15–24. doi:10.1016/j.brainresbull.2019.12.004

Ray-Coquard, I. L., Kaminsky-Forrett, M., Ohkuma, R., De Montfort, A., Joly, F., Treilleux, I., et al. (2023). *In situ* immune impact of nivolumab + ipilimumab combination before standard chemoradiation therapy (RTCT) for FIGO IB3-IVA in patients (pts) with cervical squamous carcinoma: COLIBRI trial, a GINECO study. *J. Clin. Oncol. Clin. Oncol.* 41, 5501. doi:10.1200/JCO.2023.41.16_suppl.5501

Roden, R., and Stern, P. L. (2018). Opportunities and challenges for human papillomavirus vaccination in cancer. *Nat. Rev. Cancer* 18, 240–254. doi:10.1038/nrc.2018.13

Rohaan, M. W., Wilgenhof, S., and Haanen, J. (2019). Adoptive cellular therapies: the current landscape. *Virchows Arch.* 474, 449–461. doi:10.1007/s00428-018-2484-0

Sahin, U., and Türeci, Ö. (2018). Personalized vaccines for cancer immunotherapy. *Science* 359, 1355–1360. doi:10.1126/science.aar7112

Santin, A. D., Bellone, S., Palmieri, M., Zanolini, A., Ravaggi, A., Siegel, E. R., et al. (2008). Human papillomavirus type 16 and 18 E7-pulsed dendritic cell vaccination of stage IB or IIA cervical cancer patients: a phase I escalating-dose trial. *J. Virol.* 82, 1968–1979. doi:10.1128/JVI.02343-07

Saxena, M., van der Burg, S. H., Melief, C., and Bhardwaj, N. (2021). Therapeutic cancer vaccines. *Nat. Rev. Cancer* 21, 360–378. doi:10.1038/s41568-021-00346-0

Siegel, R. L., Miller, K. D., Fuchs, H. E., and Jemal, A. (2022). Cancer statistics, 2022. *CA Cancer J. Clin.* 72, 7–33. doi:10.3322/caac.21708

Stevanović, S., Draper, L. M., Langhan, M. M., Campbell, T. E., Kwong, M. L., Wunderlich, J. R., et al. (2015). Complete regression of metastatic cervical cancer after treatment with human papillomavirus-targeted tumor-infiltrating T cells. *J. Clin. Oncol.* 33, 1543–1550. doi:10.1200/JCO.2014.58.9093

Sugiyama, T., Fujiwara, K., Ohashi, Y., Yokota, H., Hatae, M., Ohno, T., et al. (2014). Phase III placebo-controlled double-blind randomized trial of radiotherapy for stage IIB-IVA cervical cancer with or without immunomodulator Z-100: a JGOG study. *Ann. Oncol.* 25, 1011–1017. doi:10.1093/annonc/mdu057

Sukari, A., Abdallah, N., and Nagasaka, M. (2019). Unleash the power of the mighty T cells-basis of adoptive cellular therapy. *Crit. Rev. Oncol. Hematol.* 136, 1–12. doi:10.1016/j.critrevonc.2019.01.015

Sung, H., Ferlay, J., Siegel, R. L., Laversanne, M., Soerjomataram, I., Jemal, A., et al. (2021). Global cancer statistics 2020: GLOBOCAN estimates of incidence and mortality worldwide for 36 cancers in 185 countries. *CA Cancer J. Clin.* 71, 209–249. doi:10.3322/caac.21660

Suran, M. (2022). Why US cervical cancer survival rates haven't improved for decades. *JAMA* 327, 1943–1945. doi:10.1001/jama.2022.4681

Synnestvedt, M. B., Chen, C., and Holmes, J. H. (2005). CiteSpace II: visualization and knowledge discovery in bibliographic databases. *AMIA . Annu. Symp. Proc. AMIA Symp.* 2005, 724–728.

Takeuchi, S., Kagabu, M., Shoji, T., Nitta, Y., Sugiyama, T., Sato, J., et al. (2020). Anti-cancer immunotherapy using cancer-derived multiple epitope-peptides cocktail vaccination clinical studies in patients with refractory/persistent disease of uterine cervical cancer and ovarian cancer [phase 2]. *Oncoimmunology* 9, 1838189. doi:10.1080/2162402X.2020.1838189

Tan, K. T., Yeh, C. N., Chang, Y. C., Cheng, J. H., Fang, W. L., Yeh, Y. C., et al. (2020). PRKDC: new biomarker and drug target for checkpoint blockade immunotherapy. *J. Immunother. Cancer* 8, e000485. doi:10.1136/jitc-2019-000485

Tewari, K. S., Monk, B. J., Vergote, I., Miller, A., de Melo, A. C., Kim, H. S., et al. (2022). Survival with cemiplimab in recurrent cervical cancer. *N. Engl. J. Med.* 386, 544–555. doi:10.1056/NEJMoa2112187

Trimble, C. L., Morrow, M. P., Kraynyak, K. A., Shen, X., Dallas, M., Yan, J., et al. (2015). Safety, efficacy, and immunogenicity of VGX-3100, a therapeutic synthetic DNA vaccine targeting human papillomavirus 16 and 18 E6 and E7 proteins for cervical intraepithelial neoplasia 2/3: a randomised, double-blind, placebo-controlled phase 2b trial. *Lancet* 386, 2078–2088. doi:10.1016/S0140-6736(15)00239-1

van Eck, N. J., and Waltman, L. (2010). Software survey: VOSviewer, a computer program for bibliometric mapping. *Scientometrics* 84, 523–538. doi:10.1007/s11192-009-0146-3

van Elsas, M. J., van Hall, T., and van der Burg, S. H. (2020). Future challenges in cancer resistance to immunotherapy. *Cancers (Basel)* 12, 935. doi:10.3390/cancers12040935

Vici, P., Pizzuti, L., Mariani, L., Zampa, G., Santini, D., Di Lauro, L., et al. (2016). Targeting immune response with therapeutic vaccines in premalignant lesions and cervical cancer: hope or reality from clinical studies. *Expert Rev. Vaccines* 15, 1327–1336. doi:10.1080/14760584.2016.1176533

Vicier, C., Isambert, N., Cropet, C., Hamimed, M., Osanno, L., Legrand, F., et al. (2022). MOVIE: a phase I, open-label, multicenter study to evaluate the safety and tolerability of metronomic vinorelbine combined with durvalumab plus tremelimumab in patients with advanced solid tumors. *ESMO Open* 7, 100646. doi:10.1016/j.esmoop.2022.100646

Vinokurova, S., Wentzensen, N., Kraus, I., Klaes, R., Driesch, C., Melsheimer, P., et al. (2008). Type-dependent integration frequency of human papillomavirus genomes in cervical lesions. *Cancer Res.* 68, 307–313. doi:10.1158/0008-5472.CAN-07-2754

Wang, J., Lou, H., Cai, H., Huang, X., Li, G., Wang, L., et al. (2022). A study of AK104 (an anti-PD1 and anti-CTLA4 bispecific antibody) combined with standard therapy for the first-line treatment of persistent, recurrent, or metastatic cervical cancer (R/M CC). *J. Clin. Oncol. Clin. Oncol.* 40, 106. doi:10.1200/JCO.2022.40.16_suppl.106

Wang, R., Pan, W., Jin, L., Huang, W., Li, Y., Wu, D., et al. (2020). Human papillomavirus vaccine against cervical cancer: opportunity and challenge. *Cancer Lett.* 471, 88–102. doi:10.1016/j.canlet.2019.11.039

Welters, M. J., Kenter, G. G., Piersma, S. J., Vloon, A. P., Löwik, M. J., Berends-van der Meer, D. M., et al. (2008). Induction of tumor-specific CD4+ and CD8+ T-cell immunity in cervical cancer patients by a human papillomavirus type 16 E6 and E7 long peptides vaccine. *Clin. Cancer Res.* 14, 178–187. doi:10.1158/1078-0432.CCR-07-1880

Wheeler, C. M. (2007). Advances in primary and secondary interventions for cervical cancer: human papillomavirus prophylactic vaccines and testing. *Nat. Clin. Pract. Oncol.* 4, 224–235. doi:10.1038/ncponc0770

Wu, L., Chen, B., Yao, W., Li, X., Xiao, Z., Liu, H., et al. (2021). 1300P A phase Ib/II trial of AK104 (PD-1/CTLA-4 bispecific antibody) in combination with anlotinib in advanced NSCLC. *Ann. Oncol. Oncol.* 32, S1006. doi:10.1016/j.annonc.2021.08.1902

Wu, X., Ji, J., Lou, H., Li, Y., Feng, M., Xu, N., et al. (2022). Efficacy and safety of cadonilimab, an anti-PD-1/CTLA4 bi-specific antibody, in previously treated recurrent or metastatic (R/M) cervical cancer: a multicenter, open-label, single-arm, phase II trial (075). *Gynecol. Oncol. Oncol.* 166, S47–S48. doi:10.1016/S0090-8258(22)01293-8

Xing, Y., Yasinjan, F., Du, Y., Geng, H., Zhang, Y., He, M., et al. (2023). Immunotherapy in cervical cancer: from the view of scientometric analysis and clinical trials. *Front. Immunol.* 14, 1094437. doi:10.3389/fimmu.2023.1094437

Xu, Q., Wang, J., Sun, Y., Lin, Y., Liu, J., Zhuo, Y., et al. (2022). Efficacy and safety of Sintilimab plus anlotinib for PD-L1-positive recurrent or metastatic cervical cancer: a multicenter, single-arm, prospective phase II trial. *J. Clin. Oncol.* 40, 1795–1805. doi:10.1200/JCO.21.02091

Yan, W. T., Lu, S., Yang, Y. D., Ning, W. Y., Cai, Y., Hu, X. M., et al. (2021). Research trends, hot spots and prospects for necroptosis in the field of neuroscience. *Neural Regen. Res.* 16, 1628–1637. doi:10.4103/1673-5374.303032

Yao, R. Q., Ren, C., Wang, J. N., Wu, G. S., Zhu, X. M., Xia, Z. F., et al. (2020). Publication trends of research on sepsis and host immune response during 1999-2019: a 20-year bibliometric analysis. *Int. J. Biol. Sci.* 16, 27–37. doi:10.7150/ijbs.37496

Zhao, P., Li, L., Jiang, X., and Li, Q. (2019). Mismatch repair deficiency/microsatellite instability-high as a predictor for anti-PD-1/PD-L1 immunotherapy efficacy. *J. Hematol. Oncol.* 12, 54. doi:10.1186/s13045-019-0738-1

frontiers | Frontiers in Pharmacology

TYPE Original Research
PUBLISHED 31 May 2024
DOI 10.3389/fphar.2024.1349459

OPEN ACCESS

EDITED BY
Zhongrui Li,
Nanjing University of Chinese Medicine, China

REVIEWED BY
Shixiang Wang,
Sun Yat-Sen University Cancer Center (SYSUCC), China
Qian Zhang,
Guangdong Pharmaceutical University, China

*CORRESPONDENCE
Peng Chen,
chenpengde220@163.com
Longfei Zhao,
longfei@sjtu.edu.cn
Yongshun Gao,
gaoys@zzu.edu.cn

†These authors have contributed equally to this work and share first authorship

RECEIVED 04 December 2023
ACCEPTED 08 May 2024
PUBLISHED 31 May 2024

CITATION
Sun J, Li X, Wang Q, Chen P, Zhao L and Gao Y (2024), Proteomic profiling and biomarker discovery for predicting the response to PD-1 inhibitor immunotherapy in gastric cancer patients.
Front. Pharmacol. 15:1349459.
doi: 10.3389/fphar.2024.1349459

Proteomic profiling and biomarker discovery for predicting the response to PD-1 inhibitor immunotherapy in gastric cancer patients

Jiangang Sun[1†], Xiaojing Li[2†], Qian Wang[1], Peng Chen[1*], Longfei Zhao[3*] and Yongshun Gao[1*]

[1]Department of Gastrointestinal Surgery, The First Affiliated Hospital of Zhengzhou University, Zhengzhou, Henan, China, [2]Department of Pharmacy, The First Affiliated Hospital of Zhengzhou University, Zhengzhou, Henan, China, [3]School of Biomedical Engineering, Shanghai Jiao Tong University, Shanghai, China

Background: Immune checkpoint inhibitors (ICIs) have revolutionized cancer treatment; however, a significant proportion of gastric cancer (GC) patients do not respond to this therapy. Consequently, there is an urgent need to elucidate the mechanisms underlying resistance to ICIs and identify robust biomarkers capable of predicting the response to ICIs at treatment initiation.

Methods: In this study, we collected GC tissues from 28 patients prior to the administration of anti-programmed death 1 (PD-1) immunotherapy and conducted protein quantification using high-resolution mass spectrometry (MS). Subsequently, we analyzed differences in protein expression, pathways, and the tumor microenvironment (TME) between responders and non-responders. Furthermore, we explored the potential of these differences as predictive indicators. Finally, using machine learning algorithms, we screened for biomarkers and constructed a predictive model.

Results: Our proteomics-based analysis revealed that low activity in the complement and coagulation cascades pathway (CCCP) and a high abundance of activated CD8 T cells are positive signals corresponding to ICIs. By using machine learning, we successfully identified a set of 10 protein biomarkers, and the constructed model demonstrated excellent performance in predicting the response in an independent validation set (N = 14; area under the curve [AUC] = 0.959).

Conclusion: In summary, our proteomic analyses unveiled unique potential biomarkers for predicting the response to PD-1 inhibitor immunotherapy in GC patients, which may provide the impetus for precision immunotherapy.

KEYWORDS

gastric cancer, immune checkpoint inhibitor, proteomics, machine learning, biomarkers

1 Introduction

Unprecedented advances have been made in cancer treatment with the use of immune checkpoint inhibitors (ICIs). However, the response to ICIs is limited to a subset of patients (Morad et al., 2021). Different studies on ICI treatment revealed a highly variable objective response rate, ranging from 10% to 23% in gastric cancer (GC) patients (Kang et al., 2017; Shitara et al., 2018; Huang et al., 2019). Therefore, it is urgent to identify the mechanism of resistance to ICI treatment and discover reliable biomarkers capable of predicting the treatment response at the onset of therapy.

Various factors play a crucial role in influencing the response to ICIs. Among these, the expression, landscape, and composition of neoantigens within tumors emerge as robust indicators of the response (McGranahan et al., 2016; Morad et al., 2021). Additionally, oncogenic signaling, metabolic pathways, and their associated mutations have been conclusively demonstrated to drive immunogenic responses across diverse cancer types. Recent studies highlight the potential involvement of extracellular vesicles, specifically the exosome subset, in tumor immunity and resistance to ICIs (Chen et al., 2018; Poggio et al., 2019). Growing evidence suggests that the contribution of the tumor microenvironment (TME), encompassing stromal cells and immune cells, governs immune evasion and resistance to ICIs (Morad et al., 2021).

Biomarkers predictive of the ICI response are under investigation. Many biomarkers, including tumor mutation burden, programmed cell death 1 ligand 1 (PD-L1) expression, microsatellite instability, and Epstein–Barr virus infection status, identify susceptibility to PD-1/PD-L1 inhibitors (Kim et al., 2018; McGrail et al., 2021). However, the results of several clinical trials using these biomarkers at an individual level are not consistent; some are even contradictory (Ji et al., 2019; Kim et al., 2019; Di Bartolomeo et al., 2020). Therefore, to date, no single biomarker is available for adequate patient stratification (not only in GC) due to the complexity of the immune response to cancer.

Machine learning has exhibited significant potential in predicting responses to ICIs, especially when applied to omics data (Polano et al., 2019; Lu et al., 2020; Sung and Cheong, 2022). Mass spectrometry (MS)-based proteomics techniques provide accurate, specific, and high-throughput quantification capabilities. Moreover, the proteomic layer more precisely reflects cellular function. Despite these advantages, limited research has explored the application of MS-based proteomics techniques to identify predictive biomarkers for ICI response (Longuespée et al., 2023). To the best of our knowledge, no study has yet integrated machine learning and proteomics in the context of GC for this purpose.

In this study, clinical GC tissue samples were collected from a cohort of 28 GC patients before initiating treatment with camrelizumab. Through proteomic data analysis, we aimed to elucidate the underlying mechanisms that may influence patient response, including relevant signaling pathways and the TME. Additionally, by employing machine learning techniques, we successfully identified a panel of biomarkers and developed a robust prediction model, which was subsequently validated on an independent dataset. We are confident that the findings from this study will contribute to the advancement of personalized cancer treatment and ultimately lead to improvements in patients' quality of life.

2 Results

2.1 Clinical–pathological features and sample processing of the GC patients

Between June 2019 and May 2021, a total of 28 GC patients were enrolled in this study. Following the completion of immunotherapy, 17 patients exhibited a favorable response to PD-1 inhibitors, while the remaining 11 patients did not manifest a similar response. As shown in Table 1, the median age of the enrolled patients was 59 years (range: 37–78 years), with 64.2% being men. Tumors had invaded the outer lining of the stomach (T4) in 85.7% of cases, and metastasis to other parts of the body (M1) was observed in 78.5% of cases. No significant association was found between the response to immunotherapy and clinical–pathological characteristics.

Archival pre-treatment tissue specimens were available for all patients. The protein was extracted from formalin-fixed, paraffin-embedded (FFPE) tissues and subjected to quantitative analysis using MS. Stringent quality control measures were implemented to ensure the reliability of the data (see Methods for details, Supplementary Figure S1). Details of the comprehensive study design are given in Figure 1.

2.2 Differences in protein expression between responders and non-responders to immunotherapy

To gain an insight into the proteomic profile differences between responder and non-responder groups, we conducted differential expression analysis. First, our principal component analysis (PCA) revealed no significant outliers and minor intergroup variance, suggesting limited distinction among the sample sets (Figure 2A). Subsequently, by employing Student's *t*-test with a statistical threshold (p-value < 0.05; fold change > 1.2 or < 1/1.2), we identified 320 differentially expressed proteins (DEPs), consisting of 139 upregulated and 181 downregulated proteins in non-responders (Figure 2B; Supplementary Table S5). The most significantly altered DEPs included ERO1A, NCEH1, THEM6, JUP, DSP, LYAR, TFRC, IGF2BP2, COL12A1, CGN, C7, OGN, COL14A1, CYBRD1, FBLN5, ACTA1, TMEM119, VWF, GFAP, RARRES2, and FGA. These protein expression profiles across diverse patients are illustrated in Figure 2C. Notably, in non-responders, genes exhibiting higher expression levels tended to correlate with poorer prognoses in GC patients (Supplementary Figure S3). Importantly, upon incorporating validation data from an external experiment following a similar methodology, we observed a strong correlation and concordance in our findings (Figure 2D).

2.3 Functional enrichment analysis with DEPs

To gain a deeper understanding of the pathways associated with these DEPs, we conducted enrichment analyses using Gene

TABLE 1 Baseline characteristics of gastric cancer (GC) patients.

	Progressors (*n* = 11)	Responders (*n* = 17)	*p*-value
Sex (%)			
Female	4 (36.4)	6 (35.3)	1
Male	7 (63.6)	11 (64.7)	
Age [mean (SD)]	57.91 (11.72)	59.00 (8.69)	0.779
Degree of differentiation (%)			
Moderate–poorly differentiated	4 (36.4)	7 (41.2)	0.497
Moderately differentiated	1 (9.1)	4 (23.5)	
Poorly differentiated	6 (54.5)	6 (35.3)	
Lauren's criteria (%)			
Diffuse	8 (72.7)	7 (41.2)	0.206
Intestinal	1 (9.1)	6 (35.3)	
Mix	2 (18.2)	4 (23.5)	
T (%)			
1	0 (0.0)	1 (5.9)	0.361
2	0 (0.0)	3 (17.6)	
4	11 (100.0)	13 (76.5)	
N (%)			
0	1 (9.1)	7 (41.2)	0.215
1	3 (27.3)	5 (29.4)	
2	3 (27.3)	1 (5.9)	
3	4 (36.4)	4 (23.5)	
M (%)			
0	1 (9.1)	5 (29.4)	0.355
1	10 (90.9)	12 70.6)	

Ontology (GO), Kyoto Encyclopedia of Genes and Genomes (KEGG), and Gene Set Enrichment Analysis (GSEA). The outcomes of the GO enrichment analysis unveiled that the DEPs are primarily implicated in processes such as "complement activation," "humoral immune response," "regulation of blood coagulation," "collagen-containing extracellular matrix," and "blood microparticle" pathways (Figure 3A; Supplementary Table S6). Corresponding with the findings from both KEGG (Figure 3B; Supplementary Table S7) and GSEA (Figure 3C; Supplementary Table S8), the complement and coagulation cascades pathway (CCCP) emerged as notably significant. As shown in Figure 3D, nearly all genes within the CCCP exhibited upregulation in non-responders. A detailed exploration of the inter-regulatory relationships among proteins within the CCCP is given in Supplementary Figure S4.

2.4 Impact of the TME on the response to immunotherapy

The hallmarks of the response and resistance to the immune checkpoint blockade were amplified by a cross-talk between tumor cells and stromal and immune cells within the TME (Morad et al., 2021). Therefore, we observed an association between the ICI response and the TME. To investigate this relationship, we employed single-sample Gene Set Enrichment Analysis (ssGSEA) to assess the differential infiltration levels of various immune cell types (He et al., 2018). We observed significant differences in the abundance of certain tumor-infiltrating immune cells, including activated B cell, activated CD8 T cell, central memory CD8 T cell, memory B cell, natural killer T cell, and plasmacytoid dendritic cell, between the two groups. Notably, activated CD8 T cells showed consistency in the validation data (Figure 4; Supplementary Table S9).

2.5 Prediction of patient response to immunotherapy

Although some genes with significant changes also exhibit discriminative patterns (Supplementary Figure S5), individual indicators tend to lack robustness. To improve the biological comprehensibility of our predictive model, we evaluated the potential of utilizing pathway enrichment scores and levels of immune cell infiltration as predictors of patient response to immunotherapy. To provide clarity, we plotted the receiver operating characteristic (ROC) curves for the CCCP and activated CD8 T-cell infiltration. With the CCCP as the predictor, the AUC values for our data and validation data were 0.82 and 0.78, respectively (Figures 5A, B). With the level of

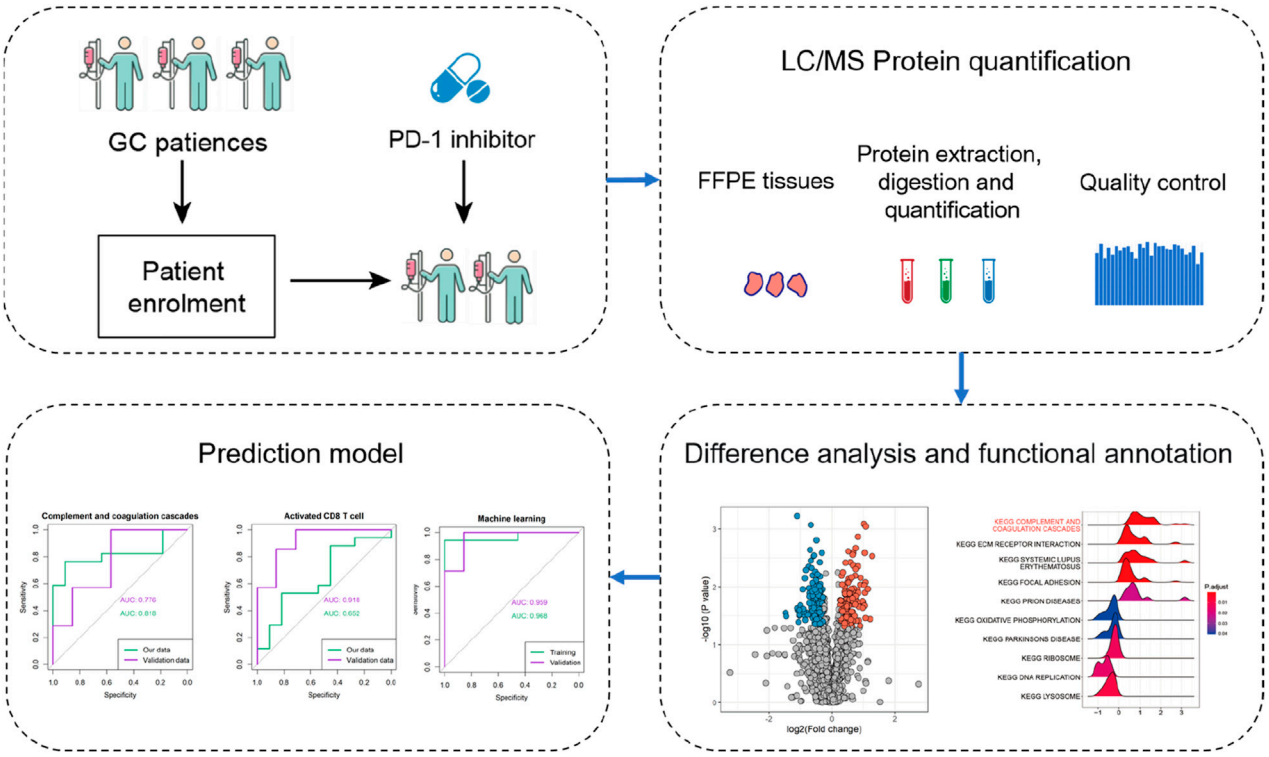

FIGURE 1
Schematic representation of the experimental design in this study.

activated CD8 T-cell infiltration as the predictor, the AUC values for our data and validation data were 0.65 and 0.92, respectively (Figures 5C, D).

While both predictors show some potential for the response to immunotherapy, we further sought to harness the power of machine learning algorithms to achieve superior predictive performance. Specifically, we implemented support vector machines (SVMs) and optimized the performance of our predictive model (Supplementary Table S10). Table 2 shows the performance achieved by our predictive model on the different datasets. The ROC curves show that our model achieved AUC values of 0.97 and 0.96 in our data and the validation data, respectively, indicating excellent prediction accuracy and robustness across datasets (Figures 5E, F).

3 Discussion and conclusion

Immunotherapy has emerged as a promising approach for treating various malignancies, leveraging the patient's immune system to target and eliminate cancer cells. However, not all patients respond uniformly to immunotherapy, and predicting individual treatment responses remains a challenge. Therefore, there is a need to identify more convenient and reliable biomarkers for predicting the benefits of ICIs in clinical practice.

We have pinpointed several differentially expressed proteins with high credibility between responders and non-responders to immunotherapy (Figure 2C). Notably, the expression of the ERO1A protein was significantly elevated in responders. *In vivo* studies demonstrated that ERO1A overexpression promoted tumor growth by suppressing antitumor immunity, acting in collaboration with protein disulfide isomerase (Kukita et al., 2015). The inhibition of ERO1A in tumors might have a synergetic antitumor effect on the immune checkpoint blockade by turning the tumor immunogenic and removing immune-suppressive signals, thereby restoring the antitumor capacity of the T cells in tumor hosts (Liu et al., 2023). Therefore, individuals with higher ERO1A levels may exhibit increased responsiveness to ICIs. ERO1A not only serves as a predictive biomarker but also emerges as a promising therapeutic target for cancer treatment (Johnson et al., 2020). Furthermore, in melanomas, the systemic levels of VWF antigen were measured, confirming VWF as a biomarker of ICI response and overall prognosis (Stadler et al., 2023). Our results also underscore the robust predictive power of VWF for ICIs (Supplementary Figure S5). Similarly, the high levels of GFAP in non-responders also deserve attention. Our findings also validate GFAP as a biomarker for both ICI response and prognosis. These robust results not only provide new evidence for existing studies but also support the value of the other new markersidentified. These molecules hold promise as potential predictive factors for immunotherapy or as novel therapeutic targets.

Our results show that DEPs are enriched in the CCCP. Previously, many studies of preclinical models of lung, colon, and liver cancers have indicated that inflammatory mediators derived from the complement system, such as C5a, together with PD-1 blockade, markedly reduce tumor growth and metastasis, leading to prolonged survival by enhancing antitumor CD8 T-cell responses (Wang et al., 2016; Ajona et al., 2017; Zha et al., 2017). Moreover,

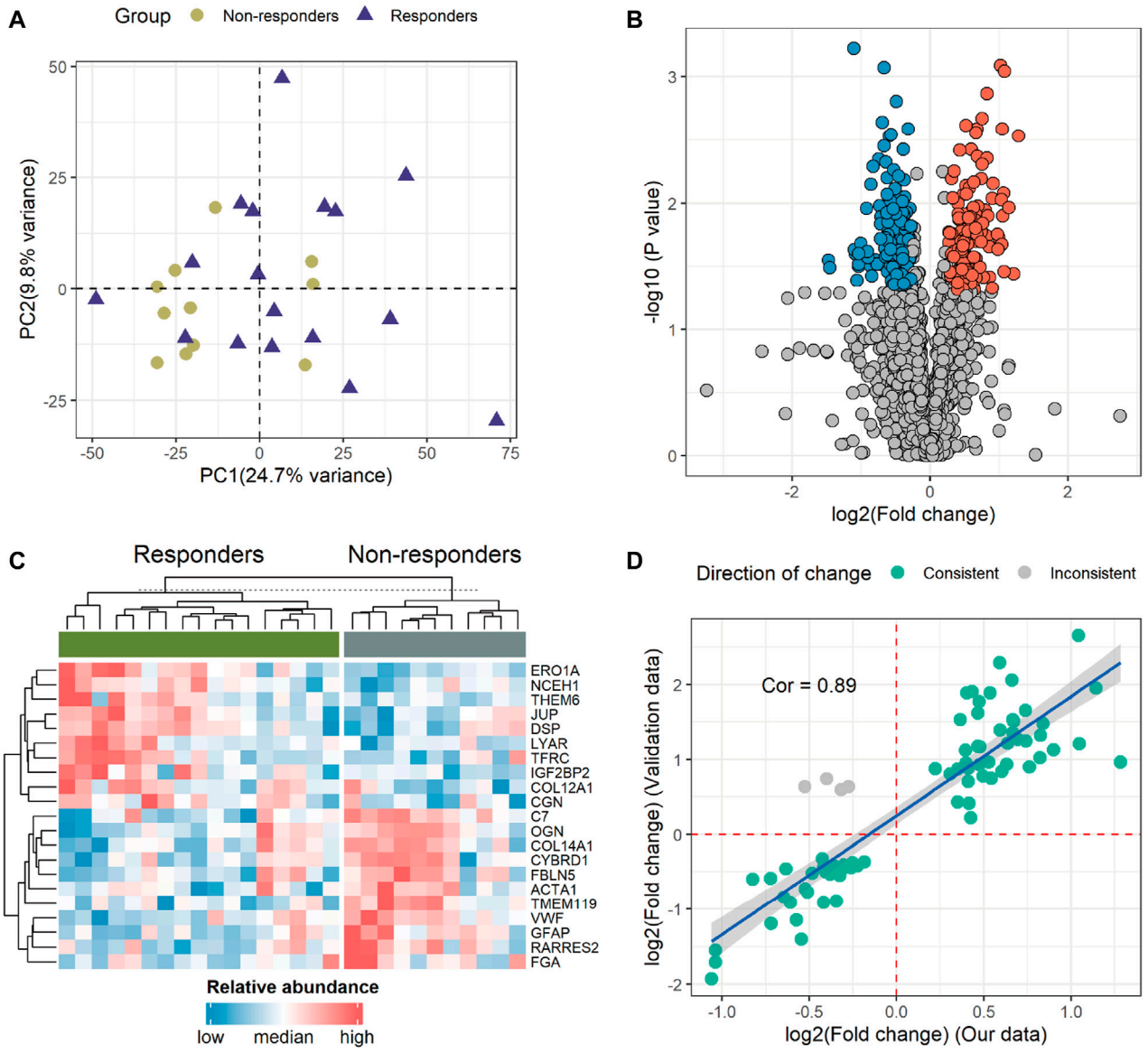

FIGURE 2
Identification and profiling of differentially expressed proteins (DEPs). **(A)** The principal component analysis (PCA) illustrates the overall variance between the two groups. **(B)** Volcano plot demonstrating 320 DEPs. The red and blue dots indicate proteins with high and low expressions in non-responders, respectively. **(C)** Heatmap displaying the 21 proteins that significantly differed ($p < 0.05$; fold change > 2 or < 1/2) between the two groups. **(D)** Correlation analysis of DEPs between our data and validation data. The green and gray dots denote consistent and opposing directions of change, respectively. Cor, correlation coefficient.

cancer cells can exploit the CCCP to shape the TME, thus impacting the efficacy of ICIs (Afshar-Kharghan, 2017; Ruf and Graf, 2020). Another study directly proved that CCCP risk score is an independent biomarker that predicts the efficacy of ICIs in metastatic urothelial cancer patients (Gong et al., 2023). Our results suggest that the CCCP may serve as a potential biomarker in GC.

The TME influences the response to ICIs. ICIs take advantage of immune cell infiltration in the tumor to reinvigorate an efficacious antitumoral immune response (Petitprez et al., 2020; Zhang and Zhang, 2020). By exploring the TME, we found that natural killer T cells, activated CD8 T cells, and memory B cells have an impact on the response to immunotherapy in GC patients. However, only activated CD8 T cells showed consistency between our data and the validation data. It is clear that the presence of infiltrating CD8 T cells in combination with increased PD-L1 expression/amplification is positively associated with the therapeutic efficacy of the PD-1 blockade (Raskov et al., 2021; Chen et al., 2022). In a study of various cancers, the abundance of CD8 T cells within a tumor was found to be the best predictive factor for the response to anti-PD-1/PD-L1 therapy (Lee and Ruppin, 2019). As expected, when protein data were used to infer the extent of CD8 T-cell infiltration, excellent response prediction ability was also shown in GC. However, different types of natural killer T cells, primarily type I and type II, may play completely opposite roles in tumor progression (Terabe et al., 2000; Terabe et al., 2003; Pilones et al., 2012; Robertson et al.,

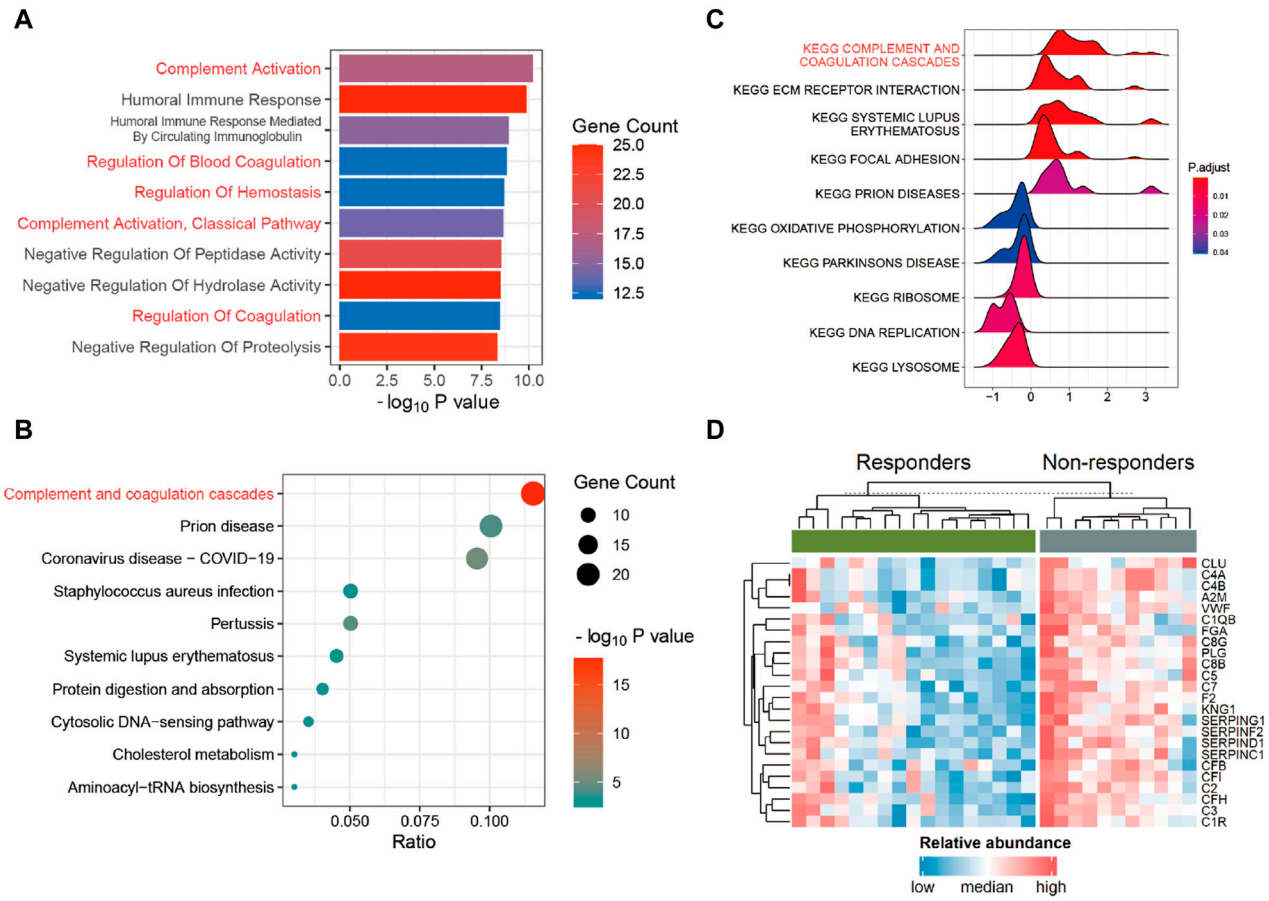

FIGURE 3
Functional enrichment analysis. **(A)** Gene Ontology (GO) enrichment analysis in DEPs. **(B)** Kyoto Encyclopedia of Genes and Genomes (KEGG) enrichment analysis in DEPs. **(C)** Gene Set Enrichment Analysis (GSEA) in all proteins. **(D)** Heatmap of DEPs within the complement and coagulation cascades pathway (CCCP) between the responders and non-responders.

2014; Altman et al., 2015; McEwen-Smith et al., 2015; Nair and Dhodapkar, 2017). Therefore, interpreting the degree of natural killer T-cell infiltration in the context of immunotherapy responses necessitates a more in-depth investigation.

While some molecules and pathways have demonstrated the ability to predict the response to ICIs, a comprehensive and diverse panel of markers providing comparable prognostic accuracy is desirable for clinical applications. Leveraging the capabilities of machine learning, we developed a prediction model utilizing the expression of a specific set of 10 proteins, namely, COL15A1, SAMHD1, DHX15, PTDSS1, CFI, ORM2, VWF, APOA1, EMC2, and COL6A2 (Supplementary Figure S6). The model exhibited robust predictive performance (Figure 5E). Upon validation set assessment, a clear differentiation between responders and non-responders was observed ($p = 0.003$).

While we have demonstrated consistency in the variation between our data and the validation cohort data (Figure 2D), we recognize that the limitations due to the small sample size and the constraints of proteomics technology are significant. Specifically, the limited number of analyzable and overlapping proteins identified across different experimental projects resulted in discrepancies when performing downstream analysis using the DEPs from each dataset (Figure 4). Furthermore, there is a scarcity of available proteomic datasets with the same experimental goals as ours, which restricts the ability to further validate the robustness of our model. Finally, despite the model presenting high sensitivity in predicting immunotherapy efficacy, its application may be limited across diverse cancer types. Tumor heterogeneity and tissue specificity are presumed to be the main reasons. Addressing these issues would require larger sample sizes and more independent datasets. In the future, we will collect many GC samples before immunotherapy to determine the robustness of the model for consequent clinical practice.

Overall, our study revealed that proteomics data and the machine learning method play a critical role in identifying predictive biomarkers that can aid in stratifying patients for immunotherapy. We acknowledge the need for more extensive and in-depth validation studies to translate these findings into clinical applications.

4 Materials and methods

4.1 Clinical trial protocol

This study was a retrospective study involving 28 enrolled patients with advanced GC between June 2019 and May 2021 at

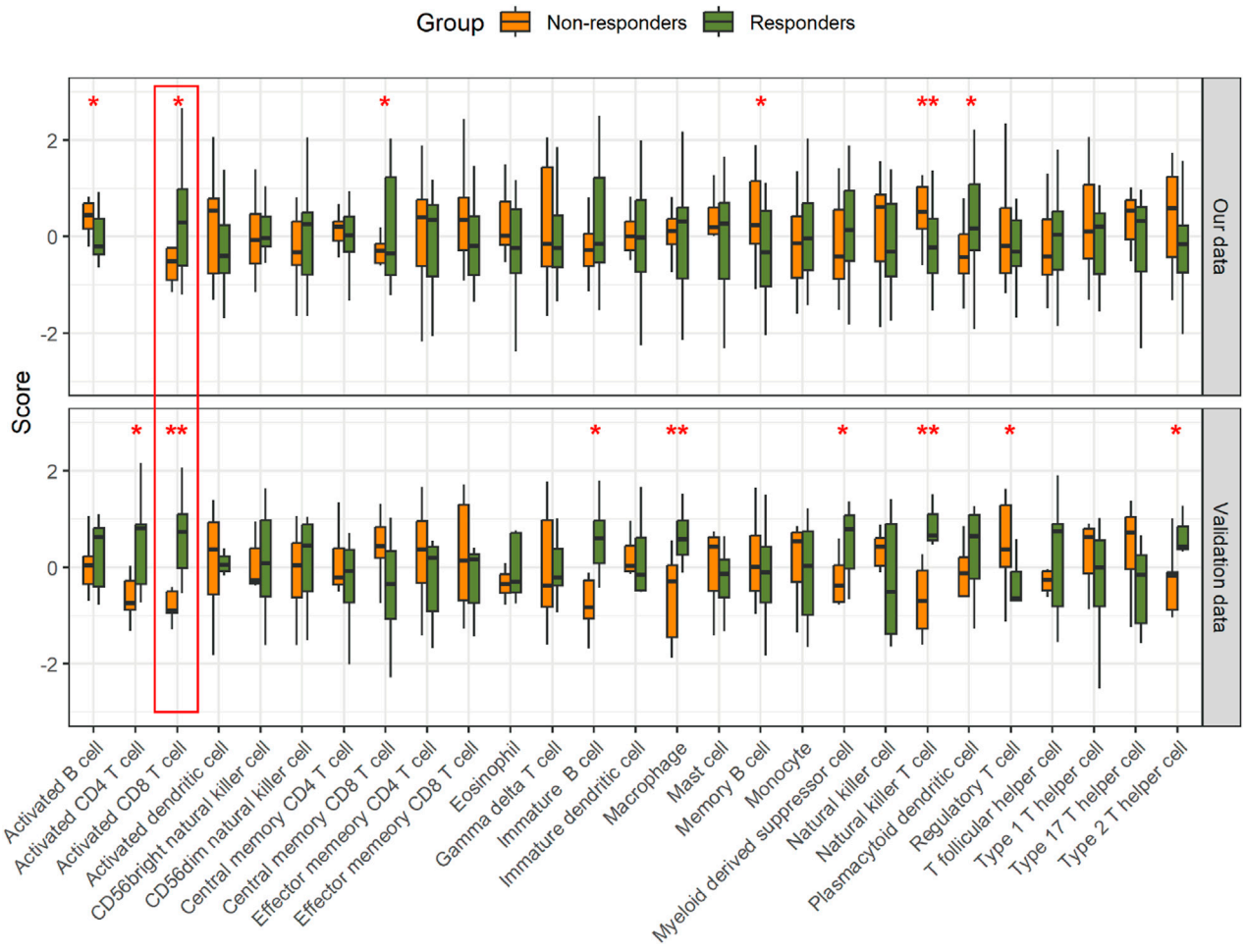

FIGURE 4
Comparison of the relative abundance of immune cell infiltration in the tumor. *$p < 0.05$ and **$p < 0.01$.

the First Affiliated Hospital of Zhengzhou University, Zhengzhou, Henan, China. The study obtained the ethical approval of our hospital with number 2020-KY-386. All cases were reexamined independently by senior pathologists, and histological diagnosis was performed based on the WHO classification of central nervous system tumors. The clinical data, including age, sex, treatment, body mass index, and pathology results, were obtained from the medical records of the enrolled patients. All patients and their families provided informed consent. The clinical information is shown in Supplementary Table S1. Patients use camrelizumab (AiRuiKa™), a PD-1 inhibitor being developed by Jiangsu Hengrui Medicine Co., Ltd. (Markham and Keam, 2019), according to the protocol. Responders were defined as patients with a RECIST complete response (CR) or partial response (PR), while non-responders were defined as those with progressive disease (PD) or stable disease (SD).

4.2 Tumor sample collection

Tumor tissues were obtained any time before initiation of study treatment. The freshly acquired tissues were first rinsed with physiological saline and subsequently fixed in a 10% formalin solution, followed by embedding in paraffin wax.

4.3 MS-based protein quantification

After protein extraction, trypsin digestion, MS analysis, and database search, we obtained the raw data of proteomics. Supplementary Information provides more detailed processing information (Supplementary Method).

4.4 Quality control and missing value imputation

Following the database search using MaxQuant, 5,107 proteins were identified, of which 4,061 were quantified (Supplementary Table S2). On average, 3,061 proteins per sample were quantified (Supplementary Figure S1A; Supplementary Table S3). Subcellular distribution analysis conducted through the Hum-mPLoc 3.0 database (Zhou et al., 2017) revealed that the majority of identified proteins were cytoplasmic, followed by nuclear and plasma membrane proteins. This distribution

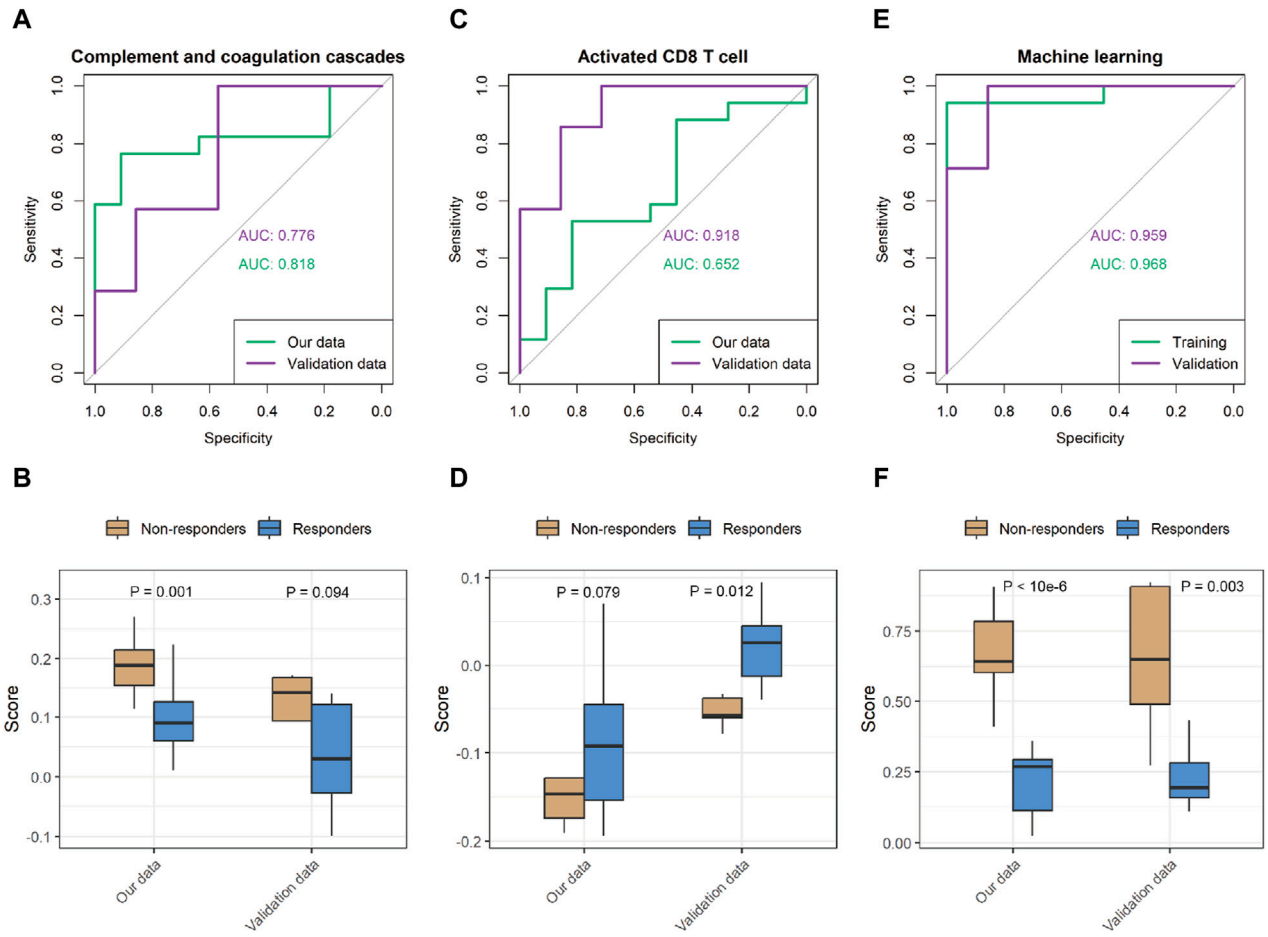

FIGURE 5
Performance of the prediction model in our data and validation data. **(A,B)** Representative receiver operating characteristic (ROC) curve with the CCCP score as the predictor, and comparison of the predicted score. **(C,D)** ROC curve with the score of the activated CD8 T-cell signature as the predictor, and comparison of the predicted scores. **(E,F)** ROC curve of the machine learning prediction score, and comparison of the predicted scores.

TABLE 2 Performance metrics for the predictive model.

	Accuracy	Precision	Recall	F1 score
Our data	0.893	0.900	0.818	0.857
Validation data	0.857	1.000	0.714	0.833

aligns with existing references and likely reflects the actual distribution within the tissue, without any subcellular bias (Supplementary Figure S1B). To control the variation among samples, 28 samples were assessed using Pearson's correlation. The results displayed high correlations among samples with an average Pearson's correlation coefficient of 0.827 (Supplementary Figure S1C). To identify samples with abnormal protein abundance distributions, the log2-transformed protein intensities were analyzed. The violin plot demonstrates that each sample exhibited a similar distribution when log2-transformed (Supplementary Figure S1D). Quantitative proteomics experiments based on MS frequently generate data with missing values, which can profoundly affect downstream analyses. To address this issue, we evaluated several methods using NAguideR (Kang et al., 2017) and selected the "SeqKNN" method for imputing missing values (Supplementary Figure S2). This imputation process resulted in a dataset consisting of 2,884 proteins for further downstream analysis across all samples (Supplementary Table S4).

4.5 Validation data processing

The validation cohort (https://www.iprox.cn//page/subproject.html?id=IPX0004819001) is a group of GC patients treated with anti-PD1 therapy, including seven responder cases and seven non-responder cases (Shi et al., 2023). The sample is also FFPE, and the proteins were quantified using an MS-based label-free method. To ensure data consistency, we downloaded the raw data and re-performed database search and quantification using MaxQuant with the same parameters. After database searching, 4,263 proteins were quantified. After missing value imputation, 2,472 proteins were used for further downstream analysis.

4.6 Statistical analysis

All statistical analyses were performed using R software. The code for proteomics-based analysis is available at https://github.

com/longfei8533/Predicting-Response-to-PD-1-Inhibitor. The relationships between the treatment response and clinical–pathological features were evaluated using Wilcoxon's test for continuous variables and Fisher's exact test for categorical variables. Pearson's correlation coefficient was used in the correlation analysis. We used two-sided Student's *t*-test to evaluate the difference in the log2-transformed protein intensity between groups. The R "clusterProfiler" package (Cell, 2023) was used for GO and KEGG functional enrichment analyses and GSEA.

4.7 Immune cell abundance inference

We selected immune-related signatures representing 28 different types of immune cells from the study by Charoentong et al. (2017). To estimate the relative abundance of immune cell infiltration in the tumor based on protein intensity, we utilized the Gene Set Variation Analysis (GSVA) package (Hänzelmann et al., 2013) with the ssGSEA method (Barbie et al., 2009). To compare the differences between responders and non-responders, we conducted unpaired one-sided Student's *t*-tests.

4.8 Construction of prediction models

For the CCCP predictor, we selected the "KEGG_COMPLEMENT_AND_COAGULATION_CASCADES" gene set from MSigDB (Liberzon et al., 2011). For the activated CD8 T-cell predictor, the signature gene set from the study by Charoentong was used. Both prediction methods through the utilization of ssGSEA were used to infer the relative activity of pathway.

Considering the small-sample size issue, we utilized SVM as a machine learning approach from the "e1071" package to predict the patient response to medication. Initially, we aligned our dataset with the validation set by selecting overlapping analyzable proteins and then normalized the data using these proteins. Subsequently, important features were chosen using Boruta (Kursa and Rudnicki, 2010), resulting in the retention of 10 proteins as features. We conducted model training after adjusting the SVM parameters; please refer to the Supplementary Material for the specific parameter values. The classifiers developed from the training cohort were then applied to the validation cohort, and the AUC of each classifier was calculated.

Data availability statement

The datasets presented in this study can be found in online repositories. The names of the repository/repositories and accession number(s) can be found at: [iProx database (https://www.iprox.cn)/IPX0008285000].

Ethics statement

The studies involving humans were approved by the Ethics Review Committee of the First Affiliated Hospital of Zhengzhou University. The studies were conducted in accordance with the local legislation and institutional requirements. The participants provided their written informed consent to participate in this study. Written informed consent was obtained from the individual(s) for the publication of any potentially identifiable images or data included in this article.

Author contributions

JS: writing–original draft. XL: writing–review and editing, visualization, and data curation. QW: writing–review and editing, formal analysis, and data curation. PC: writing–review and editing and supervision. LZ: writing–review and editing and validation. YG: writing–review and editing and conceptualization.

Funding

The author(s) declare that financial support was received for the research, authorship, and/or publication of this article. This work was supported by the Henan Provincial Medical Science and Technology Joint Construction Project (No. LHGJ20220423) and the National Natural Science Foundation for Youth of China (No. 82103664).

Conflict of interest

The authors declare that the research was conducted in the absence of any commercial or financial relationships that could be construed as a potential conflict of interest.

Publisher's note

All claims expressed in this article are solely those of the authors and do not necessarily represent those of their affiliated organizations, or those of the publisher, the editors, and the reviewers. Any product that may be evaluated in this article, or claim that may be made by its manufacturer, is not guaranteed or endorsed by the publisher.

Supplementary material

The Supplementary Material for this article can be found online at: https://www.frontiersin.org/articles/10.3389/fphar.2024.1349459/full#supplementary-material

References

Afshar-Kharghan, V. (2017). The role of the complement system in cancer. *J. Clin. Invest.* 127, 780–789. doi:10.1172/JCI90962

Ajona, D., Ortiz-Espinosa, S., Moreno, H., Lozano, T., Pajares, M. J., Agorreta, J., et al. (2017). A combined PD-1/C5a blockade synergistically protects against lung cancer growth and metastasis. *Cancer Discov.* 7, 694–703. doi:10.1158/2159-8290.CD-16-1184

Altman, J. B., Benavides, A. D., Das, R., and Bassiri, H. (2015). Antitumor responses of invariant natural killer T cells. *J. Immunol. Res.* 2015, 652875–652910. doi:10.1155/2015/652875

Barbie, D. A., Tamayo, P., Boehm, J. S., Kim, S. Y., Moody, S. E., Dunn, I. F., et al. (2009). Systematic RNA interference reveals that oncogenic KRAS-driven cancers require TBK1. *Nature* 462, 108–112. doi:10.1038/nature08460

Cell (2023). ClusterProfiler 4.0: a universal enrichment tool for interpreting omics data: the innovation. Available at: https://www.cell.com/the-innovation/fulltext/S2666-6758(21)00066-7?_returnURL=https%3A%2F%2Flinkinghub.elsevier.com%2Fretrieve%2Fpii%2FS2666675821000667%3Fshowall%3Dtrue (Accessed November 8, 2023).

Charoentong, P., Finotello, F., Angelova, M., Mayer, C., Efremova, M., Rieder, D., et al. (2017). Pan-cancer immunogenomic analyses reveal genotype-immunophenotype relationships and predictors of response to checkpoint blockade. *Cell Rep.* 18, 248–262. doi:10.1016/j.celrep.2016.12.019

Chen, G., Huang, A. C., Zhang, W., Zhang, G., Wu, M., Xu, W., et al. (2018). Exosomal PD-L1 contributes to immunosuppression and is associated with anti-PD-1 response. *Nature* 560, 382–386. doi:10.1038/s41586-018-0392-8

Chen, Y., Jia, K., Sun, Y., Zhang, C., Li, Y., Zhang, L., et al. (2022). Predicting response to immunotherapy in gastric cancer via multi-dimensional analyses of the tumour immune microenvironment. *Nat. Commun.* 13, 4851. doi:10.1038/s41467-022-32570-z

Di Bartolomeo, M., Morano, F., Raimondi, A., Miceli, R., Corallo, S., Tamborini, E., et al. (2020). Prognostic and predictive value of microsatellite instability, inflammatory reaction and PD-L1 in gastric cancer patients treated with either adjuvant 5-FU/LV or sequential folfiri followed by cisplatin and docetaxel: a translational analysis from the itaca-S trial. *Oncologist* 25, e460–e468. doi:10.1634/theoncologist.2019-0471

Gong, Z., He, Y., Mi, X., Li, C., Sun, X., Wang, G., et al. (2023). Complement and coagulation cascades pathway-related signature as a predictor of immunotherapy in metastatic urothelial cancer. *Aging (Albany NY)* 15, 9479–9498. doi:10.18632/aging.205022

Hänzelmann, S., Castelo, R., and Guinney, J. (2013). GSVA: gene set variation analysis for microarray and RNA-seq data. *BMC Bioinf.* 14, 7. doi:10.1186/1471-2105-14-7

He, Y., Jiang, Z., Chen, C., and Wang, X. (2018). Classification of triple-negative breast cancers based on immunogenomic profiling. *J. Exp. Clin. Cancer Res.* 37, 327. doi:10.1186/s13046-018-1002-1

Huang, J., Mo, H., Zhang, W., Chen, X., Qu, D., Wang, X., et al. (2019). Promising efficacy of SHR-1210, a novel anti-programmed cell death 1 antibody, in patients with advanced gastric and gastroesophageal junction cancer in China. *Cancer Soc.* 125, 742–749. doi:10.1002/cncr.31855

Ji, Z., Peng, Z., Gong, J., Zhang, X., Li, J., Lu, M., et al. (2019). Hyperprogression after immunotherapy in patients with malignant tumors of digestive system. *BMC Cancer* 19, 705. doi:10.1186/s12885-019-5921-9

Johnson, B. D., Geldenhuys, W. J., and Hazlehurst, L. A. (2020). The role of ERO1α in modulating cancer progression and immune escape. *J. Cancer Immunol.* 2, 103–115. doi:10.33696/cancerimmunol.2.023

Kang, Y.-K., Boku, N., Satoh, T., Ryu, M.-H., Chao, Y., Kato, K., et al. (2017). Nivolumab in patients with advanced gastric or gastro-oesophageal junction cancer refractory to, or intolerant of, at least two previous chemotherapy regimens (ONO-4538-12, ATTRACTION-2): a randomised, double-blind, placebo-controlled, phase 3 trial. *Lancet (Lond. Engl.)* 390, 2461–2471. doi:10.1016/S0140-6736(17)31827-5

Kim, J. Y., Kim, W. G., Kwon, C. H., and Park, D. Y. (2019). Differences in immune contextures among different molecular subtypes of gastric cancer and their prognostic impact, Gastric Cancer: off. *J. Int. Gastric Cancer Assoc. Jpn. Gastric Cancer Assoc.* 22, 1164–1175. doi:10.1007/s10120-019-00974-4

Kim, S. T., Cristescu, R., Bass, A. J., Kim, K.-M., Odegaard, J. I., Kim, K., et al. (2018). Comprehensive molecular characterization of clinical responses to PD-1 inhibition in metastatic gastric cancer. *Nat. Med.* 24, 1449–1458. doi:10.1038/s41591-018-0101-z

Kukita, K., Tamura, Y., Tanaka, T., Kajiwara, T., Kutomi, G., Saito, K., et al. (2015). Cancer-associated oxidase ERO1-α regulates the expression of MHC class I molecule via oxidative folding. *J. Immunol.* 194, 4988–4996. doi:10.4049/jimmunol.1303228

Kursa, M. B., and Rudnicki, W. R. (2010). Feature selection with the boruta package. *J. Stat. Softw.* 36, 1–13. doi:10.18637/jss.v036.i11

Lee, J. S., and Ruppin, E. (2019). Multiomics prediction of response rates to therapies to inhibit programmed cell death 1 and programmed cell death 1 ligand 1. *JAMA Oncol.* 5, 1614–1618. doi:10.1001/jamaoncol.2019.2311

Liberzon, A., Subramanian, A., Pinchback, R., Thorvaldsdóttir, H., Tamayo, P., and Mesirov, J. P. (2011). Molecular signatures database (MSigDB) 3.0. *Biochem. Anal.* 27, 1739–1740. doi:10.1093/bioinformatics/btr260

Liu, L., Li, S., Qu, Y., Bai, H., Pan, X., Wang, J., et al. (2023). Ablation of ERO1A induces lethal endoplasmic reticulum stress responses and immunogenic cell death to activate anti-tumor immunity. *Med.* 4, 101206. doi:10.1016/j.xcrm.2023.101206

Longuespée, R., Theile, D., Zörnig, I., Hassel, J. C., Lindner, J. R., Haefeli, W. E., et al. (2023). Molecular prediction of clinical response to anti-PD-1/anti-PD-L1 immune checkpoint inhibitors: new perspectives for precision medicine and mass spectrometry-based investigations. *Int. J. Cancer* 153, 252–264. doi:10.1002/ijc.34366

Lu, Z., Chen, H., Jiao, X., Zhou, W., Han, W., Li, S., et al. (2020). Prediction of immune checkpoint inhibition with immune oncology-related gene expression in gastrointestinal cancer using a machine learning classifier. *J. Immunother. Cancer* 8, e000631. doi:10.1136/jitc-2020-000631

Ma, J., Chen, T., Wu, S., Yang, C., Bai, M., Shu, K., et al. (2019). iProX: an integrated proteome resource. *Nucleic Acids Res.* 47, D1211–D1217. doi:10.1093/nar/gky869

Markham, A., and Keam, S. J. (2019). Camrelizumab: first global approval. *Drugs* 79, 1355–1361. doi:10.1007/s40265-019-01167-0

McEwen-Smith, R. M., Salio, M., and Cerundolo, V. (2015). The regulatory role of invariant NKT cells in tumor immunity. *Cancer Immunol. Res.* 3, 425–435. doi:10.1158/2326-6066.CIR-15-0062

McGrail, D. J., Pilié, P. G., Rashid, N. U., Voorwerk, L., Slagter, M., Kok, M., et al. (2021). High tumor mutation burden fails to predict immune checkpoint blockade response across all cancer types. *Ann. Oncol. Off. J. Eur. Soc. Med. Oncol.* 32, 661–672. doi:10.1016/j.annonc.2021.02.006

McGranahan, N., Furness, A. J. S., Rosenthal, R., Ramskov, S., Lyngaa, R., Saini, S. K., et al. (2016). Clonal neoantigens elicit T cell immunoreactivity and sensitivity to immune checkpoint blockade. *Science* 351, 1463–1469. doi:10.1126/science.aaf1490

Morad, G., Helmink, B. A., Sharma, P., and Wargo, J. A. (2021). Hallmarks of response, resistance, and toxicity to immune checkpoint blockade. *Cell* 184, 5309–5337. doi:10.1016/j.cell.2021.09.020

Nair, S., and Dhodapkar, M. V. (2017). Natural killer T cells in cancer immunotherapy. *Front. Immunol.* 8, 1178. doi:10.3389/fimmu.2017.01178

Petitprez, F., Meylan, M., de Reyniès, A., Sautès-Fridman, C., and Fridman, W. H. (2020). The tumor microenvironment in the response to immune checkpoint blockade therapies. *Front. Immunol.* 11, 784. doi:10.3389/fimmu.2020.00784

Pilones, K. A., Aryankalayil, J., and Demaria, S. (2012). Invariant NKT cells as novel targets for immunotherapy in solid tumors. *J. Immunol. Res.* 2012, e720803. doi:10.1155/2012/720803

Poggio, M., Hu, T., Pai, C.-C., Chu, B., Belair, C. D., Chang, A., et al. (2019). Suppression of exosomal PD-L1 induces systemic anti-tumor immunity and memory. *Cell* 177, 414–427. doi:10.1016/j.cell.2019.02.016

Polano, M., Chierici, M., Dal Bo, M., Gentilini, D., Di Cintio, F., Baboci, L., et al. (2019). A pan-cancer approach to predict responsiveness to immune checkpoint inhibitors by machine learning. *Cancers* 11, 1562. doi:10.3390/cancers11101562

Raskov, H., Orhan, A., Christensen, J. P., and Gögenur, I. (2021). Cytotoxic CD8+ T cells in cancer and cancer immunotherapy. *Br. J. Cancer* 124, 359–367. doi:10.1038/s41416-020-01048-4

Robertson, F. C., Berzofsky, J. A., and Terabe, M. (2014). NKT cell networks in the regulation of tumor immunity. *Front. Immunol.* 5, 543. doi:10.3389/fimmu.2014.00543

Ruf, W., and Graf, C. (2020). Coagulation signaling and cancer immunotherapy. *Thromb. Res.* 191 (Suppl. 1), S106–S111. doi:10.1016/S0049-3848(20)30406-0

Shi, W., Wang, Y., Xu, C., Li, Y., Ge, S., Bai, B., et al. (2023). Multilevel proteomic analyses reveal molecular diversity between diffuse-type and intestinal-type gastric cancer. *Nat. Commun.* 14, 835. doi:10.1038/s41467-023-35797-6

Shitara, K., Özgüroğlu, M., Bang, Y.-J., Bartolomeo, M. D., Mandalà, M., Ryu, M.-H., et al. (2018). Pembrolizumab versus paclitaxel for previously treated, advanced gastric or gastro-oesophageal junction cancer (KEYNOTE-061): a randomised, open-label, controlled, phase 3 trial. *Lancet* 392, 123–133. doi:10.1016/S0140-6736(18)31257-1

Stadler, J.-C., Keller, L., Mess, C., Bauer, A. T., Koett, J., Geidel, G., et al. (2023). Prognostic value of von willebrand factor levels in patients with metastatic melanoma treated by immune checkpoint inhibitors. *J. Immunother. Cancer* 11, e006456. doi:10.1136/jitc-2022-006456

Sung, J.-Y., and Cheong, J.-H. (2022). Machine learning predictor of immune checkpoint blockade response in gastric cancer. *Cancers* 14, 3191. doi:10.3390/cancers14133191

Terabe, M., Matsui, S., Noben-Trauth, N., Chen, H., Watson, C., Donaldson, D. D., et al. (2000). NKT cell–mediated repression of tumor immunosurveillance by IL-13 and the IL-4R–STAT6 pathway. *Nat. Immunol.* 1, 515–520. doi:10.1038/82771

Terabe, M., Matsui, S., Park, J.-M., Mamura, M., Noben-Trauth, N., Donaldson, D. D., et al. (2003). Transforming growth factor-beta production and myeloid cells are an effector mechanism through which CD1d-restricted T cells block cytotoxic T lymphocyte-mediated tumor immunosurveillance: abrogation prevents tumor recurrence. *J. Exp. Med.* 198, 1741–1752. doi:10.1084/jem.20022227

Wang, Y., Sun, S.-N., Liu, Q., Yu, Y.-Y., Guo, J., Wang, K., et al. (2016). Autocrine complement inhibits IL10-dependent T-cell-mediated antitumor immunity to promote tumor progression. *Cancer Discov.* 6, 1022–1035. doi:10.1158/2159-8290.CD-15-1412

Zha, H., Han, X., Zhu, Y., Yang, F., Li, Y., Li, Q., et al. (2017). Blocking C5aR signaling promotes the anti-tumor efficacy of PD-1/PD-L1 blockade. *Oncoimmunology* 6, e1349587. doi:10.1080/2162402X.2017.1349587

Zhang, Y., and Zhang, Z. (2020). The history and advances in cancer immunotherapy: understanding the characteristics of tumor-infiltrating immune cells and their therapeutic implications. *Cell. Mol. Immunol.* 17, 807–821. doi:10.1038/s41423-020-0488-6

Zhou, H., Yang, Y., and Shen, H.-B. (2017). Hum-mPLoc 3.0: prediction enhancement of human protein subcellular localization through modeling the hidden correlations of gene ontology and functional domain features. *Biochem. Anal.* 33, 843–853. doi:10.1093/bioinformatics/btw723

frontiers | Frontiers in Pharmacology

TYPE Original Research
PUBLISHED 11 June 2024
DOI 10.3389/fphar.2024.1387949

OPEN ACCESS

EDITED BY
Zhongrui Li,
Nanjing University of Chinese Medicine, China

REVIEWED BY
Iman Azimi,
University of Tasmania, Australia
Yu Zhao,
Shanghai Normal University, China

*CORRESPONDENCE
Tianqing Liu,
michelle.tianqing.liu@gmail.com
Yongmei Zhao,
ymzhao@ntu.edu.cn
Kaikai Wang,
kirk2008@126.com

RECEIVED 19 February 2024
ACCEPTED 15 May 2024
PUBLISHED 11 June 2024

CITATION
Ding K, Li H, Xu Q, Zhao Y, Wang K and Liu T (2024), Real-time label-free three-dimensional invasion assay for anti-metastatic drug screening using impedance sensing. *Front. Pharmacol.* 15:1387949. doi: 10.3389/fphar.2024.1387949

Real-time label-free three-dimensional invasion assay for anti-metastatic drug screening using impedance sensing

Kai Ding[1], Hailong Li[1], Qian Xu[1], Yongmei Zhao[1]*, Kaikai Wang[1]* and Tianqing Liu[2]*

[1]School of Pharmacy, Nantong University, Nantong, China, [2]NICM Health Research Institute, Western Sydney University, Westmead, NSW, Australia

Tumor metastasis presents a formidable challenge in cancer treatment, necessitating effective tools for anti-cancer drug development. Conventional 2D cell culture methods, while considered the "gold standard" for invasive studies, exhibit limitations in representing cancer hallmarks and phenotypes. This study proposes an innovative approach that combines the advantages of 3D tumor spheroid culture with impedance-based biosensing technologies to establish a high-throughput 3D cell invasion assay for anti-metastasis drug screening through multicellular tumor spheroids. In addition, the xCELLigence device is employed to monitor the time-dependent kinetics of cell behavior, including attachment and invasion out of the 3D matrix. Moreover, an iron chelator (deferoxamine) is employed to monitor the inhibition of epithelial–mesenchymal transition in 3D spheroids across different tumor cell types. The above results indicate that our integrated 3D cell invasion assay with impedance-based sensing could be a promising tool for enhancing the quality of the drug development pipeline by providing a robust platform for predicting the efficacy and safety of anti-metastatic drugs before advancing into preclinical or clinical trials.

KEYWORDS

tumor metastasis, tumor spheroid, biosensing, drug screening, drug development

Introduction

Tumor metastasis poses a significant challenge in cancer treatment, with the complex biological processes involved making it difficult to study (Lyden et al., 2022). However, it is very challenging to screen anti-cancer drugs against tumor metastasis *in vitro*, mostly because there is a lack of effective tools for drug development that can be a good mimic for tumor metastasis (Wan et al., 2020; Collins et al., 2021). As a result, it is difficult to identify the potential compounds to treat tumor metastasis, leading to poor prediction of the drug's therapeutic efficacy and safety before preclinical or clinical trials. This increased the cost of drug development due to the failure of the anti-cancer drug candidates to go to market. Therefore, establishing an advanced, high-throughput platform for anti-metastatic drug screening is in high demand to increase the pipeline quality.

Conventional 2D cell invasion assays, such as the well-established scratch assay, are widely acknowledged as the gold standard methods for studying invasive processes

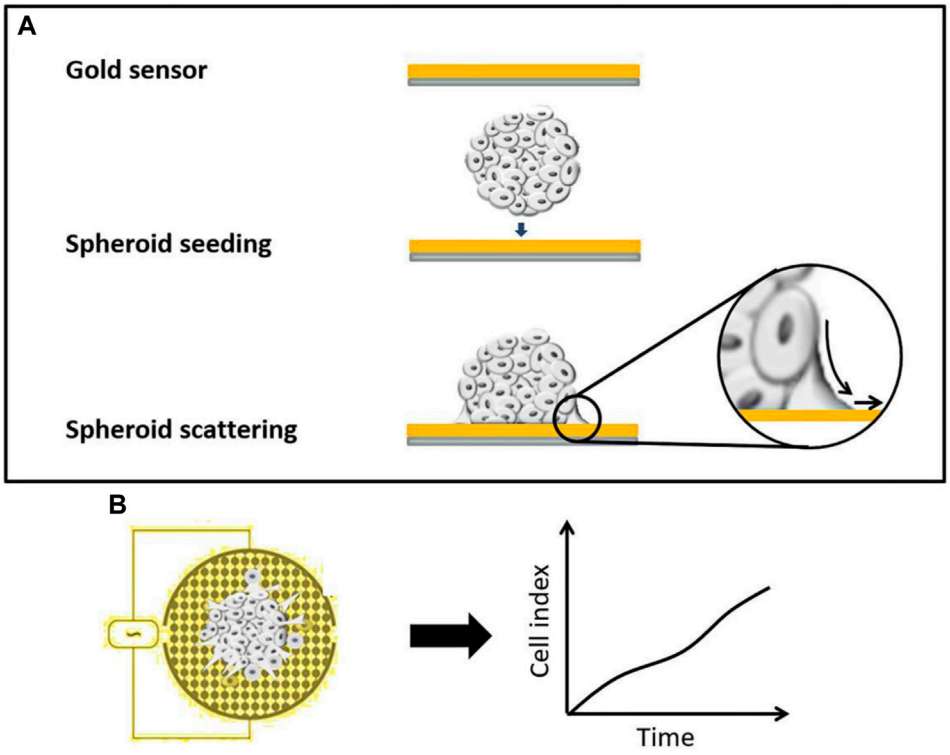

FIGURE 1
Schematic of the impedance-based spheroid spreading assay.

(Bouchalova and Bouchal, 2022). However, it has been reported that 2D cancer cell culture could not represent some hallmarks of cancer in the expression of some phenotypes, while cancer cells cultured in a 3D environment undergo significant phenotypical changes, such as epithelial–mesenchymal transition (EMT), due to 3D cell–cell interactions, the presence of complex extracellular matrix, and the physiological spatial heterogeneity (Liu et al., 2014; Liu et al., 2014; Golinelli et al., 2021; Leineweber, 2023; Zhu et al., 2023). An improved assay to mimic tumor invasion using *in vitro* models combines 3D with 2D cell culture by placing multicellular tumor cell spheroids either on a conventional cell culture dish or on collagen-coated surfaces (Manini et al., 2018; Weydert et al., 2020; Rodrigues et al., 2021). After the spheroids are attached to the surface, the cancer cells start to migrate on the dish surface opposite to the center of the spheroids in a scattering manner or invade toward the collagen as the extracellular matrix. Cell invasion behavior can be monitored using microscopes over a certain period of time or recorded at endpoints. The invasion of cancer cells toward the surfaces from the spheroids can closely mimic tumor aggressiveness and response to biological or drug conditions (Zuela-Sopilniak and Lammerding, 2019). Therefore, this invasion assay has been used for anti-migratory effects of drugs or biomolecules on 3D tumor tissues.

Impedance-based cell substrate sensing has emerged as a powerful, real-time, non-invasive, and label-free approach to assess various cell events, such as attachment, adhesion, proliferation, and invasion (Ramasamy et al., 2014; Zhang et al., 2021; Chen et al., 2023). Traditionally, the standard method for impedance-based cell sensing is to culture cells as a monolayer on the gold electrode, which can detect the changes in resistance caused by the cell behavior responding to the treatment (Mojena-Medina et al., 2020; Sagir et al., 2022). However, there is a lack of impedance-based cell assays developed to study cell invasion using 3D tissue models. Here, we present an integrated strategy for combining 3D tumor spheroid culture with commercially available impedance-based biosensing technologies in order to develop a 3D cell invasion assay for high-throughput anti-metastasis drug screening (Figures 1A,B). Multicellular tumor spheroids are cultured in a concave microwell device and then transferred to the impedance sensor (Tevlek et al., 2023). Cell attachment to the substrate and cell invasion out of the 3D matrix can be monitored over time by recording time-dependent kinetics of cell behavior using the xCELLigence device (Yan et al., 2018). The system is established to evaluate the anti-migratory effects of drugs on 3D tumor spheroids using a commercially available technology. The data are compared with parallel data obtained from conventional 2D and 3D observation-based invasion assays using cell lines, which are known to have different invasion capabilities, to confirm the reliability of this method. Furthermore, the application of the iron chelator (deferoxamine) adds a specific dimension to the study. The treatment-induced inhibition of EMT can be monitored using this 3D spheroid assay across different types of tumor cells. This comprehensive approach not only advances our understanding of cell invasion in 3D environments but also provides a valuable tool for high-throughput screening of anti-metastasis drugs in a physiologically relevant context.

Materials and methods

Cell culture

Two cell lines with different tumor metastasis status were used in this study. Human adenocarcinomas MCF-7 and MDA-MB-231 were purchased from the American Type Culture Collection (ATCC, United States). MCF-7 and MDA-MB-231 cells were grown in a complete medium consisting of DMEM supplemented with 10% (v/v) FBS in a humidified incubator at 37°C in 5% CO_2 and at 100% humidity. Cells were maintained by a once-weekly passage using trypsin/EDTA.

Cell seeding and tumor spheroid formation

Tumor spheroids were prepared using our previously developed method (Liu et al., 2014). The microwell devices were equilibrated with cell culture medium for 30 min before cell seeding. Cancer cell suspensions of MCF-7 or MDA-MB-231 cells (400 μL, 1×10^5 cells/mL) were seeded into the devices. Cell sedimentation in the microwells was aided by gentle vibration. The culture medium was removed every 2 days and refilled with fresh medium. The microwell devices were typically kept in an incubator for several days to enable the formation of dense multicellular tumor spheroids.

2D cell scratch assay monitored using time-lapse microscopy

Cancer cells were seeded on the 96-well plates with a cell seeding density of 200 μL, 1×10^6 cells/mL, and attached to the surface overnight. After the cells reached confluence, a line was drawn on the cell monolayer using a cell scraper, and a scratched region was created. Cell invasion over the scratched region was monitored over 24 h (Huang et al., 2020; Pijuan et al., 2019). The distance of the recovery over time was monitored using a time-lapse microscope with a stage-top incubator.

3D spheroid invasion assay

Cells were seeded into agarose microwells to form 3D tissue. The formed spheroids were harvested from the microwell devices and manually transferred to the collagen-coated E-plate. The cell motion and the invasion of 3D spheroids were tracked using a time-lapse microscope equipped with impedance-sensing technology.

Antiproliferative and metastasis- predictive drug treatment

An iron chelator, deferoxamine (DFO), was dissolved and diluted using a culture medium as the treatment. The anti-proliferative effects of the drug on different cancer cells were measured after 72 h of incubation at 37°C (Sandoval-Acuña et al., 2021; Wijesinghe et al., 2021). The proliferation of the MCF-7 and MDA-MB-231 cells was first monitored using an xCELLigence System (Roche, Penzberg, Germany). The cell index, defined based on the cell adhesion rate, was recorded throughout the incubation and treatment periods. IC_{50} values were obtained directly from the measurement. The drug response was evaluated using both 2D cell scratch assays monitored with a time-lapse microscope and 3D spheroid invasion assays were monitored using a time-lapse microscope and impedance-sensing equipment.

Western blot of EMT biomarkers

The proteins were extracted from the 2D cells and 3D tumor spheroids using RIPA buffer containing a protease inhibitor, a phosphatase inhibitor, and phenylmethanesulfonyl fluoride (PMSF). They were separated with SDS-PAGE gel and transferred onto a polyvinylidene fluoride (PVDF) membrane. After being blocked in 5% BSA for 2 h at room temperature, the membranes were incubated with primary antibodies for EMT markers (vimentin, E-cadherin, and N-cadherin) and β-actin at a 1:1000 dilution in 5% BSA at 4°C overnight. After being washed three times with TBST every 15 min, the membranes were incubated with the secondary antibody at room temperature for 2 h. The blots were visualized using an ECL chemiluminescence kit. β-Actin was used as a loading control, and Image-Pro software (National Institutes of Health, Bethesda, MD, United States) was used for the densitometric analysis of the bands.

Results and discussion

2D cell scratch assay using cancer cells with different metastatic statuses

Two distinct metastatic statuses of human breast cancer cells, namely MCF-7 cells (Figure 2A) and MDA-MB-231 cells (Figure 2B), were chosen for the 2D cell scratch assay. MDA-MB-231 cells, which are characterized by their spindle shape, estrogen receptor (ER) negativity, adherent growth, and robust invasion and metastatic capabilities, were selected as representatives of highly invasive human breast cancer cells. On the other hand, MCF-7 cells, which are estrogen receptor-positive breast cancer cell lines, exhibit lower invasiveness compared to MDA-MB-231. The healing process in the MCF-7 cell line showed only 40% closure at the 12th hour and approximately 70% at the 24th hour, indicating incomplete healing. In contrast, the MDA-MB-231 cell line exhibited 80% wound closure at the 12th hour and complete healing at the 24th hour (Figures 2C,D). These findings suggest that MDA-MB-231 cells are highly invasive, while MCF-7 cells exhibit lower invasiveness. Importantly, the observed experimental outcomes align with the existing literature data, supporting the reliability and consistency of our results (Izdebska et al., 2021).

Verification of the epithelial–mesenchymal transition (EMT) induced by 3D cell culture

Furthermore, tumor spheroids were prepared by culturing MDA-MB-231 and MCF-7 cells in microwells at a concentration

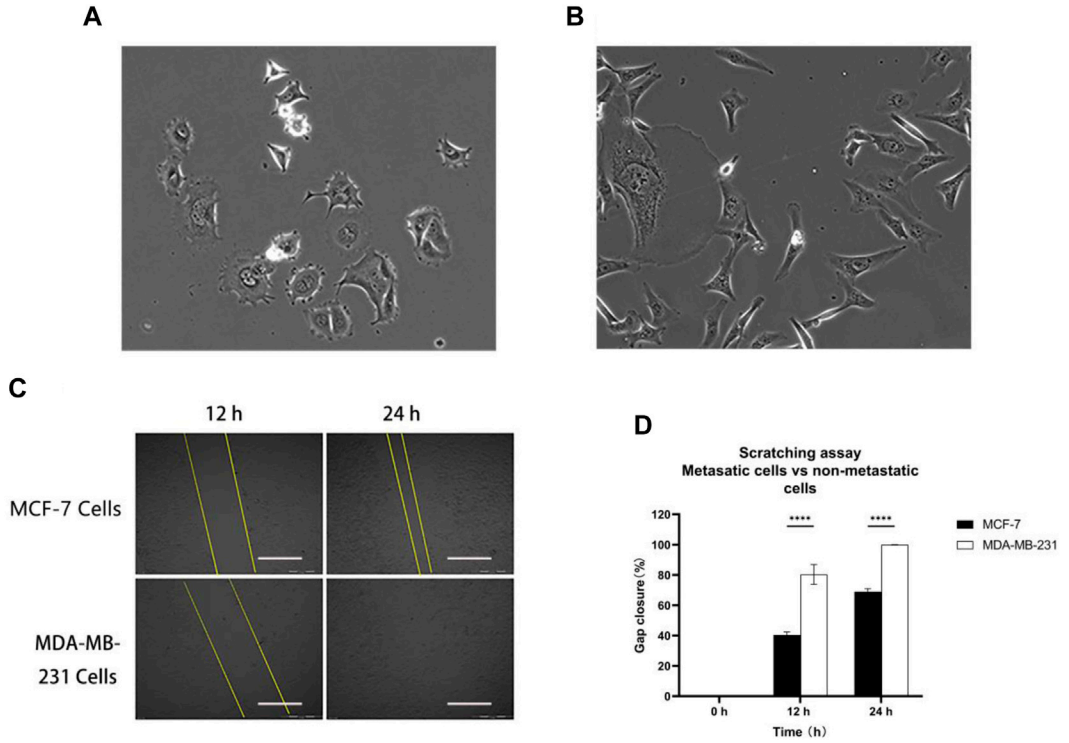

FIGURE 2
Metastatic cells vs. non-metastatic cells: **(A)** MCF-7 and **(B)** MDA-MB-231 cell morphology; **(C)** and **(D)** MCF-7 and MDA-MB-231 cells were scratched and monitored over 24 h. Scale bar, 0.5 mm. Then, wound healing was analyzed using ImageJ software. Data are expressed as mean ± SD of three independent replicates. ****$p < 0.0001$ *versus* the 2D group.

of 1×10^5 cells/device. The growth of multicellular tumor spheroids was monitored using a time-lapse microscope, and changes in spheroid size were quantified using Image-Pro Analyzer software. Experimental findings revealed that, by day 7, the radius of MDA-MB-231 tumor spheroids was approximately 250 μm, surpassing that of MCF-7 tumor spheroids (Figure 3A). Real-time tumor images further illustrated the larger size of MDA-MB-231 cell-derived spheroids compared to those derived from MCF-7 cells (Figure 3B). Concurrently, protein extraction from both 2D and 3D cultured MDA-MB-231 and MCF-7 cells enabled a comparison of the expression of epithelial–mesenchymal transition (EMT)-related proteins using Western blot analysis (Figures 3C, D). In 2D culture, vimentin protein expression in MDA-MB-231 cells exceeded that in MCF-7 cells, suggesting a higher invasiveness of MDA-MB-231 cells. Interestingly, 3D culture led to a significant increase in vimentin expression in MCF-7 cells, indicating an elevation in the invasiveness of the initially less-invasive tumor. Notably, the absence of E-cadherin expression is indicative of EMT, and MDA-MB-231 cells exhibited lower E-cadherin expression compared to MCF-7 cells, reinforcing the higher invasiveness of MDA-MB-231 cells. Moreover, the expression of E-cadherin in 3D tumor spheroids for both cell types was lower than that in 2D culture, suggesting that 3D culture increased the invasiveness of tumor cells. Furthermore, N-cadherin, which is associated with increased motility and invasiveness, exhibited elevated expression in 3D-cultured tumor spheroids compared to 2D culture. In summary, 3D culture promoted the enhanced epithelial–mesenchymal transition in tumors. Tumor spheroids cultured in 3D more closely resembled real tumors compared to their 2D counterparts, making them more conducive to subsequent experimental analyses.

Comparison of the 3D spheroid scattering assay

There are limitations associated with 2D cell culture. Studies have indicated that 2D cancer cell culture fails to fully capture certain characteristics of cancer phenotypes. In contrast, cancer cells cultured in a 3D environment undergo substantial phenotypic changes, such as epithelial–mesenchymal transition (EMT), owing to 3D cell–cell interactions, the presence of a complex extracellular matrix, and physiological spatial heterogeneity (Leggett et al., 2021). To address these limitations, we employ a method that combines *in vitro* 3D-cultured tumor spheroids with an impedance sensor capable of monitoring real-time changes in cell morphology, proliferation, and differentiation quantitatively.

In this approach, multicellular tumor spheroids are cultured in a concave microwell device and then transferred onto the impedance sensor (Lee and Kim, 2021). Over the course of several hours, tumor cells spread from the spheroid onto the coated surface, and their invasion is recorded at intervals of up to 72 h. Using an inverted microscope, images are captured and subsequently analyzed using

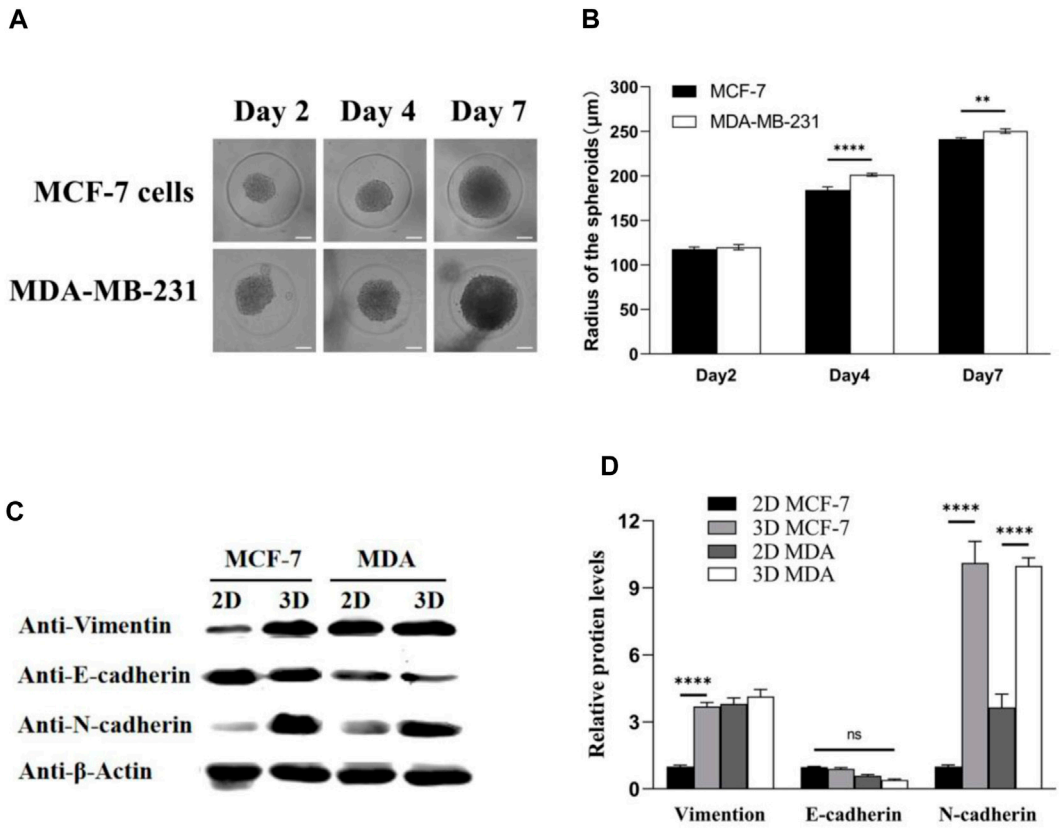

FIGURE 3
MDA-MB-231 spheroids significantly contribute to the expression levels of EMT biomarkers compared with 2D culture. **(A)** MCF-7 and MDA-MB-231 spheroids in microwells; **(B)** spheroid radius was analyzed by Image-Pro Analyzer software; and **(C,D)** Western blotting analysis on the expression of EMT biomarkers: vimentin, E-cadherin, and N-cadherin. β-Actin was used as the internal reference. Scale bar, 100 μm. (**$p < 0.01$, ****$p < 0.0001$, N = 3, six spheroids per group).

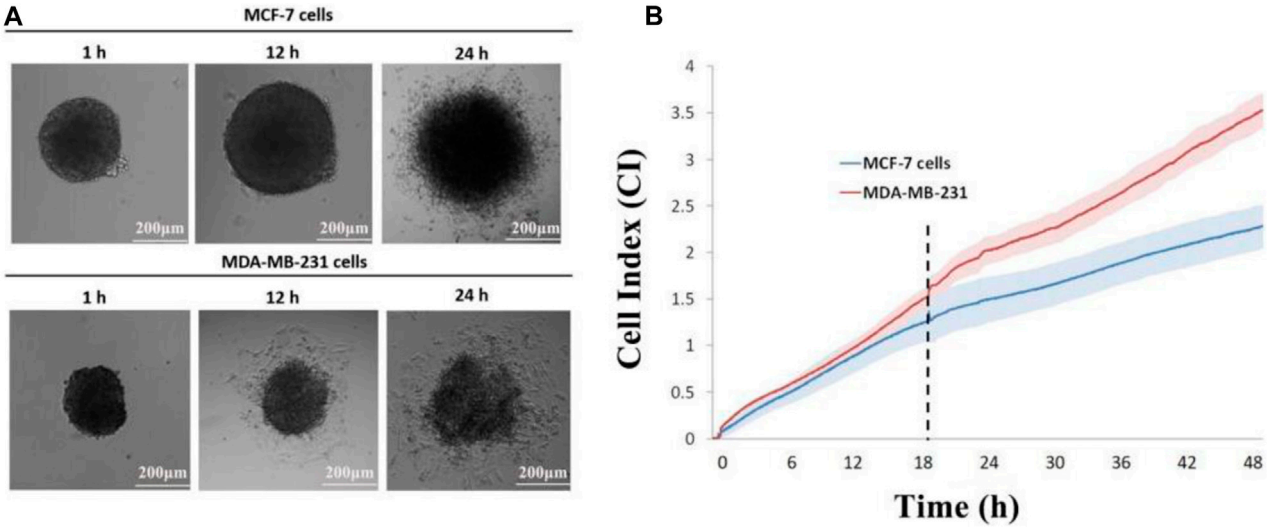

FIGURE 4
Impedance sensing of both cell lines. **(A)** Morphological changes in MCF-7 and MDA-MB-231 spheroids on E-plate; **(B)** real-time monitoring of cell index changes in tumor spheroids using impedance sensors. Scale bar, 200 μm. (N = 3, six spheroids per group).

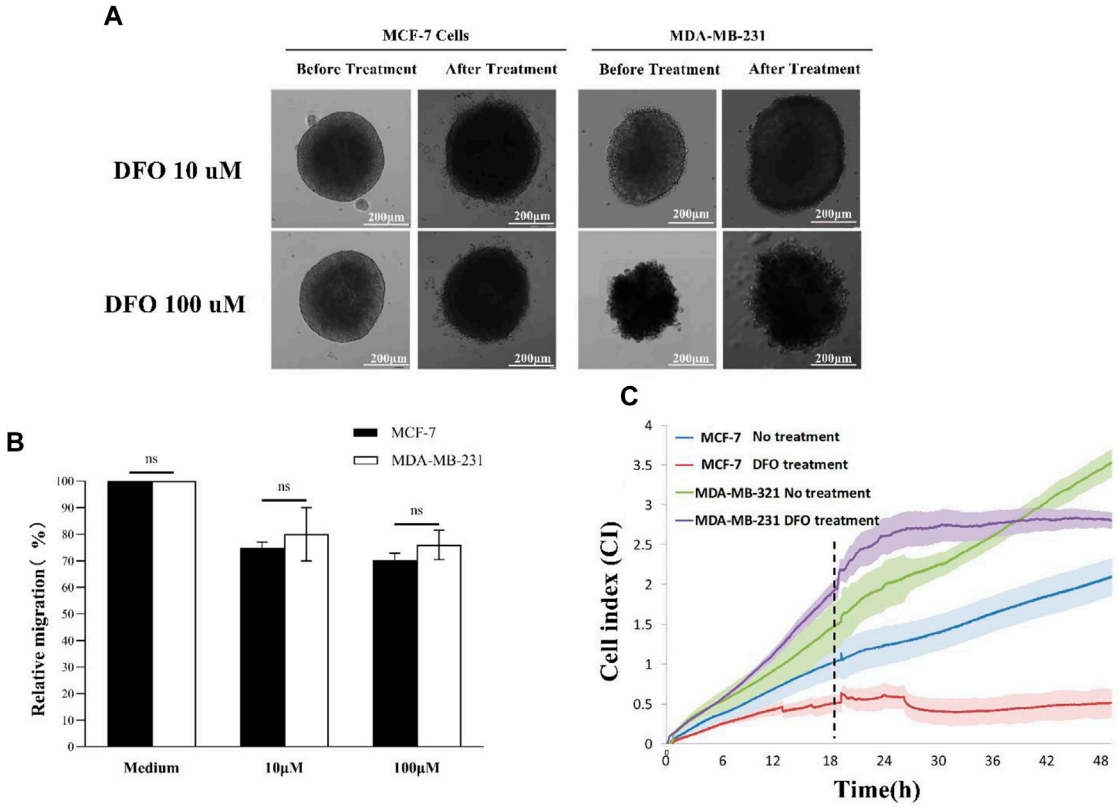

FIGURE 5
DFO treatment: **(A)** 3D scattering assay recorded using time-lapse microscopy; **(B)** relative invasion of 3D tumor spheroids; and **(C)** impedance sensing. Scale bar, 200 μm. (N = 3, six spheroids per group).

Image-Pro Analyzer software. Manual recording of the leading edge of migrating cells allows the software application to calculate the covered area, offering valuable qualitative insights into different cell invasion patterns (Figure 4B). The recorded cell index (CI) demonstrates a positive correlation with the invasive capacity of the tumor cells. Notably, MDA-MB-231 achieved the highest CI value in the invasion (without Matrigel) setting, indicating that the 3D tumor spheroid from the MDA-MB-231 cell line exhibited greater mobility than that from the MCF-7 cell line (Figure 4B). The experimental monitoring results align with the observations made through real-time imaging using a time-lapse microscope (Figure 4A).

Inhibition of EMT using iron chelators monitored by the impedance-sensing-based 3D spheroid scattering assay

Following the experimental validation of the real-time 3D spheroid invasion monitoring capability of the impedance sensor, our objective was to utilize this sensor for tracking the inhibition of epithelial–mesenchymal transition (EMT) in 3D spheroids of distinct tumor cells through iron chelator (DFO) treatment. Initially, we assessed the impact of different concentrations of iron chelators on the dispersion of 3D spheroids by monitoring changes in cell index (CI) values. Subsequently, the selected concentration of iron chelators was applied to 3D tumor spheroids on E-plates, and impedance curves were recorded from the initiation. The addition of the iron chelator (DFO) occurred during the plateau period of the impedance curves, concurrent with the real-time documentation of the 3D spheroid states.

Time-lapse microscopy data revealed a diminished invasion of both MCF-7 and MDA-MB-231 spheroids, following DFO treatment, with invasion capacity decreasing in correlation with the increasing DFO concentration (Figure 5A). Consistent findings were obtained through Image-Pro Analyzer software analysis, further indicating that MCF-7 spheroids exhibited lower relative invasion compared to MDA-MB-231 spheroids, aligning with previous experimental outcomes (Figure 5B). Real-time impedance values demonstrated that the MCF-7 DFO treatment group exhibited the lowest cell index, while the MDA-MB-231-no treatment group reached the highest cell index at the 48th hour post-chelating agent administration. In the MDA-MB-231 DFO treatment group, the cell index briefly increased to around 2.5 following chelating agent administration before plateauing for a period, whereas in the no-treatment groups, the cell index continued to rise, surpassing that of the treated group after 18 h. These observations indicated that the EMT of MDA-MB-231 tumor spheroids was suppressed by iron chelator treatment. Similar trends were observed in the less-invasive MCF-7 cells (Figure 5C).

Conclusion

In conclusion, our investigation not only confirmed the augmented expression of epithelial–mesenchymal transition (EMT)-related biomarkers within 3D tumor spheroids when compared to their 2D cultured counterparts, as validated by Western blot analysis but also extended its scope to encompass the real-time monitoring of cell invasion using the impedance sensor system. This multifaceted approach provided a better understanding of the dynamic changes in cellular behavior under three-dimensional conditions. Furthermore, we successfully demonstrated the efficacy of the impedance sensor system in verifying the inhibitory effects of the DFO drug on the invasion of 3D spheroids. The real-time label-free monitoring of cell invasion afforded by the impedance sensor system allowed for precise and quantitative assessment, offering insight into the temporal dynamics of cell responses. Our results underscore the potential of impedance sensing as a valuable tool for studying the intricate interplay between cells and their microenvironment in three-dimensional settings. This integrated methodology holds promise for advancing anti-metastasis drug screening strategies. Moreover, the successful validation of the DFO drug as an inhibitor of 3D spheroid invasion highlights the translational potential of our findings. By bridging the gap between traditional 2D cell culture models and more complex 3D systems, our study establishes a robust foundation for future investigations into anti-metastasis drug screening.

Data availability statement

The raw data supporting the conclusions of this article will be made available by the authors, without undue reservation.

Ethics statement

Ethical approval was not required for the studies on humans in accordance with local legislation and institutional requirements, because only commercially available established cell lines were used.

Author contributions

HL: data curation, formal analysis, methodology, and writing–review and editing. QX: data curation, formal analysis, methodology, and writing–review and editing. YZ: conceptualization, funding acquisition, methodology, supervision, and writing–review and editing. KW: conceptualization, supervision, and writing–review and editing. KD: data curation, formal analysis, methodology, and writing–original draft. TL: conceptualization, data curation, funding acquisition, methodology, supervision, and writing–review and editing.

Funding

The authors declare that financial support was received for the research, authorship, and/or publication of this article. TL is supported by the National Health and Medical Research Council (NHMRC) Early Career Fellowship (Grant No. 1112258) and the WSU Vice-Chancellor's Senior Research Fellowship. YZ is supported by Jiangsu's Mass Entrepreneurship and Innovation Program.

Conflict of interest

The authors declare that the research was conducted in the absence of any commercial or financial relationship that could be construed as a potential conflict of interest.

Publisher's note

All claims expressed in this article are solely those of the authors and do not necessarily represent those of their affiliated organizations, or those of the publisher, the editors, and the reviewers. Any product that may be evaluated in this article, or claim that may be made by its manufacturer, is not guaranteed or endorsed by the publisher.

References

Bouchalova, P., and Bouchal, P. (2022). Current methods for studying metastatic potential of tumor cells. *Cancer Cell Int.* 22 (1), 394. doi:10.1186/s12935-022-02801-w

Chen, Y. S., Huang, C. H., Pai, P. C., Seo, J., and Lei, K. F. (2023). A review on microfluidics-based impedance biosensors. *Biosens. (Basel)* 13 (1), 83. doi:10.3390/bios13010083

Collins, T., Pyne, E., Christensen, M., Iles, A., Pamme, N., and Pires, I. M. (2021). Spheroid-on-chip microfluidic technology for the evaluation of the impact of continuous flow on metastatic potential in cancer models *in vitro*. *Biomicrofluidics* 15 (4), 044103. doi:10.1063/5.0061373

Golinelli, G., Talami, R., Frabetti, S., Candini, O., Grisendi, G., Spano, C., et al. (2021). A 3D platform to investigate dynamic cell-to-cell interactions between tumor cells and mesenchymal progenitors. *Front. Cell Dev. Biol.* 9, 767253. doi:10.3389/fcell.2021.767253

Huang, Z., Yu, P., and Tang, J. (2020). Characterization of triple-negative breast cancer MDA-MB-231 cell spheroid model. *Onco Targets Ther.* 13, 5395–5405. doi:10.2147/OTT.S249756

Izdebska, M., Zielińska, W., Krajewski, A., Hałas-Wiśniewska, M., Mikołajczyk, K., Gagat, M., et al. (2021). Downregulation of MMP-9 enhances the anti-migratory effect of cyclophosphamide in MDA-MB-231 and MCF-7 breast cancer cell lines. *Int. J. Mol. Sci.* 22 (23), 12783. doi:10.3390/ijms222312783

Lee, K. H., and Kim, T. H. (2021). Recent advances in multicellular tumor spheroid generation for drug screening. *Biosens. (Basel)* 11 (11), 445. doi:10.3390/bios11110445

Leggett, S. E., Hruska, A. M., Guo, M., and Wong, I. Y. (2021). The epithelial-mesenchymal transition and the cytoskeleton in bioengineered systems. *Cell Commun. Signal* 19 (1), 32. doi:10.1186/s12964-021-00713-2

Leineweber, W. (2023). Integrated biophysical imaging of cell interactions with 3D extracellular matrices. *Nat. Rev. Mol. Cell Biol.* 24 (11), 773. doi:10.1038/s41580-023-00639-2

Liu, T., Chien, C. C., Parkinson, L., and Thierry, B. (2014). Advanced micromachining of concave microwells for long term on-chip culture of multicellular tumor spheroids. *ACS Appl. Mater Interfaces* 6 (11), 8090–8097. doi:10.1021/am500367h

Liu, T., Winter, M., and Thierry, B. (2014). Quasi-spherical microwells on superhydrophobic substrates for long term culture of multicellular spheroids and high throughput assays. *Biomaterials* 35 (23), 6060–6068. doi:10.1016/j.biomaterials.2014.04.047

Lyden, D., Ghajar, C. M., Correia, A. L., Aguirre-Ghiso, J. A., Cai, S., Rescigno, M., et al. (2022). Metastasis. *Cancer Cell* 40 (8), 787–791. doi:10.1016/j.ccell.2022.07.010

Manini, I., Caponnetto, F., Bartolini, A., Ius, T., Mariuzzi, L., Di Loreto, C., et al. (2018). Role of microenvironment in glioma invasion: what we learned from *in vitro* models. *Int. J. Mol. Sci.* 19 (1), 147. doi:10.3390/ijms19010147

Mojena-Medina, D., Hubl, M., Bäuscher, M., Jorcano, J. L., Ngo, H. D., and Acedo, P. (2020). Real-time impedance monitoring of epithelial cultures with inkjet-printed interdigitated-electrode sensors. *Sensors (Basel)* 20 (19), 5711. doi:10.3390/s20195711

Pijuan, J., Barceló, C., Moreno, D. F., Maiques, O., Sisó, P., Marti, R. M., et al. (2019). *In vitro* cell migration, invasion, and adhesion assays: from cell imaging to data analysis. *Front. Cell Dev. Biol.* 7, 107. doi:10.3389/fcell.2019.00107

Ramasamy, S., Bennet, D., and Kim, S. (2014). Drug and bioactive molecule screening based on a bioelectrical impedance cell culture platform. *Int. J. Nanomedicine* 9, 5789–5809. doi:10.2147/IJN.S71128

Rodrigues, J., Heinrich, M. A., Teixeira, L. M., and Prakash, J. (2021). 3D *in vitro* model (R)evolution: unveiling tumor-stroma interactions. *Trends Cancer* 7 (3), 249–264. doi:10.1016/j.trecan.2020.10.009

Sagir, T., Huysal, M., Senel, M., Isık, S., Burgucu, N., Tabakoglu, O., et al. (2022). Folic acid conjugated PAMAM-modified mesoporous silica-coated superparamagnetic iron oxide nanoparticles for potential cancer therapy. *J. Colloid Interface Sci.* 625, 711–721. doi:10.1016/j.jcis.2022.06.069

Sandoval-Acuña, C., Torrealba, N., Tomkova, V., Jadhav, S. B., Blazkova, K., Merta, L., et al. (2021). Targeting mitochondrial iron metabolism suppresses tumor growth and metastasis by inducing mitochondrial dysfunction and mitophagy. *Cancer Res.* 81 (9), 2289–2303. doi:10.1158/0008-5472.CAN-20-1628

Tevlek, A., Kecili, S., Ozcelik, O. S., Kulah, H., and Tekin, H. C. (2023). Spheroid engineering in microfluidic devices. *ACS Omega* 8 (4), 3630–3649. doi:10.1021/acsomega.2c06052

Wan, L., Neumann, C. A., and LeDuc, P. R. (2020). Tumor-on-a-chip for integrating a 3D tumor microenvironment: chemical and mechanical factors. *Lab. Chip* 20 (5), 873–888. doi:10.1039/c9lc00550a

Weydert, Z., Lal-Nag, M., Mathews-Greiner, L., Thiel, C., Cordes, H., Küpfer, L., et al. (2020). A 3D heterotypic multicellular tumor spheroid assay platform to discriminate drug effects on stroma versus cancer cells. *SLAS Discov.* 25 (3), 265–276. doi:10.1177/2472555219880194

Wijesinghe, T. P., Dharmasivam, M., Dai, C. C., and Richardson, D. R. (2021). Innovative therapies for neuroblastoma: the surprisingly potent role of iron chelation in up-regulating metastasis and tumor suppressors and down-regulating the key oncogene, N-myc. *Pharmacol. Res.* 173, 105889. doi:10.1016/j.phrs.2021.105889

Yan, G., Du, Q., Wei, X., Miozzi, J., Kang, C., Wang, J., et al. (2018). Application of real-time cell electronic analysis system in modern pharmaceutical evaluation and analysis. *Molecules* 23 (12), 3280. doi:10.3390/molecules23123280

Zhang, Z., Huang, X., Liu, K., Lan, T., Wang, Z., and Zhu, Z. (2021). Recent advances in electrical impedance sensing technology for single-cell analysis. *Biosens. (Basel)* 11 (11), 470. doi:10.3390/bios11110470

Zhu, D., Trinh, P., Liu, E., and Yang, F. (2023). Cell-cell interactions enhance cartilage zonal development in 3D gradient hydrogels. *ACS Biomater. Sci. Eng.* 9 (2), 831–843. doi:10.1021/acsbiomaterials.2c00469

Zuela-Sopilniak, N., and Lammerding, J. (2019). Engineering approaches to studying cancer cell migration in three-dimensional environments. *Philos. Trans. R. Soc. Lond B Biol. Sci.* 374 (1779), 20180219. doi:10.1098/rstb.2018.0219

frontiers | Frontiers in Pharmacology

TYPE Original Research
PUBLISHED 15 July 2024
DOI 10.3389/fphar.2024.1388038

OPEN ACCESS

EDITED BY
Luping Pang,
Zhengzhou University, China

REVIEWED BY
Sumei Ren,
Zhengzhou University, China
Jing-Quan Wang,
St. John's University, United States

*CORRESPONDENCE
Marwa M. Abu-Serie,
marwaelhedaia@gmail.com

RECEIVED 19 February 2024
ACCEPTED 18 June 2024
PUBLISHED 15 July 2024

CITATION
Abu-Serie MM, Barakat A, Ramadan S and Habashy NH (2024), Superior cuproptotic efficacy of diethyldithiocarbamate-Cu_4O_3 nanoparticles over diethyldithiocarbamate-Cu_2O nanoparticles in metastatic hepatocellular carcinoma.
Front. Pharmacol. 15:1388038.
doi: 10.3389/fphar.2024.1388038

Superior cuproptotic efficacy of diethyldithiocarbamate-Cu_4O_3 nanoparticles over diethyldithiocarbamate-Cu_2O nanoparticles in metastatic hepatocellular carcinoma

Marwa M. Abu-Serie[1]*, Assem Barakat[2], Sherif Ramadan[3,4] and Noha Hassan Habashy[5]

[1]Medical Biotechnology Department, Genetic Engineering and Biotechnology Research Institute (GEBRI), City of Scientific Research and Technological Applications (SRTA-City), Alexandria, Egypt, [2]Department of Chemistry, College of Science, King Saud University, Riyadh, Saudi Arabia, [3]Chemistry Department, Michigan State University, East Lansing, MI, United States, [4]Department of Chemistry, Benha University, Benha, Egypt, [5]Biochemistry Department, Faculty of Science, Alexandria University, Alexandria, Egypt

Metastatic hepatocellular carcinoma (HC) is a serious health concern. The stemness of cancer stem cells (CSCs) is a key driver for HC tumorigenesis, apoptotic resistance, and metastasis, and functional mitochondria are critical for its maintenance. Cuproptosis is Cu-dependent non-apoptotic pathway (mitochondrial dysfunction) via inactivating mitochondrial enzymes (pyruvate dehydrogenase "PDH" and succinate dehydrogenase "SDH"). To effectively treat metastatic HC, it is necessary to induce selective cuproptosis (for halting cancer stemness genes) with selective oxidative imbalance (for increasing cell susceptibility to cuproptosis and inducing non-CSCs death). Herein, two types of Cu oxide nanoparticles (Cu_4O_3 "C(I + II)" NPs and Cu_2O "C(I)" NPs) were used in combination with diethyldithiocarbamate (DD, an aldehyde dehydrogenase "ALDH" inhibitor) for comparative anti-HC investigation. DC(I + II) NPs exhibited higher cytotoxicity, mitochondrial membrane potential, and anti-migration impact than DC(I) NPs in the treated human HC cells (HepG2 and/or Huh7). Moreover, DC(I + II) NPs were more effective than DC(I) NPs in the treatment of HC mouse groups. This was mediated via higher selective accumulation of DC(I + II) NPs in only tumor tissues and oxidant activity, causing stronger selective inhibition of mitochondrial enzymes (PDH, SDH, and ALDH2) than DC(I)NPs. This effect resulted in more suppression of tumor and metastasis markers as well as stemness gene expressions in DC(I + II) NPs-treated HC mice. In addition, both nanocomplexes normalized liver function and hematological parameters. The computational analysis found that DC(I + II)

showed higher binding affinity to most of the tested enzymes. Accordingly, DC(I + II) NPs represent a highly effective therapeutic formulation compared to DC(I) NPs for metastatic HC.

KEYWORDS

metastatic liver cancer, diethyldithiocarbamate-Cu_4O_3 nanocomplex (DC(I+II)NPs), diethyldithiocarbamate-Cu_2O nanocomplex (DC(I)NPs), stemness genes, cuproptosis induction, oxidant activity

1 Introduction

Hepatocellular carcinoma (HC) is one of the most common types of primary malignant liver tumors and the second-leading cause of cancer death (Liu and Qian, 2021). Its incidence and mortality rates are increasing, making it a challenging global health issue. According to estimations, over a million people will be diagnosed with HC annually by 2025 (Philips et al., 2021; Wang et al., 2021). Metastasis is the main cause of HC death; the lungs are the most frequent site of metastatic HC (Terada and Maruo, 2013; Chang et al., 2019). The stemness of liver cancer stem cells (CSCs) represents the main driver of HC initiation, progression, therapeutic resistance, recurrence, and metastasis (Chang et al., 2019; Jing et al., 2021). CSCs maintain stemness by up-regulating unique genes, including CD133 (prominin1) and aldehyde dehydrogenase (ALDH)2, to activate Notch and Wnt/β-catenin signaling pathways, resulting in the expression of self-renewal transcription factors (SOX2, OCT-4, and NANOG) and drug efflux transporters (e.g., ATP binding cassette subfamily G member 2, ABCG2). This condition confers more metastatic and chemoresistance effects (Wang and Sun, 2018; Liu and Qian, 2021; Zhang and Fu, 2021). The latter is also mediated by glutathione-S-transferase (GST), particularly GST π (GSTP1), which is highly expressed in malignant tumors and maintains stemness by detoxifying reactive oxygen species (ROS) and DNA-damaging compounds, conferring apoptosis resistance (Cui et al., 2020; Niitsu et al., 2022). The stemness markers in HC are also associated with overexpression of the fetal liver cell marker (α-fetoprotein, AFP), which is an indicator of poorly differentiated HC (Sell, 2008). Functional mitochondria (tricarboxylic acid cycle (TCA) and respiratory chain) are essential for maintaining the stemness of apoptotic resistance CSCs (Loureiro et al., 2017; Yadav et al., 2020). Therefore, finding other forms of regulated cell death (apoptosis) depending on mitochondrial dysfunction is critical for effectively eradicating metastatic seeds, CSCs.

Cuproptosis, which is based on cellular Cu accumulation, mediates nonapoptotic mitochondrial cell death via inactivation of mitochondrial lipoylated TCA enzymes (e.g., pyruvate dehydrogenase complex (PDH), α-ketoglutarate dehydrogenase, 2-oxoadipate dehydrogenase, and branched-chain ketoacid dehydrogenase) and mitochondrial Fe-S cluster-containing enzymes (Lv et al., 2022). This high intracellular Cu binds specifically to the lipoyl moiety of dihydrolipoamide S-acetyltransferase (DLAT, regenerating lipoamide cofactor), a component E2 of PDH, which is a crucial enzyme for the transformation of glycolysis to TCA. This binding results in disulfide-mediated aggregation of Cu-lipoylated proteins and then halts TCA (Tang et al., 2022). On the other hand, this accumulated Cu binds to sulfur and displaces the catalytic iron atom of mitochondrial Fe-S cluster proteins, causing cluster degradation (Vallieres et al., 2017; Tang et al., 2022). Mitochondrial Fe-S cluster proteins are key cofactors for electron transfer complexes of the respiratory chain with dual functions in TCA (e.g., succinate dehydrogenase "SDH", complex II"), whereas nuclear Fe-S cofactors are involved in DNA replication, DNA repair, and genome integrity (regulator of telomere length helicase 1, RTEL1) (Paul and Lill, 2015; Read et al., 2021; Li et al., 2022). The latter contributes to stability of the whole genome and telomere and is associated with HC risk (Margalef et al., 2018). The resultant toxic lipoylated protein aggregation and mitochondrial Fe-S protein degradation caused by Cu accumulation induce mitochondrial proteotoxic stress, causing loss of mitochondrial membrane potential (MP) and ultimately cell death, particularly in the case of proteasomal dysfunction (Li et al., 2022; Tang et al., 2022). Notably, the depletion of glutathione (GSH, a nonenzymatic antioxidant) makes cancer cells more susceptible to cuproptosis (Tsvetkov et al., 2022).

As a consequence, in this study, green chemically synthesized Cu oxide nanoparticles (NPs) were used to improve cuproptotic selectivity in combination with diethyldithiocarbamate (DD). The latter (an active metabolite of FDA-approved anti-alcoholism remedy) was used, herein as Cu oxide NPs ionophore to maximize the cuproptosis effect via its potency for suppressing ALDH, depleting GSH, and inhibiting the S26 proteasome (a major protease for degrading damaged toxic proteins) (Cvek et al., 2008; Abu-Serie and Eltarahony, 2021; Abu-Serie and Abdelfattah, 2023; Abu-Serie et al., 2024; Abu-Serie, 2024). Abu-Serie and Eltarahony (2021) illustrated that a new nanocomplex of cuprous oxide NPs and DD (DC(I) NPs) can repress the growth of human lung, colon, liver, and prostate cancer cells at IC_{50} < 2.5 μg/mL by inhibiting ALDH1A1 and elevating the cellular content of ROS. Furthermore, this nanocomplex (DC(I) NPs) exhibited potent anti-migration efficacy on the above-mentioned cell lines (Abu-Serie and Eltarahony, 2021). Another recent study by the author demonstrated that a unique nanocomplex of DD-Cu_4O_3 NPs (DC(I + II) NPs) can eradicate metastatic breast cancer by suppressing CSC genes and the metastasis marker (matrix metalloproteinase (MMP)9), as well as disturbing redox markers, using MDA-MB 231 cells and an orthotopic animal model (Abu-Serie and Abdelfattah, 2023). These recent findings prompted us to investigate the cuproptosis and oxidative alteration effects of DC(I + II) NPs in comparison with DC(I) NPs for suppressing the HC markers (α-fetoprotein and GST), stemness and GSTP1 genes, ALDH2 activity, and metastasis markers (MMP9 gene and TWIST1) in the treatment of

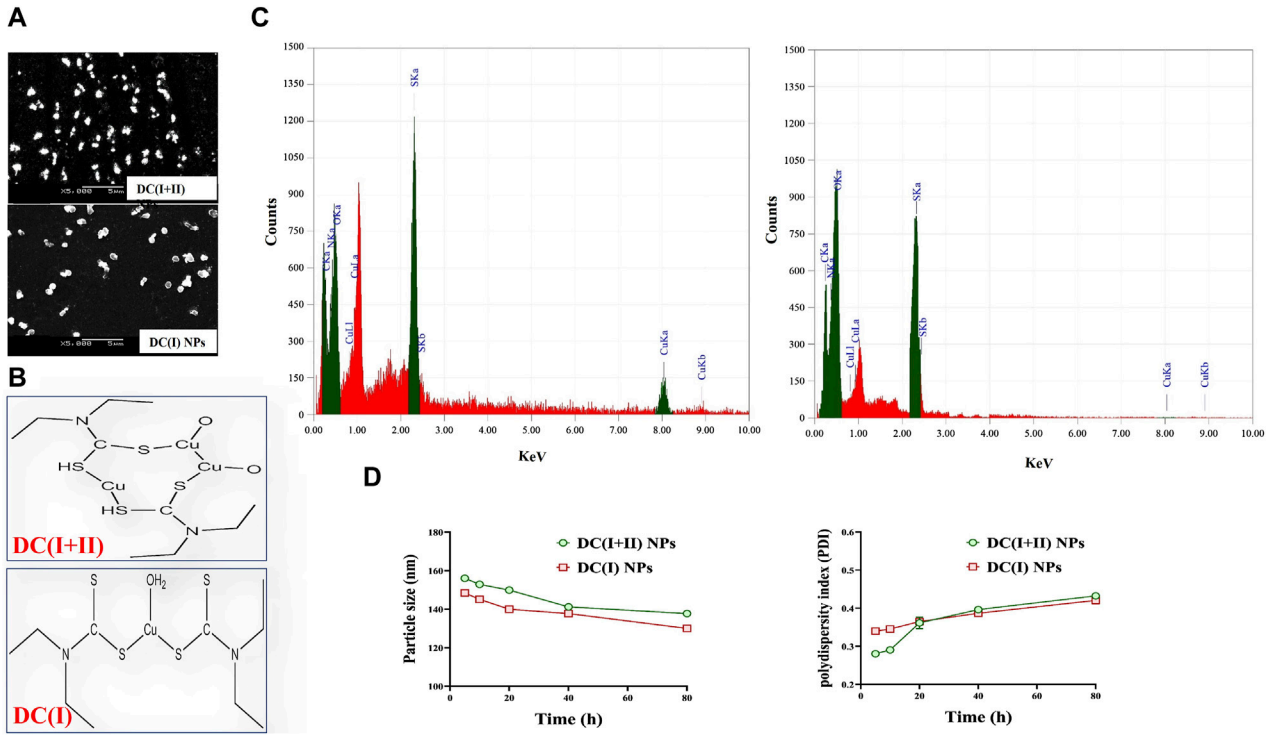

FIGURE 1
Morphology, ChemDraw 2D structures, elemental composition analysis, and stability of nanocomplexes. **(A)** Scanning electron microscope images of diethyldithiocarbamate (DD)-Cu_4O_3 "C(I + II)" nanoparticles (DC(I + II) NPs) and DD-Cu_2O NPs "C(I)" NPs (DC(I) NPs) (magnification ×5000). **(B)** 2D structures of nanocomplexes of DC(I + II) NPs and DC(I) NPs, as generated by ChemDraw software. **(C)** Elemental composition of nanocomplexes of DC(I + II) NPs and DC(I) NPs, as analyzed by energy dispersive X-ray spectroscopy. **(D)** Biostability of the prepared nanocomplexes during 80 h incubation in phosphate buffer saline-contained 50% fetal bovine serum at 37°C in terms of variations in particle size and aggregation index (PDI). Data are shown as mean ± SD (n = 3).

metastatic HC. The current study also used molecular docking analysis to predict the inhibitory mechanisms of these nanocomplexes on the activity of the biochemically investigated enzymes, including GSTP1, MMP9, PDH, SDH, and ALDH2.

2 Materials and methods

2.1 Materials

Copper salts, (3-(4,5-dimethylthiazol-2-yl)-2,5-diphenyltetrazolium bromide (MTT), ethidium bromide, acridine orange, phenobarbital (PB), p-dimethylaminobenzene (DAB), Tris-HCL, glutathione (GSH), and 5,5′-dithiobis2-nitrobenzoic acid (Ellman's reagent) were purchased from Sigma-Aldrich (Saint Louis, MO, USA). In addition, reagents of mitochondrial enzyme activity assays were from Sigma-Aldrich (Saint Louis, MO, USA). Chitosan and DD were obtained from Acros Organics (Morris Plains, NJ, USA). RPMI 1640 medium, HEPES buffer, phosphate buffer saline (PBS), and fetal bovine serum (FBS) were supplied from GIBCO (Grand Island, NY, USA). Primary antibodies to Ki-67 (Cat#PA1-21520) and Twist family bHLH transcription factor 1 (TWIST1, Cat #PA5-116628), tetramethylrhodamine ethyl ester (TMRE) dye, GeneJET RNA purification kit, one-step qPCR SYBR green kit, and primers were purchased from Thermo Fisher Scientific (Waltham, MA, USA). α-Fetoprotein (AFP) electrochemiluminescence kit (code# 10121) and liver function kits were obtained from Roche Diagnostics (USA) and Spectrum Diagnostics (Cairo, Egypt), respectively. Other chemicals were analytical grades (El-Nasr Pharmaceutical Chemicals Company, Cairo, Egypt).

2.2 Methods

2.2.1 Preparation and characterization of nanocomplexes of DD-Cu oxide NPs

As described in author recent studies, Cu_4O_3 NPs and Cu_2O NPs were green synthesized using copper chloride and copper nitrate as Cu precursors, respectively, in the presence of chitosan and vitamin C. Both copper oxide NPs were well characterized, as mentioned in author's recent studies, using a zetasizer, X-ray diffractometer (XRD), energy dispersive X-ray analysis (EDX), and electron microscopes. These NPs were mixed with DD (10:1), forming DC(I + II) NPs and DC(I) NPs, respectively. The size and zeta potential of two generated nanocomplexes were assessed and mentioned in the author's recent studies (Abu-Serie and Eltarahony, 2021; Abu-Serie and Abdelfattah, 2023). Additionally, the scanning electron microscope (SEM, JEOL "JSM-5300", Japan) was used to demonstrate the morphology of these nanoformulations. The elemental composition of DC(I + II) NPs and DC(I) NPs was identified through energy dispersive X-ray

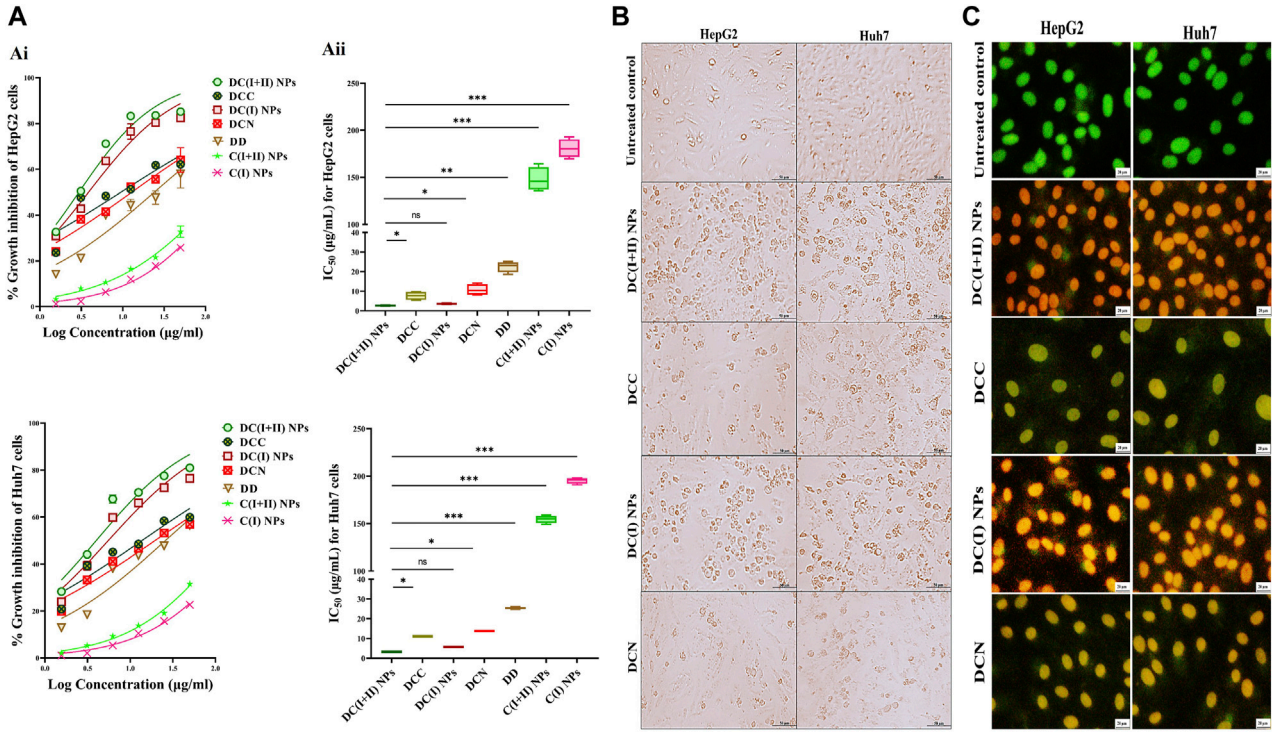

FIGURE 2
Cytotoxicity on human liver cancer (HepG2 and Huh7) cell lines and cellular morphology alterations using phase contrast and fluorescence microscopes. **(A)** Cytotoxicity on HepG2 and Huh7 using MTT assay as demonstrated by (Ai) dose-response curves and (Aii) IC_{50} values of nanocomplex of diethyldithiocarbamate (DD)-Cu_4O_3 "C(I + II)" NPs (DC(I + II) NPs), nanocomplex of DD-Cu_2O NPs "C(I)" NPs (DC(I) NPs), their corresponding typical complexes (DCC and DCN) of DD with precursors of copper oxide NPs (copper chloride and copper nitrate, respectively), DD, and Cu oxide NPs of C(I + II) NPs and C(I) NPs. Morphological changes of nanocomplexes-treated HepG2 and Huh7 cells, compared to DCC- and DCN-treated cells **(B)** using phase contrast microscope (magnification ×100) and **(C)** after staining with dual nuclear dyes (ethidium bromide and acridine orange), dead cells show yellowish green or yellow and orange or reddish orange nuclei at the early and late cell death, respectively, in comparison to viable green fluorescence nuclei, as demonstrated using fluorescence microscope (magnification ×200). Data are shown as mean ± SD (n = 3). DC(I + II) NPs were compared to other tested compounds, and values are considered statistically significant at $p < 0.05$*, <0.005**, and <0.0001***.

analysis (EDX, JEOL "JEM-1230", Japan) at a voltage of 200 KV. Concurrently, typical complexes of DD-Cu chloride (DCC) and DD-Cu nitrate (DCN) were prepared in the same ratio.

Importantly, the chemical stability of DC(I + II) NPs and DC(I) NPs was investigated by incubation in conditions (PBS-contained 50% FBS, pH 7.4, 37°C) resembling the biological system by measuring their size and polydispersity index (PDI, aggregation index) throughout 80 h, using a particle size analyzer (Malvern Panalytical, United Kingdom).

2.2.2 *In vitro* assessment of the anti-liver cancer efficacy of the prepared nanoformulations

2.2.2.1 MTT cytotoxicity assay and detection of morphological alteration using the fluorescence microscope

This assay determines the cellular growth inhibition potential based on the intact membrane and active mitochondria. The latter reduces tetrazolium dye (MTT) to insoluble formazan by its oxidoreductase enzymes. Briefly, WRL68 (normal human liver cell line, ATCC CL-48, passage no. "P#"17), HepG2 (human liver cancer cells, ATCC HB-8065, P#35) and Huh7 (PTA-4583, ATCC, P#29) were cultured in EMEM, DMEM, and RPMI 1640, respectively, containing 10% FBS. These cell lines were seeded as 6×10^3 cells/well in 96-well plates and allow to attach for 24 h. Then serial concentrations of nanocomplexes (DC(I + II) NPs and DC(I) NPs), traditional complexes (DCC and DCN), DD, and Cu oxide NPs, as well as their corresponding Cu salts, were added. After 72 h in 5% CO_2 incubator, MTT was added, incubated for 4 h, discarded, and DMSO was added (Mosmann, 1983). The cell viability was determined by measuring the absorbance of wells at 590 nm (spectrophotometer plate reader, BMG LabTech, Germany). The dose of 50% cell growth inhibition (IC_{50}) was estimated using GraphPad Prism version 9, and the morphological variations in the most active compounds-treated cells were recorded using a digital camera-supplemented phase contrast inverted microscope (Olympus, Japan).

More importantly, alteration in the nuclear morphology of the treated cells was recorded using a digital camera-supplemented fluorescence microscope (Olympus, Japan) after 15 min of incubation with dual fluorescence dye (acridine orange-ethidium bromide at a final concentration of 50 µg/mL) and washing with PBS.

2.2.2.2 Flow cytometry analysis of mitochondrial damage

The mitochondrial dysfunction was measured in terms of decreasing MP after staining with cationic dye (TMRE), which

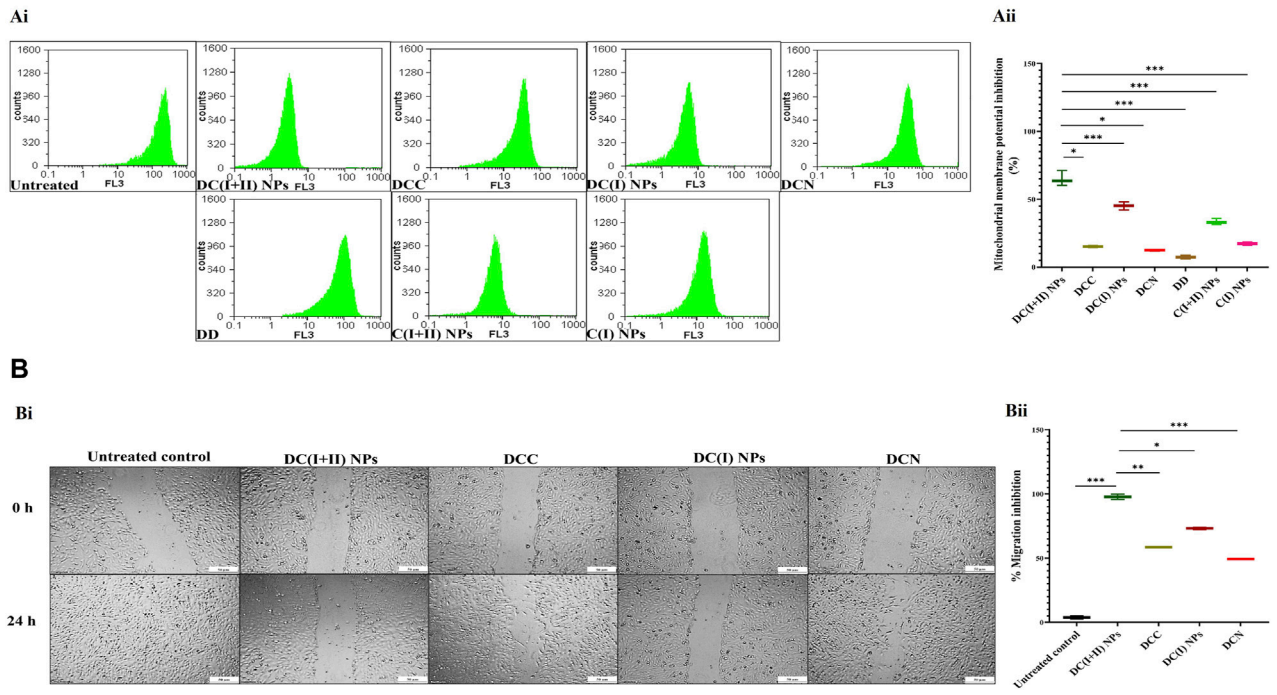

FIGURE 3
Mitochondrial damage and migration inhibition in the treated HepG2 cells. **(A)** Flow cytometry analysis of mitochondrial membrane potential (MP) damage in the treated HepG2 cells using tetramethylrhodamine (TMRE) staining, as illustrated by (Ai) flow charts and (Aii) the percentage of MP inhibition in terms of the relative percentages of low TMRE fluorescence intensity of the treated HepG2. **(B)** Anti-migration efficacy of nanocomplexes (nanocomplex of diethyldithiocarbamate (DD)-Cu_4O_3 nanoparticles (DC(I + II) NPs) and nanocomplex of DD-Cu_2O NPs (DC(I) NPs)) compared to traditional DD-copper complexes (DCC and DCN) of DD with precursors of copper oxide NPs (copper chloride and copper nitrate, respectively), as demonstrated by (Bi) microscopic images of HepG2 cell migration (at 0 and 24 h) and (Bii) the percentage of migration inhibition. Data are shown as mean ± SD (n = 3). DC(I + II) NPs were compared to other tested compounds, and values are considered statistically significant at $p < 0.05$*, <0.005**, and <0.0001***. C(I + II) NPs and C(I) NPs; Cu oxides (Cu_4O_3 and Cu_2O, respectively) NPs.

accumulates only in active mitochondria and emits red fluorescence that was quantified using flow cytometry (Crowley et al., 2016). After 72 h incubation with the lowest IC_{50} ~2.7 μg/mL, HepG2 cells were stained with 150 nM TMRE in 25 mM HEPES buffer (pH 7.4) containing 75 mM KCl, 80 mM NaCl, and 25 mM D-glucose. Following 10 min of incubation at 37°C, cells were washed and analyzed by flow cytometry (Partec, Germany) at the FL-3 channel (excitation at 549 nm and emission at 575 nm) with FloMax software for gating cells with low fluorescence relative to the untreated cells.

2.2.2.3 Wound healing (migration) assay

Briefly, 90%-confluent HepG2 cells were scratched and incubated with safe doses (0.1 μg/mL) of nanocomplexes or corresponding typical complexes. The scratched area was pictured at 0 h and 24 h, then measured using ImageJ software to estimate the percentage of migration inhibition.

2.2.3 *In vivo* assessment of anti-metastatic liver cancer potential

2.2.3.1 Experimental design

Swiss albino male mice (n = 75, 20–25 g) were divided into two main groups: the normal healthy group (N, n = 36 mice) and the hepatocellular carcinoma group (HC, n = 39 mice). The animals in the latter group were fed 165 mg DAB/kg body weight (b.wt) and given orally 0.05% PB (1.2 mg/kg b. wt) daily for 6 weeks to induce HC (Pathak and Khuda-Bukhsh, 2007). The metastatic HC was confirmed by hematoxylin and eosin staining of the liver and lung tissues of three mice (Figure 4E). Then the two groups (N and HC) were randomly subdivided into three sub-groups (12 mice each), including untreated, DC(I + II) NPs, and DC(I) NPs. The latter two groups of each main group (i.e., N-DC(I + II) NPs, N-DC(I) NPs, HC-DC(I + II) NPs, and HC-DC(I) NPs) were intraperitoneally injected, three times/week, with 2 mg nanocomplex/kg b. wt for 3 weeks. The doses, route and frequencies of nanocomplexes administration were selected based on a previous study (Abu-Serie, 2023). Throughout the 3 weeks of period treatment, the mice's body weights were measured every 3 days. On the 8th week, six mice from each group were decapitated by anaesthetization with isoflurane (2%–3%, inhalation), then liver and lung tissues were collected for assessment of the redox parameters (ROS, GSH, lipid peroxidation, and ALDH2). At the termination of the experiment (after 9 weeks), all mice were sacrificed, and then blood and tissues (liver, lung, and spleen) were collected. Blood samples were harvested in EDTA tubes for hematological and AFP assays. Liver, lung, and spleen were weighted relative to the recorded b. wt. Minor portions of tissues were 10% formalin-

fixed for histological and immunohistochemical examinations, whereas the remaining portions were stored at −80°C for biochemical and molecular studies.

2.2.3.2 Quantification of AFP level and GST activity, and histological, immunohistochemical, and molecular assessments of tumor tissues

The blood level of AFP (primary liver tumor marker) was determined according to the instructions of AFP chemiluminescent immunoassay kit.

For determination of GST activity, liver nodules of the untreated HC group and liver tissues of other groups were homogenized in PBS and centrifuged (10,000 xg for 30 min) at 4°C. The resulting supernatants were added to 0.1 M PBS (pH 6.5), 1 mM 1-chloro-2,4-dinitrobenzene, and 1 mM GSH. The absorbance of the formed conjugate of CDNB-GSH was measured every minute for 5 min at 340 nm (Habig et al., 1974). The activity was calculated in relation to protein content that was assessed by the Bradford method (Bradford, 1976).

Regarding histological (H&E staining of liver, lung, and spleen) and immunohistochemical (Ki-67 immunostaining of liver and lung tumor tissues as well as TWIST1 immunostaining of liver) investigations, tissue slides were prepared using typical protocols. The obtained immunostaining images were analyzed using CellSens and ImageJ software.

Total RNA was extracted from the tumor tissues (liver and lung) of the untreated and treated HC groups based on the kit's usual protocol. After RNA quantification, one-step SYBR green master mix qPCR kit with specific primers (Supplementary Table S1) was used to determine the alteration in gene expressions in the untreated HC group (positive control) and treated HC groups relative to the untreated N group (negative control). These genes included ABCG2, prominin 1 (CD133), NOTCH1, WNT1, SOX2, OCT-4, NANOG, GSTP1, telomerase reverse transcriptase (TERT), MMP9, vascular endothelial growth factor (VEGF)A, and cyclin D genes by the equation of $2^{-\Delta\Delta Ct}$.

2.2.3.3 Biodistribution and histological investigation of nanocomplexes' safety

In a separate experiment, fifteen HC-bearing mice (~20 g) were divided into three groups (untreated, HC-DC(I + II) NPs, and HC-DC(I) NPs). The two latter groups received intraperitoneal injections of the corresponding nanocomplex, as described above. Mice were then sacrificed, and tissues (liver, lung, spleen, brain, heart, and kidney) were collected for quantification of Cu, which correlates with the accumulated tissue uptake of nanocomplexes using graphite atomic absorption spectroscopy (Analytik Jena AG, Germany).

Moreover, the nanocomplexes' safety was investigated by H&E staining of various tissues (liver, lung, spleen, brain, and kidney) in the treated N groups *versus* the healthy N group.

2.2.3.4 Evaluation of the selective inactivation impact of nanocomplexes on mitochondrial metabolic enzymes

To investigate the efficacy of nanocomplexes in inducing selective cuproptosis, PDH and SDH inhibition percentages were assessed in liver and lung tissues in all HC subgroups compared to their corresponding N groups. A mitochondrial pellet was prepared by homogenizing tissue in a solution of 10 mM Tris-HCl (pH 7.2), 250 mM sucrose, and 1 mM EDTA. The homogenate was centrifuged (600 xg, 10 min), and the obtained supernatant was further centrifuged at 10,000 xg for 10 min (Munujos et al., 1993; Schwab et al., 2005). After freezing (>15 min) and thawing the resulting pellet, it was suspended in 20 mM Tris-HCl (pH 7.5), 1 mM $CaCl_2$, 50 mM KCl, 5 mM $MgCl_2$, 1 mL/L Triton X-100, and 250 mM sucrose for PDH activity determination (Schwab et al., 2005). Meanwhile, for the SDH activity assay, this pellet was suspended in 10 mM HEPES, 5 mM potassium phosphate buffer (PPB, pH 7.2), 220 mM sucrose, and 20 mM KCl (Munujos et al., 1993). The activity of PDH was measured in the presence of 0.6 mM INT, phenazine methosulfate in PPB (pH 7.5), and 5 mM pyruvate using the Schwab et al. method [31]. While the SDH activity was assayed following the method of Munujos et al., using 2 mM INT, 20 mM succinate, and 1.2% Cremophor EL (pH 7.4). The percent inhibition of both enzymes was detected by measuring the decrease in color development of the produced formazan at 500 nm compared to the untreated group (Munujos et al., 1993). The protein content was determined according to the Bradford method (Bradford, 1976).

2.2.3.5 Biochemical assessment of redox parameters

To detect the prooxidant selectivity of the tested nanocomplexes, levels of ROS (Socci et al., 1999), GSH (Sedlak and Lindsay, 1968), and lipid peroxidation (Ohkawa et al., 1979), as well as ALDH2 activity (Josan et al., 2013) were determined in the liver and lung tumor tissues of untreated and treated HC-bearing mice compared to N groups. All these indicators were calculated using the corresponding standard curves and in relative to tissue protein content that was quantified using the Bradford method (Bradford, 1976).

2.2.3.6 Investigation of liver function and hematological parameters

The main liver function parameters (alanine aminotransferase (ALT), aspartate aminotransferase (AST), and albumin) were detected in liver homogenate (1 g of liver homogenized in 150 mM Tris-KCl buffer, pH 7.4) (Gaskill et al., 2005). These parameters were measured using commercial colorimetric kits. Additionally, a complete blood count (CBC) was assessed in all groups using the hematology analyzer (Mindray, China).

2.2.4 *In silico* studies

The current study performed a set of computational analyses to predict the complex structures of DD with Cu_2O [DC(I)] or Cu_4O_3 [DC(I + II)] and the inhibitory effects of these complexes on certain enzymes, including GSTP1, PDH (DLAT), SDH, ALDH, and MMP9.

2.2.4.1 2D and 3D structures of the studied compounds and proteins

ChemDraw v.16.0 was used to draw the 2D structures (.mol) of DC(I + II) and DC(I) complexes. The structures were then converted to 3D format (.pdb) using the ChemAxon Chemical Sketch Tool (https://www.rcsb.org/chemical-sketch). The 3D structures of GSTP1 (PDB: 3GUS), DLAT (PDB: 1FYC), SDH (PDB: 1NEN),

ALDH2 (PDB: 4FR8), and MMP9 (PDB: 1L6J) were retrieved from the Protein Data Bank (PDB, https://www.rcsb.org/).

2.2.4.2 Docking analysis

The Discovery Studio 2020 Client program (v20.1.0.19295) was used to pre-process the protein structure before further analysis by removing water and ligands. Then the 3D structure of the DC(I + II) or DC(I) complex was docked with GSTP1, DLAT, SDH, ALDH, and MMP9 using the HDOCK server (http://hdock.phys.hust.edu.cn/) (Yan et al., 2017). The highest-scoring docked complexes were used, and their interfaces were visualized and analyzed by the Discovery Studio program.

To study the effect of DC(I + II) and DC(I) on DLAT aggregation, the 3D structure of DLAT or the docked complex of DLAT-Cu complex structures were docked sequentially with another two DLAT structures. The binding affinity between DLAT molecules in the resulting docked complexes was determined and compared. While the iron displacement capability of the studied Cu complexes was evaluated by docking each of these complexes with SDH 3D structure without Fe-S centers. The resulting Cu complex-SDH docked complexes were then docked with Fe-S to examine the binding affinity between SDH and Fe-S in the presence and absence of the Cu complexes. Furthermore, the binding affinity between ALDH or MMP9 and DC(I + II) or DC(I) was evaluated and compared for each enzyme.

2.2.4.3 Binding affinity analysis in the docked complexes

The gained solvation-free energy (change in Gibbs free energy, ΔG) during the interface fomation in the obtained docked complexes was determined using the PDBePISA (Proteins, Interfaces, Structures, and Assemblies) platform (https://www.ebi.ac.uk/msd-srv/prot_int/cgi-bin/piserver) (Krissinel and Henrick, 2007). This server is a key protein interaction analysis tool in proteomics databases and servers. It is commonly utilized to investigate macromolecular interfaces in protein-protein and protein-ligand docked complexes to obtain important information about protein interactions from complex structures. The obtained ΔG value is implemented in the prediction of the binding affinity of protein-protein or protein-ligand docked complexes.

2.2.4.4 Prediction of the competitive inhibitory impacts of DC(I + II) and DC(I) on the studied enzymes

The competitive inhibitory effect of the studied complexes on the target enzymes was analyzed by comparing the amino acid residues in the active site of these enzymes with those in the interfaces of the docked complexes using the Discovery Studio software. The PDBsum web-based database (http://www.ebi.ac.uk/pdbsum) was used to identify the active site residues of the enzymes investigated using their PDB ID (Laskowski et al., 2018).

2.2.5 Statistical analysis

Data is presented as mean ± standard deviation (SD) and replicates derived from at least three independent experiments ($n \geq 3$). Data was analyzed with GraphPad Prism version 9.3.1. via one-way analysis of variance (ANOVA), multiple comparisons (Dunnett test), and unpaired *t*-test. Statistical significance was deemed at $p < 0.05$*, <0.005**, and <0.0001***.

3 Results

3.1 Characterization of the nanocomplexes

Herein, DD was nanoformulated by chelating with Cu_4O_3 NPs or Cu_2O NPs, forming semi-spherical-shaped nanocomplexes of DC(I + II) or DC(I), respectively (Figure 1A). As demonstrated in author's recent studies (Abu-Serie and Eltarahony, 2021; Abu-Serie and Abdelfattah, 2023), these nanocomplexes have mean sizes of 156.5 nm and 148.1 nm, respectively, and their mean zeta potentials were - 4.65 mv and - 20.2 mv, respectively, with mean PDI values of 0.274 and 0.337, respectively. It is worth mentioning that the ChemDraw 2D structures of the studied nanocomplexes (Figure 1B) align with the previously established coordination complexes of DD-Cu (I + II) and DD-Cu (I) (Han et al., 2013). Figure 1D declares the elemental composition including C (19.36% and 17.99%), N (9.00% and 7.71%), O (12.36% and 13.93%), S (22.75% and 15.05%), and Cu (36.52% and 21.39%) for DC(I + II) and DC(I), respectively. Moreover, as illustrated in Figure 1D, there was no discernible shift in the ranges of the nanosizes and PDI values (<0.44) of both nanocomplexes during 80 h incubation in PBS/50%FBS, indicating their stability and acceptable particle distribution without aggregation (homogeneity) in serum condition.

3.2 *In vitro* anti-liver cancer efficacy of the prepared nanocomplexes

The estimated IC_{50} for normal liver cells demonstrated that nanocomplexes (DC(I + II) NPs and DC(I) NPs) and Cu oxide NPs (C(I + II) NPs and C(I) NPs) had higher values (97.8, 94.5, 99.6, and 97.3 μg/mL, respectively) than traditional complexes (DCC and DCN) and DD (31.1, 29.2, and 14.7 μg/mL, respectively). In a dose-dependent manner (Figure 2Ai), both nanocomplexes exhibited the lowest IC_{50} values (<5 μg/mL) compared to their corresponding typical complexes (<14 μg/mL), DD (≤25 μg/mL), and Cu oxide NPs (>147 μg/mL) for inhibiting HepG2 and Huh7 growth (Figure 2Aii). In terms of IC_{50} values, DC(I + II) NPs (2.71 and 3.26 μg/mL) showed comparable values to DC(I) NPs (4.73 and 3.56 μg/mL) against HepG2 and Huh7 cells, respectively. Additionally, the most severe collapse in morphology of both liver cancer cell lines was observed in DC(I + II) NPs-treated cells, followed by DC(I) NPs-treated cells, compared to other treated cells (Figure 2B). Furthermore, dual nuclear fluorescence dyes were used to discriminate the grades of cell death in the treated HC cell lines. It is based on the acridine orange staining cells with green fluorescence, while ethidium bromide is only taken up by the damaged cells; as damage increases more ethidium bromide is entered, making their nuclei appear yellow to red according to damage degree. This fluorescence staining of these treated cells supported the highest lethal effect of DC(I + II) NPs,

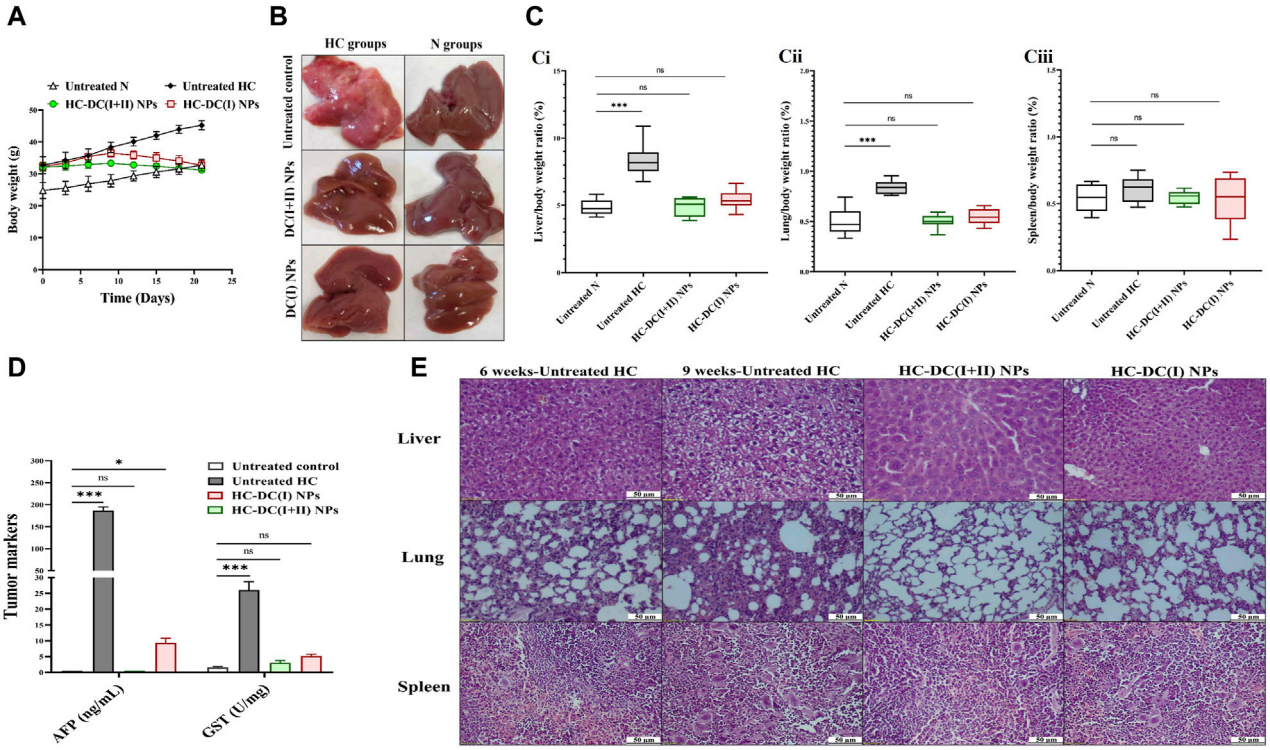

FIGURE 4
In vivo impact of nanocomplexes on the liver tumor in terms of weight, histological analysis, and tumor markers (α-fetoprotein (AFP) level and glutathione-S-transferase (GST) activity). **(A)** The measured body weight of mice during 3 weeks of treatment. **(B)** Liver morphology images of the untreated and treated hepatocellular carcinoma (HC) and normal (N) groups. **(C)** The relative weight of (Ci) liver, (Cii) lung, and **(B)** (Ciii) spleen to body weight of N, untreated HC, and nanocomplexes-treated HC [HC-diethyldithiocarbamate-Cu_4O_3 nanoparticles (DC(I + II) NPs) and HC-diethyldithiocarbamate-Cu_2O nanoparticles (HC-DC(I) NPs)] groups. **(D)** Blood AFP level (ng/mL) and hepatic activity of GST (U/mg protein) in the untreated N, HC, and nanocomplexes-treated HC groups. **(E)** H&E-stained liver, lung, and spleen tissues of the untreated HC group at the sixth week of HC induction (showing neoplastic hepatocytes and a small area of lung cancer cells without alteration in the spleen) and at the ninth week of HC induction (demonstrating marked anaplasia in clear cell HC, a larger area of lung cancer, and nodular hyperplasia in spleen), and two nanocomplexes-treated HC groups after 6 weeks of induction and 3 weeks of treatment (showing a higher therapeutic impact of DC(I + II) NPs than DC(I) NPs for eradicating liver tumor cells and inhibiting metastasis to lung and spleen as well as normal spleen in both treated groups). Data are shown as mean ± SD ($n \geq 6$). All the studied groups were compared to the untreated N group, and values are considered statistically significant at $p <$ 0.05*, <0.005**, and <0.0001***.

as demonstrated by organ fluorescence nuclei in comparison with the yellowish orange nuclei of DC(I + II) NPs, the yellow or yellowish green nuclei of traditional complexes, and the green nuclei of the untreated control (Figure 2C). Because there was no statistically significant difference between HepG2 and Huh7 in the cytotoxicity efficacy of the tested nanocomplexes, the following parameters were only investigated *in vitro* using 1 cell line.

Regarding cuproptosis-mediated mitochondrial damage, nanocomplexes-treated HepG2 cells revealed the lowest MP (65.05% ± 3.26% and 45.24% ± 1.78%, respectively), followed by C(I + II) NPs (33.37% ± 1.33%), relative to other treated cells (Figures 3Ai, Aii). These results are evidenced by the lowest fluorescence intensity of TMRE with DC(I + II) NPs-treated HepG2 cells compared to those treated with DC(I) NPs (Figure 3Ai). Moreover, DC(I + II) NPs demonstrated the highest anti-migration potency on HepG2 cells (97.67% ± 2.03%), followed by DC(I) NPs (73.15% ± 0.89%), compared to the lowest percentages for their typical complexes (58.49% ± 0.28% and 49.21% ± 0.53%, respectively), as illustrated in Figures 3Bi, Bii.

3.3 Superior therapeutic potency of DC(I + II) NPs against metastatic HC (*in vivo* study) in terms of

3.3.1 Morphology, weight, tumor markers, histology, immunostaining, and key gene expression of tumor tissues, as well as the proposed GSTP1 and MMP9 inhibition

Following induction of HC by DMAB and PB, oval nodules (the mean number~21/liver organ) appeared only in the collected pale-colored livers of the untreated HC group. This group showed a 1.6-fold increase in body weight, ~ 2-fold increase in weight of the liver and lung, no increment in spleen weight, as well as > 185-fold and >15-fold elevation in AFP level and GST activity, respectively, relative to the healthy N group (Figures 4A–D). Before starting treatment (at the sixth week), the induction of metastatic HC was investigated by H&E staining of liver, lung, and spleen tissues showing hepatic neoplastic changes (increased nuclear to cytoplasmic ratio and multinucleated giant cells), lung cancer cells, and no alterations in spleen (Figure 4E). At the end of the experiment (9 weeks), H&E staining of these tissues from the untreated HC-bearing animals demonstrated clear cell HC with marked

anaplasia (irregular-shaped hyperchromatic nuclei and clear cytoplasm), an increasing area of lung cancer cells, and nodular lymphoid hyperplasia in the spleen (Figure 4E). Moreover, the results showed an elevation in the percentages of the Ki-67^{+}-immunostaining and the metastatic marker (TWIST1^{+}-immunostaining) in both liver and lung tissues (Figure 5Ai, Aii), indicating HC lung metastasis (Figure 5A).

The findings of the current study showed no differences in body weight, liver morphology or liver, lung, and spleen weights between the nanocomplexes-treated HC group and the untreated N group (Figures 4A–C). Both nanocomplexes (in the treated HC groups) also suppressed the AFP level (<10 ng/mL compared to >150 ng/mL in the HC untreated group); importantly, DC(I + II) NPs can normalize this tumor marker. Moreover, two nanocomplexes normalized the elevation in hepatic GST activity from 26.1 U/mg to <6 U/mg (Figure 4D). Histological and immunohistochemical investigations illustrated that DC(I + II) NPs had superior therapeutic efficacy against HC by showing normal hepatocytes with complete inhibiting metastasis to lung and normal splenic nodules, compared to DC(I) NPs (Figures 4E, 5A). As shown in Figures 5Ai, Aii, the treatment with this nanocomplex repressed the elevation of Ki-67 in the liver and lung as well as the metastatic marker (TWIST1) in the liver by 17.58, 2.810, and 16.56 folds, respectively, relative to DC(I) NPs. The latter showed significantly higher positive immunostaining percentages of Ki-67 and TWIST1 than DC(I + II) NPs (Figure 5A).

The inhibitory mechanism of the studied Cu complexes (DC(I + II) and DC(I)) on the activity of GSTP1 was studied using molecular docking analysis (Figures 5Bi,Bii). The retrieved 3D structure of GSTP1 is two chains: chain A and chain B, with 209 amino acid residues. The results showed that the two Cu complexes could bind to the enzyme with a superior binding affinity (Table 1) of DC(I + II), which bound firmly to the enzyme at different positions. The DC(I + II) interacted with 13 amino acid residues (9 of them are active site residues) of GSTP1 chain A. Whereas DC(I) is bound to 14 amino acid residues of chain A and one residue of chain B (11 of them are active site residues) of GSTP1 (Figures 5Bi, ii, respectively).

MMP9 (gelatinase B) was also examined using *in silico* analysis, as shown in Figures 5Biii, Biv. The PDB 3D structure of MMP9 contains one chain with 425 amino acids. Both DC(I + II) and DC(I) complexes could bind to MMP9 with 13 and 11 amino acid residues, respectively (Figures 5Biii,Biv),

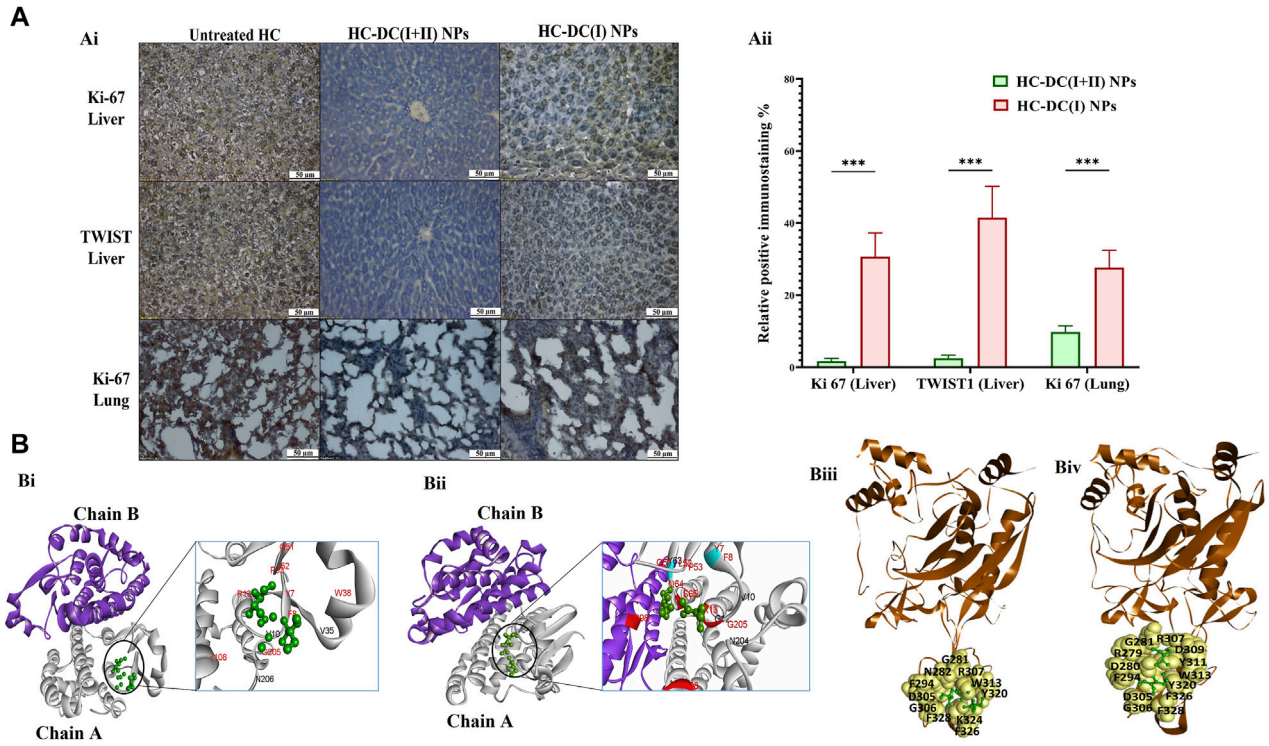

FIGURE 5
Immunohistological investigations for tumor markers in nanocomplexes-treated hepatocellular carcinoma mouse groups as well as computational inhibitory effect on GSTP1 and matrix metalloproteinase (MMP)9. **(A)** Ki-67 and TWIST1 immunostaining tumor tissues of the liver and lung in the untreated hepatocellular carcinoma (HC) group and nanocomplexes-treated HC [HC-diethyldithiocarbamate-Cu_4O_3 nanoparticles (DC(I + II) NPs) and HC-diethyldithiocarbamate-Cu_2O nanoparticles (HC-DC(I) NPs)] groups, as demonstrated by (Ai) microscopic images and (Aii) the percentages of positive immunostained cells. Data are shown as mean ± SD (n ≥ 6). HC-DC(I + II) NPs group was compared to HC-DC(I) NPs groups, and values are considered statistically significant at $p < 0.05$*, <0.005**, and <0.0001***. **(B)** The computational results, as presented by (Bi, Bii) the docked complexes of GSTP1 (PDB ID: 3GUS, white "chain A" and purple "chain B") with DC(I + II) or DC(I) (green-colored ball and stick style), respectively. The interface residues (black and red) in the docked complexes of GSTP1 with DC(I) and DC(I + II) are magnified and show the binding of the Cu complexes to the active site residues of GSTP1 (red), and (Biii, Biv) the docked complexes of MMP9 (PDB ID: 1L6J, brown-colored cartoon) with DC(I + II) or DC(I) (green-colored ball and stick style), respectively. The interface residues are represented by yellow-colored space-filling spheres labeled with black-colored amino acids. These docked complexes were given by the HDOCK server (http://hdock.phys.hust.edu.cn/) and visualized by Discovery Studio 2020 Client software.

and slightly higher affinity (Δ^iG) to DC(I + II) (Table 1). However, neither DC(I + II) nor DC(I) could bind to the active site residues of the enzyme.

Importantly, DC(I + II) NPs surpassed DC(I) NPs in downregulating key oncogene expression. DC(I + II) NPs repressed stemness genes (NOTCH1, WNT1, chemoresistance gene, prominin1, SOX2, OCT-4, and NANOG), GSTP1, telomerase, MMP9-stimulated metastasis, VEGFA, and cyclin D-mediated cell cycle by two to six folds, 5 folds, 2 folds, two to three folds, two to three folds, and two to four folds, respectively, in both tumor tissues (Figures 6A–C).

3.3.2 Selective accumulation in tumor tissues, safety in normal tissues, and selective inhibition of mitochondrial lipoylated and Fe-S cluster enzymes with *in silico* analysis

The nanocomplex biodistribution results illustrated that the investigated NPs were mostly accumulated in tumor tissues of the liver (>68%), followed by the lung (>14%), and then the spleen (≥2%), while other normal (non-tumor) tissues contained less than 0.09% (Figure 7A). Tumor uptake of DC(I + II) NPs was significantly higher in liver (82.20% ± 0.30%) and lung (14.17% ± 0.67%) tissues than that of DC(I) NPs (68.17% ± 0.88% and 7.32% ± 0.183%, respectively). This high tumor selectivity of nanocomplexes with their lowest uptake by normal tissues indicates the safety of these nanoformulations in normal tissues. These results were supported by the histological findings of the liver, lung, spleen, brain, and kidney tissues of normal mice treated with these nanocomplexes and revealed no alterations compared to the healthy N group (Figure 7B). Nanocomplexes of DC(I + II) and DC(I) selectively suppressed PDH (lipoylated enzyme) and SDH (Fe-S cluster protein) activities by > 41% and >27%, respectively, in both tumor tissues of the liver and lung, without affecting their activities in the corresponding tissues of the treated N groups (Figure 7C). The DC(I + II) nanocomplex inhibited hepatic PDH and hepatic SDH more effectively (38.10 ± 1.58 and 5.24 ± 0.07 U/mg protein, respectively) than the DC(I) nanocomplex (74.56 ± 2.18 and 7.07 ± 0.03 U/mg protein, respectively), compared to the untreated HC (126.89 ± 1.46 and 11.27 ± 0.45 U/mg protein, respectively). Also, in lung tissues, DC(I + II) NPs-treated HC animals had lower activities of these enzymes (40.20 ± 0.955 and 5.18 ± 0.05 U/mg protein, respectively) than the DC(I) NPs-treated HC mice (62.25 ± 1.46 and 6.46 ± 0.05 U/mg protein, respectively), relative to the untreated HC (86.26 ± 1.28 and 8.93 ± 0.25 U/mg protein, respectively).

The impact of both DC(I + II) and DC(I) on DLAT aggregation was evaluated using molecular docking analysis. DLAT is a single-chain 3D structure with 106 amino acid residues; it could bind to DC(I + II) with more affinity than DC(I) (Table 1). Binding of DLAT with these Cu complexes effectively increased the binding affinity between DLAT molecules (enhancing aggregation) with higher efficiency to DC(I + II) (Table 1). Analysis of the obtained docked complexes revealed that DC(I) could bind to 10 amino acid residues of $DLAT_1$ and 17 amino acids of $DLAT_2$, while DC(I + II) bound to $DLAT_1$ with 7 amino acid residues and $DLAT_2$ with 15 amino acid residues (Figure 7D).

The *in silico* analysis was also utilized to evaluate the probable iron displacement influence of DC(I + II) and DC(I) on SDH. The PDB-retrieved 3D structure of SDH has four subunits: A (succinate dehydrogenase flavoprotein, 588 amino acids), B (succinate dehydrogenase iron-sulfur protein, 238 amino acids), C (succinate dehydrogenase cytochrome b-556, 129 amino acids), and D (succinate dehydrogenase hydrophobic membrane anchor protein, 115 amino acids). The structure contains two dimeric (Fe_2S_2) and one tetrameric (Fe_4S_4) iron-sulfur centers that bind to chain B. The results showed that both the tested Cu complexes could bind to SDH with superior affinity to DC(I + II) (Table 1). DC(I) is bound to about 50 amino acid residues (of which 28 Fe-S binding residues) of the enzyme at chains B, C, and D. While DC(I + II) is bound to nearly 27 amino acid residues of the enzyme at chain A only. The binding affinity of the Fe-S to the enzyme was decreased from–57 kcal/mol to–56.8 kcal/mol and–54.1 kcal/mol after binding of DC(I + II) and DC(I), respectively, to the enzyme (Table 1). After comparing the interface residues of the obtained docked complexes with the enzyme active site residues, the outcomes revealed the binding of DC(I) and DC(I + II) complexes to 30 and 25 residues, respectively (Figure 7E).

TABLE 1 The predicted binding affinity (solvation-free energy gain upon interface formation, Δ^iG) between the studied enzymes and DC(I+II) or DC(I) in the obtained docked complexes.

Docked complex	Δ^iG kcal/mol	Binding affinity between
MMP9_ DC(I+II)	−0.4	MMP9, DC(I+II)
MMP9_ DC(I)	−0.3	MMP9, DC(I)
DLAT_ DC(I+II)	−0.8	DLAT1, DC(I+II)
DLAT_ DC(I)	−0.2	DLAT1, DC(I)
DLAT1_DLAT2	−3.7	DLAT1, DLAT2
DLAT1_ DC(I+II)_DLAT2	−5.2	DLAT1, DLAT2
DLAT1_ DC(I)_DLAT2	−5.0	DLAT1_DLAT2
DLAT1_DLAT2_DLAT3	−0.1	DLAT2, DLAT3
DLAT1_ DC(I+II)_DLAT2_DLAT3	−3.7	DLAT2, DLAT3
DLAT1_ DC(I)_DLAT2_DLAT3	−2.5	DLAT2, DLAT3
SDH_DC(I+II)	−0.8	SDH, DC(I+II)
SDH_DC(I)	−0.6	SDH, DC(I)
SDH_(Fe-S)	−57	SDH, (Fe-S)
SDH_DC(I+II)_(Fe-S)	−56.8	SDH, (Fe-S)
SDH_ DC(I)_(Fe-S)	−54.1	SDH, (Fe-S)
ALDH2_DC(I+II)	−0.2	ALDH2, DC(I+II)
ALDH2_DC(I)	−0.0	ALDH2, DC(I)

The Δ^iG was generated by the PDBePISA server, which is available at https://www.ebi.ac.uk/pdbe/pisa/; ALDH2 aldehyde dehydrogenase 2, DLAT dihydrolipoamide S-acetyltransferase, DC(I+II) diethyldithiocarbamate-Cu4O3 complex; DC(I) diethyldithiocarbamate-Cu2O complex, MMP9 matrix metalloproteinase 9, MTA1 metastasis-associated protein1, SDH succinate dehydrogenase. The Cu complex with the highest binding affinity to the tested enzymes are highlighted in light green.

3.3.3 Selective prooxidant potential in tumor tissues and docking results

Both nanocomplexes demonstrated selective elevation of ROS (≥5 folds) and lipid peroxidation (≥2.5 folds) with

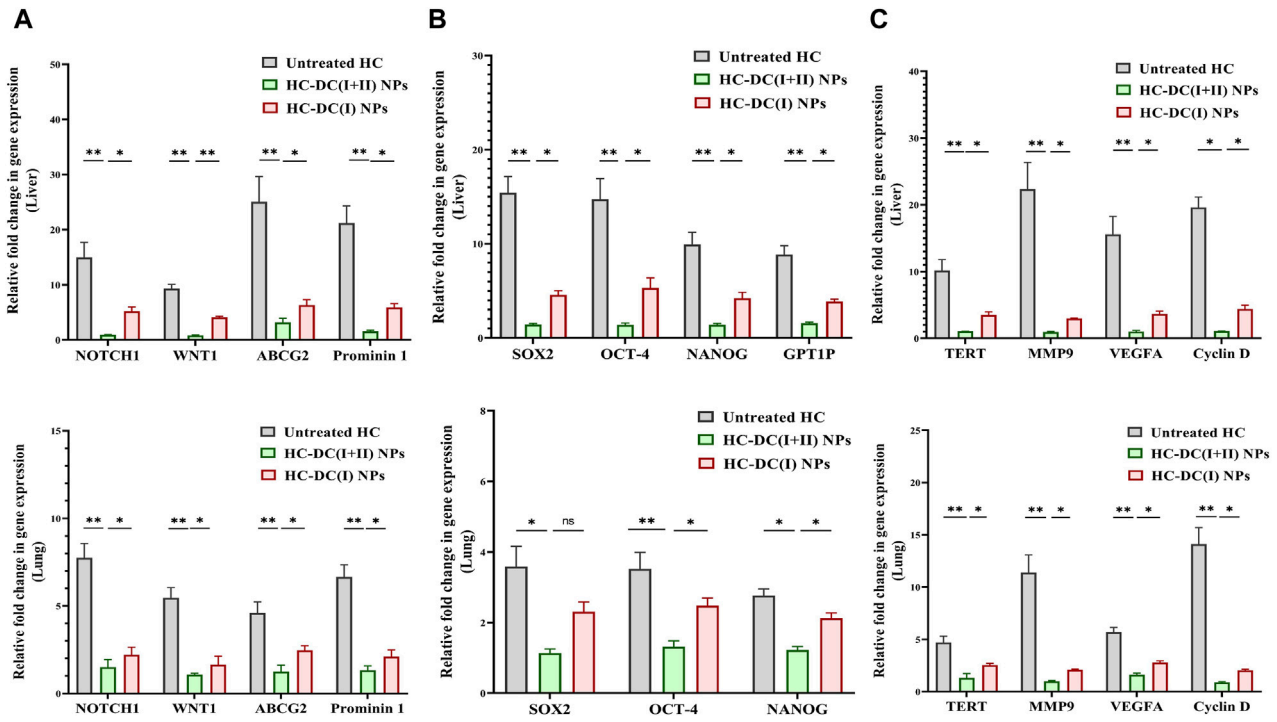

FIGURE 6
The inhibitory impact of nanocomplexes on fundamental stemness genes and oncogenes. Relative fold changes in gene expression of **(A)** NOTCH1, WNT1, ATP binding cassette subfamily G member 2 (ABCG2), and prominin 1 (CD133), **(B)** SOX2, OCT-4, NANOG, and glutathione-S-transferase (GST)P1, and **(C)** telomerase reverse transcriptase (TERT), matrix metalloproteinase (MMP)9, vascular endothelial growth factor (VEGF)A, and cyclin D in tumor tissues of the liver and lung in all the studied groups. The nanocomplex of diethyldithiocarbamate- Cu_4O_3 nanoparticles-treated hepatocellular carcinoma animal group (HC-DC(I + II) NPs) was compared to the untreated HC group and the nanocomplex of diethyldithiocarbamate-Cu_2O nanoparticles-treated HC animal group (HC-DC(I) NPs). Data are shown as mean ± SD (n ≥ 6). Values are considered statistically significant at $p <$ 0.05*, <0.005**, and <0.0001***.

lowering GSH level (>1.3 fold) and inhibiting ALDH2 activity (>36%) in tumor tissues (liver and lung). These parameters showed no alterations in the respective normal tissues of mice in the nanocomplex-treated N groups (Figures 8A–D). The DC(I + II) NPs were more effective than DC(I) NPs in increasing ROS (9.1 and 4.7 folds) and lipid peroxidation (3.5 and 2.5 folds), as well as depleting GSH (9.3 and 2.51 folds) and ALDH2 activity (81.82% and 56.07%) in tumor tissues of the liver and lung, respectively.

The proposed inhibitory mechanisms of DC(I + II) and DC(I) on the activity of ALDH2 were determined by docking analysis. ALDH2 has eight chains (Figure 8Ei) with 500 amino acid residues in its 3D structure. The results revealed that both the investigated Cu complexes could bind to the enzyme at different chains and amino acids. Hence, DC(I) is bound to the enzyme with 21 amino acids at chains E, F, G, and H (Figure 8Eii), whereas DC(I + II) is attached to chains A, B, C, and D with 20 amino acids (Figure 8Eiii). The DC(I + II) complex interacted with the enzyme with a higher binding affinity (Table 1) than DC(I), but neither complex could bind to the enzyme active site residues.

3.3.4 Normalization of liver function and hematological parameters

In comparison to the healthy N group, the liver tissue of animals in the untreated HC group showed a significant depletion in ALT and AST activities (2 and 1.28 folds, respectively) and albumin (1.31 folds). All of the aforementioned hepatic functional indices were normalized after the treatment with the investigated nanocomplexes (DC(I + II) NPs- and D(I) NPs-treated HC groups, Table 2. Furthermore, DC(I + II) NPs and D(I) NPs can ameliorate the HC-induced suppression in lymphocyte (lymph)% and elevation in monocyte (Mid)% and neutrophil (Gran)%. Moreover, no hematological variations were observed between nanocomplexes-treated N groups and healthy N group in all assessed parameters of RBCs, WBCs, and platelets (Table 2).

4 Discussion

Because of mitochondrial importance as an energy provider (through TCA and the respiratory chain) for maintaining cancer stemness, cuproptosis (a novel regulated cell death manner dependent on mitochondrial stress) is deemed an effective therapeutic approach for halting CSC metastasis and self-renewal (Yadav et al., 2020). Cuproptosis thus exclusively targets apoptotic-resistant CSCs while having little effect on non-CSCs that rely mainly on anaerobic glycolysis to sustain their rapid proliferation (Loureiro et al., 2017; Yadav et al., 2020). Therefore, the Cu ionophore must have a suppressive effect on non-CSCs, such as pro-oxidant activity, to aggravate the cuproptotic effect. Two recent

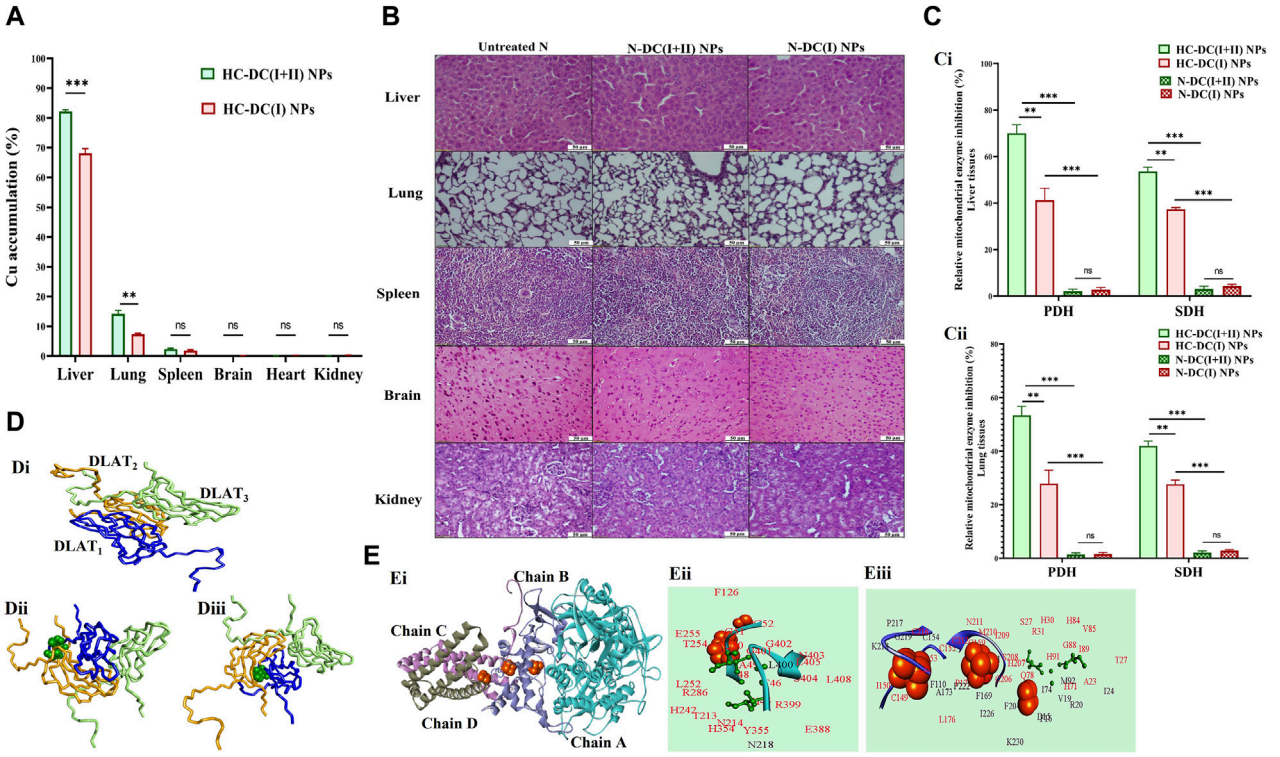

FIGURE 7
Selective accumulation in tumor tissues with a histological indication of safety in normal tissues and the cuproptosis-mediated inhibition of mitochondrial enzymes by the studied nanocomplexes with molecular docking analysis. **(A)** Atomic absorption spectroscopy results of nanocomplexes' distribution in the liver, lung, spleen, brain, heart, and kidney after nanocomplexes' injections into hepatocellular carcinoma (HC)-bearing mice. The nanocomplex of diethyldithiocarbamate-Cu_4O_3 nanoparticles-treated HC animal group (HC-DC(I + II) NPs) was compared to the nanocomplex of diethyldithiocarbamate-Cu_2O nanoparticles-treated HC animal group (HC-DC(I) NPs). Data are shown as mean ± SD (n ≥ 6) and values were considered statistically significant at $p < 0.05$*, <0.005**, and <0.0001***. **(B)** H&E staining tissues of the untreated normal healthy mice (N) and treated N groups. **(C)** The relative inhibition percentage of pyruvate dehydrogenase (PDH) and succinate dehydrogenase (SDH) in nanocomplexes-treated HC groups and nanocomplexes-treated N groups in (Ci) liver and (Cii) lung tissues, respectively. Data are shown as mean ± SD (n ≥ 6). HC-DC(I + II) NPs group was compared to HC-DC(I) NPs and N-DC(I + II) NPs. Also, the HC-DC(I) NPs group was compared to the N-DC(I) NPs group, and the two N-nanocomplex groups were compared. The values are considered statistically significant at $p < 0.05$*, <0.005**, and <0.0001***. **(D)** Molecular docking with dihydrolipoamide S-acetyltransferase (DLAT, a component of PDH), as illustrated by (Di) the 3D structure of the docked complex of three DLAT (PDB: 1FYC, blue, orange, and light green wire style) molecules. (Dii, Diii) Docking models of $DLAT_1$ (blue-colored wire style) with DC(I + II) or DC(I) (stick style and green-colored ball), respectively, followed by $DLAT_2$ (orange-colored wire style), and then $DLAT_3$ (light green-colored wire style). **(E)** Molecular docking with SDH as demonstrated by (Ei) the 3D structure of SDH (PDB: 1NEN, turquoise "chain A", light blue "chain B", violet "chain C", and gray "chain D"-colored cartoons). (Eii, Eiii) The interacting residues (black and red) in the docked complexes of SDH with DC(I + II) and DC(I) (stick style and green-colored ball), respectively, are magnified and show the binding of the Cu complexes to the active site residues of SDH (red). The brown-colored space-filling spheres are referred to as the Fe-S centers of the SDH. The docked complexes were given by the HDOCK server (http://hdock.phys.hust.edu.cn/) and visualized by Discovery Studio 2020 Client software.

green chemically synthesized Cu oxide NPs (C(I + II) NPs and C(I) NPs) were chelated by DD, forming nanocomplexes of DC(I + II) NPs and DC(I) NPs. These semi-spherical-shaped DC(I + II) NPs and global-shaped DC(I) NPs whose elemental compositions were identified, demonstrated appropriate stability profiles in serum condition at 37°C (Figures 1A–D) as well as higher safety on normal liver cells than their corresponding complexes and DD. Recently, these nanocomplexes exhibited high anti-metastatic effects with suppressing ALDH1A activity and elevating ROS levels in cancer cells (Abu-Serie and Eltarahony, 2021; Abu-Serie and Abdelfattah, 2023). In line with these recent findings, the current study revealed their highest growth inhibitory potential against both liver cancer cell lines, compared to C(I + II) NPs, C(I) NPs, DD, and their corresponding typical complexes, as well as their most potent anti-migratory efficacy. More importantly, both nanocomplexes showed the highest cuproptotic potential in the treated HepG2 cells, as evidenced by the lowest MP (65.05% and 45.24%, respectively, Figure 3A). This could be attributed to the nanocomplex nanosizes that positively affect cellular uptake of their included Cu, as well as the GSH-suppressive effect of DD, where GSH depletion increases cancer cells' sensitivity to cuproptosis (Abu-Serie and Eltarahony, 2021; Li et al., 2022; Tsvetkov et al., 2022; Abu-Serie and Abdelfattah, 2023). Interestingly, this study is the first to evaluate the cuproptotic efficacy of these promising nanocomplexes against metastatic HC.

The DC(I + II) exhibited significantly higher therapeutic potential than DC(I) not only toward cells but also against the metastatic HC animal model (in terms of histological investigations and tumor markers "AFP, GST, Ki-67, CSC genes, and metastasis mediators "TWIST1-induced epithelial-mesenchymal transition (EMT), and MMP9"). Due to their nanosizes, both nanocomplexes had a higher accumulation rate in tumor tissues than normal tissues, but DC(I + II)

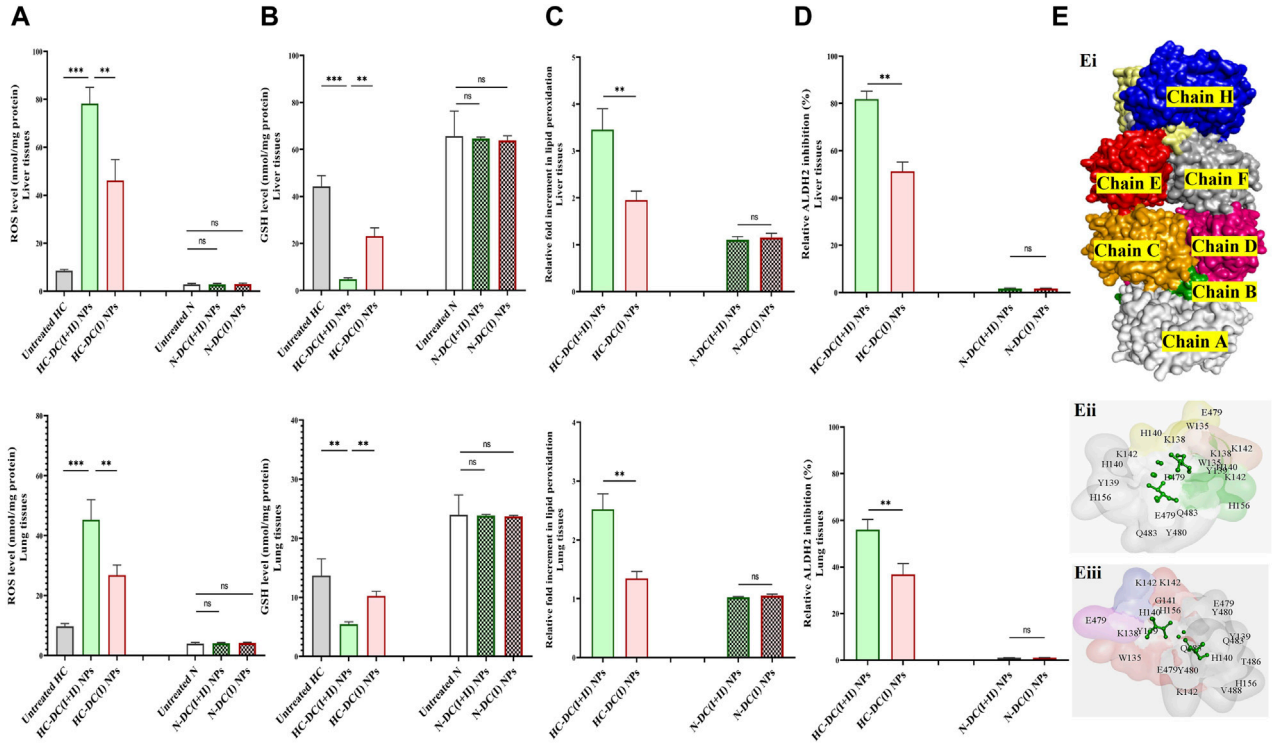

FIGURE 8
Selective oxidant impact of the studied nanocomplexes in the treated hepatocellular carcinoma (HC)-bearing mice as well as their molecular docking analysis with aldehyde dehydrogenase (ALDH) 2. **(A)** Reactive oxygen species (ROS) content (nmol/mg protein), **(B)** glutathione (GSH) level (nmol/mg protein), **(C)** relative fold increment of lipid peroxidation, and **(D)** relative ALDH2 inhibition in tumor tissues (liver and lung) of the untreated HC and treated HC groups (nanocomplex of diethyldithiocarbamate-Cu_4O_3 nanoparticles-treated HC (HC-DC(I + II) NPs) and nanocomplex of diethyldithiocarbamate-Cu_2O nanoparticles-treated HC (HC-DC(I) NPs), as well as in normal corresponding tissues of the untreated and treated N groups. Data are shown as mean ± SD ($n \geq 6$). The N group was compared to other groups, and the values are considered statistically significant at $p <$ 0.05*, <0.005**, and <0.0001***. **(E)** Predicted inhibition of ALDH2, as shown by (Ei) the 3D structure of ALDH2 (PDB: 4FR8, white "chain A″, green "chain B″, orange "chain C″, pink "chain D″, yellow "chain E″, blue "chain F″, red "chain G″, and gray "chain H″-colored surface). (Eii, Eiii) Magnification of the interacting residues (gray) in the docked complexes of ALDH2 with diethyldithiocarbamate-Cu_4O_3 "DC(I + II)" or diethyldithiocarbamate-Cu_2O "DCI)(I)" (stick style and green-colored ball), respectively.

NPs showed greater distribution percentages in tumor tissues than DC(I) NPs (Figure 7A). This may be owing to DC(I + II) NPs have a lower negative surface charge than DC(I) NPs, which results in superior binding to the negatively charged tumor cell plasma membrane (Frohlich, 2012). In the HC-DC(I + II) NPs group, the highly accumulated Cu in only tumor tissues, as the main initiator of selective cuproptosis, led to more aggregating lipoylated enzymes (e.g., PDH) and more destabilization of Fe-S cluster protein (e.g., SDH), resulting in high mitochondrial stress. Interestingly, docking results revealed that the DC(I + II) complex had a higher affinity for DLAT of PDH and enhanced its aggregation more than the DC(I) complex. Furthermore, both complexes could inhibit competitively the activity of this enzyme and decrease its affinity for Fe-S. The computational findings also showed that DC(I) had more capability to reduce the affinity between SDH and Fe-S (Fe displacement) than DC(I + II). However, DC(I + II) showed a higher affinity for SDH (Table 1) and suppressed SDH activity more effectively than DC(I) (Figures 7Ci, Cii). In addition to higher Cu content in HC-treated HC-DC(I + II) NPs' tumor tissues, the freed Fe from Cu displacement in the Fe-S cluster (Table 1) can induce the Fenton reaction (Vallieres et al., 2017), causing oxidative stress. Liver tumor cells defend against the generated oxidative stress products by elevating the expression of ALDH2 (Abu-Serie, 2023) and GST, practically GSTP1. The latter is closely coincident with malignant transformation of liver cells and mediates chemoresistance via conjugating proapoptotic drugs with GSH (Muramatsu and Sakai, 2006; Sell, 2008; Li et al., 2013; Mazari et al., 2023). Furthermore, AFP which promotes HC's malignant transformation, involves in the process of multidrug resistance and acts as an immunosuppressor (Li et al., 2021). Therefore, suppression of these tumor markers represents potential therapeutic targets. Thiol affinity of DD may be attributed to the inhibition potency of both complexes for ALDH2 and GST activities by forming disulfide adducts with cysteine residues of catalytically active sites of these enzymes. Additionally, a recent study illustrated that DD can inhibit transcriptional activation of nuclear factor erythroid-2, which induces GSTP1 expression (Satoh et al., 2002; Abu-Serie and Abdelfattah, 2022).

Telomerase reverse transcriptase is also essential for maintaining cancer stemness and stimulates the conversion of non-CSCs to CSCs by protecting them from oxidative stress and inducing VEGF expression-mediated angiogenesis and EMT-mediated metastasis via the promotion of NF-κB-dependent MMP expression (Kong et al., 2014; Zou et al., 2020). As demonstrated in the current study, DC(I + II) NPs inhibited

TABLE 2 Liver function and hematological parameters.

Liver function parameters								
Groups	ALT (U/mg)			AST (U/mg)		Albumin (g/dL)		
N	64.1±0.83			24.4±0.63		1.78±0.03		
Untreated HC	32.6±0.71*			19.1±1.12*		1.36±0.04*		
HC-DC(I+II) NPs	65.4±2.02			25.8±0.53		1.76±0.04		
HC-DC(I) NPs	71.2±2.99			27.9±0.58		1.77±0.04		
RBCs								
	RBC (10^6/μL)	Hg (g/dL)	HCT (%)	MCV (fL)	MCH (pg)	MCHC (g/dL)	RDW-CV (%)	RDW-SD (fL)
N	7.25±0.09	12.2±0.05	35.8±0.85	50.4±0.92	17.0±0.02	34.3±1.15	15.4±1.25	27.9±1.62
N-DC(I+II) NPs	8.16±0.14	13.1±0.3	39.6±0.95	51.0±2.05	16.0±0.05	31.5±1.40	17.6±1.3	32.4±1.05
N-DC(I) NPs	7.51±0.11	12.5±0.25	39.0±3.00	57.0±1.95	16.6±0.15	29.2±1.25	15.2±1.25	27.2±0.65
Untreated HC	7.75±0.01	11.6±0.25	34.0±3.05	43.9±4.05	15.7±0.30	35.9±2.55	15.3±0.5	24.4±3
HC-DC(I+II) NPs	8.06±0.14	12.3±0.1	38.8±1.70	48.1±1.25	15.1±0.20	31.4±1.30	14.9±0.65	26.1±1.85
HC-DC(I) NPs	7.58±0.105	12.6±0.65	36.6±4.70	48.3±6.80	16.0±1.75	33.4±1.20	17.0±0.4	29.8±4.95
WBCs					PLT			
	WBC (10^3/μL)	Lymph (%)	Mid (%)	Gran (%)	PLT (10^3/μL)	MPV (fL)	PDW	PCT (mL/L)
N	9.16±0.20	83.8±0.08	5.58±0.67	10.6±0.59	1205±52	5.72±0.20	14.8±0.15	6.62±0.82
N-DC(I+II) NPs	9.80±0.59	86.6±0.86	5.06±0.71	8.31±1.57	1207±33	5.70±0.10	14.9±0.01	6.92±0.29
N-DC(I) NPs	8.61±0.21	87.1±1.01	4.22±0.65	8.69±0.36	1281±13	6.03±0.23	15.2±0.35	7.76±0.23
Untreated H	8.81±1.01	68.2±1.04*	10.9±0.55*	19.3±0.08*	1172±58	5.40±0.01	14.9±0.2	6.58±1.11
HC-DC(I+II) NPs	8.93±0.10	78.9±0.75	5.43±0.10	15.7±0.86	1197±3.0	5.55±0.15	15.4±0.05	7.06±0.04
HC-DC(I) NPs	9.90±0.43	84.3±0.84	3.89±0.02	11.8±0.82	1192±11	6.00±0.20	15.0±0.25	7.20±0.09

All values are expressed as mean±SD. All groups were compared to the normal healthy (N) mouse group and considered significantly different at $p < 0.05$*, <0.005**, and <0.0001***. Liver function indexes were measured in liver homogenates, including ALT; alanine aminotransferase, and AST; aspartate aminotransferase. Hg; hemoglobin, HCT; hematocrit, MCV; mean corpuscular volume, fL; 10^{-15} liter, MCH; mean corpuscular Hg, MCHC; mean corpuscular Hg concentration, RDW-SD and RDW-CV; RBC distribution width-coefficient of standard deviation and variation, WBCs; white blood cells, Lymph; lymphocyte, Gran; granulocyte, Mid; monocytes, basophils, and eosinophils, MPV; mean PLT volume, PCT; plateletcrit, and PDW; PLT distribution width. Untreated HC; hepatocellular carcinoma-bearing mice, HC-DC(I+II) NPs; nanocomplex of diethyldithiocarbamate-Cu_3O_4 nanoparticles-treated HC animal group, HC-DC(I) NPs; nanocomplex of diethyldithiocarbamate-Cu_2O nanoparticles-treated HC animal group; and the treated N groups (N-DC(I+II) NPs and N-DC(I) NPs).

not only the expression of stemness genes but also the TERT gene and its downstream genes (MMP9 and VEGF2) in both tumor tissues (Figures 6A–C). The *in silico* results revealed a higher binding affinity of DC(I + II) to MMP9 than DC(I), as well as the ability of these nanocomplexes to inhibit its activity via non- or uncompetitive mechanisms due to their proposed inability to bind the enzyme active sites (Figures 5Biii, Biv).

Besides the thiol affinity-dependent oxidant activity of DD resulting in GSH inactivation (Skrott and Cvek, 2012), Cu(II) of Cu_4O_3 "$(Cu^{+1})_2$ $(Cu^{+2})_2$ O_3" in DC(I + II) NPs depleted the GSH level by catalyzing its oxidation, producing its oxide form (GSSG) and Cu (I) (Ngamchuea et al., 2016). Consequently, tumor tissues of HC-DC(I + II) NPs had a lower level of GSH than those of DC(I) NPs (Figure 8B). The released Cu(I) or Cu (I) of DC(I) NPs could directly generate hydroxyl radicals via the Fenton reaction, but DC(I + II) NPs-treated tumor tissues had a lesser antioxidant defense, resulting in more oxidative damage (lipid peroxidation) than DC(I) NPs. Moreover, DC(I + II) NPs revealed stronger inhibition potency on mitochondrial ALDH2 activity than DC(I) NPs (Figures 8D, E; Table 1). The predicted analysis also supported that DC(I + II) had a higher binding affinity to ALDH2 than DC(I), and the mechanism of inhibition by both nanocomplexes was non- or uncompetitive since they did not bind to the enzyme active site residues (Figures 8Eii, Eiii). In addition to being a CSC marker, ALDH2 is crucial functional regulator that enhances hepatic CSC self-renewal, proliferation, and metastasis by increasing the expression of SOX2, OCT-4, and NANOG and activating EMT (Chen et al., 2020; Zhang and Fu, 2021). It also acts a CSC protector by detoxifying reactive aldehydes, such as those generated by lipid peroxidation (Zhang and Fu, 2021). Therefore, its inhibition causes stemness suppression and elevates lipid peroxidation. Accordingly, following treatment with DC(I + II) NPs as opposed to its counterpart, stemness gene expressions were more repressed and cellular lipid peroxidation content was higher. In clinical trials (phase I/II), disulfiram (parent compound of DD) demonstrated a safe and effective response in increasing cancer patients' survival rates (Kang et al., 2023). Elesclomol (cuproptosis inducer) alone or in combination with paclitaxel had a favourable safety profile but a low response rate (Zheng et al., 2022).

5 Conclusion

In comparison with DC(I) NPs, DC(I + II) nanocomplex demonstrated a significantly higher accumulation rate in tumor tissues, inhibition-dependent cuproptotic activity for mitochondrial enzymes, and depletion of antioxidant indices (GSH and ALDH2). As a result of these effects, the DC(I + II) nanocomplex exhibited a more potent anti-metastatic HC impact, as evidenced by histological, immunohistological, molecular, and biochemical investigations for key tumor, stemness gene, and metastasis markers. Both nanocomplexes showed high selectivity against tumor tissues without causing any alterations in normal healthy cells. Consequently, DC(I + II) NPs could be promising against a variety of aggressive tumors.

Data availability statement

The original contributions presented in the study are included in the article/Supplementary Material, further inquiries can be directed to the corresponding author.

Ethics statement

Ethical approval was not required for the studies on humans in accordance with the local legislation and institutional requirements because only commercially available established cell lines were used. The animal study was approved by Institutional Animal Care and Use Committee (Alex-IACUC)-International Council for Laboratory Animal Science (ICLAS) with an approval code of AU-0122172833. The study was conducted in accordance with the local legislation and institutional requirements.

Author contributions

MA-S: Conceptualization, Data curation, Formal Analysis, Investigation, Methodology, Software, Validation, Visualization, Writing–original draft, Writing–review and editing. AB: Funding acquisition, Project administration, Writing–original draft, Writing–review and editing. SR: Writing–original draft, Writing–review and editing, Software. NH: Data curation, Methodology, Software, Validation, Visualization, Writing–original draft, Writing–review and editing.

Funding

The author(s) declare that financial support was received for the research, authorship, and/or publication of this article. This work was supported by the Researchers Supporting Project (RSP2024R64), King Saud University, Riyadh, Saudi Arabia.

Acknowledgments

Authors acknowledge Dr. Mohamed Salah Ayoup (Faculty of Science, Alexandria University, Egypt) and Dr. Mohamed Teleb Ismail (Faculty of Pharmacy, Alexandria University, Egypt) for their kind help in drawing the chemical structures of Cu_4O_3-diethyldithiocarbamate (DC(I + II) NPs) and Cu_2O-diethyldithiocarbamate (DC(I) NPs) for molecular docking analysis. Also, authors acknowledge Ghada M. Ahmad (Assistant lecturer, Medical Laboratory Technology, Alexandria University, Egypt) and Walaa Haghazy Ali (Assistant lecturer, Biochemistry department, Faculty of Science, Alexandria University, Egypt) for their assistance during the animal experiment.

Conflict of interest

The authors declare that the research was conducted in the absence of any commercial or financial relationships that could be construed as a potential conflict of interest.

Publisher's note

Supplementary material

The Supplementary Material for this article can be found online at: https://www.frontiersin.org/articles/10.3389/fphar.2024.1388038/full#supplementary-material

References

Abu-Serie, M. M. (2023). Targeted ferroptotic potency of ferrous oxide nanoparticles-diethyldithiocarbamate nanocomplex on the metastatic liver cancer. *Front. Pharmacol.* 13, 1089667. doi:10.3389/fphar.2022.1089667

Abu-Serie, M. M., and Abdelfattah, A. E. Z. (2023). A comparative study of smart nanoformulations of diethyldithiocarbamate with Cu_4O_3 nanoparticles or zinc oxide nanoparticles for efficient eradication of metastatic breast cancer. *Sci. Rep.* 13, 3529. doi:10.1038/s41598-023-30553-8

Abu-Serie, M. M., and Abdelfattah, E. Z. A. (2022). Anti-metastatic breast cancer potential of novel nanocomplexes of diethyldithiocarbamate and green chemically synthesized iron oxide nanoparticles. *Int. J. Pharm.* 627, 122208. doi:10.1016/j.ijpharm.2022.122208

Abu-Serie, M. M., Osuka, S., Heikal, L. A., Teleb, M., Barakat, A., and Dudeja, V. (2024). Diethyldithiocarbamate-ferrous oxide nanoparticles inhibit human and mouse glioblastoma stemness: aldehyde dehydrogenase 1A1 suppression and ferroptosis induction. *Front. Pharmacol.* 15, 1363511. doi:10.3389/fphar.2024.1363511

Abu-Serie, M. M. (2024). Synergistic eradicating impact of 5-fluouracil with FeO nanoparticles-diethyldithiocarbamate in colon cancer spheroids. *Nanomedicine (Lond).* 19 (11), 979–994. doi:10.2217/nnm-2024-0007

Abu-Serie, M. M., and Eltarahony, M. (2021). Novel nanoformulated diethyldithiocarbamate complexes with biosynthesized or green chemosynthesized copper oxide nanoparticles: an *in vitro* comparative anticancer study. *Int. J. Pharm.* 609, 121149. doi:10.1016/j.ijpharm.2021.121149

Bradford, M. M. (1976). A rapid and sensitive method for the quantitation of microgram quantities of protein utilizing the principle of protein-dye binding. *Anal. Biochem.* 72, 248–254. doi:10.1006/abio.1976.9999

Chang, C. W., Lo, J. F., and Wang, X. W. (2019). Roles of mitochondria in liver cancer stem cells. *Differentiation* 107, 35–41. doi:10.1016/j.diff.2019.04.001

Chen, L., Wu, M., Ji, C., Yuan, M., Liu, C., and Yin, Q. (2020). Silencing transcription factor FOXM1 represses proliferation, migration, and invasion while inducing apoptosis of liver cancer stem cells by regulating the expression of ALDH2. *IUBMB Life.* 72, 285–295. doi:10.1002/iub.2166

Crowley, L. C., Christensen, M. E., and Waterhouse, N. J. (2016). Measuring mitochondrial transmembrane potential by TMRE staining. *Cold Spring Harb. Protoc.* 2016, pdb.prot087361. doi:10.1101/pdb.prot087361

Cui, J., Li, G., Yin, J., Li, L., Tan, Y., Wei, H., et al. (2020). GSTP1 and cancer: expression, methylation, polymorphisms and signaling (Review). *Int. J. Oncol.* 56, 867–878. doi:10.3892/ijo.2020.4979

Cvek, B., Milacic, V., Taraba, J., and Dou, Q. P. (2008). Ni(II), Cu(II), and Zn(II) diethyldithiocarbamate complexes show various activities against the proteasome in breast cancer cells. *J. Med. Chem.* 51, 6256–6258. doi:10.1021/jm8007807

Frohlich, E. (2012). The role of surface charge in cellular uptake and cytotoxicity of medical nanoparticles. *Int. J. Nanomed.* 7, 5577–5591. doi:10.2147/IJN.S36111

Gaskill, C. L., Miller, L. M., Mattoon, J. S., Hoffmann, W. E., Burton, S. A., Gelens, H. C., et al. (2005). Liver histopathology and liver and serum alanine aminotransferase and alkaline phosphatase activities in epileptic dogs receiving phenobarbital. *Vet. Pathol.* 42, 147–160. doi:10.1354/vp.42-2-147

Habig, W. H., Pabst, M. J., and Jakoby, W. B. (1974). Glutathione S-transferases. *J. Biol. Chem.* 249, 7130–7139. doi:10.1016/s0021-9258(19)42083-8

Han, J., Liu, L., Yue, X., Chang, J., Shi, W., and Hua, Y. (2013). A binuclear complex constituted by diethyldithiocarbamate and copper(I) functions as a proteasome activity inhibitor in pancreatic cancer cultures and xenografts. *Toxicol. Appl. Pharmacol.* 273, 477–483. doi:10.1016/j.taap.2013.09.009

Jing, N., Gao, W. Q., and Fang, Y. X. (2021). Regulation of formation, stemness and therapeutic resistance of cancer stem cells. *Front. Cell Dev. Biol.* 9, 641498. doi:10.3389/fcell.2021.641498

Josan, S., Xu, T., Yen, Y. F., Hurd, R., Ferreira, J., Chen, C. H., et al. (2013). *In vivo* measurement of aldehyde dehydrogenase-2 activity in rat liver ethanol model using dynamic MRSI of hyperpolarized [1-(13) C] pyruvate. *NMR Biomed.* 26, 607–612. doi:10.1002/nbm.2897

Kang, X., Jadhav, S., Annaji, M., Huang, C. H., Amin, R., Shen, J., et al. (2023). Advancing cancer therapy with copper/disulfiram nanomedicines and drug delivery systems. *Pharmaceutics* 15 (6), 1567. doi:10.3390/pharmaceutics15061567

Kong, F., Zheng, C., and Xu, D. (2014). Telomerase as a "stemness" enzyme. *Sci. China Life Sci.* 57, 564–570. doi:10.1007/s11427-014-4666-6

Krissinel, E., and Henrick, K. (2007). Inference of macromolecular assemblies from crystalline state. *J. Mol. Biol.* 372, 774–797. doi:10.1016/j.jmb.2007.05.022

Laskowski, R. A., Jabłońska, J., Pravda, L., Vařeková, R. S., and Thornton, J. M. (2018). PDBsum: structural summaries of PDB entries. *Protein Sci.* 27, 129–134. doi:10.1002/pro.3289

Li, S. R., Bu, L. L., and Cai, L. (2022). Cuproptosis: lipoylated TCA cycle proteins-mediated novel cell death pathway. *Signal Transduct. Target Ther.* 7, 158. doi:10.1038/s41392-022-01014-x

Li, T., Zhao, X. P., Wang, L. Y., Gao, S., Zhao, J., Fan, Y. C., et al. (2013). Glutathione S-transferase P1 correlated with oxidative stress in hepatocellular carcinoma. *Int. J. Med. Sci.* 10, 683–690. doi:10.7150/ijms.5947

Li, W., Liu, K., Chen, Y., Zhu, M., and Li, M. (2021). Role of alpha-fetoprotein in hepatocellular carcinoma drug resistance. *Curr. Med. Chem.* 28, 1126–1142. doi:10.2174/0929867327999200729151247

Liu, F., and Qian, Y. (2021). The role of CD133 in hepatocellular carcinoma. *Cancer Biol. Ther.* 22, 291–300. doi:10.1080/15384047.2021.1916381

Loureiro, R., Mesquita, K. A., Magalhães-Novais, S., Oliveira, P. J., and Vega-Naredo, I. (2017). Mitochondrial biology in cancer stem cells. *Semin. Cancer Biol.* 47, 18–28. doi:10.1016/j.semcancer.2017.06.012

Lv, H., Liu, X., Zeng, X., Liu, Y., Zhang, C., Zhang, Q., et al. (2022). Comprehensive analysis of cuproptosis-related genes in immune infiltration and prognosis in melanoma. *Front. Pharmacol.* 13, 930041. doi:10.3389/fphar.2022.930041

Margalef, P., Kotsantis, P., Borel, V., Bellelli, R., Panier, S., and Boulton, S. J. (2018). Stabilization of reversed replication forks by telomerase drives telomere catastrophe. *Cell* 172, 439–453. doi:10.1016/j.cell.2017.11.047

Mazari, A. M. A., Zhang, L., Ye, Z. W., Zhang, J., Tew, K. D., and Townsend, D. M. (2023). The multifaceted role of glutathione S-transferases in health and disease. *Biomolecules* 13, 688. doi:10.3390/biom13040688

Mosmann, T. (1983). Rapid colorimetric assay for cellular growth and survival: application to proliferation and cytotoxicity assays. *J. Immunol. Method.* 65, 55–63. doi:10.1016/0022-1759(83)90303-4

Munujos, P., Coll-Cantí, J., González-Sastre, F., and Gella, F. J. (1993). Assay of succinate dehydrogenase activity by a colorimetric-continuous method using iodonitrotetrazolium chloride as electron acceptor. *Anal. Biochem.* 212, 506–509. doi:10.1006/abio.1993.1360

Muramatsu, M., and Sakai, M. (2006). Mechanisms of a tumor marker, glutathione transferase P, expression during hepatocarcinogenesis of the rat. *Proc. Jpn. Acad. Ser. B Phys. Biol. Sci.* 82, 339–352. doi:10.2183/pjab.82.339

Ngamchuea, K., Batchelor-McAuley, C., and Compton, R. G. (2016). The copper(ii)-catalyzed oxidation of glutathione. *Chem.* 22, 15937–15944. doi:10.1002/chem.201603366

Niitsu, Y., Sato, Y., and Takayama, T. (2022). Implications of glutathione-S transferase P1 in MAPK signaling as a CRAF chaperone: in memory of Dr. Irving Listowsky. *Proc. Jpn. Acad. Ser. B Phys. Biol. Sci.* 98, 72–86. doi:10.2183/pjab.98.005

Ohkawa, H., Ohishi, N., and Yagi, K. (1979). Assay for lipid peroxides in animal tissues by thiobarbituric acid reaction. *Anal. Biochem.* 95, 351–358. doi:10.1016/0003-2697(79)90738-3

Pathak, S., and Khuda-Bukhsh, A. R. (2007). Assessment of hepatocellular damage and hematological alterations in mice chronically fed p-dimethyl aminoazobenzene and phenobarbital. *Exp. Mol. Pathol.* 83, 104–111. doi:10.1016/j.yexmp.2006.10.003

Paul, V. D., and Lill, R. (2015). Biogenesis of cytosolic and nuclear iron-sulfur proteins and their role in genome stability. *Biochim. Biophys. Acta.* 1853, 1528–1539. doi:10.1016/j.bbamcr.2014.12.018

Philips, C. A., Rajesh, S., Nair, D. C., Ahamed, R., Abduljaleel, J. K., and Augustine, P. (2021). Hepatocellular carcinoma in 2021: an exhaustive update. *Cureus* 13, e19274. doi:10.7759/cureus.19274

Read, A. D., Bentley, R. E., Archer, S. L., and Dunham-Snary, K. J. (2021). Mitochondrial iron-sulfur clusters: structure, function, and an emerging role in vascular biology. *Redox Biol.* 47, 102164. doi:10.1016/j.redox.2021.102164

Satoh, K., Itoh, K., Yamamoto, M., Tanaka, M., Hayakari, M., Ookawa, K., et al. (2002). Nrf2 transactivator-independent GSTP1-1 expression in "GSTP1-1 positive" single cells inducible in female mouse liver by DEN: a preneoplastic character of possible initiated cells. *Carcinog* 23 (3), 457–462. doi:10.1093/carcin/23.3.457

Schwab, M. A., Kölker, S., van den Heuvel, L. P., Sauer, S., Wolf, N. I., Rating, D., et al. (2005). Optimized spectrophotometric assay for the completely activated pyruvate dehydrogenase complex in fibroblasts. *Clin. Chem.* 51, 151–160. doi:10.1373/clinchem.2004.033852

Sedlak, J., and Lindsay, R. H. (1968). Estimation of total, protein-bound, and nonprotein sulfhydryl groups in tissue with Ellman's reagent. *Anal. Biochem.* 25, 192–205. doi:10.1016/0003-2697(68)90092-4

Sell, S. (2008). Alpha-fetoprotein, stem cells and cancer: how study of the production of alpha-fetoprotein during chemical hepatocarcinogenesis led to reaffirmation of the stem cell theory of cancer. *Tumour Biol.* 29, 161–180. doi:10.1159/000143402

Skrott, Z., and Cvek, B. (2012). Diethyldithiocarbamate complex with copper: the mechanism of action in cancer cells. *Mini Rev. Med. Chem.* 12, 1184–1192. doi:10.2174/138955712802762068

Socci, D. J., Bjugstad, K. B., Jones, H. C., Pattisapu, J. V., and Arendash, G. W. (1999). Evidence that oxidative stress is associated with the pathophysiology of inherited hydrocephalus in the H-Tx rat model. *Exper. Neurol.* 155, 109–117. doi:10.1006/exnr.1998.6969

Tang, D., Chen, X., and Kroemer, G. (2022). Cuproptosis: a copper-triggered modality of mitochondrial cell death. *Cell Res.* 32, 417–418. doi:10.1038/s41422-022-00653-7

Terada, T., and Maruo, H. (2013). Unusual extrahepatic metastatic sites from hepatocellular carcinoma. *Int. J. Clin. Exp. Pathol.* 6, 816–820.

Tsvetkov, P., Coy, S., Petrova, B., Dreishpoon, M., Verma, A., Abdusamad, M., et al. (2022). Copper induces cell death by targeting lipoylated TCA cycle proteins. *Sci* 375, 1254–1261. doi:10.1126/science.abf0529

Vallieres, C., Holland, S. L., and Avery, S. V. (2017). Mitochondrial ferredoxin determines vulnerability of cells to copper excess. *Cell Chem. Biol.* 24, 1228–1237. doi:10.1016/j.chembiol.2017.08.005

Wang, K., and Sun, D. (2018). Cancer stem cells of hepatocellular carcinoma. *Oncotarget* 9, 23306–23314. doi:10.18632/oncotarget.24623

Wang, Z. G., He, Z. Y., Chen, Y., Gao, H., and Du, X. L. (2021). Incidence and survival outcomes of secondary liver cancer: a Surveillance epidemiology and end results database analysis. *Transl. Cancer Res.* 10, 1273–1283. doi:10.21037/tcr-20-3319

Yadav, U. P., Singh, T., Kumar, P., Sharma, P., Kaur, H., Sharma, S., et al. (2020). Metabolic adaptations in cancer stem cells. *Front. Oncol.* 10, 1010. doi:10.3389/fonc.2020.01010

Yan, Y., Zhang, D., Zhou, P., Li, B., and Huang, S. Y. (2017). HDOCK: a web server for protein-protein and protein-DNA/RNA docking based on a hybrid strategy. *Nucleic Acids Res.* 45, W365–W373. doi:10.1093/nar/gkx407

Zhang, H., and Fu, L. (2021). The role of ALDH2 in tumorigenesis and tumor progression: targeting ALDH2 as a potential cancer treatment. *Acta Pharm. Sin. B* 11, 1400–1411. doi:10.1016/j.apsb.2021.02.008

Zheng, P., Zhou, C., Lu, L., Liu, B., and Ding, Y. (2022). Elesclomol: a copper ionophore targeting mitochondrial metabolism for cancer therapy. *J. Exp. Clin. Cancer Res.* 41 (1), 271. doi:10.1186/s13046-022-02485-0

Zou, Y., Cong, Y. S., and Zhou, J. (2020). Implications of telomerase reverse transcriptase in tumor metastasis. *BMB Rep.* 53, 458–465. doi:10.5483/BMBRep.2020.53.9.108

frontiers | Frontiers in Pharmacology

TYPE Original Research
PUBLISHED 06 September 2024
DOI 10.3389/fphar.2024.1439497

OPEN ACCESS

EDITED BY
Jing-Quan Wang,
St. John's University, United States

REVIEWED BY
Chao Han,
China Pharmaceutical University, China
Wenli Wang,
Nantong University, China

*CORRESPONDENCE
Pei-Chun Sun,
sunpeichunyz@126.com
Wen-Chao Chen,
chenwenchao1122@126.com
Qiu-Rong Zhang,
zhangqr@zzu.edu.cn

†These authors have contributed equally to this work and share first authorship

RECEIVED 28 May 2024
ACCEPTED 26 August 2024
PUBLISHED 06 September 2024

CITATION
Zhang Y-T, Zhao L-J, Zhou T, Zhao J-Y, Geng Y-P, Zhang Q-R, Sun P-C and Chen W-C (2024) The lncRNA CADM2-AS1 promotes gastric cancer metastasis by binding with miR-5047 and activating NOTCH4 translation. *Front. Pharmacol.* 15:1439497. doi: 10.3389/fphar.2024.1439497

The lncRNA CADM2-AS1 promotes gastric cancer metastasis by binding with miR-5047 and activating NOTCH4 translation

Yu-Tong Zhang[1,2†], Li-Juan Zhao[1,3†], Teng Zhou[1], Jin-Yuan Zhao[2], Yin-Ping Geng[2], Qiu-Rong Zhang[2*], Pei-Chun Sun[1*] and Wen-Chao Chen[1*]

[1]Department of Gastrointestinal Surgery, Henan Provincial People's Hospital, Henan University People's Hospital, Zhengzhou University People's Hospital, Academy of Medical Sciences, Tianjian Laboratory of Advanced Biomedical Sciences, Zhengzhou University, Zhengzhou, China, [2]State Key Laboratory of Esophageal Cancer Prevention and Treatment, Key Laboratory of Advanced Drug Preparation Technologies, Ministry of Education of China, Institute of Pharmaceutical Sciences, Zhengzhou University, Zhengzhou, China, [3]State Key Laboratory of Esophageal Cancer Prevention and Treatment, Academy of Medical Sciences, Tianjian Laboratory of Advanced Biomedical Sciences, Zhengzhou University, Zhengzhou, China

Background: Multi-organ metastasis has been the main cause of death in patients with Gastric cancer (GC). The prognosis for patients with metastasized GC is still very poor. Long noncoding RNAs (lncRNAs) always been reported to be closely related to cancer metastasis.

Methods: In this paper, the aberrantly expressed lncRNA CADM2-AS1 was identified by lncRNA-sequencing in clinical lymph node metastatic GC tissues. Besides, the role of lncRNA CADM2-AS1 in cancer metastasis was detected by Transwell, Wound healing, Western Blot or other assays *in vitro* and *in vivo*. Further mechanism study was performed by RNA FISH, Dual-luciferase reporter assay and RT-qPCR. Finally, the relationship among lncRNA CADM2-AS1, miR-5047 and NOTCH4 in patient tissues was detected by RT-qPCR.

Results: In this paper, the aberrantly expressed lncRNA CADM2-AS1 was identified by lncRNA-sequencing in clinical lymph node metastatic GC tissues. Besides, the role of lncRNA CADM2-AS1 in cancer metastasis was detected *in vitro* and *in vivo*. The results shown that overexpression of the lncRNA CADM2-AS1 promoted GC metastasis, while knockdown inhibited it. Further mechanism study proved that lncRNA CADM2-AS1 could sponge and silence miR-5047, which targeting mRNA was NOTCH4. Elevated expression of lncRNA CADM2-AS1 facilitate GC metastasis by up-regulating NOTCH4 mRNA level consequently. What's more, the relationship among lncRNA CADM2-AS1, miR-5047 and NOTCH4 was further detected and verified in metastatic GC patient tissues.

Abbreviations: ASO, The antisense oligonucleotide; ceRNAs, Competing endogenous RNAs; GC, Gastric cancer; HE staining, Hematoxylin-eosin staining; lncRNAs, Long noncoding RNAs; miRNAs, MicroRNAs; NOTCH4, neurogenic locus notch homolog protein; 4RPMI, Roswell Park Memorial Institute; RT-qPCR, Quantitative reverse transcription PCR.

Conclusions: LncRNA CADM2-AS1 promoted metastasis in GC by targeting the miR-5047/NOTCH4 signaling axis, which may be a potential target for GC metastasis.

KEYWORDS

lncRNA CADM2-AS1, gastric cancer, metastasis, NOTCH4, miR-5047

1 Introduction

Gastric cancer (GC) was a malignant tumor originating from the epithelial cells of the gastric mucosa (Machlowska et al., 2020). In 2022, GC has emerged as the fifth leading cause of cancer-related mortality globally, posing a grave threat to the nation's public health (Siegel et al., 2024). According to 2020 statistics, China accounted for 44% and 48.6% of global GC cases and fatalities respectively, with the extremely high disease burden (He et al., 2024). The high incidence of local recurrence and distant metastasis was the main reason of the high mortality (Li G. Z. et al., 2022). In China, more than 80% of GC patients were locally advanced or advanced GC. The GC could metastasize not only to distant lymph nodes, liver and peritoneum, but also to lung, adrenal gland, brain and other sites (Oki et al., 2016; Ma et al., 2022; Fang et al., 2022; Kroese et al., 2022).The treatment of GC was still based on traditional methods such as surgical resection and chemotherapy, but these treatments were more suitable for patients with early GC without metastasis. The treatment of GC patients with metastasis was limited, and the prognosis was poor (Smyth et al., 2020; Thrumurthy et al., 2015). Therefore, it was essential to deeply study the development mechanism of GC metastasis, excavate the related biomarkers of GC metastasis, and propose new treatment plans for GC.

About 70% of the human genome could be transcribed, but only less than 2% of transcript could encode proteins, while almost 98% of transcript was non-coding RNA (Xue and He, 2014). Long noncoding RNAs (lncRNAs) were noncoding RNAs longer than 200 nucleotides (Xing C. et al., 2021). The present study indicated that lncRNAs played a key role in multiple biological processes such as cancer proliferation, metastasis and immunity (Li Y. et al., 2022; Li B. et al., 2022; Gao et al., 2022). Changes in the expression of lncRNAs could lead to abnormal expression of transcriptome genes, thus promoting the formation and development of cancer. For example, lncRNA H19 was not only highly expressed in colorectal cancer, breast cancer and other tumor tissues, but also significantly abnormal expression in prostate cancer and oral cancer. Moreover, the high expression of H19 shortened the survival time of cancer patients and was closely associated with poor prognosis of cancer patients (Zhang et al., 2020; Wang J. et al., 2019; Singh et al., 2021; Yang et al., 2021). The expression level of lncRNA XIST was downregulated in breast cancer, and the deletion of lncRNA XIST promoted breast cancer cells metastasize to brain (Xing F. et al., 2021). LncRNAs may have the potential to be biomarkers of cancer initiation and progression and therapeutic targets for cancer. LncRNAs could regulate the biological behavior of cancer cells by interacting with proteins, RNA or DNA. The classical pathway of lncRNAs was working as competing endogenous RNAs (ceRNAs) of miRNAs, blocking the inhibitory effect of miRNAs on mRNA by reducing the binding of microRNAs (miRNAs) to 3′UTR regions of target genes mRNAs. At the same time, as a miRNA sponge, it also reduced the expression of miRNAs (Wang L. et al., 2019; Braga et al., 2020; Han et al., 2020). For instance, the upregulated lncRNA CCAT1 competitively bound to miR-28-5P, inhibiting its anticancer effect and promoting prostate cancer cell proliferation (You et al., 2019). LncRNA MIAT competitively bound to miR-50-5p, inhibiting the function of miR-50-5p to downregulate EZH2 protein, and promoted the invasion and metastasis of papillary thyroid carcinoma (Guo et al., 2021). LncRNAs interferes target genes mainly through miRNAs, following play their biological functions to participate in the occurrence and development of tumors.

There were a large number of lncRNAs, but the current functional studies of lncRNAs in GC often focused on a small number of classical lncRNAs (Sun et al., 2021; Xu et al., 2021; Syllaios et al., 2021). However, most of these lncRNAs have not yet been well studied and applicated in clinic. It's imperative to develop some potential and deeply studied lncRNAs for clinical application. Therefore, we screen the abnormally expressed lncRNAs in metastatic GC based on clinical samples and analysis in database. LncRNA CADM2-AS1 was found to be abnormally expressed in lymph node metastatic GC tissues. Thus, we focus on lncRNA CADM2-AS1 and further study its role and mechanism in GC metastasis in this paper. By combining with clinical samples, it was expected to identify new potential lncRNAs involved in the metastasis process of GC, providing new ideas for the clinical application of lncRNAs in GC metastasis.

2 Materials and methods

2.1 Cells

GC cell line was purchased from the Cell Bank of the Shanghai Institute of Cell Biology, Chinese Academy of Sciences. The cells were maintained in Roswell Park Memorial Institute (RPMI) 1,640 medium (BI, Israel), supplemented with 10% fetal bovine serum (BI, Israel). All cells were cultured in a humidified atmosphere at 5% CO_2 and 37°C.

2.2 Transfection assays

The antisense oligonucleotide (ASO) to knock down lncRNA CADM2-AS1 expression was produced and packaged by Guangzhou RIBOBIO Biotechnology Co. LTD., China; the siRNA to knock down NOTCH4 mRNA was produced and packaged by Suzhou Genepharma Co. LTD., China. The ASO/siRNA transfection was performed as follows, the HGC-27/BGC-823 cells (5×10^5 cells/well) were seeded in 6-well plates and cultured overnight in RPMI-1640 medium supplemented with

10% FBS. The ASO/siRNA was added to 1 mL blank medium at a final concentration of 100 nM. After 12 h of co-incubation with cells, the blank medium was replaced with complete medium, and the incubation continued for 24–48 h.

2.3 Infection assays

The lentiviral vector containing lncRNA CADM2-AS1/miR-5047 to overexpress was produced and packaged by Shanghai Genechem Co. Ltd., China. The lentivirus infection was performed as follows, the HGC-27/BGC-823 cells (4×10^3 cells/well) were seeded in 96-well plates and cultured with RPMI-1640 medium containing 10% FBS. The lentivirus was added to 100 μL complete medium at a final concentration of 10^7 TU/mL. After 20 h of incubation, the lentivirus-containing medium was replaced with complete medium. After 2 days 2 infection, the cells were incubated with 0.5 μg/mL puromycin in culture medium for 2 days to select the stable pCADM2-AS1/pmiR-5047 cell line.

2.4 Quantitative reverse transcription PCR (RT-qPCR)

The total mRNA was extracted by Total RNA Isolation Kit (Beibei Biotechnology, China). Then, each mRNA sample was reverse transcribed into cDNAs using lnRcute lncRNA First-Strand cDNA Kit (TIANGEN Biotechnology, China), HiScript II Q RT SuperMix for qPCR (Vazyme, China), riboSCRIPT Reverse Transcription Kit (RIBOBIO Biotechnology, China). The relative RNA levels of lncRNA CADM2-AS1, NOTCH4, has-miR-5047, has-miR-5706, has-miR-1184, and has-miR-1301-3p were detected with indicated primers. The primers of lncRNA CADM2-AS1, has-miR-5047, has-miR-5706, has-miR-1184, and has-miR-1301-3p were designed by RIBOBIO Biotechnology. The primer of NOTCH4 was designed by Tsingke Biotechnology.

2.5 Transwell assays

For silencing of lncRNA CADM2-AS1 (NC or ASO-CADM2-AS1) and NOTCH4 (NC or siNOTCH4), 8×10^3 HGC-27 or BGC-823 cells were seeded in the upper transwell chambers. For overexpression of lncRNA CADM2-AS1 (CON or pCADM2-AS1) and miR-5047 (CON or pmiR-5047), 8×10^3 HGC-27 or BGC-823 cells were added in the chambers. The medium containing 10% FBS (700 μL) was added to the lower wells. After 48 h, the cells in upper chambers were removed by cotton swab, and they migrated to the lower wells through pores were fixed with 4% paraformaldehyde and stained with 4,6-diamidino-2-phenylindole (DAPI) or 0.2% crystal violet solution, which followed by observing and counting with microscope.

2.6 Wound healing assay

For Wound healing assay, 5×10^5 cells were seeded in 6-well. A wound was made in each well 24 h later. Plates were imaged every 24 h. Wound width was imaged and measured bymicroscope (Nikon, Japan).

2.7 Western blot

The cell total protein was extracted with Native lysis Buffer (Solarbio, China), adding PSMF and protein enzyme inhibitors (Meilunbio, China), which followed by degeneration with 6 × Loading buffer for 10 min at 100°C. Western Blot was performed according to the standard methods. Approximately 30 μg of protein was subjected to sodium dodecyl sulfate-polyacrylamide gel electrophoresis (SDS–PAGE) gel. The resolved proteins were transferred to a 0.2-μm nitrocellulose membrane (Pall, United States). The membrane carrying proteins was blocked with 5% milk in PBS for 2 h, following by first-antibody incubation like anti-CDH1 (CST, United States), anti-N-cadherin (CST, United States), anti-snail (CST, United States), anti-vimentin (Abcam, England), and anti-GAPDH (Hangzhou Goodhere Biotechnology, China), overnight at 4°C. Next, the membrane was washed with PBS containing 0.05% Tween-20 (PBST) at room temperature and incubated with peroxidase-conjugated goat anti-rabbit IgG (ZEN-BIOSCIENCE, China) for 2 h at room temperature. The membrane was then washed with PBST at room temperature and developed using an enhanced chemiluminescence reagent (Meilunbio, China).

2.8 MTT assay

Cell proliferation was detected by the 3-(4,5-Dimethyl-2-Thiazolyl)-2,5-Diphenyl Tetrazolium Bromide (MTT, Meilunbio, China) method. The cells were seeded and grown in 96-well plates. After the grown period, 20 μL MTT solution was added to each well and incubated with cells for 4 h. Then the supernatant was discarded and 200 μL Dimethyl sulfoxide (DMSO, Meilunbio, China) was added to each well. The absorbance was measured with microplate reader (Envision, PerkinElmer, United States) at 570 nm.

2.9 RNA FISH

HGC-27 or BGC-823 cells were seeded on cell climbing piece and cultured overnight in 24-well plates. Then the cells were fixed in 4% paraformaldehyde for 15–20 min. The location of lncRNA CADM2-AS1 was detected by RNA FISH SA-Biotin amplification System Kit, which was purchased from Genepharma (Suzhou, China). The general operation was as follows: Cells were permeabilized with 0.1% Buffer A, which followed by blocking with 1 × blocking solution for 30 min. The blocked cells then incubated with appropriate probe overnight. After the incubation, cells were washed with 2 × Buffer C for three times, and nuclei were stained with DAPI. Finally, the cells were imaged using a Nikon C2 Plus confocal microscope (Nikon, Japan), lncRNA CADM2-AS1, Red; miR-5047, Green; nuclei, Blue.

2.10 Dual-luciferase reporter assay

The binding sites of NOTCH4 mRNA and miR-5047 were predicted by the Targetscan database (https://www.targetscan.org/vert_80/) (Mcgeary et al., 2019). The binding sites of lncRNA CADM2-AS1 and miR-5047 were predicted by the RNA22 database (https://cm.jefferson.edu/rna22/Interactive/RNA22Controller) (Loher and RIGOUTSOS, 2012). The lncRNA CADM2-AS1 and NOTCH4 mRNA serial truncations were cloned into pmirGLO vector, which were purchased from Suzhou Genepharma Co. LTD. Then, 2 μg reporter vector, 2 μg ectopic expression vector and 2 μg pmirGLO vector were transfected into 293T cells with EntransterTM-H4000 (Engreen, China). For miR-5047 stability assay, 2 μg reporter vector and 100 nmol mimic (Genepharma, China) were co-transfected into 293T cells with EntransterTM-H4000. About 48 h later, cells were lysed in 500 μL of passive lysis buffer. The firefly luciferase activity and the Renilla activity were determined by Dual-Luciferase® Reporter Assay System (Promega, United States). For each experiment, the firefly luciferase activity was normalized by Renilla activity.

2.11 *In vivo* assay

Five-week-old male NOD/SCID immunodeficiency mice were purchased from the Gempharmatech Co., Ltd., China. All animals were housed in a pathogen-free environment, and the experimental protocols were approved by the Ethics Committee of Zhengzhou University Health Science Center. The mice were randomized into three groups (n = 7 in each group). 5×10^5 or 7×10^6 HGC-27 cells were diluted in 200 μL of sterile PBS and injected through tail vein (5×10^5 for the animal experiment in Figure 3, and 5×10^6 for the animal experiment in Figure 7), and the mice were weighted every week. After 8 weeks, mice were euthanized and dissected to detect the GC cell metastasis *in vivo*.

2.12 Hematoxylin-eosin staining (HE staining)

The lung tissues of the mice were dissected and fixed in 10% buffered formalin solution, which followed by embedding in paraffin wax. The serial sections (5 μm) were cut from the tissue blocks, deparaffinized in xylene, and hydrated in an alcohol series (75%, 85%, 95%, and 100%). The tissue sections were then incubated with hematoxylin (Solarbio, China) and eosin (Solarbio, China), which staining cell nuclei and cytoplasm separately. Finally, the sections were dehydrated in an alcohol series (75%, 85%, 95%, and 100%) and xylene. The HE stained sections were imaged and analyzed with a microscope (Nikon, Japan).

2.13 Patients tissue specimens

GC tissues and adjacent tissues of 60 patients were collected from the Henan Provincial people's Hospital. All tissue's collections were authorized by the Ethics Committee of Zhengzhou University People's Hospital (approval date 2020, code 172). Detailed characteristics of patients were showed in Supplementary Table 1.

2.14 Statistical analysis

Three independent trials were performed for each *in vitro* experiment. Spearman's correlation coefficient was used to evaluate the correlation between two groups. RNA sequencing and GC tissues analysis were performed by using Volcano and BOX plot tools in Hiplot Pro (https://hiplot.com.cn/), a comprehensive web service for biomedical data analysis and visualization. All statistical analyses were performed using GraphPad 8.0. The data difference was analyzed using Student's *t*-test. The differences were considered significant at $p < 0.05$. $^{*}p < 0.05$, $^{**}p < 0.01$, $^{***}p < 0.001$, $^{****}p < 0.0001$.

3 Results

3.1 LncRNA CADM2-AS1 overexpressed in metastatic GC

To develop and explore lncRNAs related to the GC metastasis, GC tissues with lymph node metastasis and adjacent tissues were collected for lncRNA sequencing. The results showed that multiple lncRNAs were abnormally expressed in GC tissues, and significantly differentially expressed lncRNA CADM2-AS1 was found (Figure 1A). For a preliminary understanding of lncRNA CADM2-AS1, we start with a preliminary validation in the lncRNASNP-human database (http://bioinfo.life.hust.edu.cn/lncRNASNP/#!/), and the database displayed that lncRNA CADM2-AS1 was significantly highly expressed in GC (Figure 1B) (Miao et al., 2018; Yang et al., 2023). Besides, Kaplan Meier plotter database (http://kmplot.com/analysis/) showed that high expression of lncRNA CADM2-AS1 was associated with poor prognosis of GC patients (Figure 1C) (Győrffy, 2021). Then, the overexpression of lncRNA CADM2-AS1 in GC tissues with lymph node metastasis was detected and verified by RT-qPCR, and the result was shown in Figure 1D. It was speculated that lncRNA CADM2-AS1 may be involved in GC metastasis. To explore the differential expression of lncRNA CADM2-AS1 in GC cell lines, total RNA was extracted from GC cells (AGS, BGC-823, HGC-27, MKN-1, MKN-45 and MGC-803). The result of RT-qPCR shown that lncRNA CADM2-AS1 was highly expressed in HGC-27 and low in BGC-823 (Figure 1E). Therefore, HGC-27 and BGC-823 cells were used as cell models to explore the regulatory effects of lncRNA CADM2-AS1 on metastasis of GC.

3.2 Knockdown of lncRNA CADM2-AS1 inhibited the migration of GC cells

To investigate the effect of lncRNA CADM2-AS1 on the metastasis of GC cells, lncRNA CADM2-AS1 was knocked down in HGC-27 and BGC-823 by ASO (HGC-27 ASO-CADM2-AS1 and BGC-823 ASO-CADM2-AS1) (Figure 2A). With knocking down of lncRNA CADM2-AS1, the ability of HGC-27 and BGC-823 to

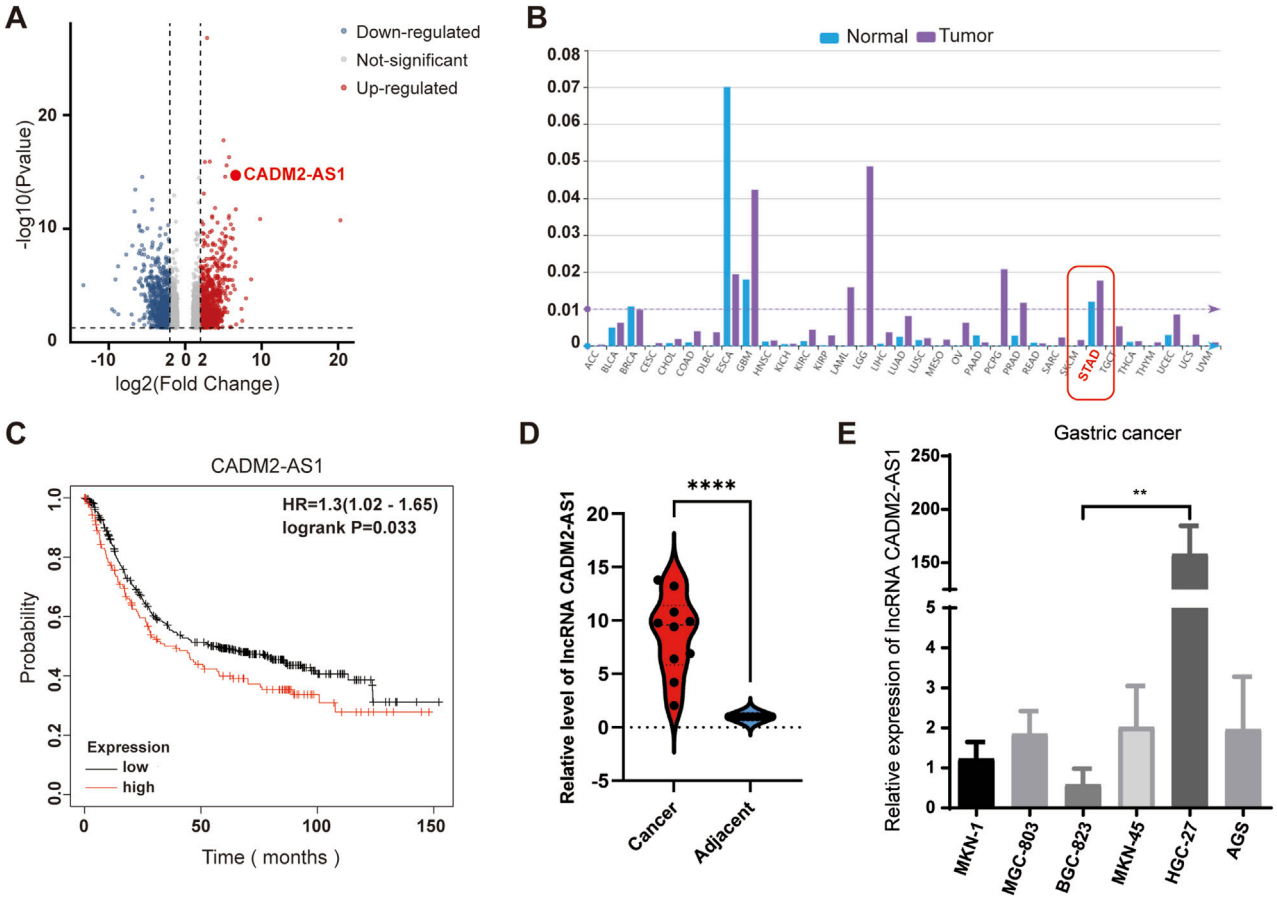

FIGURE 1
Overexpression of lncRNA CADM2-AS1 in metastatic GC. **(A)** Volcano plot of lncRNA sequencing of clinical GC tissues with lymph node metastasis and normal samples; **(B)** LncRNA CADM2-AS1 was significantly overexpressed in GC in LncRNASNP-human database; **(C)** The analysis in Kaplan Meier plotter database showed that high expression of lncRNA CADM2-AS1 was associated with poor prognosis in patients with GC. **(D)** The overexpression of lncRNA CADM2-AS1 in GC tissues with lymph node metastasis was detected and verified by RT-qPCR. **(E)** The expression of lncRNA CADM2-AS1 in GC cell lines was detected by RT-qPCR assay; n = 3, $^{**}p < 0.01$.

invade through the Transwell membrane was reduced (Figures 2B, C). Besides, the wound healing ability of HGC-27 and BGC-823 was also diminished when lncRNA CADM2-AS1 was knocked down (Figure 2D). Meanwhile, with lncRNA CADM2-AS1 knocking down, the expression of epithelial cell marker (E-cadherin) was increased but the expression of mesenchymal cell markers (N-cadherin, Vimentin, Snail) was decreased, which were the markers of inhibited epithelial-mesenchymal transition (EMT) progress (Figure 2E). All these results shown that lncRNA CADM2-AS1 knockdown hindered the migration of GC cells.

3.3 Overexpression of lncRNA CADM2-AS1 promoted the migration of GC cells *in vitro* and *in vivo*

To confirm that lncRNA CADM2-AS1 could promote metastasis in GC cells, the lncRNA CADM2-AS1 overexpression cell models were constructed by lentiviral infection (HGC-27 pCADM2-AS1 and BGC-823 pCADM2-AS1) (Figure 3A). Compared to CON, the ability of HGC-27 and BGC-823 to invade through the Transwell membrane was increased with lncRNA CADM2-AS1 overexpression and the wound healing ability of HGC-27 and BGC-823 was also enhanced (Figures 3B–D). Similarly, the overexpression of lncRNA CADM2-AS1 downregulated the expression of epithelial cell marker (E-cadherin) and upregulated the expression of mesenchymal cell markers (N-cadherin, Vimentin, Snail) (Figure 3E). With the consideration of the cell proliferation may affect cell migration ability, we also detected the effect of lncRNA CADM2-AS1 on the proliferation of GC cells by MTT assay. The results showed that the overexpression of lncRNA CADM2-AS1 had no significant effect on cell proliferation of HGC-27 and BGC-823 cells (Figure 3F). It was further demonstrated that lncRNA CADM2-AS1 overexpression could promote the migration ability of GC cells.

To explore whether lncRNA CADM2-AS1 overexpression had the promoting metastasis biological effect of GC cells *in vivo*, we established the lung metastasis models in NOD/SCID mouse by injecting HGC-27 CON and pCADM2-AS1 through tail vein (Figure 3G). Compared to CON group, there was no conspicuous change of weight in pCADM2-AS1 group (Figure 3H). However, 8 weeks later, it was found that the lung nodules were formed in the

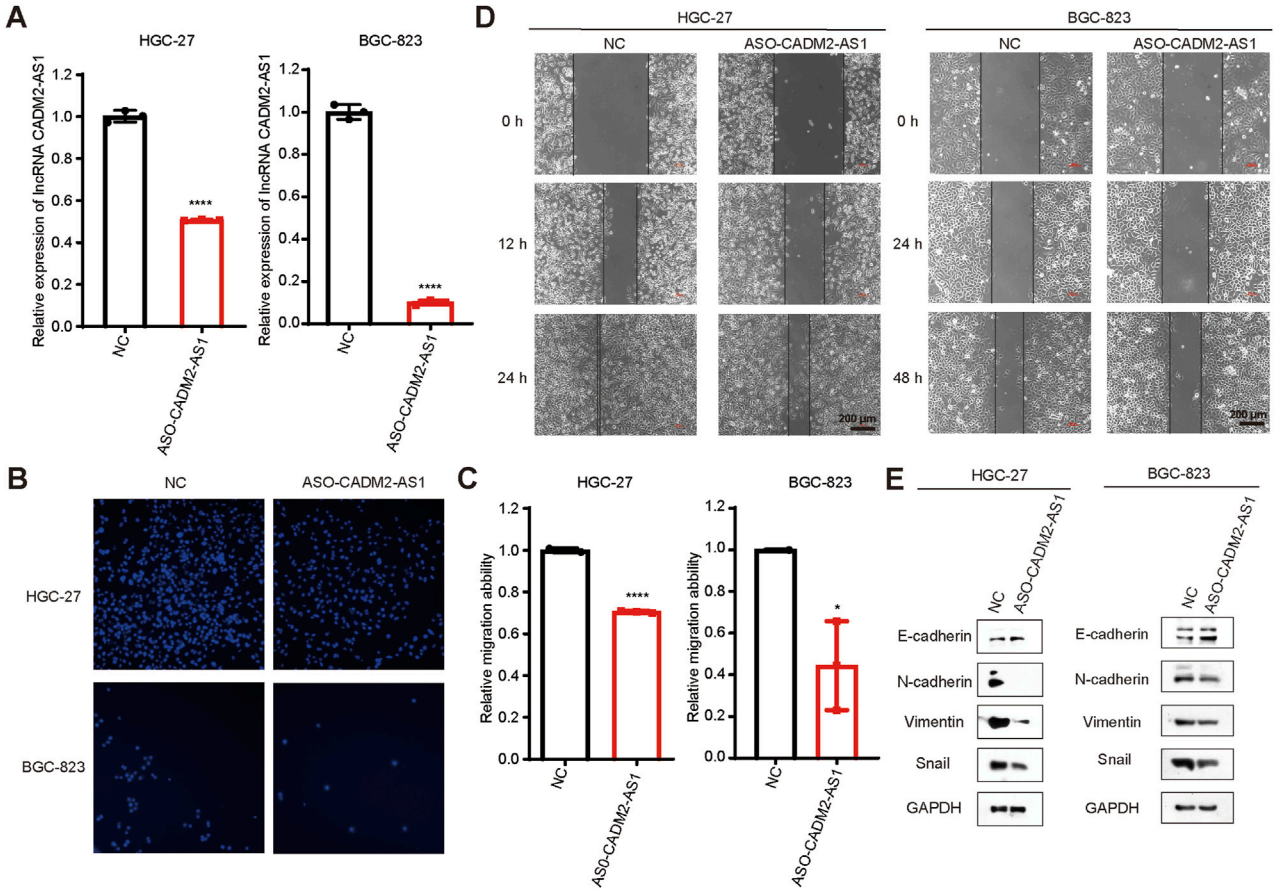

FIGURE 2
Knockdown of lncRNA CADM2-AS1 inhibited the migration activities of GC cells. **(A)** The expression of lncRNA CADM2-AS1 in HGC-27 and BGC-823 was detected by RT-qPCR assay; **(B)** Transwell verified that after knocking down lncRNA CADM2-AS1, the migration ability of HGC-27 and BGC-823 was reduced; **(C)** Figure C was the quantitative statistics of figure B; **(D)** Wound healing assay verified that knocking down lncRNA CADM2-AS1 reduced the speed of wound healing in HGC-27 and BGC-823, scale = 200 μm; **(E)** The markers of EMT progress were detected in HGC-27and BGC-823 with different conditions by Western Blot; n = 3, $*p < 0.05$, $****p < 0.0001$, $****p < 0.001$.

lungs of pCADM2-AS1 group (Figure 3I). Besides, the results of HE staining shown that the nuclei were large and stained deeply, the normal structure of the lung was destroyed, and the number of pulmonary nodules were increased in pCADM2-AS1 group, which proved that the metastasis ability of GC cells was significantly enhanced in pCADM2-AS1 group (Figure 3J). All these data proved that overexpression of lncRNA CADM2-AS1 could promote the metastasis of GC cells *in vivo*.

3.4 Overexpression of lncRNA CADM2-AS1 promotes metastasis in GC by upregulating NOTCH4 mRNA

Based on the above experiments, it has proved that the lncRNA CADM2-AS1 could promote metastasis of GC cells *in vitro* and *vivo*. However, the mechanism of lncRNA CADM2-AS1 promoting the metastasis of GC cells was still unclear, which need to be further explored. Due to different localization in cells, lncRNAs played biological functions in different ways. The result of RNA FISH assay revealed that lncRNA CADM2-AS1 was found in both the cytoplasm and nucleus of HGC-27 and BGC-823 (Figure 4A). LncRNAs competed with mRNA to bind to miRNAs, which is a classical molecular pathway for intracellular lncRNAs to function. Therefore, it is pondered that lncRNA CADM2-AS1 may encourage the metastasis of GC cells by regulating metastasis-related mRNA expression through miRNAs.

To analyze whether lncRNA CADM2-AS1 fostered metastasis of GC cells by regulating metastasis-related mRNA expression, HGC-27 pCADM2-AS1 and HGC CON GC cells were subjected to RNA-seq. It was found that mRNA levels of neurogenic locus notch homolog protein 4 (NOTCH4) was obviously upregulated after lncRNA CADM2-AS1 overexpression, which is a close regulator of tumor metastasis (Figure 4B). NOTCH4, with two intracellular and extracellular domains, is one of the four transmembrane receptors of NOTCH family (Xiu et al., 2021; Katoh and KATOH, 2020). NOTCH4 is activated binding to its corresponding ligand to participate in the NOTCH pathway, closely involving in regulating the EMT process and promoting the invasion and metastasis of colorectal cancer, breast cancer, melanoma, lung adenocarcinoma and other cancers (Zhou et al., 2020; Lin et al., 2016; Li et al., 2021; Scheurlen et al., 2022; Wu et al., 2018).

10.3389/fphar.2024.1439497

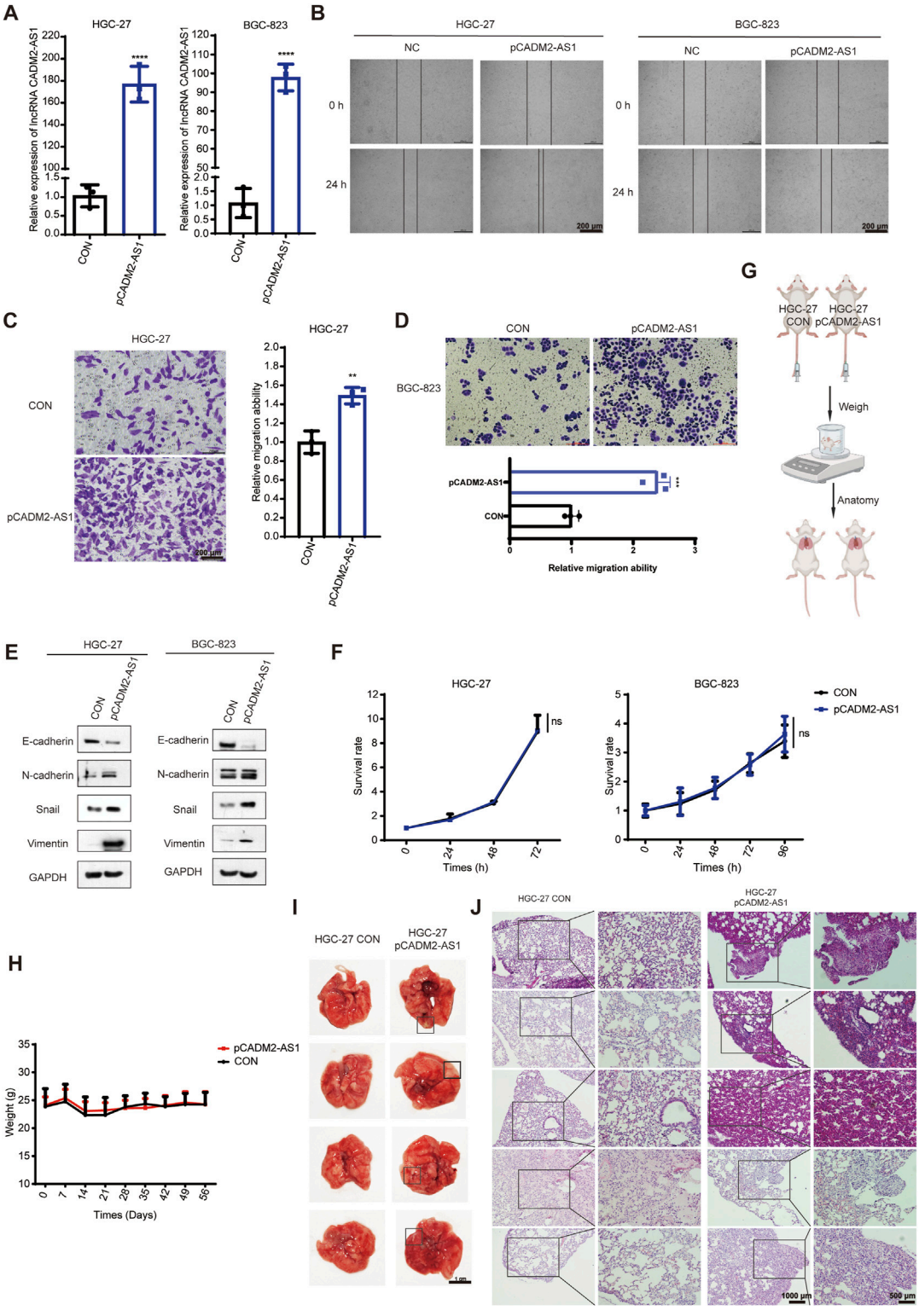

FIGURE 3
LncRNA CADM2-AS1 promoted the migration activities of GC cells. **(A)** The expression of lncRNA CADM2-AS1 in HGC-27 and BGC-823 with lentivirus infection were detected by RT-qPCR assay; **(B)** Wound healing assay was performed to detected the migration ability of HGC-27 and BGC-823 in different conditions, scale = 200 μm; **(C,D)** The effect of lncRNA CADM2-AS1 on migration ability of HGC-27 and BGC-823 was detected by Transwell assay, scale = 200 μm; **(E)** The markers of EMT progress were detected in HGC-27and BGC-823 with different conditions by Western Blot; **(F)** MTT assay was performed to detect proliferation of CON and pCADM2-AS1 cells in 96 h; n = 3; **(G)** The construction pattern diagram of mouse lung metastasis model; **(H)** The mouse in pCADM2-AS1 group and CON group was recorded; **(I)** Brightfield map of fresh lung tissues in pCADM2-AS1 group and CON group, scale = 1 cm; **(J)** Images of HE staining of lung tissues sections in pCADM2-AS1 group and CON group, scale = 1,000 μm; The right side figures were local magnification view of left side figures, scale = 500 μm; n = 6. ns, not statistically significant, $^{**}p < 0.01$, $^{****}p < 0.0001$.

10.3389/fphar.2024.1439497

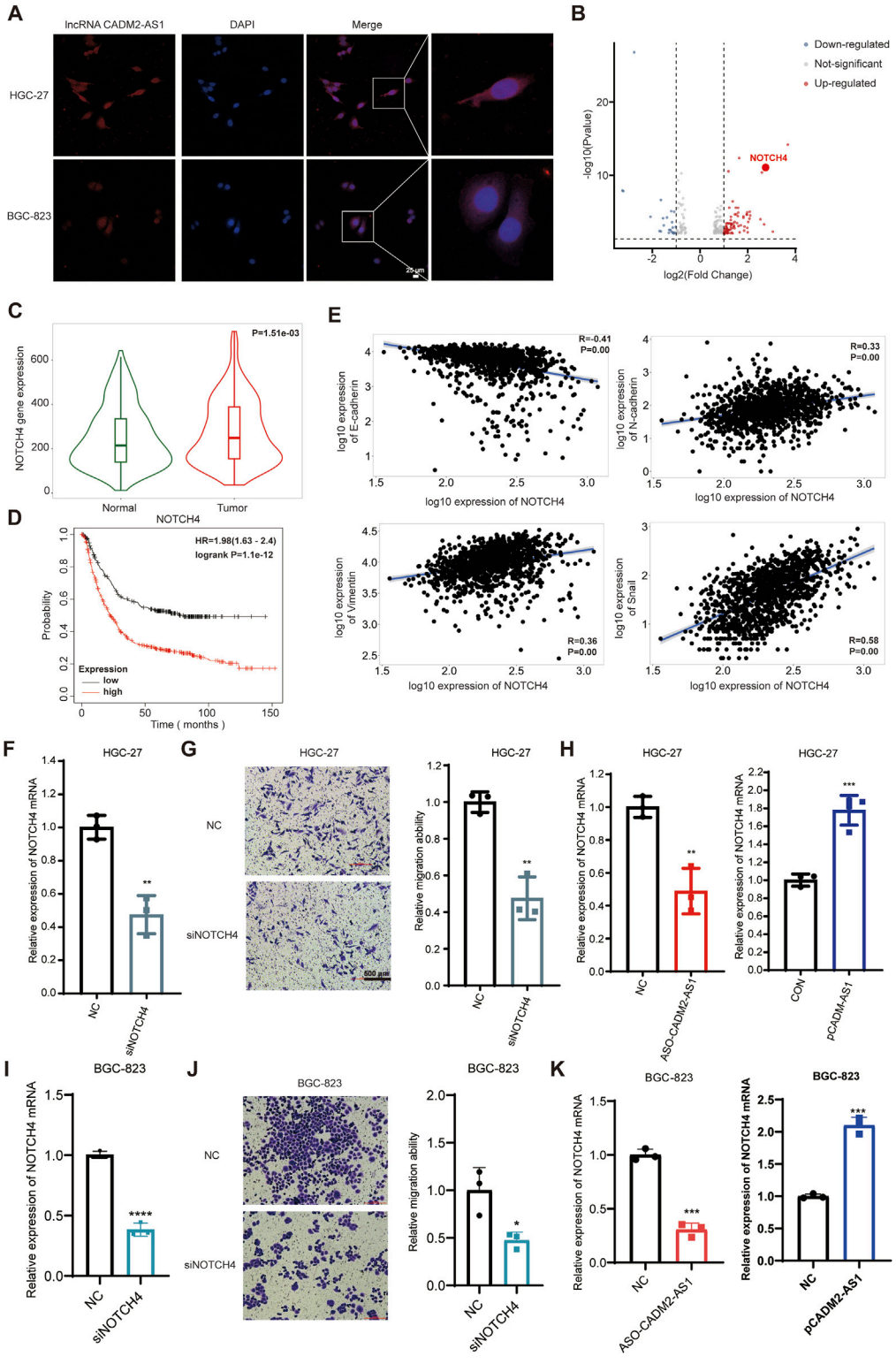

FIGURE 4
LncRNA CADM2-AS1 promote metastasis in GC by upregulating NOTCH4 mRNA. **(A)** RNA FISH assay was performed to detect subcellular localization of lncRNA CADM2-AS1 in HGC-27 and BGC-823, scale = 25 μm; Red, the Cy3 fluorescent probe represented lncRNA CADM2-AS1; Blue, DAPI represented nucleus; Merge, a merge channel graph; **(B)** Volcano plot of RNA sequencing result in HGC CON and HGC-27 pCADM2-AS1 cells; n = 3, $p < 0.05$; **(C)** The expression of NOTCH4 in GC tissues and normal tissues was searched in TNMplot database; **(D)** The relationship between NOTCH4 and prognosis in GC patients was searched in Kaplan Meier plotter database; **(E)** The relationships between NOTCH4 and EMT markers were searched in TNMplot database respectively; **(F)** RT-qPCR assay was performed to detect NOTCH4 knockdown efficiency in HGC-27 after transfecting siRNA; **(G)** The effect of NOTCH4 on migration ability of HGC-27 was detected by Transwell assay, scale = 100 μm; **(H)** The effect of lncRNA CADM2-AS1

(*Continued*)

FIGURE 4 (Continued)
on NOTCH4 in HGC-27 was detected by RT-qPCR assay; **(I)** RT-qPCR assay was performed to detect NOTCH4 knockdown efficiency in BGC-823 after transfecting siRNA; **(J)** The effect of NOTCH4 on migration ability of BGC-823 was detected by Transwell assay, scale = 100 μm; **(K)** The effect of lncRNA CADM2-AS1 on NOTCH4 in BGC-823 was detected by RT-qPCR assay; n = 3, $^{**}p < 0.01$, $^{***}p < 0.001$.

Based on the close relationship between NOTCH4 and tumor metastasis, we verify the relationship between NOTCH4 and metastasis of GC firstly. It was discovered that NOTCH4 expression in GC was higher than it in paracancerous tissues with 273 pairs of GC samples in TNMplot database (https://tnmplot.com/analysis/) (Figure 4C) (Bartha and GYŐRFFY, 2021). Moreover, high expression of NOTCH4 was associated with poor prognosis of GC patients in Kaplan Meier plotter database (Figure 4D). In addition, it was initiated NOTCH4 was negatively correlated with epithelial cell marker (E-cadherin), and was positively correlated with mesenchymal cell markers (N-cadherin, vimentin and Snail) by TNMplot database (Figure 4E). These data provide preliminary evidence that NOTCH4 contributes to the metastasis of GC. Then, we construct NOTCH4 knockdown GC cell line with NOTCH4 siRNA to verify the role of NOTCH4 in GC metastasis (Figure 4F). Compared to HGC-27 NC, the ability of HGC-27 siNOTCH4 to invade through the Transwell membrane was reduced (Figure 4G). Meanwhile, similar results were also obtained in BGC-823 cells (Figures 4I, J). All these results confirmed that NOTCH4 promoted GC metastasis. To verify the regulatory effect of lncRNA CADM2-AS1 on NOTCH4, RT-qPCR assay was performed. It was discovered that lncRNA CADM2-AS1 knockdown downregulated the level of NOTCH4 mRNA, while lncRNA CADM2-AS1 overexpression upregulated it (Figures 4H, K). These results proved that lncRNA CADM2-AS1 facilitated GC cell metastasis by raising NOTCH4 mRNA expression, but the molecular mechanism was still unknown.

3.5 LncRNA CADM2-AS1 upregulates NOTCH4 mRNA by decreasing miR-5047

To inspect the molecular mechanism of lncRNA CADM2-AS1 regulation on NOTCH4 mRNA, we search for the potential miRNAs who both bind to lncRNA CADM2-AS1 and NOTCH4 mRNA in database. There were 268 miRNAs binding to NOTCH4 mRNA were retrieved from Targetscan database (https://www.targetscan.Org/vert_80/), and 57 miRNAs binding to lncRNA CADM2-AS1 were retrieved from lncRNASNP2 database (http://bioinfo.life.hust.edu.cn/lncRNASNP/#!/); Among them, a total of 4 miRNAs (miR-1301-3p, miR-5047, miR-5706, and miR-1184) bound to lncRNA CADM2-AS1 and NOTCH4 mRNA simultaneously (Figure 5A) (Mcgeary et al., 2019; Miao et al., 2018). To verify whether lncRNA CADM2-AS1 can competitively bind to the above miRNAs, the above four miRNAs were detected by RT-qPCR with overexpression of lncRNA CADM2-AS1 firstly. Compared to CON, there were no significant differences in the level of miR-1301-3p, miR-5706 and miR-1184 when lncRNA CADM2-AS1 overexpression, while the level of miR-5047 was downregulated in HGC-27 pCADM2-AS1 (Figure 5B). The significant regulatory effect of lncRNA CADM2-AS1 on miR-5047 prompted us to speculate that miR-5047 may be the intermediate molecule between lncRNA CADM2-AS1 and NOTCH4 during the metastasis of GC.

The existing literature indicates that miR-5047 was a key negative regulator of osteosarcoma cell stemness and metastasis by target SOX2 mRNA (Chen et al., 2020). Similarly, miR-5047 significantly inhibit cervical cancer metastasis and chemoresistance by down-regulating VEGFA (Guo et al., 2019). Therefore, miR-5047 is closely related to tumor metastasis, which may also participate the metastasis of GC caused by lncRNA CADM2-AS1 overexpression.

To validate the inference of miR-5047, we detected the regulatory function of miR-5047 on the metastatic ability in GC cells firstly. The overexpression of miR-5047 GC cell line was constructed with miR-5047 mimic (Figure 5C). Besides, the result of Transwell showed that overexpression of miR-5047 inhibited the migration ability of GC cells (Figures 5D, E). The wound healing ability of HGC-27 pmiR-5047 was also weakened (Figure 5F). Meanwhile, transfecting miR-5047 mimic, the expression of epithelial cell marker (E-cadherin) was increased but the expression of mesenchymal cell markers (N-cadherin, Vimentin, Snail) was decreased when miR-5047 mimic was transfected in HGC-27 cells (Figure 5G). The overexpression of miR-5047 hindered the metastasis of GC cells. After confirming the metastasis inhibiting biological function of miR-5047 in GC, we further detected the regulatory effect of miR-5047 on NOTCH4 mRNA by RT-qPCR. The result shown that the expression of NOTCH4 mRNA was decreased while miR-5047 overexpression, which suggested that NOTCH4 was a potential target mRNA of miR-5047 (Figure 5H).

Based on the above results, we found miR-5047 may be the mediator of lncRNA CADM2-AS1 upregulation of NOTCH4 in promoting GC metastasis. To verify this inference, we recovered the level of miR-5047 in HGC-27 pCADM2-AS1 cells by transfecting miR-5047 mimic (Figure 6A). The results of Transwell and Wound healing assay shown that, with miR-5047 recovered, the enhanced migration ability of HGC-27 by lncRNA CADM2-AS1 overexpression was also re-diminished (Figures 6B–D). Similarly, with miR-5047 mimic transfecting, the downregulated expression of epithelial cell marker (E-cadherin) by lncRNA CADM2-AS1 overexpression was increased, while the upregulated expression of mesenchymal cell markers (N-cadherin, Vimentin, Snail) by lncRNA CADM2-AS1 overexpression were decreased. Furthermore, the upregulated NOTCH4 was also re-decreased by miR-5047 mimic (Figure 6E). Meanwhile, RT-qPCR showed that the low level of NOTCH4 mRNA was restored with miR-5047 re-expression in HGC-27 pCADM2-AS1 (Figure 6F). In conclusion, the results preliminarily confirmed miR-5047 may be the mediator of lncRNA CADM2-AS1 upregulation of NOTCH4 in promoting GC metastasis, which still need more experimental verification.

To confirm that miR-5047 may be the mediator between lncRNA CADM2-AS1 and NOTCH4 mRNA, the cellular

10.3389/fphar.2024.1439497

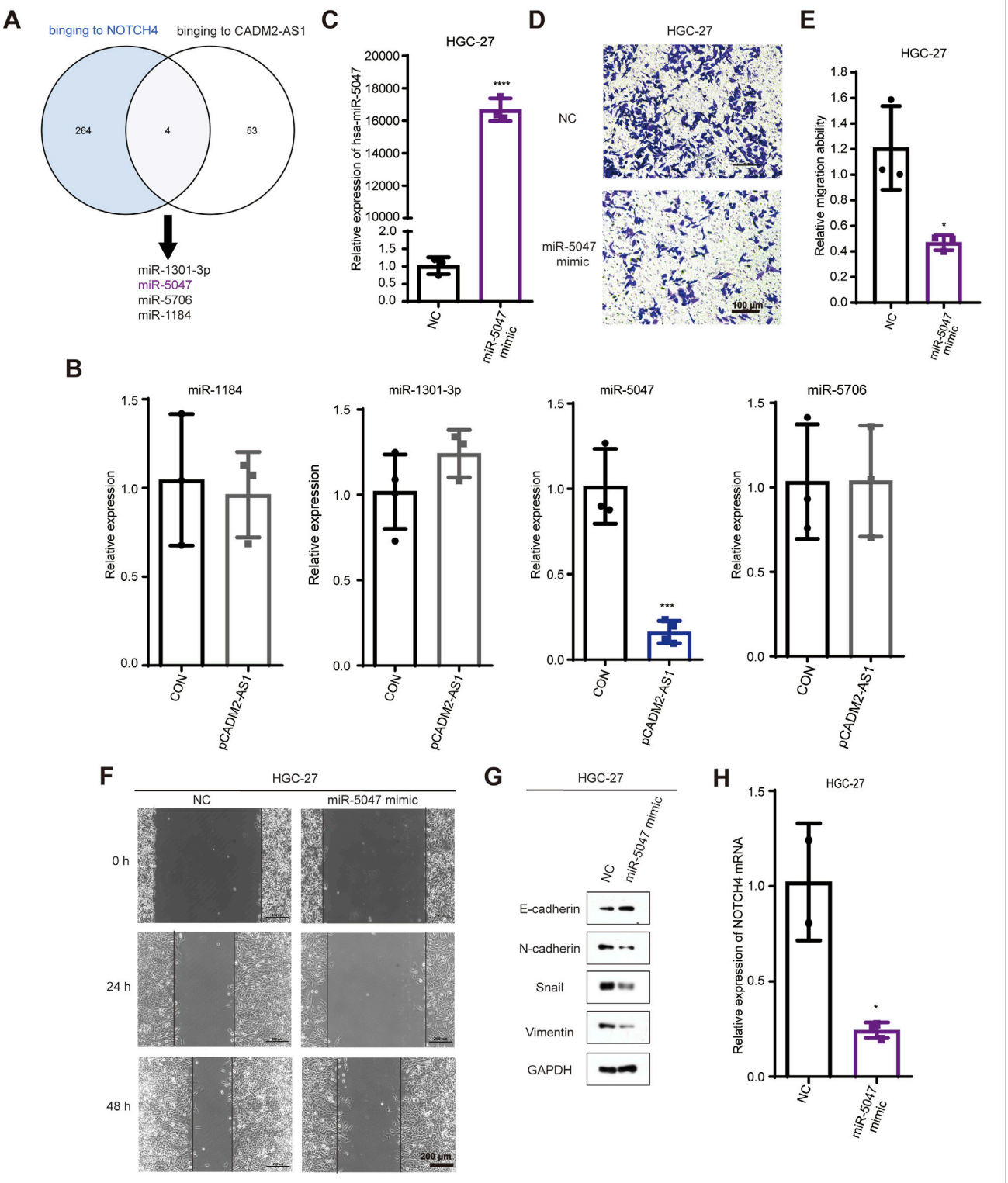

FIGURE 5
MiR-5047 may be the mediator of lncRNA CADM2-AS1 upregulation of NOTCH4 in promoting GC metastasis. **(A)** Venn Diagram of 268 miRNAs bound to NOTCH4 mRNA and 57 miRNAs bound to lncRNA CADM2-AS1 retrieved from database respectively; **(B)** RT-qPCR detected the expression of miR-1301 -3p, miR-5047, miR-5706 and miR-1184 in HGC-27 pCADM2-AS1 cells; **(C)** MiR-5047 overexpression was detected by RT-qPCR in HGC-27 which transfected with miR-5047 mimic; **(D)** The migration ability of HGC-27 with miR-5047 mimic was detected by Transwell assay, scale = 100 μm; **(E)** Figure E was the quantitative statistics of figure D; **(F)** The migration ability of HGC-27 with miR-5047 overexpression was detected by Wound healing assay, scale = 200 μm; **(G)** The expression of EMT markers in HGC-27 with the overexpression of miR-5047 were detected by Western Blot; **(H)** RT-qPCR verified the level of NOTCH4 mRNA in HGC-27 cells with overexpression of miR-5047; n = 3, *$p < 0.05$, ***$p < 0.001$, ****$p < 0.0001$.

10.3389/fphar.2024.1439497

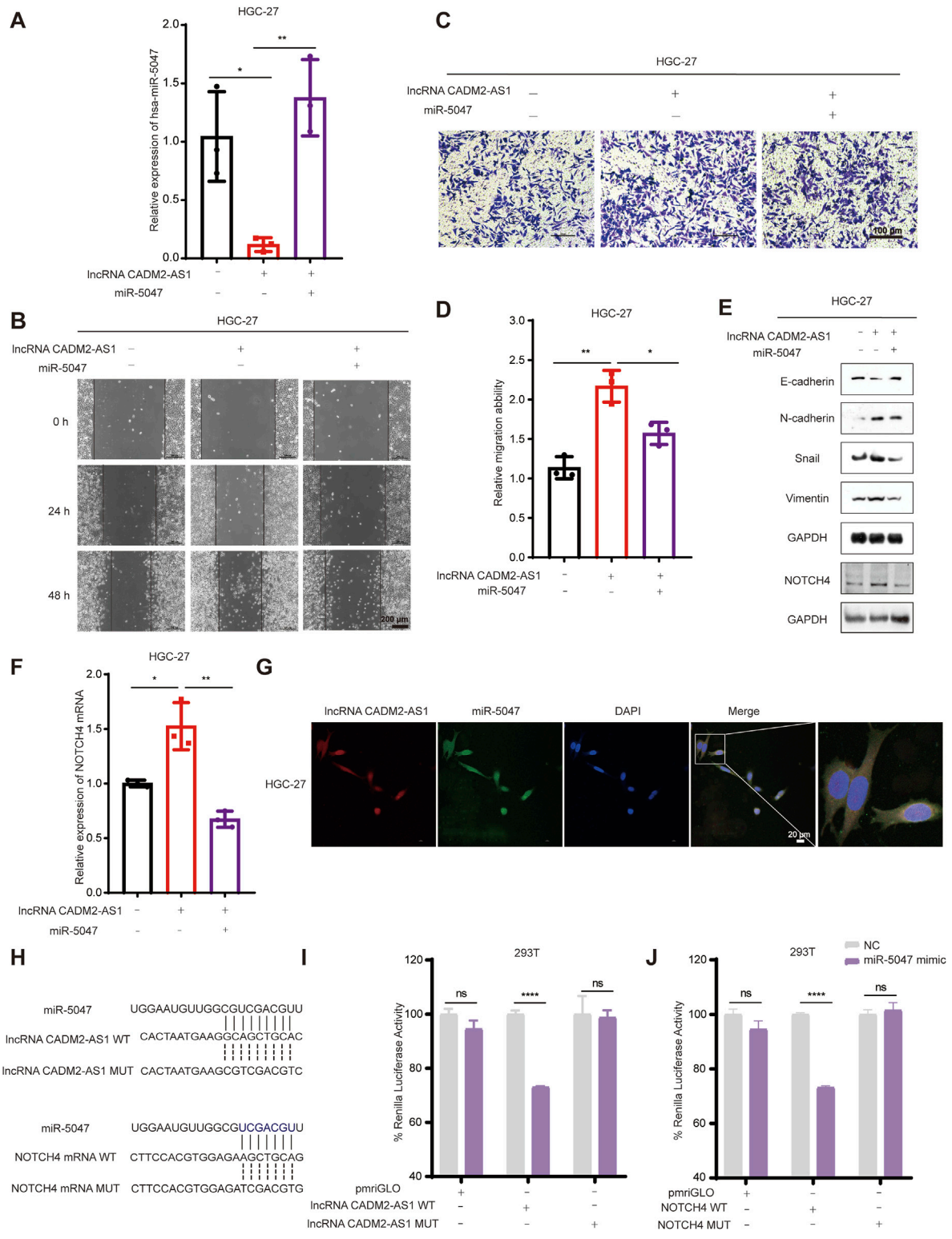

FIGURE 6
LncRNA CADM2-AS1 promoted GC metastasis by targeting the miR-5047/NOTCH4 signaling axis. **(A)** RT-qPCR assay was performed to detect miR-5047 overexpression efficiency in HGC-27 pCADM2-AS1 cell after transfecting miR-5047 mimic; **(B)** Wound healing assay was performed to detect the migration ability of HGC-27 cells in different conditions, scale = 200 μm; **(C)** Transwell assay was performed to detect the migration ability of HGC-27 cells in different conditions, scale = 100 μm; **(D)** Figure D was the quantitative statistics of figure C; **(E)** The expression of EMT-associated markers and NOTCH4 protein in HGC-27 cells were detected by Western Blot; **(F)** The level of NOTCH4 mRNA in HGC-27 cells with different treatment were detected by RT-qPCR assay; **(G)** RNA FISH assay was performed to detect colocalization between lncRNA CADM2-AS1 and miR-5047, scale = 20 μm; Red, Cy3 fluorescent probe represented lncRNA CADM2-AS1; Green, FAM fluorescent probe represented miR-5047; Blue, DAPI represented the nucleus;
(*Continued*)

FIGURE 6 (Continued)
Merge, a merge channel graph; **(H)** The predicted targeting sequence of miR-5047 on the lncRNA CADM2-AS1 and NOTCH4 mRNA. **(I)** Dual-luciferase reporter assay was performed to detect the targeting binding between lncRNA CADM2-AS1 and miR-5047; **(J)** Dual-luciferase reporter assay was performed to detect the targeting binding between NOTCH4 mRNA and miR-5047; Gray, represented the NC; Purple, represented 293T cells with miR-5047 overexpression; n = 3, $*p < 0.05$, $**p < 0.01$, $***p < 0.001$, $****p < 0.0001$.

sublocalization of lncRNA CADM2-AS1 and miR-5047 was detected by RNA FISH assay firstly. The miR-5047 and lncRNA CADM2-AS1 were substantially co-localized in the cells, which signified that they had the possibility to combine with each other (Figure 6G). Meanwhile, bioinformatics prediction by RNA22 and Targetscan databases showed both lncRNA CADM2-AS1 and NOTCH4 mRNA might directly bind with the seed sequence (2-8 nucleotides) of miR-5047 (Figure 6H). Therefore, the Dual-luciferase reporter assay was performed to verify the binding between lncRNA CADM2-AS1 and miR-5047, as well as the binding between NOTCH4 mRNA and miR-5047. The result of Dual-luciferase reporter assay showed that overexpression of miR-5047 significantly reduced the fluorescence intensity of firefly luciferase from lncRNA CADM2-AS1 WT plasmid, while the fluorescence intensity of firefly luciferase from lncRNA CADM2-AS1 MUT plasmid had no obvious variation (Figure 6I). LncRNA CADM2-AS1 targeting bind with miR-5047. Identically, miR-5047 overexpression considerably reduced the fluorescence intensity of firefly luciferase from NOTCH4 WT plasmid, nevertheless, the fluorescence intensity of firefly luciferase from NOTCH4 MUT plasmid had no obvious change. The NOTCH4 was the target mRNA of miR-5047 (Figure 6J). To sum up, miR-5047 was the mediator of lncRNA CADM2-AS1 upregulation of NOTCH4 in promoting GC metastasis, which means that lncRNA CADM2-AS1 promoted GC metastasis by targeting the miR-5047/NOTCH4 signaling axis.

To explore whether lncRNA CADM2-AS1 promote metastasis by miR-5047/NOTCH4 signaling axis, the lung metastasis model in NOD/SCID mouse was established by injecting HGC-27 CON, pCADM2-AS1 and pCADM2-AS1+miR-5047 cells into tail vein separately (Figure 7A). The weights were performed once a week. There was no significant difference in weight among the three groups (Figure 7B), while the lung nodules were obviously formed only in the lungs of pCADM2-AS1 group (Figure 7C). Compared to pCADM2-AS1 group, the recovery of miR-5047 in pCADM2-AS1 HGC-27 cells alleviated the ability of lncRNA CADM2-AS1 to promote metastasis of GC cells (Figures 7D, E). These phenomena proved lncRNA CADM2-AS1 can promote the metastasis of GC cells to the lung via miR-5047/NOTCH4 signaling axis *in vivo*.

3.6 LncRNA CADM2-AS1/miR-5047/NOTCH4 mRNA signaling axis was explored in clinical samples

To verify the molecular mechanism of lncRNA CADM2-AS1 promoting GC metastasis by lncRNA CADM2-AS1/miR-5047/NOTCH4 mRNA signaling axis in metastatic GC patient tissues, 50 pair GC tissues and tumor-adjacent tissue were collected (Supplementary Table 1). There were 24 GC patients with lymph node metastasis and 25 GC patients without lymph node metastasis in the 50 pair tissues. Total RNA and miRNA were extracted respectively to detect the levels of lncRNA CADM2-AS1, NOTCH4 and miR-5047. It was found that the levels of lncRNA CADM2-AS1 and NOTCH4 mRNA in GC tissues with lymph node metastasis were notably higher than that in tumor-adjacent tissues respectively (Figures 8A, B), while the level of miR-5047 in GC tissues with lymph node metastasis was lower than that in tumor-adjacent tissues (Figure 8C). However, in tissues without lymph node metastasis, the expression of lncRNA CADM2-AS1, NOTCH4 mRNA and miR-5047 were no differences between GC tissues and tumor-adjacent tissues (Figures 8A–C). Moreover, it was discovered that the expression of lncRNA CADM2-AS1 was positively correlated with the expression of NOTCH4 mRNA (Figure 8D), while the expression of miR-5047 was negatively correlated with the expression of lncRNA CADM2-AS1 and NOTCH4 mRNA in GC tissues with lymph node metastasis (Figures 8E, F). However, in the tissues without lymph node metastasis, although the expression of lncRNA CADM2-AS1 was positively correlated with the expression of NOTCH4 mRNA, the relationships among miR-5047, lncRNA CADM2-AS1 and NOTCH4 mRNA has no statistical significance (Figures 8D–F). The regulation of lncRNA CADM2-AS1 on miR-5047 and NOTCH4 also existed in clinical tissues of GC with lymph node metastasis, which provided a new potential idea for the treatment of metastatic GC.

4 Conclusions

The number of new cases and deaths of GC were plentiful for long time (Siegel et al., 2022; Liu et al., 2022). It is becoming increasingly clear that lncRNAs are ubiquitous and novel classes of genes involved in GC (Okada et al., 2019). However, it has not been extensively studied how lncRNAs drive metastasis of GC. After profiling lncRNAs dysregulated between GC lymph node metastasis and normal tissues via lncRNA-seq, we identified plenty of lncRNAs with continuously elevated or decreased expression patterns in these tissues. Among them, the expression of lncRNA CADM2-AS1 increased obviously, which suggested that lncRNA CADM2-AS1 may involve in metastasis of GC.

The further study demonstrated that lncRNA CADM2-AS1 knockdown inhibited migration abilities of GC cells, while lncRNA CADM2-AS1 overexpression promoted the metastasis of GC cells. Moreover, epithelial cell marker (E-cadherin) was upregulated and mesenchymal cell markers (N-cadherin, Vimentin, Snail) were downregulated with lncRNA CADM2-AS1 knockdown; lncRNA CADM2-AS1 overexpression also enhanced the expression of N-cadherin, Vimentin and Snail and decreased the

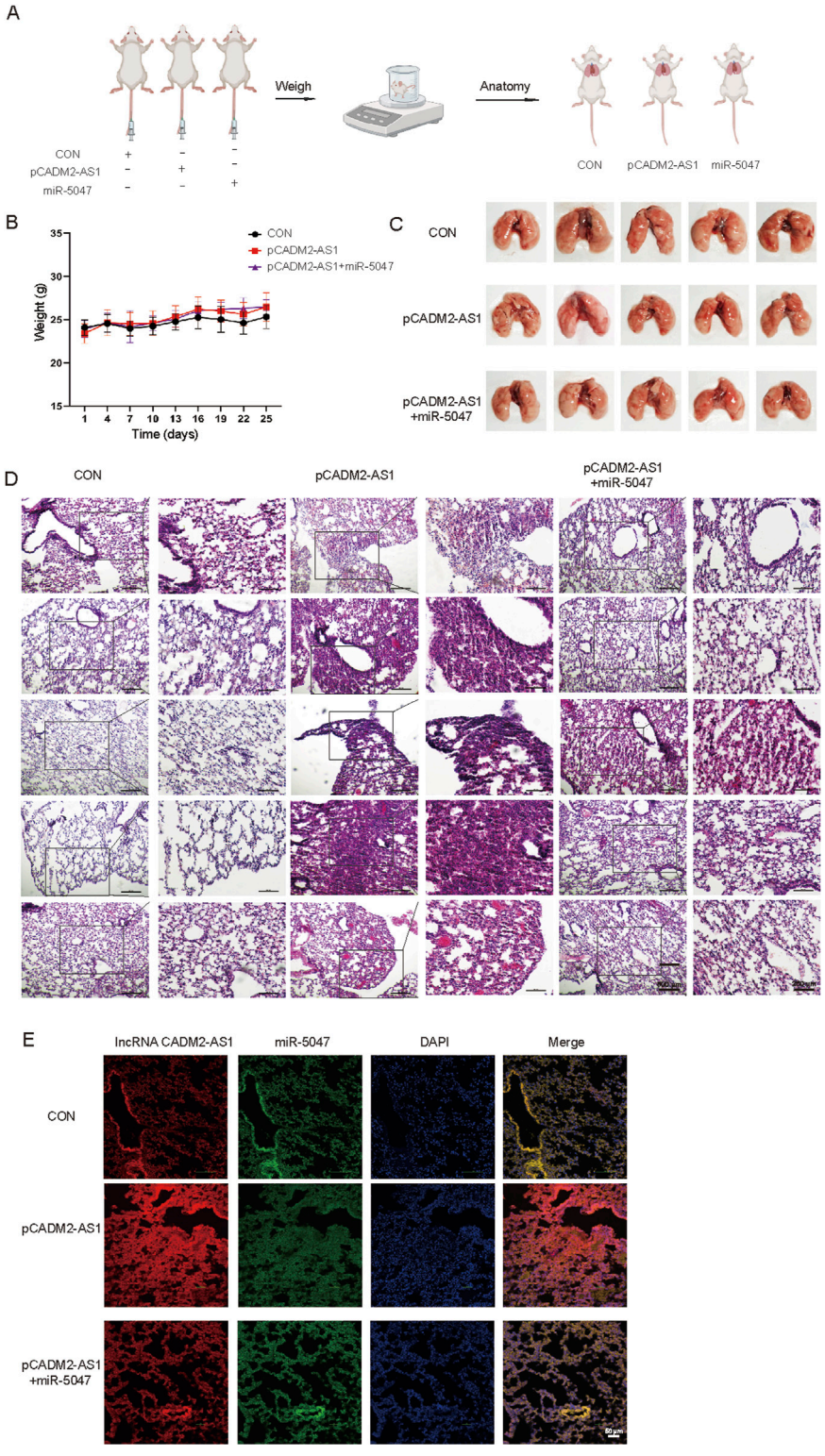

FIGURE 7
LncRNA CADM2-AS1 promoted the metastasis of GC cells via miR-5047/NOTCH4 signaling axis *in vivo*. **(A)** Mouse lung metastasis model construction pattern diagram; **(B)** With the lung metastasis model constructed, the mice were weighted in three groups once a week; **(C)** Brightfield map of fresh lung in pCADM2-AS1+miR-5047 group, pCADM2-AS1 group and control group; **(D)** HE staining of lung section in pCADM2-AS1+miR-5047 group, pCADM2-AS1 group and control group, scale = 500 μm; The figure on the right-side was a local magnification view, scale = 250 μm; n = 6; **(E)** RNA FISH assay was performed to detect the expression of lncRNA CADM2-AS1 and miR-5047 in GC, scale = 50 μm; Red, the Cy3 fluorescent probe represented lncRNA CADM2-AS1; Green, the FAM fluorescent probe represented miR-5047; Blue, DAPI represented nucleus; Merge, a merge channel graph.

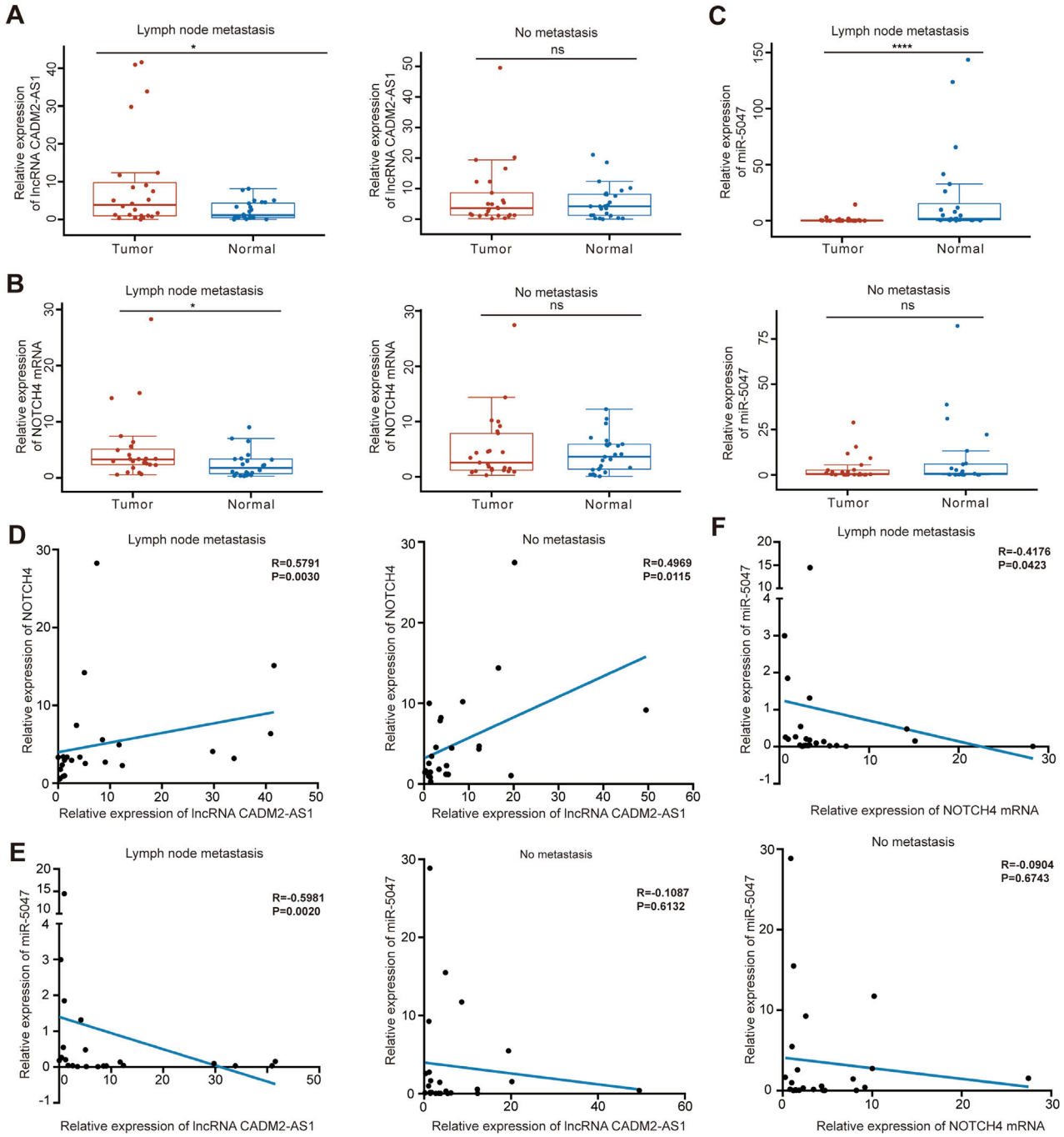

FIGURE 8
LncRNA CADM2-AS1/miR-5047/NOTCH4 mRNA signaling axis was explored in clinical tissues. **(A)**. The level of lncRNA CADM2-AS1 in GC tissues and tumor-adjacent were detected by RT-qPCR, the data were analyzed in GC tissues with or without lymph node metastasis separately and plotted in Hiplot Pro website; **(B)**. The level of NOTCH4 mRNA in GC tissues and tumor-adjacent were detected and analyzed; **(C)** The level of miR-5047 in GC tissues and tumor-adjacent were detected and analyzed; **(D)** The relationship between lncRNA CADM2-AS1 and NOTCH4 mRNA was analyzed by spearman analysis in GC tissues with or without lymph node metastasis respectively; **(E)** The relationship between lncRNA CADM2-AS1 and miR-5047 was analyzed by spearman analysis in GC tissues with or without lymph node metastasis respectively; **(F)** The relationship between NOTCH4 mRNA and miR-5047 was analyzed by spearman analysis in GC tissues with or without lymph node metastasis respectively; ns, not significantly different, $*p < 0.05$, $****p < 0.0001$.

expression of E-cadherin, which were necessary for GC cell metastasis. In addition, the results of lung metastasis models shown that overexpression of lncRNA CADM2-AS1 increased the number of pulmonary nodules. All these data proved that high expression of lncRNA CADM2-AS1 facilitate GC cells metastasis *in vitro* and *in vivo*.

However, there have been not enough reports on the role of lncRNA CADM2-AS1 in GC metastasis. The location of lncRNA

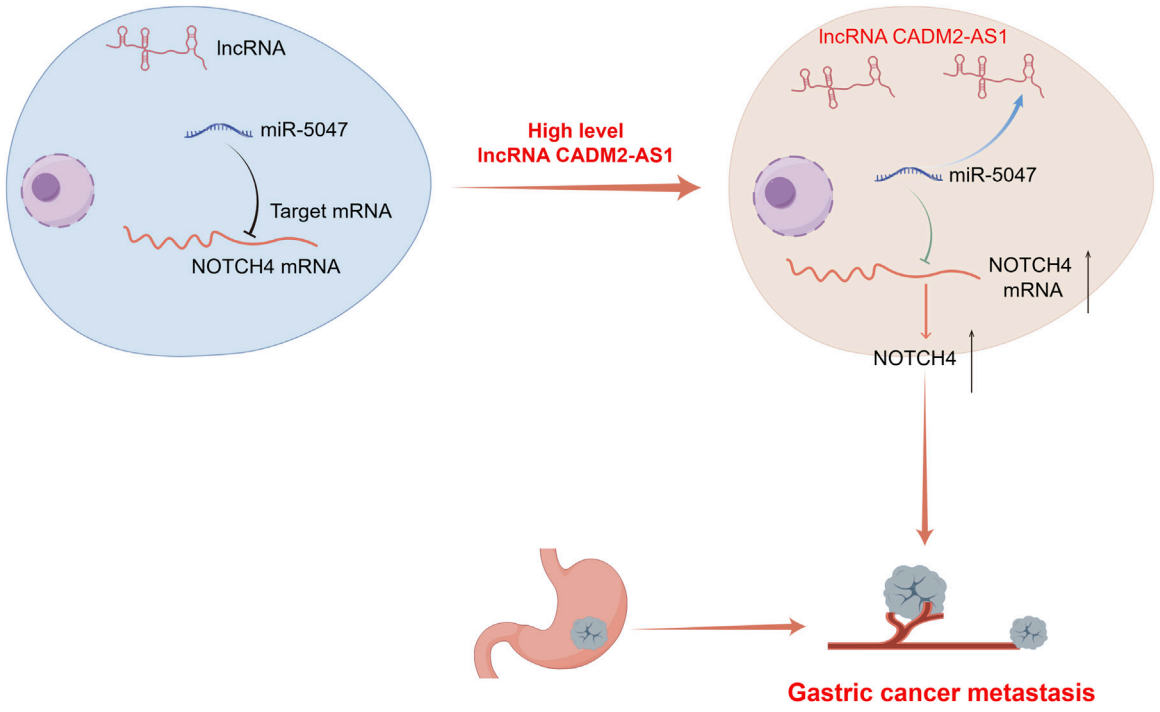

FIGURE 9
A diagram for this article. Elevated expression of LncRNA CADM2-AS1 promoted metastasis in GC by targeting the miR-5047/NOTCH4 signaling axis. Diagram drew by Figdraw.

CADM2-AS1 in cytoplasm suggested that it might act through the miRNA/mRNA signaling axis. In addition, the result of RNA-seq revealed that overexpression of lncRNA CADM2-AS1 could markedly increase NOTCH4 mRNA expression. Therefore, we speculated that lncRNA CADM2-AS1 improved metastasis of GC by raising NOTCH4 mRNA.

As expected, our results confirmed our hypothesis. NOTCH4 was a significant promoter of GC metastasis, and lncRNA CADM2-AS1 overexpression could upregulate NOTCH4 mRNA by down-regulating miR-5047. Meanwhile, the results of Dual-luciferase reporter assays showed that miR-5047 bound to both lncRNA CADM2-AS1 and NOTCH4. Besides, with miR-5047 recovered in HGC-27 pCADM2-AS1, the enhanced migration ability of HGC-27 by lncRNA CADM2-AS1 upregulated NOTCH4 mRNA was also re-diminished *in vitro* and *in vivo*. MiR-5047 was the mediator of lncRNA CADM2-AS1 upregulation of NOTCH4 in promoting GC metastasis.

What is more, lncRNA CADM2-AS1 expression was positively correlated with the expression of NOTCH4 mRNA in GC tissues with lymph node metastasis, while miR-5047 expression was negatively correlated with the expression of lncRNA CADM2-AS1 and NOTCH4 mRNA. The regulation of lncRNA CADM2-AS1 on miR-5047 and NOTCH4 also existed in clinical tissues of GC with lymph node metastasis, which give lncRNA CADM2-AS1 the potential to a prognostic and predictive biomarker in treatment of metastatic GC.

In conclusion, high lncRNA CADM2-AS1 expression upregulated NOTCH4 mRNA to promote metastasis of GC cells by silencing miR-5047 both *in vitro* and *in vivo* (Figure 9). The relationship among lncRNA CADM2-AS1, miR-5047 and NOTCH4 was further detected and verified in metastatic GC patient tissues. These results offered strong support for the hypothesis that LncRNA CADM2-AS1 may be a potential target for metastasic GC prognosis in the clinic. Targeting reduced LncRNA CADM2-AS1 may contribute to inhibit the progression of GC metastasis, which has great significance to propose a new treatment plan for metastasic GC.

5 Discussion

In the present study, the overexpression of lncRNA CADM2-AS1 was found and verified from clinic GC patient tissues, which endows this study with high research significance because it starts from clinical phenomena. Based on the exploration the mechanism that high expression of lncRNA CADM2-AS1 promote metastasis of GC cells by upregulated the target mRNA of miR-5047, NOTCH4, *in vitro* and *in vivo*. The relationship among lncRNA CADM2-AS1, miR-5047 and NOTCH4 was further detected and verified in metastatic GC patient tissues. These results offered strong support for the hypothesis that lncRNA CADM2-AS1 may be a potential target for metastasic GC prognosis in the clinic. Therefore, inhibition of GC metastasis via precisely controlling lncRNA CADM2-AS1 levels might represent as potential therapeutic methods. Uncovering the precise role of lncRNA CADM2-AS1/miR-5047/NOTCH4 regulatory axis in GC metastasis will not only increase our knowledge of noncoding RNAs-regulated therapeutic effect in cancer metastasis and the underlying regulatory mechanism, but also help develop more efficient strategies to reduce the incidence of GC metastasis.

Data availability statement

The datasets presented in this study can be found in online repositories. The mRNA-seq data have been submitted in SRA database, and the number was PRJNA1115977.

Ethics statement

The studies involving humans were approved by Ethics Committee of Zhengzhou University People's Hospital. The studies were conducted in accordance with the local legislation and institutional requirements. The participants provided their written informed consent to participate in this study. The animal study was approved by Ethics Committee of Zhengzhou University Health Science Center. The study was conducted in accordance with the local legislation and institutional requirements.

Author contributions

Y-TZ: Data curation, Formal Analysis, Methodology, Writing–original draft. L-JZ: Conceptualization, Investigation, Supervision, Writing–review and editing. TZ: Resources, Validation, Writing–review and editing. J-YZ: Data curation, Validation, Writing–review and editing. Y-PG: Data curation, Validation, Writing–review and editing. Q-RZ: Investigation, Project administration, Supervision, Writing–review and editing. P-CS: Funding acquisition, Resources, Writing–review and editing. W-CC: Funding acquisition, Resources, Writing–review and editing.

Funding

The author(s) declare that financial support was received for the research, authorship, and/or publication of this article. This study was supported by the National Natural Science Foundation of China (No. U21A20416 and 82020108030, No. 82103997); Science and Technology Project of Henan Province (No. 232102311179); the China Postdoctoral Science Foundation (Nos 2021M692950 and 2021M702942); the Basic Research of the Key Project of the High Education from the Education Department of Henan Province (No. 22ZX008); Youth Supporting Program from Henan Province (No. 2021HYTP060); Youth Supporting Program from Zhengzhou University (No. JC202044046); Medical Science and Technique Foundation of Henan province (Nos LHGJ20220021, SBGJ202102025 and SBGJ202102028).

Conflict of interest

The authors declare that the research was conducted in the absence of any commercial or financial relationships that could be construed as a potential conflict of interest.

Publisher's note

All claims expressed in this article are solely those of the authors and do not necessarily represent those of their affiliated organizations, or those of the publisher, the editors and the reviewers. Any product that may be evaluated in this article, or claim that may be made by its manufacturer, is not guaranteed or endorsed by the publisher.

Supplementary material

The Supplementary Material for this article can be found online at: https://www.frontiersin.org/articles/10.3389/fphar.2024.1439497/full#supplementary-material

References

Bartha, Á., and Győrffy, B. (2021). TNMplot.com: a web tool for the comparison of gene expression in normal, tumor and metastatic tissues. *Int. J. Mol. Sci.* 22 (5), 2622. doi:10.3390/ijms22052622

Braga, E. A., Fridman, M. V., Moscovtsev, A. A., Filippova, E. A., Dmitriev, A. A., and Kushlinskii, N. E. (2020). LncRNAs in ovarian cancer progression, metastasis, and main pathways: ceRNA and alternative mechanisms. *Int. J. Mol. Sci.* 21 (22), 8855. doi:10.3390/ijms21228855

Chen, C., Jiang, L., Zhang, Y., and Zheng, W. (2020). FOXA1-induced LINC01207 facilitates head and neck squamous cell carcinoma via up-regulation of TNRC6B. *Biomed. and Pharmacother. = Biomedecine and Pharmacother.* 128, 110220. doi:10.1016/j.biopha.2020.110220

Fang, Y., Dou, R., Huang, S., Han, L., Fu, H., Yang, C., et al. (2022). LAMC1-mediated preadipocytes differentiation promoted peritoneum pre-metastatic niche formation and gastric cancer metastasis. *Int. J. Biol. Sci.* 18 (7), 3082–3101. doi:10.7150/ijbs.70524

Gao, Y., Zhang, N., Zeng, Z., Wu, Q., Jiang, X., Li, S., et al. (2022). LncRNA PCAT1 activates SOX2 and suppresses radioimmune responses via regulating cGAS/STING signalling in non-small cell lung cancer. *Clin. Transl. Med.* 12 (4), e792. doi:10.1002/ctm2.792

Guo, J., Chen, M., Ai, G., Mao, W., Li, H., and Zhou, J. (2019). Hsa_circ_0023404 enhances cervical cancer metastasis and chemoresistance through VEGFA and autophagy signaling by sponging miR-5047. *Biomed. and Pharmacother. = Biomedecine and Pharmacother.* 115, 108957. doi:10.1016/j.biopha.2019.108957

Guo, K., Qian, K., Shi, Y., Sun, T., and Wang, Z. (2021). LncRNA-MIAT promotes thyroid cancer progression and function as ceRNA to target EZH2 by sponging miR-150-5p. *Cell death and Dis.* 12 (12), 1097. doi:10.1038/s41419-021-04386-0

Győrffy, B. (2021). Survival analysis across the entire transcriptome identifies biomarkers with the highest prognostic power in breast cancer. *Comput. Struct. Biotechnol. J.* 19, 4101–4109. doi:10.1016/j.csbj.2021.07.014

Han, T. S., Hur, K., Cho, H. S., and Ban, H. S. (2020). Epigenetic associations between lncRNA/circRNA and miRNA in hepatocellular carcinoma. *Cancers* 12 (9), 2622. doi:10.3390/cancers12092622

He, F., Wang, S., Zheng, R., Gu, J., Zeng, H., Sun, K., et al. (2024). Trends of gastric cancer burdens attributable to risk factors in China from 2000 to 2050. *Lancet Regional Health-Western Pac.* 44, 101003. doi:10.1016/j.lanwpc.2023.101003

Katoh, M., and Katoh, M. (2020). Precision medicine for human cancers with Notch signaling dysregulation (Review). *Int. J. Mol. Med.* 45 (2), 279–297. doi:10.3892/ijmm.2019.4418

Kroese, T. E., Van Laarhoven, H. W. M., Nilsson, M., Lordick, F., Guckenberger, M., Ruurda, J. P., et al. (2022). Definition of oligometastatic esophagogastric cancer and impact of local oligometastasis-directed treatment: A systematic review and meta-analysis. *Eur. J. Cancer* 166, 254–269. doi:10.1016/j.ejca.2022.02.018

Li, B., Kang, H., Xiao, Y., Du, Y., Song, G., et al. (2022c). LncRNA GAL promotes colorectal cancer liver metastasis through stabilizing GLUT1. *Oncogene* 41 (13), 1882–1894. doi:10.1038/s41388-022-02230-z

Li, G. Z., Doherty, G. M., and Wang, J. (2022a). Surgical management of gastric cancer: a review. *JAMA Surg.* 157 (5), 446–454. doi:10.1001/jamasurg.2022.0182

Li, X., Cao, X., Zhao, H., Guo, M., Fang, X., Li, K., et al. (2021). Hypoxia activates Notch4 via ERK/JNK/P38 MAPK signaling pathways to promote lung adenocarcinoma

progression and metastasis. *Front. Cell Dev. Biol.* 9, 780121. doi:10.3389/fcell.2021.780121

Li, Y., Hu, J., Guo, D., Ma, W., Zhang, X., Zhang, Z., et al. (2022b). LncRNA SNHG5 promotes the proliferation and cancer stem cell-like properties of HCC by regulating UPF1 and Wnt-signaling pathway. *Cancer gene Ther.* 29 (10), 1373–1383. doi:10.1038/s41417-022-00456-3

Lin, X., Sun, B., Zhu, D., Zhao, X., Sun, R., Zhang, Y., et al. (2016). Notch4+ cancer stem-like cells promote the metastatic and invasive ability of melanoma. *Cancer Sci.* 107 (8), 1079–1091. doi:10.1111/cas.12978

Liu, Q., Tang, J., Chen, S., Hu, S., Shen, C., Xiang, J., et al. (2022). Berberine for gastric cancer prevention and treatment: Multi-step actions on the Correa's cascade underlie its therapeutic effects. *Pharmacol. Res.* 184, 106440. doi:10.1016/j.phrs.2022.106440

Loher, P., and Rigoutsos, I. (2012). Interactive exploration of RNA22 microRNA target predictions. *Bioinforma. Oxf. Engl.* 28 (24), 3322–3323. doi:10.1093/bioinformatics/bts615

Ma, D., Zhang, Y., Shao, X., Wu, C., and Wu, J. (2022). PET/CT for predicting occult lymph node metastasis in gastric cancer. *Curr. Oncol. Tor. Ont.* 29 (9), 6523–6539. doi:10.3390/curroncol29090513

Machlowska, J., Baj, J., Sitarz, M., Maciejewski, R., and Sitarz, R. (2020). Gastric cancer: epidemiology, risk factors, classification, genomic characteristics and treatment strategies. *Int. J. Mol. Sci.* 21 (11), 4012. doi:10.3390/ijms21114012

Mcgeary, S. E., Lin, K. S., Shi, C. Y., Pham, T. M., Bisaria, N., Kelley, G. M., et al. (2019). The biochemical basis of microRNA targeting efficacy. *Sci. (New York, NY)* 366 (6472), eaav1741. doi:10.1126/science.aav1741

Miao, Y. R., Liu, W., Zhang, Q., and Guo, A. Y. (2018). lncRNASNP2: an updated database of functional SNPs and mutations in human and mouse lncRNAs. *Nucleic Acids Res.* 46 (D1), D276–D280. doi:10.1093/nar/gkx1004

Okada, S., Vaeteewoottacharn, K., and Kariya, R. (2019). Application of highly immunocompromised mice for the establishment of patient-derived xenograft (PDX) models. *Cells* 8, 889. doi:10.3390/cells8080889

Oki, E., Tokunaga, S., Emi, Y., Kusumoto, T., Yamamoto, M., Fukuzawa, K., et al. (2016). Surgical treatment of liver metastasis of gastric cancer: a retrospective multicenter cohort study (KSCC1302). *Gastric cancer* 19 (3), 968–976. doi:10.1007/s10120-015-0530-z

Scheurlen, K. M., Chariker, J. H., Kanaan, Z., Littlefield, A. B., George, J. B., Seraphine, C., et al. (2022). The NOTCH4-GATA4-IRG1 axis as a novel target in early-onset colorectal cancer. *Cytokine and growth factor Rev.* 67, 25–34. doi:10.1016/j.cytogfr.2022.06.002

Siegel, R. L., Giaquinto, A. N., and Jemal, A. (2024). Cancer statistics, 2024. *CA a cancer J. Clin.* 74 (1), 12–49. doi:10.3322/caac.21820

Siegel, R. L., Miller, K. D., Fuchs, H. E., and Jemal, A. (2022). Cancer statistics, 2022. *CA a cancer J. Clin.* 72 (1), 7–33. doi:10.3322/caac.21708

Singh, N., Ramnarine, V. R., Song, J. H., Pandey, R., Padi, S. K. R., Nouri, M., et al. (2021). The long noncoding RNA H19 regulates tumor plasticity in neuroendocrine prostate cancer. *Nat. Commun.* 12 (1), 7349. doi:10.1038/s41467-021-26901-9

Smyth, E. C., Nilsson, M., Grabsch, H. I., van Grieken, N. C., and Lordick, F. (2020). Gastric cancer. *Lancet (London, Engl.)* 396 (10251), 635–648. doi:10.1016/S0140-6736(20)31288-5

Sun, L., Li, J., Yan, W., Yao, Z., Wang, R., Zhou, X., et al. (2021). H19 promotes aerobic glycolysis, proliferation, and immune escape of gastric cancer cells through the microRNA-519d-3p/lactate dehydrogenase A axis. *Cancer Sci.* 112 (6), 2245–2259. doi:10.1111/cas.14896

Syllaios, A., Moris, D., Karachaliou, G. S., Sakellariou, S., Karavokyros, I., Gazouli, M., et al. (2021). Pathways and role of MALAT1 in esophageal and gastric cancer. *Oncol. Lett.* 21 (5), 343. doi:10.3892/ol.2021.12604

Thrumurthy, S. G., Chaudry, M. A., Chau, I., and Allum, W. (2015). Does surgery have a role in managing incurable gastric cancer? *Nat. Rev. Clin. Oncol.* 12 (11), 676–682. doi:10.1038/nrclinonc.2015.132

Wang, J., Xie, S., Yang, J., Xiong, H., Jia, Y., Zhou, Y., et al. (2019a). The long noncoding RNA H19 promotes tamoxifen resistance in breast cancer via autophagy. *J. Hematol. and Oncol.* 12 (1), 81. doi:10.1186/s13045-019-0747-0

Wang, L., Cho, K. B., Li, Y., Tao, G., Xie, Z., and Guo, B. (2019b). Long noncoding RNA (lncRNA)-Mediated competing endogenous RNA networks provide novel potential biomarkers and therapeutic targets for colorectal cancer. *Int. J. Mol. Sci.* 20 (22), 5758. doi:10.3390/ijms20225758

Wu, G., Chen, Z., Li, J., Ye, F., Chen, G., Fan, Q., et al. (2018). NOTCH4 is a novel prognostic marker that correlates with colorectal cancer progression and prognosis. *J. Cancer* 9 (13), 2374–2379. doi:10.7150/jca.26359

Xing, C., Sun, S. G., Yue, Z. Q., and Bai, F. (2021a). Role of lncRNA LUCAT1 in cancer. *Biomed. and Pharmacother. = Biomedecine and Pharmacother.* 134, 111158. doi:10.1016/j.biopha.2020.111158

Xing, F., Liu, Y., Wu, S. Y., et al. (2021b). Loss of XIST in breast cancer activates MSN-c-met and reprograms microglia via exosomal miRNA to promote brain metastasis. *Cancer Res.* 81 (21), 5582. doi:10.1158/0008-5472.CAN-21-3056

Xiu, M., Zeng, X., Shan, R., Wen, W., Li, J., and Wan, R. (2021). Targeting Notch4 in cancer: molecular mechanisms and therapeutic perspectives. *Cancer Manag. Res.* 13, 7033–7045. doi:10.2147/CMAR.S315511

Xu, W., Ding, M., Wang, B., Cai, Y., Guo, C., and Yuan, C. (2021). Molecular mechanism of the canonical oncogenic lncRNA MALAT1 in gastric cancer. *Curr. Med. Chem.* 28 (42), 8800–8809. doi:10.2174/0929867328666210521213352

Xue, B., and He, L. (2014). An expanding universe of the non-coding genome in cancer biology. *Carcinogenesis* 35 (6), 1209–1216. doi:10.1093/carcin/bgu099

Yang, J., Shi, X., Yang, M., Luo, J., Gao, Q., Wang, X., et al. (2021). Glycolysis reprogramming in cancer-associated fibroblasts promotes the growth of oral cancer through the lncRNA H19/miR-675-5p/PFKFB3 signaling pathway. *Int. J. oral Sci.* 13 (1), 12. doi:10.1038/s41368-021-00115-7

Yang, Y., Wang, D., Miao, Y. R., Wu, X., Luo, H., Cao, W., et al. (2023). lncRNASNP v3: an updated database for functional variants in long non-coding RNAs. *Nucleic acids Res.* 51 (D1), D192–D198. doi:10.1093/nar/gkac981

You, Z., Liu, C., Wang, C., Ling, Z., Wang, Y., Wang, Y., et al. (2019). LncRNA CCAT1 promotes prostate cancer cell proliferation by interacting with DDX5 and MIR-28-5P. *Mol. cancer Ther.* 18 (12), 2469–2479. doi:10.1158/1535-7163.MCT-19-0095

Zhang, Y., Huang, W., Yuan, Y., Li, J., Wu, J., Yu, J., et al. (2020). Long non-coding RNA H19 promotes colorectal cancer metastasis via binding to hnRNPA2B1. *J. Exp. and Clin. cancer Res. CR* 39 (1), 141. doi:10.1186/s13046-020-01619-6

Zhou, L., Wang, D., Sheng, D., Xu, J., Chen, W., Qin, Y., et al. (2020). NOTCH4 maintains quiescent mesenchymal-like breast cancer stem cells via transcriptionally activating SLUG and GAS1 in triple-negative breast cancer. *Theranostics* 10 (5), 2405–2421. doi:10.7150/thno.38875

frontiers | Frontiers in Pharmacology

TYPE Review
PUBLISHED 16 September 2024
DOI 10.3389/fphar.2024.1442196

OPEN ACCESS

EDITED BY
Jing-Quan Wang,
St. John's University, United States

REVIEWED BY
Magesh Muthu,
Wayne State University, United States
Hiba Muwafaq Saleem,
University of Anbar, Iraq

*CORRESPONDENCE
Wan'an Xiao,
waxiao@cmu.edu.cn

RECEIVED 01 June 2024
ACCEPTED 30 August 2024
PUBLISHED 16 September 2024

CITATION
Liu J, Chang X, Manji L, Xu Z and Xiao W (2024) Roles of small peptides encoded by non-coding RNAs in tumor invasion and migration. *Front. Pharmacol.* 15:1442196. doi: 10.3389/fphar.2024.1442196

Roles of small peptides encoded by non-coding RNAs in tumor invasion and migration

Jie Liu[1,2], Xiyue Chang[1,2], Laeeqa Manji[1], Zhijie Xu[1] and Wan'an Xiao[1]*

[1]Department of Orthopedics, Shengjing Hospital of China Medical University, Shenyang, Liaoning, China, [2]Department of Epidemiology, School of Public Health, China Medical University, Shenyang, Liaoning, China

Non-coding RNAs (ncRNAs), which are usually considered not to encode proteins, are widely involved in important activities including signal transduction and cell proliferation. However, recent studies have shown that small peptides encoded by ncRNAs (SPENs) have important roles in the development of malignant tumors. Some SPENs participate in the regulation of skeleton reorganization, intercellular adhesion, signaling and other processes of tumor cells, with effects on the invasive and migratory abilities of the cells. Therefore, SPENs have potential applications as therapeutic targets and biomarkers of malignant tumors. Invasion and migration of malignant tumor cells are the main reasons for poor prognosis of cancer patients and represent the most challenging aspects of treatment of malignant tumors. Currently, the main treatments for tumors include surgery, radiotherapy, targeted drug therapy. Surgery, however, is reserved for early stages of cancer and carries risks and costs. Radiotherapy and targeted therapy have serious side effects. This review describes the mechanisms of SPENs and their roles in tumor invasion and migration, with the aim of providing new targets for tumor diagnosis and treatment.

KEYWORDS

non-coding RNA, tumor, small peptide, invasion, migration

1 Introduction

Malignant tumors, which are associated with high morbidity and mortality, represent a global public health challenge (Liu et al., 2024). Owing to the difficulty of early diagnosis, some tumors are found in the middle to late stages of the disease, with serious effects on patient survival and prognosis. Therefore, in-depth research is needed to identify biomarkers involved in the regulation of malignant transformation to better predict the progression of malignant tumors. These could have applications in both clinical diagnosis and targeted adjuvant therapy to improve the overall survival of patients (Li et al., 2022).

Only about 2% of the genes in the human genome are coding genes; the vast majority of transcripts lack coding open reading frames and are regarded as non-coding RNAs (ncRNAs); these include microRNAs, circular RNAs, and long ncRNAs (Miano et al., 2021; Panni et al., 2020; Wang J. et al., 2019; Wang Y. et al., 2019). However, owing to

Abbreviations: ncRNA, Non-coding RNAs; SPENs, small peptides encoded by non-coding RNAs; aa, amino acids; mRNA, messenger RNAs; ECM, extracellular matrix; EMT, epithelial-mesenchymal transition; FABP5, fatty acid binding protein 5.

technological advances, circular RNAs and lncRNAs have been found to have short open reading frames that can be translated into small peptides of about 100 amino acids (aa) in length (Gao et al., 2024; Zhou et al., 2024). These small peptides, in turn, have been shown to have various biological functions, which are listed in the corresponding databases (Andrews and Rothnagel, 2014; Dragomir et al., 2020). Many ncRNAs are similar to coding RNAs (messenger RNAs, mRNAs) and are also transcribed by RNA polymerase II via the processes of polyadenylation, 5′-end capping and RNA splicing (Chen, 2016). In addition, deep sequencing of ribosomal profiles has shown that many transcripts of ncRNAs bind to the ribosome (Gelsinger et al., 2020), suggesting that ncRNAs may be able to encode proteins in the same way as mRNAs.

Small peptides encoded by ncRNAs (SPENs) have important roles in organisms. In recent years, studies published in *Science*, *Nature*, *Cell*, *Molecular Cancer* and other journals have reported that some SPENs (less than 100 aa in length, e.g., sarco-endoplasmic reticulum Ca^{2+}, Toddler, myoregulin, small regulatory polypeptide of amino acid response) are involved in the processes of myogenesis, embryogenesis, and tumorigenesis (Nelson et al., 2016; Matsumoto et al., 2017; Anderson et al., 2015; Wu et al., 2020) Cancer-associated small integral membrane open reading frame 1 was the first functional small peptide found to be carcinogenic; it interacts with squalene epoxidase, a key enzyme in cholesterol synthesis, to regulate the metabolic homeostasis of cancer cells. Knockdown of cancer-associated small integral membrane open reading frame 1 led to a reduction in the proliferation of breast cancer cells (Polycarpou-Schwarz et al., 2018). In another study, HOXB-AS3, a 53-aa conserved small peptide encoded by the lncRNA HOXB-AS3, was shown to inhibit the growth of colon cancer, and its deletion was identified as a key oncogenic factor in colon cancer metabolism (Huang et al., 2017). In addition, the 59-aa small peptide SMIM30, encoded by lncRNA LINC00998, has been reported to promote hepatocellular carcinoma development by regulating cell proliferation and migration (Pang et al., 2020) These studies indicate that SPENs participate in tumorigenesis and development of tumors through complex mechanisms. This enriches our knowledge of tumor regulatory molecules, providing new directions for tumor research with potential clinical applications (Zhu et al., 2020).

Invasion and migration are central processes in tumor biology. They are critical to tumor development owing to their role in metastasis and are major causes of poor patient prognosis and cancer-related mortality (Ahmad et al., 2023). This review focuses on the mechanisms of SPENs and their roles in tumor invasion and migration, aiming to provide new strategies for clinical diagnosis and treatment of various cancers.

2 Invasion and migration

2.1 Overview of tumor cell invasion and migration

Invasion is the process by which tumor cells break out of their original location of growth and invade surrounding normal tissues. The cancer cells use a variety of mechanisms to destroy the structure of the surrounding tissue so that they can spread and metastasize to other sites. Migration, on the other hand, refers to the ability of tumor cells to spread to other parts of the body through the blood or lymphatic system. This process can be roughly divided into the following three steps. First, the migration ability of cancer cells is enhanced after they are detached from the tumor, enabling them to further destroy the extracellular matrix (ECM) and basement membrane and form an invasive growth in normal tissue (Joshi et al., 2023). Second, the surviving cancer cells escape from the wall of the blood vessels, grow and proliferate in suitable tissues and organs, and form a metastatic cancerous focus. Last, a network of neovascularization is formed inside the metastatic focus, which promotes proliferation of the cancerous cells and enables a new round of metastasis (Spano et al., 2012). Invasion and migration processes have crucial roles in the development and progression of tumors. Abnormally active cell migration and invasion mechanisms lead to the formation of abnormal structures around the tumor, resulting in the development of invasive cancers. Therefore, elucidating the mechanisms of these processes can provide a better understanding the mechanisms of cancer development and enable the development more effective therapeutic strategies to improve patient survival and quality of life.

2.2 Roles of invasion and migration in tumorigenesis and development of tumors

Invasion and migration are important aspects of tumor dissemination, and together they constitute the process of tumor metastasis (van Zijl et al., 2011). This process can cause extensive harm and also represents a challenge in cancer treatment, as widespread metastasis often means that advanced cancer cannot be surgically eradicated (Izdebska et al., 2023).

Invasion and migration are central processes in tumor biology (Wu et al., 2021). Invasion involves the degradation and penetration of tumor cells into surrounding tissues, whereas migration involves the movement of tumor cells and colonization of new sites. The two processes are usually driven by complex interactions between tumor cells and the surrounding environment. The molecular mechanisms of invasion and migration are complex and varied. Cancer cells gain motility by remodeling of their tight cell–cell and cell–matrix adhesions, which allows them to leave the primary tumor and invade surrounding tissues (Valastyan and Weinberg, 2011; Christofori, 2006; Lim et al., 2017). Then, the cancer cells secrete a variety of enzymes to degrade the matrix of surrounding tissues. These enzymes break down the ECM and basement membrane stroma, thereby providing a pathway for cancer cells to spread and metastasize (Mondal et al., 2020). In addition, cancer cells release signaling factors, which promote invasion and metastasis by activating signals associated with these processes (Hashemi Goradel et al., 2019; Todd and Johnson, 2020) These changes allow tumor cells to escape the primary site and form new tumor foci at distant sites.

3 SPENs

For a long time, RNAs have been divided into two main categories: mRNAs and ncRNAs (Yasuda and Hayashizaki, 2008).

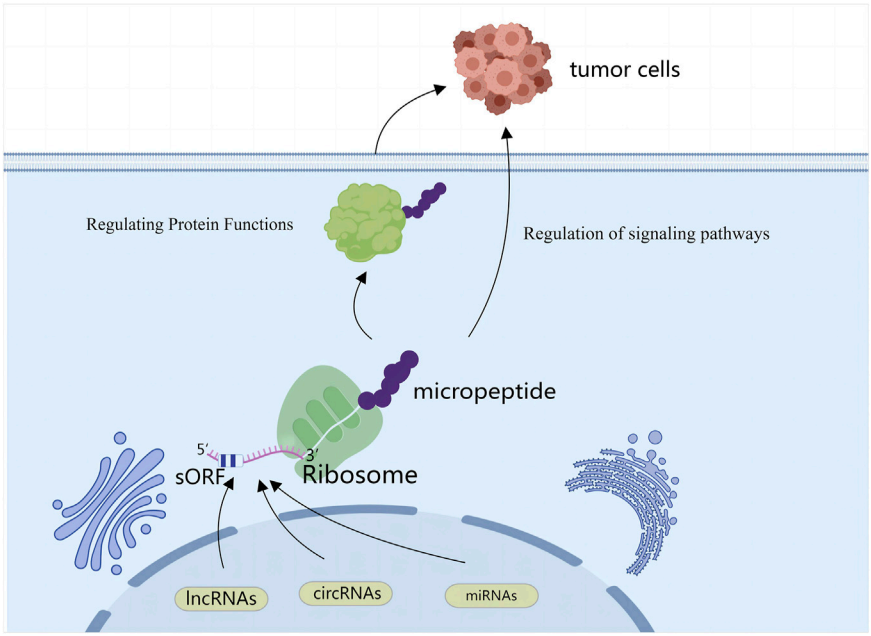

FIGURE 1
SPENs refer to small peptides encoded by ncRNAs (lncRNAs, circRNAs, miRNAs). Some ncRNAs can generate small peptides through unconventional translation mechanisms, and these peptides influence behaviors of cancer cells by regulating protein functions and participating in signaling pathways.

mRNAs act as carriers of genetic information and direct protein synthesis, whereas ncRNAs were once called the "dark matter of the genome" because they were thought to not directly code for proteins. However, recent studies have revealed that some ncRNAs can encode small peptides. This discovery has greatly expanded our understanding of RNA function and opened a new chapter in biological research.

Small peptides encoded by ncRNAs are synthesized through different mechanisms from those associated with classical mRNA-encoded proteins. These comprise ribosome-independent mechanisms, involving the regulation of tRNA half-life, editing, and modification; and ribosome-dependent mechanisms, in which the open reading frames of the ncRNAs are recognized by the ribosome and translated into small peptides.

SPENs have a small molecular weight, usually between 10 and 100 aa. Despite their small molecular weight, these peptides have important regulatory functions in organisms, including signal transduction, protein interactions, and regulation of gene expression (Dong et al., 2023). In addition, SPENs usually have high specificity and sensitivity and function under specific physiological or pathological conditions. SPENs perform a wide variety of functions in organisms, participating in cell signal transduction, cell proliferation, differentiation and apoptosis. SPENs can also interact with specific proteins to change their activity or localization, as well as acting as molecular chaperones and participating in the assembly and regulation of other biomolecules. SPENs also have important roles in the onset and development of cancers.

4 Mechanisms of SPENs in tumor invasion and migration

Although relatively little research has focused on the roles of SPENs in tumor biology, some studies have provided insight into their functions. SPENs play important parts in cancer cell invasion and migration through a variety of mechanisms (Figure 1). For example, they can regulate protein functions and activities by binding to specific proteins and forming complexes. These proteins may be involved in processes such as cell adhesion and cell signaling, which have crucial roles in tumor cell invasion and migration; thus the regulation of these processes by SPENs may directly affect the migratory and invasive behavior of tumor cells. In addition, SPENs can influence the reorganization and dynamics of the cytoskeleton, an important structure within the cell that maintains cell morphology and motility. Through effects on the assembly and stability of the cytoskeleton, small peptides proximally alter cell morphology and motility, thereby playing a key part in tumor invasion and migration (Hu et al., 2022; Zhang Y. et al., 2024; Ye et al., 2023) (Figure 2).

In recent years, studies of SPENs have confirmed that several ncRNAs can encode small peptides and regulate various malignant tumor phenotypes (Polycarpou-Schwarz et al., 2018). Mechanisms of tumor-associated functional peptides encoded by ncRNAs in invasion and migration have been reported in the following tumor types: gastric cancer, intestinal cancer, clear cell renal cell carcinoma, osteosarcoma, neuroblastoma, lung cancer, and breast cancer (Table 1).

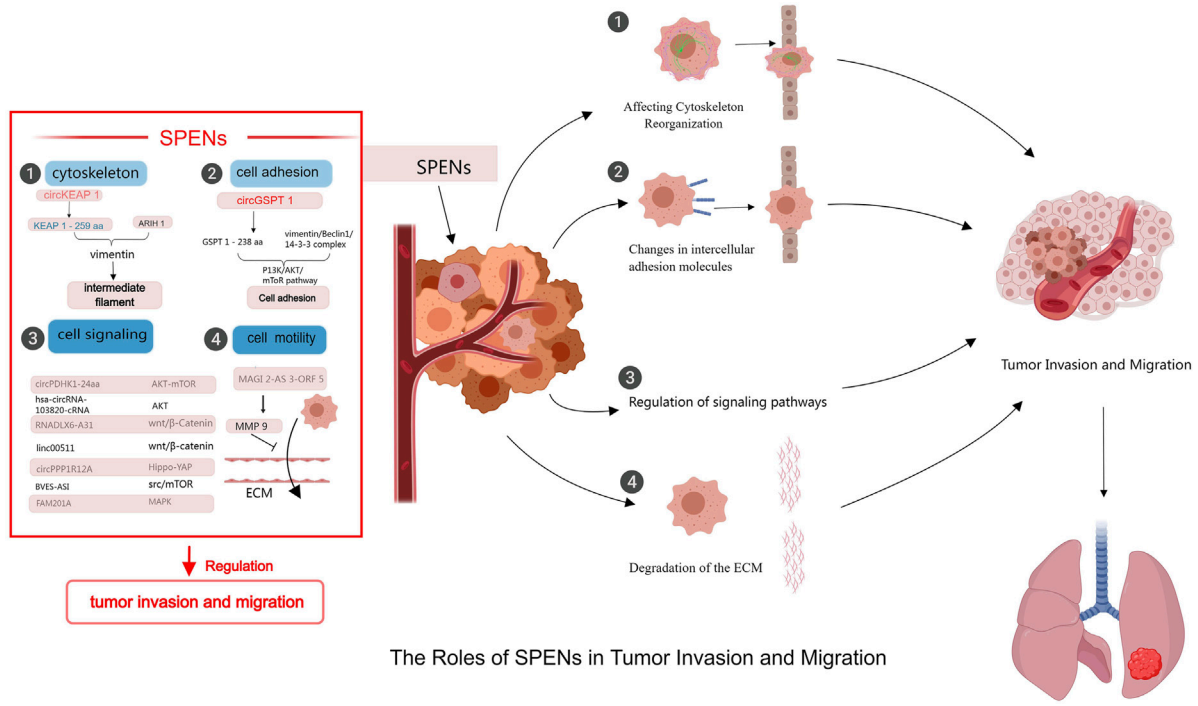

FIGURE 2
Mechanisms of SPENs on tumor invasion and migration. SPENs play significant roles in tumor invasion and metastasis by regulating protein functions, participating in signal transduction, affecting cytoskeleton reorganization, and influencing the extracellular matrix.

4.1 Changes in intercellular adhesion molecules

In normal tissues, cells adhere to each other, forming an interdependent system that promotes their survival. By contrast, cancer cells weaken intercellular adhesion and enhance cell migration by altering the expression of intercellular adhesion molecules, such as those involved in epithelial–mesenchymal transition (EMT) (Lee et al., 2017). EMT is the phenotypic transformation of epithelial cells to acquire mesenchymal features, a crucial process in tumor cell migration (Pantia et al., 2023). Waveform protein, an important marker of EMT, can cause tumor cells to lose adhesion and disrupt their tight junction structure, change the structure of the cytoskeleton, and increase the invasiveness and distant metastasis of tumor cells (Strouhalova et al., 2020; Ohara et al., 2020). Hu et al., (2022) demonstrated that a novel tumor suppressor protein, GSPT1-238aa, encoded by circGSPT1, interacts with the waveform protein/Beclin 1/14-3-3 complex and regulates autophagy in gastric cancer cells through the PI3K/AKT/mTOR signaling pathway. Zhang Y. et al., (2024) showed that KEAP1-259aa, a small peptide encoded by circKEAP1, binds to waveform proteins in the cytoplasm, where it promotes the proteasomal degradation of waveform proteins through interaction with ARIH1, an E3 ligase. In addition to mediating cell adhesion, cell adhesion molecules act as tumor suppressors, limiting tumor growth and migration through contact inhibition. Weakening of cell adhesion allows tumor cells to gain motility and invasiveness, escape the original tumor site, and metastasize to distant organs. Important adhesion molecules include integrin, cadherin, selectin, the immunoglobulin superfamily (e.g., intercellular adhesion molecule-1, neural cell adhesion molecule, vascular cell adhesion molecule, carcinoembryonic antigen, and deleted in colon cancer), CD44, and the 67 kD laminin receptor (Staff, 2001; Moh and Shen, 2009). Calcineurin family members form relatively strong calcium-dependent homotypic adhesions with neighboring cells through their cytoplasmic structural domains, thereby maintaining the stability of cell–cell adhesion. Integrin receptors are calcium-dependent heterodimers composed of noncovalently linked alpha and beta subunits. Members of the integrin family of molecules connect the ECM to the cytoskeleton and transduce signals controlling adhesion and migration in both directions. Members of the selectin family enable transient cell–cell adhesion by interacting with ligands on glycoproteins and glycolipids in the carbohydrate portion of the sialic acid-Lewis X tetrasaccharide. Members of the immunoglobulin superfamily mediate calcium-independent cell–cell adhesion through structural domains, regulate adhesion, and recognize both homophilic and heterophilic ligands (von Lersner et al., 2019).

4.2 Degradation of the ECM

The ECM is a fundamental core component of body tissues and organs and is essential for the existence of multicellular organisms (Cox, 2021). The ECM, which consists of collagen, polysaccharides,

TABLE 1 Mechanisms of SPENs in tumor invasion and migration.

Tumor types		ncRNAs	SPENs	Mechanisms of SPENs	Published Journals	References information
Gastric cancer		CircGSPT1	GSPT1-238aa	Waveform protein/Beclin 1/14-3-3 complex interacts with GSPT1-238aa and regulates autophagy in gastric cancer cells via the PI3K/AKT/mTOR signaling pathway	*Cancer Letters*	Hu et al. (2022)
Colorectal cancer	Colon	circPPP1R12A	circPPP1R12A-73aa	Promotion of colon cancer growth and metastasis through activation of the Hippo-YAP signaling pathway	*Molecular Cancer*	Zheng et al. (2019)
	Colorectal cancer	lncRNA BVES-AS1	BVES-AS1-201-50aa	BVES-AS1-201-50aa enhances activation of the Src/mTOR pathway in colorectal cancer cells and promotes cell migration and invasion of colorectal cancer cells	*PLoS One*	Zheng et al. (2023)
Clear cell renal cell carcinoma		circPDHK1	PDHK1-241aa	Inhibition of AKT dephosphorylation and activation of the AKT-mTOR signaling pathway through interaction with PPP1CA promotes clear cell renal cell carcinoma progression	*Molecular Cancer*	Huang et al. (2024)
Osteosarcoma		circKEAP1	KEAP1-259aa	Binds to wave proteins in the cytoplasm to promote wave protein proteasomal degradation through interaction with the E3 ligase ARIH1	*Journal of Experimental and Clinical Cancer Research*	Zhang et al. (2024a)
Neuroblastoma		FAM201A	NBASP	Neuroblastoma- associated small protein interacts with FABP5 via the ubiquitin proteasome pathway and reduces FABP5 expression, thereby inhibiting neuroblastoma through the MAPK signaling pathway	*Communications Biology*	Ye et al. (2023)
		circSHPRH	SHPRH-146aa	Apoptosis is induced mainly by regulating key apoptotic proteins caspase-3 and Bcl-2; in addition, circ-SHPRH peptide-RUNX 1 interaction enhances expression of NFKBIA in neuroblastoma, which plays an important part in inhibiting the malignant progression of neuroblastoma	*PeerJ*	Gao et al. (2024)
Lung cancer	Uncategorized lung cancer	hsa_circRNA_103820	hsa_circRNA_103820 188-aa	Suppression of malignant progression of lung cancer cells by inhibiting the AKT pathway	*Chemical Biology and Drug Design*	Zhou et al. (2024)
	Non-small-cell lung cancer	DLX6-AS1	SMIM30	Exogenous overexpression of SMIM30 promotes non-small-cell lung cancer growth through activation of the Wnt/β-catenin pathway	*Critical Reviews in Eukaryotic Gene Expression*	Xu et al. (2022)

(Continued on following page)

TABLE 1 (*Continued*) Mechanisms of SPENs in tumor invasion and migration.

Tumor types		ncRNAs	SPENs	Mechanisms of SPENs	Published Journals	References information
		circβ-catenin	circβ-catenin-β370aa	Inhibition of β-catenin degradation by binding GSK3β promotes a malignant phenotype in non-small-cell lung cancer cells	*Journal of Clinical Laboratory Analysis*	Zhao et al. (2021)
	Adenocarcinoma of the lungs	LINC 00954	LINC 00954-ORF	Enhances sensitivity to PEM (anticancer drug) and inhibits A549/PEM cell growth	*Amino Acids*	Han et al. (2024)
Lymphoma		MAGI2-AS3	magi2-as3-orf5	Regulation of BRCA cell migration by ECM-related proteins	*Molecular Biotechnology*	Zhang et al. (2024b)

proteoglycans, etc., not only provides physical support for cells but also participates in essential processes such as cell growth, differentiation, migration, and signaling. ECM degradation is the pathological basis for the development of many diseases; moreover, degradation of the ECM, including the basement membrane, is a key step in tumor invasion and metastasis, because tumor cells must cross the basement membrane several times to invade surrounding tissues. The various components of the ECM are degraded by specific protein hydrolases; thus, the degradation of the entire ECM requires the synergistic action of multiple matrix hydrolases. Tumor cells facilitate their own invasion and migration by secreting enzymes that rupture the structure of the ECM, enabling them to penetrate the ECM barrier and invade surrounding tissues and blood vessels; they then travel via the circulatory system to other sites, eventually forming metastatic tumors. The proteolytic enzymes associated with ECM degradation by tumor cells can be divided into four major groups: serine proteases (e.g., plasma fibrinolytic plasminogen activator), metalloproteinases, elastases, and cysteine proteases; the first two groups have been investigated in depth. Tumor biomarkers have key roles in cancer screening, diagnosis and prognosis, detection of progression, prediction of recurrence, and evaluation of treatment efficacy (Huang, 2018). MMP9 regulates ECM degradation during tumor metastasis. Degradation and is considered a marker of cell migration and invasion. Zhang Z. et al., (2024) showed that the fluorescence intensity of MMP9 was significantly reduced by overexpression of MAGI2-AS3-ORF5, a small peptide encoded by a non-coding RNA. A transwell assay further revealed that accumulation of MAGI2-AS3-ORF5 reduced numbers of migrating breast cancer cells. In addition, it was found to regulate the migration of breast cancer cells through ECM-associated proteins.

4.3 Cytoskeletal alterations

The cytoskeleton, which comprises cytoplasmic cytoskeleton and nuclear cytoskeleton parts, consists of intermediate fibers, microfilaments, and microtubules, which exist in the cytoplasm and are assembled by a network of proteins. As well as its involvement in activities such as cell division, motility, material movement, and signal transduction, it plays a crucial part in maintaining the basic shape and structure of the cell. Dysfunction or abnormal expression of constituents of the cytoskeleton may thus lead to changes in cell morphology and structure, which in turn may trigger a series of physiopathological processes. Recent studies have also identified an important role of the cytoskeleton in tumor migration and invasion. Cancer cells have a high degree of plasticity, and the deformability of cells is increased by altering the structure and function of the cytoskeleton, thereby promoting cell migration and invasion. Microfilaments, the most important component of the cytoskeleton, consist of fibrinogen, actin, and microkeratin; they enable cell migration and invasion through dynamic reorganization and depolymerization. Intermediate fibers are the most stable part of the cytoskeleton and have an important role in supporting cells. Waveform protein, which is among the most important intermediate fiber proteins, provides physical scaffolding for various organelles in the cell, thereby maintaining cytoskeletal conformation and cellular morphology as well as the integrity and mobility of bridge particles (Guo et al., 2013). Zhang Y. et al. (2024) found that circKEAP1 encodes the protein KEAP1-259aa, which binds to waveform proteins and facilitates their degradation by interacting with the E3 ligase ARIH1, which in turn inhibits tumor migration.

4.4 Regulation of signaling pathways

Signaling pathways are intracellular information transfer systems that involve various biochemical reactions and signal transduction processes. Abnormalities of these signaling pathways may lead to cellular dysfunction. Cancer cells participate in the regulation of cell invasion and migration through activation of various signaling pathways, including the Rho GTPase family, PI3k/Akt, and MAPK pathways. A newly discovered circular RNA, circPPP1R12A, encodes a small peptide named circPPP1R12A-73aa. Zheng et al. (2019) demonstrated experimentally that circPPP1R12A-73aa promotes the migration ability and invasiveness of colon cancer through activation of the

Hippo-YAP signaling pathway. Zheng et al. (2023) found that lncRNA BVES-AS1 encodes peptide BVES-AS1-201-50aa, which promotes cell migration and invasion of colorectal cancer cells by enhancing activation of the Src/mTOR pathway. Ye et al. (2023) showed that neuroblastoma-associated small protein, a small peptide encoded by FAM201A, interacts with fatty acid binding protein 5 (FABP5) through the ubiquitin proteasome pathway to reduce the expression of FABP5, thereby suppressing cellular migration and invasion through the MAPK signaling pathway and inhibiting neuroblastoma tumorigenesis. Huang et al. (2024) demonstrated that circPDHK1 encodes a novel peptide, PDHK1-241aa, which promotes invasion and metastasis of clear cell renal cell carcinoma by inhibiting AKT dephosphorylation and activating the AKT-mTOR signaling pathway through its interaction with PPP 1CA. Zhou et al., (2024) demonstrated that a 188-aa peptide encoded by hsa_circRNA_103820 inhibits cell migration and invasion by inactivating the AKT pathway in lung cancer. Xu et al., (2022) showed that the lncRNA DLX6-AS1, encoding peptide SMIM30, promotes migration and invasion of non-small-cell lung cancer cells through activation of the Wnt/β-catenin signaling pathway. Tan et al. (2023) showed that the small peptide LINC00511-133 aa is encoded by LINC00511 and promotes invasiveness of breast cancer cells by regulating expression levels of Wnt/β-catenin-pathway-associated proteins Bax, cMyc, and cyclin D1, as well as facilitating the entry of β-catenin proteins into the nucleus.

5 Conclusion and outlook

This article focuses on an emerging area of research: the role of SPENs in tumor invasion and migration. We review the mechanisms by which SPENs act in tumor invasion and migration, highlighting the previously unrecognized complexity of ncRNAs. It is an exciting issue to address why discove the role of SPENs in tumor invasion and migration. Invasion and migration are key processes in tumor metastasis, which is of clinical significance as the vast majority of cancer patients die from metastatic rather than primary tumors. In-depth studies of the mechanisms underlying these processes are thus conducive to the development of diagnostic and therapeutic strategies for cancer. SPENs, which represent a newly discovered function of RNAs, both enrich existing protein libraries and provide new directions for protein-related research; they also opens up new avenues for cancer treatment. Research into the coding properties of ncRNAs is ongoing; however, the detection and identification of small peptides remains challenging owing to the immaturity of experimental techniques. In addition, many studies have failed to distinguish between the functions of SPENs and those of ncRNAs themselves; this should be considered in the future. Moreover, although some SPENs have been shown to have functional features, their mechanisms of action are not yet clear; challenges remain regarding how to verify their activities and functions. Therefore, further studies are needed. However, despite our current limited understanding in this field, we expect more breakthroughs and advances as research continues and the technology develops. SPENs have the potential to play important parts in drug development and in the diagnosis and treatment of various diseases, which will be beneficial to human health and quality of life.

Author contributions

JL: Writing–original draft, Writing–review and editing. XC: Writing–original draft, Investigation. LM: Methodology, Writing–review and editing. ZX: Investigation, Methodology, Writing–review and editing. WX: Writing–review and editing, Funding acquisition, Project administration, Resources, Supervision.

Funding

The authors declare that financial support was received for the research, authorship, and/or publication of this article. This study was financially supported by General Scientific Research Project of Liaoning Provincial Department of Education (No. JYTMS20230100).

Conflict of interest

The authors declare that the research was conducted in the absence of any commercial or financial relationships that could be construed as a potential conflict of interest.

Publisher's note

Supplementary material

The Supplementary Material for this article can be found online at: https://www.frontiersin.org/articles/10.3389/fphar.2024.1442196/full#supplementary-material

References

Ahmad, M., Weiswald, L. B., Poulain, L., Denoyelle, C., and Meryet-Figuiere, M. (2023). Involvement of lncRNAs in cancer cells migration, invasion and metastasis: cytoskeleton and ECM crosstalk. *J. Exp. Clin. Cancer Res.* 42, 173. doi:10.1186/s13046-023-02741-x

Anderson, D. M., Anderson, K. M., Chang, C. L., Makarewich, C. A., Nelson, B. R., McAnally, J. R., et al. (2015). A micropeptide encoded by a putative long noncoding RNA regulates muscle performance. *Cell.* 160, 595–606. doi:10.1016/j.cell.2015.01.009

Andrews, S. J., and Rothnagel, J. A. (2014). Emerging evidence for functional peptides encoded by short open reading frames. *Nat. Rev. Genet.* 15, 193–204. doi:10.1038/nrg3520

Chen, L. L. (2016). Linking long noncoding RNA localization and function. *Trends biochem. Sci.* 41, 761–772. doi:10.1016/j.tibs.2016.07.003

Christofori, G. (2006). New signals from the invasive front. *Nature* 441, 444–450. doi:10.1038/nature04872

Cox, T. R. (2021). The matrix in cancer. *Nat. Rev. Cancer* 21, 217–238. doi:10.1038/s41568-020-00329-7

Dong, X., Zhang, K., Xun, C., Chu, T., Liang, S., Zeng, Y., et al. (2023). Small open reading frame-encoded micro-peptides: an emerging protein world. *Int. J. Mol. Sci.* 24, 10562. doi:10.3390/ijms241310562

Dragomir, M. P., Manyam, G. C., Ott, L. F., Berland, L., Knutsen, E., Ivan, C., et al. (2020). FuncPEP: a database of functional peptides encoded by non-coding RNAs. *Noncoding RNA* 6, 41. doi:10.3390/ncrna6040041

Gao, J., Pan, H., Li, J., Jiang, J., and Wang, W. (2024). A peptide encoded by the circular form of the SHPRH gene induces apoptosis in neuroblastoma cells. *PeerJ* 12, e16806. doi:10.7717/peerj.16806

Gelsinger, D. R., Dallon, E., Reddy, R., Mohammad, F., Buskirk, A. R., and DiRuggiero, J. (2020). Ribosome profiling in archaea reveals leaderless translation, novel translational initiation sites, and ribosome pausing at single codon resolution. *Nucleic Acids Res.* 48, 5201–5216. doi:10.1093/nar/gkaa304

Guo, M., Ehrlicher, A. J., Mahammad, S., Fabich, H., Jensen, M. H., Moore, J. R., et al. (2013). The role of vimentin intermediate filaments in cortical and cytoplasmic mechanics. *Biophys. J.* 105, 1562–1568. doi:10.1016/j.bpj.2013.08.037

Han, X., Chen, L., Sun, P., Wang, X., Zhao, Q., Liao, L., et al. (2024). A novel lncRNA-hidden polypeptide regulates malignant phenotypes and pemetrexed sensitivity in A549 pulmonary adenocarcinoma cells. *Amino Acids* 56, 15. doi:10.1007/s00726-023-03361-7

Hashemi Goradel, N., Najafi, M., Salehi, E., Farhood, B., and Mortezaee, K. (2019). Cyclooxygenase-2 in cancer: a review. *J. Cell. Physiol.* 234, 5683–5699. doi:10.1002/jcp.27411

Hu, F., Peng, Y., Chang, S., Luo, X., Yuan, Y., Zhu, X., et al. (2022). Vimentin binds to a novel tumor suppressor protein, GSPT1-238aa, encoded by circGSPT1 with a selective encoding priority to halt autophagy in gastric carcinoma. *Cancer Lett.* 545, 215826. doi:10.1016/j.canlet.2022.215826

Huang, B., Ren, J., Ma, Q., Yang, F., Pan, X., Zhang, Y., et al. (2024). A novel peptide PDHK1-241aa encoded by circPDHK1 promotes ccRCC progression via interacting with PPP1CA to inhibit AKT dephosphorylation and activate the AKT-mTOR signaling pathway. *Mol. Cancer* 23, 34. doi:10.1186/s12943-024-01940-0

Huang, H. (2018). Matrix metalloproteinase-9 (MMP-9) as a cancer biomarker and MMP-9 biosensors: recent advances. *Sensors (Basel)* 18, 3249. doi:10.3390/s18103249

Huang, J. Z., Chen, M., Chen, D., Gao, X. C., Zhu, S., Huang, H., et al. (2017). A peptide encoded by a putative lncRNA HOXB-AS3 suppresses colon cancer growth. *Mol. Cell.* 68, 171–184. doi:10.1016/j.molcel.2017.09.015

Izdebska, M., Zielińska, W., Krajewski, A., and Grzanka, A. (2023). Fascin in migration and metastasis of breast cancer cells – a review. *Adv. Med. Sci.* 68, 290–297. doi:10.1016/j.advms.2023.08.003

Joshi, V. B., Gutierrez Ruiz, O. L., and Razidlo, G. L. (2023). The cell biology of metastatic invasion in pancreatic cancer: updates and mechanistic insights. *Cancers (Basel)* 15, 2169. doi:10.3390/cancers15072169

Lee, H. M., Hwang, K. A., and Choi, K. C. (2017). Diverse pathways of epithelial mesenchymal transition related with cancer progression and metastasis and potential effects of endocrine disrupting chemicals on epithelial mesenchymal transition process. *Mol. Cell. Endocrinol.* 457, 103–113. doi:10.1016/j.mce.2016.12.026

Li, H., Gao, J., Liu, L., and Zhang, S. (2022). LINC00958: a promising long non-coding RNA related to cancer. *Biomed. Pharmacother.* 151, 113087. doi:10.1016/j.biopha.2022.113087

Lim, W. C., Kim, H., Kim, Y. J., Choi, K. C., Lee, I. H., Lee, K. H., et al. (2017). Dioscin suppresses TGF-β1-induced epithelial-mesenchymal transition and suppresses A549 lung cancer migration and invasion. *Bioorg. Med. Chem. Lett.* 27, 3342–3348. doi:10.1016/j.bmcl.2017.06.014

Liu, W., Wang, Y., Xia, L., and Li, J. (2024). Research progress of plant-derived natural products against drug-resistant cancer. *Nutrients* 16, 797. doi:10.3390/nu16060797

Matsumoto, A., Pasut, A., Matsumoto, M., Yamashita, R., Fung, J., Monteleone, E., et al. (2017). mTORC1 and muscle regeneration are regulated by the LINC00961-encoded SPAR polypeptide. *Nature* 541, 228–232. doi:10.1038/nature21034

Miano, V., Codino, A., Pandolfini, L., and Barbieri, I. (2021). The non-coding epitranscriptome in cancer. *Brief. Funct. Genomics* 20, 94–105. doi:10.1093/bfgp/elab003

Moh, M. C., and Shen, S. (2009). The roles of cell adhesion molecules in tumor suppression and cell migration: a new paradox. *Cell. adh. Migr.* 3, 334–336. doi:10.4161/cam.3.4.9246

Mondal, S., Adhikari, N., Banerjee, S., Amin, S. A., and Jha, T. (2020). Matrix metalloproteinase-9 (MMP-9) and its inhibitors in cancer: a minireview. *Eur. J. Med. Chem.* 194, 112260. doi:10.1016/j.ejmech.2020.112260

Nelson, B. R., Makarewich, C. A., Anderson, D. M., Winders, B. R., Troupes, C. D., Wu, F., et al. (2016). A peptide encoded by a transcript annotated as long noncoding RNA enhances SERCA activity in muscle. *Science* 351, 271–275. doi:10.1126/science.aad4076

Ohara, M., Ohara, K., Kumai, T., Ohkuri, T., Nagato, T., Hirata-Nozaki, Y., et al. (2020). Phosphorylated vimentin as an immunotherapeutic target against metastatic colorectal cancer. *Cancer Immunol. Immunother.* 69, 989–999. doi:10.1007/s00262-020-02524-9

Pang, Y. N., Liu, Z. Y., Han, H., Wang, B., Li, W., Mao, C., et al. (2020). Peptide SMIM30 promotes HCC development by inducing SRC/YES1 membrane anchoring and MAPK pathway activation. *J. Hepatol.* 73, 1155–1169. doi:10.1016/j.jhep.2020.05.028

Panni, S., Lovering, R. C., Porras, P., and Orchard, S. (2020). Non-coding RNA regulatory networks. *Biochim. Biophys. Acta Gene Regul. Mech.* 1863, 194417. doi:10.1016/j.bbagrm.2019.194417

Pantia, S., Kangsamaksin, T., Janvilisri, T., and Komyod, W. (2023). Asiatic acid inhibits nasopharyngeal carcinoma cell viability and migration via suppressing STAT3 and Claudin-1. *Pharm. (Basel)* 16, 902. doi:10.3390/ph16060902

Polycarpou-Schwarz, M., Groß, M., Mestdagh, P., Schott, J., Grund, S. E., Hildenbrand, C., et al. (2018). The cancer-associated microprotein CASIMO1 controls cell proliferation and interacts with squalene epoxidase modulating lipid droplet formation. *Oncogene* 37, 4750–4768. doi:10.1038/s41388-018-0281-5

Spano, D., Heck, C., De Antonellis, P., Christofori, G., and Zollo, M. (2012). Molecular networks that regulate cancer metastasis. *Semin. Cancer Biol.* 22, 234–249. doi:10.1016/j.semcancer.2012.03.006

Staff, A. C. (2001). An introduction to cell migration and invasion. *Scand. J. Clin. Lab. Investig.* 61, 257–268. doi:10.1080/00365510152378978

Strouhalova, K., Přechová, M., Gandalovičová, A., Brábek, J., Gregor, M., and Rosel, D. (2020). Vimentin intermediate filaments as potential target for cancer treatment. *Cancers (Basel)* 12, 184. doi:10.3390/cancers12010184

Tan, Z., Zhao, L., Huang, S., Jiang, Q., Wei, Y., Wu, J. L., et al. (2023). Small peptide LINC00511-133aa encoded by LINC00511 regulates breast cancer cell invasion and stemness through the Wnt/β-catenin pathway. *Mol. Cell. Probes* 69, 101913. doi:10.1016/j.mcp.2023.101913

Todd, V. M., and Johnson, R. W. (2020). Hypoxia in bone metastasis and osteolysis. *Cancer Lett.* 489, 144–154. doi:10.1016/j.canlet.2020.06.004

Valastyan, S., and Weinberg, R. A. (2011). Tumor metastasis: molecular insights and evolving paradigms. *Cell.* 147, 275–292. doi:10.1016/j.cell.2011.09.024

van Zijl, F., Krupitza, G., and Mikulits, W. (2011). Initial steps of metastasis: cell invasion and endothelial transmigration. *Mutat. Res.* 728, 23–34. doi:10.1016/j.mrrev.2011.05.002

von Lersner, A., Droesen, L., and Zijlstra, A. (2019). Modulation of cell adhesion and migration through regulation of the immunoglobulin superfamily member ALCAM/CD166. *Clin. Exp. Metastasis* 36, 87–95. doi:10.1007/s10585-019-09957-2

Wang, J., Zhu, S., Meng, N., He, Y., Lu, R., and Yan, G. R. (2019a). ncRNA-encoded peptides or proteins and cancer. *Mol. Ther.* 27, 1718–1725. doi:10.1016/j.ymthe.2019.09.001

Wang, Y., Huang, T., Sun, X., and Wang, Y. (2019b). Identification of a potential prognostic lncRNA-miRNA-mRNA signature in endometrial cancer based on the competing endogenous RNA network. *J. Cell. Biochem.* 120, 18845–18853. doi:10.1002/jcb.29200

Wu, J. S., Jiang, J., Chen, B. J., Wang, K., Tang, Y. L., and Liang, X. H. (2021). Plasticity of cancer cell invasion: patterns and mechanisms. *Transl. Oncol.* 14, 100899. doi:10.1016/j.tranon.2020.100899

Wu, P., Mo, Y., Peng, M., Tang, T., Zhong, Y., Deng, X., et al. (2020). Emerging role of tumor-related functional peptides encoded by LncRNA and circRNA. *Mol. Cancer* 19, 22. doi:10.1186/s12943-020-1147-3

Xu, X., Zhang, Y., Wang, M., Zhang, X., Jiang, W., Wu, S., et al. (2022). A peptide encoded by a long non-coding RNA DLX6-AS1 facilitates cell proliferation, migration, and invasion by activating the wnt/β-Catenin signaling pathway in non-small-cell lung cancer cell. *Crit. Rev. Eukaryot. Gene Expr.* 32, 43–53. doi:10.1615/CritRevEukaryotGeneExpr.2022043172

Yasuda, J., and Hayashizaki, Y. (2008). The RNA continent. *Adv. Cancer Res.* 99, 77–112. doi:10.1016/S0065-230X(07)99003-X

Ye, M., Gao, R., Chen, S., Bai, J., Chen, J., Lu, F., et al. (2023). FAM201A encodes small protein NBASP to inhibit neuroblastoma progression via inactivating MAPK pathway mediated by FABP5. *Commun. Biol.* 6, 714. doi:10.1038/s42003-023-05092-7

Zhang, Y., Liu, Z., Zhong, Z., Ji, Y., Guo, H., Wang, W., et al. (2024a). A tumor suppressor protein encoded by circKEAP1 inhibits osteosarcoma cell stemness and metastasis by promoting vimentin proteasome degradation and activating anti-tumor immunity. *J. Exp. Clin. Cancer Res.* 43, 52. doi:10.1186/s13046-024-02971-7

Zhang, Z., Yi, Y., Wang, Z., Zhang, H., Zhao, Y., He, R., et al. (2024b). LncRNA MAGI2-AS3-encoded polypeptide restrains the proliferation and migration of breast cancer cells. *Mol. Biotechnol.* 66, 1409–1423. doi:10.1007/s12033-023-00801-3

Zhao, W., Zhang, Y., and Zhu, Y. (2021). Circular RNA circβ-catenin aggravates the malignant phenotype of non-small-cell lung cancer via encoding a peptide. *J. Clin. Lab. Anal.* 35, e23900. doi:10.1002/jcla.23900

Zheng, W., Guo, Y., Zhang, G., Bai, J., Song, Y., Song, X., et al. (2023). Peptide encoded by lncRNA BVES-AS1 promotes cell viability, migration, and invasion in colorectal cancer cells via the SRC/mTOR signaling pathway. *PLoS ONE* 18, e0287133. doi:10.1371/journal.pone.0287133

Zheng, X., Chen, L., Zhou, Y., Wang, Q., Zheng, Z., Xu, B., et al. (2019). A novel protein encoded by a circular RNA circPPP1R12A promotes tumor pathogenesis and metastasis of colon cancer via Hippo-YAP signaling. *Mol. Cancer* 18, 47. doi:10.1186/s12943-019-1010-6

Zhou, J., Yao, L., Su, Y., and Tian, L. (2024). IGF2BP3 loss inhibits cell progression by upregulating has_circRNA_103820, and hsa_circRNA_103820-encoded peptide inhibits cell progression by inactivating the AKT pathway in lung cancer. *Chem. Biol. Drug Des.* 103, e14473. doi:10.1111/cbdd.14473

Zhu, S., Wang, J. Z., Chen, D., He, Y. T., Meng, N., Chen, M., et al. (2020). An oncopeptide regulates m6A recognition by the m6A reader IGF2BP1 and tumorigenesis. *Nat. Commun.* 11, 1685. doi:10.1038/s41467-020-15403-9

Frontiers in Pharmacology

Explores the interactions between chemicals and living beings

The most cited journal in its field, which advances access to pharmacological discoveries to prevent and treat human disease.

Discover the latest Research Topics

See more →

Frontiers

Avenue du Tribunal-Fédéral 34
1005 Lausanne, Switzerland
frontiersin.org

Contact us

+41 (0)21 510 17 00
frontiersin.org/about/contact